Regulation of Alzheimer's disease-associated phenotypes by the transcription factor REST

by

Mariana Santos Vidal Tomás

School of Pharmacy and Biomedical sciences

A thesis submitted in partial fulfilment for the requirements for the degree of Doctor of Philosophy at the University of Central Lancashire

April 2023

RESEARCH STUDENT DECLARATION FORM

Type of Award **PhD (via MPhil)**

School **School of Pharmacy and Biomedical sciences**

1. Concurrent registration for two or more academic awards

*I declare that while registered as a candidate for the research degree, I have not been a registered candidate or enrolled student for another award of the University or other academic or professional institution

2. Material submitted for another award

***I** declare that no material contained in the thesis has been used in any other submission for an academic award and is solely my own work

3. Collaboration

Where a candidate's research programme is part of a collaborative project, the thesis must indicate in addition clearly the candidate's individual contribution and the extent of the collaboration. Please state below:

_____

4. Use of a Proof-reader

*No proof-reading service was used in the compilation of this thesis.

Signature of Candidate Mariana Santos Vidal Tomás

Print name: Mariana Santos Vidal Tomás

Abstract

Alzheimer's disease (AD) is the major form of dementia. No cure is currently available, and a better understanding of the molecular and neurobiological mechanisms underlying AD is needed. The RE1-silencing transcription factor (REST) regulates the transcription of several genes in the brain. Recently it has been strongly implicated in AD, healthy ageing and longevity as neuroprotective (a role proposed to be lost in AD), however the exact mechanisms mediating that role are still unclear. The Director of Studies has previously generated a genetically modified conditional knockout (cKO) mouse model lacking REST specifically in neurons of the postnatal forebrain – *Rest* cKO. Characterization of this mouse model at the morphological and molecular levels is required to gain detailed insights into the role of REST in the brain, especially with relevance to AD. This research project aimed to take the next steps in this direction through a multidisciplinary approach, using biochemical, histological, molecular and computational modelling techniques.

The expression of certain key proteins (GSK3β, p35/p25) involved in one of the hallmarks of Alzheimer's disease, tau phosphorylation, as well as the levels of phosphorylated tau were found increased in the hippocampus of *Rest* cKO mice. The levels of an important postsynaptic protein, PSD-95, also appeared to be altered in the brain of *Rest* cKO mice. Moreover, *Rest* cKO mice appear to suggest the presence of a very interesting vascular phenotype associated with phospho-tau (pSer202 and pThr205) and its associated kinase GSK3β. The possible presence in *Rest* cKO mice of common cellular traits of AD, such as neuronal, dendritic and synaptic degeneration and astrocytic activation, was studied through immunohistochemical analysis of the hippocampus. Quantitation of neurons labelled for a neuronal nuclei marker revealed no major neurodegeneration phenotype. However, a mild dendritic degeneration phenotype as well as astrocytic activation was suggested in *Rest* cKO mice. Analysis of transcriptomic (RNA-seq) results, suggest that postnatal inactivation of *Rest* down-regulates synaptic activity and neuronal pathways, while also triggering an immune response and enhanced angiogenesis. Furthermore, in an attempt to assist the future design of REST enhancers as potential AD therapeutics, the 3D structures of a) the DNA-

binding domain of REST, and b) the consensus Re1 sequence (the REST binding site in the promoter of target genes) were predicted using computational modelling methods.

Overall, postnatal ablation of *Rest* appears to present a phenotype resembling several aspects of early mild AD, with pivotal mechanisms appearing affected in *Rest* cKO mice.

Contents

Acknowledgements

First, I would like to thank Dr Vassilios Beglopoulos for his guidance, incessant support, consideration, motivation and availability. For always keeping calm and positive when I would start to stress. I am very grateful for the opportunity you gave me all these years ago!

Second, I would like to thank Dr Joseph Hayes for his guidance, on the computational part of my work. Your help and teaching were invaluable. I would like to also thank Dr Jane Alder for her guidance over the course of my PhD and the kindness and sympathy she always showed me.

I would like to thank to everyone in the University of Central Lancashire, who helped me with this project and supported me during my PhD. Special thanks go out to Dr Martin Clark and Katie, your support and help with the microscope was fantastic. Thanks for always being more than ready to help me.

A special thanks to Filipa, my partner in crime. Without you these 3 and half years would have been unbearable! Thank you for always go with my crazy and sudden plans and for keeping up with me on those day that I wouldn't shut up complaining. Thanks for picking me up that very first day on the train station! Also, a special thanks to Amisha, my former colleague in the lab. Working with you was great and you helped me a lot going through COVID period. I would also like to thank my current group colleagues, Johan, Nichola and Wez and my colleagues from the office and the General lab with whom I had great chat over long hours. In particular to Wez with whom I shared my first trip to the USA.

One of the biggest thanks has to go to my family, Mom, Dad, little bro, Gradma and Aunt Clau, over in Portugal. Moving to another country was not easy for me or for you but I couldn't have done it without your support and encouragement! I want to thank my boyfriend, Marcelo, for always (!) making me laugh, even when I didn't felt like it. I can never thank you enough for all your patience and love. To my girls, Lu, Inês, Nicole

e Nininha, you showed me that although ‘we are hostages of geography’, distance is as big as we allow it to be! To my friend Eurico, from across the pond, thanks so much for the weekly talks until 4am sharing war stories from the lab. That was one of the things that kept me sane throughout the last 3 and half years!

I would like to acknowledge that this thesis was funded by the European Union’s Horizon 2020 research and innovation programme under the Marie Skłodowska-Curie grant agreement N^{o} 801604. Finally, I would like to thank the Doctoral Training Alliance (DTA) for all the support regarding this opportunity and the vote of confidence these awards entail.

List of Figures

List of Tables

Abbreviations

ABC	Avidin/Biotin Complex
AD	Alzheimer's disease
AMPA	α-amino-3-hydroxy-5-methyl-4-isoxazolepropionic acid
APP	Amyloid precursor protein
Aβ	β-amyloid
BCA	Bicinchoninic acid
BDNF	Brain derived neurotrophic factor
BLAST	Basic Local Alignment Search Tool
BSA	Bovine serum albumin
CAMKIIα	calcium/calmodulin-dependent protein kinase II
CBP	CREB binding protein
CDK5	Cyclin dependent kinase 5
cDKO	Conditional double knockout
cDNA	Complementary DNA
ChIP-Seq	Chromatin immuno-precipitation sequencing
cKO	Conditional knockout
CREB	cAMP response element-binding protein
DAB	3,3'-Diaminobenzidine
DBD	DNA binding domain
DG	Dentate gyrus
DNMT	DNA methyltransferase
DTT	Dithiothreitol
ECL	Enhanced chemiluminescence
EDTA	Ethylenediamine tetra-acetic acid
ESC	Embryonic stem cells
FC	Fold-change
FDR	False Discovery Rate
GABA	γ-Aminobutyric acid
GFAP	Glial fibrillary acidic protein
GluN2A	N-methyl D-aspartate receptor subtype 2A

GluN2B	N-methyl D-aspartate receptor subtype 2B
GOE	Gene Ontology Enrichment
GSE	Gene set enrichment
GSK-3β	Glycogen synthase kinase-3 beta
HAT	Histone acetyltransferase
HD	Huntington's Disease
HDAC	Histone deacetylase
IGBMC	Institut de Génétique et de Biologie Moléculaire et Cellulaire
IHC	Immunohistochemistry
KEGG	Kyoto Encyclopedia of Genes and Genomes
LAS X	Leica Application Suite X
LTP	Long-term potentiation
MAP2	Microtubule-associated protein 2
MAPK	Mitogen-activated protein kinase
MD	Molecular dynamics
MMB	Macro Molecular Builder
MOPS	3-(N-morpholino) Propanesulfonic acid
mRNA	Messenger RNA
NaCl	Sodium chloride
ncRNA	Non-coding RNA
NDRG2	N-Myc downstream-regulated gene 2
NFTs	Neurofibrillary tangles
NMDA	N-methyl-D-aspartate
NMR	Nuclear magnetic resonance
NPC	Neural progenitor cells
NRSE	Neuron-restrictive silencer element
NRSF	Neuron restrictive silencer factor
NtCs	Nucleotide conformers
PAGE	Polyacrylamide gel electrophoresis
PBS	Phosphate-buffered saline
PCR	Polymerase chain reaction

PD	Parkinson’s disease
PDB	Protein Data Bank
PMSF	Phenylmethylsulfonyl fluoride
PP1	Phosphatase 1
PPI	Protein-Protein Interaction
PS1	Presenilin 1
PS2	Presenilin 2
PSD-95	Postsynaptic density protein 95
pSer	Phosphorylated Serine
PVDF	Polyvinylidene difluoride
RCSB	Research Collaboratory for Structural Bioinformatics
Re1	Restrictive element 1
REST	RE1-silencing transcription factor
RIPA	Radioimmunoprecipitation assay buffer
RMSD	Root mean square deviation
RNA-seq	RNA-sequencing
rpm	Rotations per minute
SDS	Sodium dodecyl sulfate
SEM	Standard error of mean
pSer	Phosphorylated Serine
SIN3A	SIN3 transcription regulator family member A
SSA	Secondary structure assignment
TFBSPred	Transcription Factor Binding Site Prediction
TFFM	Transcription factor flexible model
pThr	Phosphorylated Threonine
TSS	Transcription start sites
VMD	Visual Molecular Dynamics
ZF	Zinc-finger

1. INTRODUCTION

1.1. Alzheimer's disease

Dementia defines a wide group of diseases characterized by the progressive decline of cognitive function, beyond what might be expected from normal ageing. Alzheimer's disease (AD) is currently the major form of dementia, comprising approximately two-thirds of all dementia cases (World Health Organization, 2022). AD is a progressive neurodegenerative disease in which the main symptom is memory loss. Age is the main risk-factor, affecting predominantly older people (over 65). Nevertheless, 6.7% of AD cases are early onset (under 65) (Alzheimer's Association, 2022). Given the rise of life-expectancy globally, the prevalence of AD keeps increasing, making it an important global health concern.

Alzheimer's disease is a heterogeneous disease with high variability concerning the age at onset, clinical presentation and biological traces (Ferreira et al., 2018). AD can be classified as sporadic, usually late onset, or familial, usually early-onset and associated with genetic alterations (Piaceri et al., 2013). To date, the diagnosis of AD is made mostly based on the cognitive deficits patients present, with decline of various types of memory being the primary symptom, manifesting with long-term memory impairment (Kumar and Tsao, 2019). Morphologically, AD major hallmarks are atrophy of the cerebral cortex and shrinkage of the hippocampus (National Institute of Ageing, 2017). The hippocampus has a major role in memory and learning, plus it is highly susceptible to be affected in degenerative diseases, being one of the first brain regions to degenerate in AD. Therefore, when diagnosed, i.e. when the patient displays symptoms, the brain has already suffered irreversible alterations. This emphasizes the importance of addressing the early events that lead to development of AD. Additionally, even though there are treatment options for AD, there is still no cure, and clinical trials have not been able to halt the progression of the disease, making it of utmost importance to try and find more effective treatments (Rasmussen and Langerman, 2019).

1.2. Mechanisms behind cognitive impairment and neurodegeneration in AD

Memory loss and cognitive impairment are the most significant traits of Alzheimer's disease. Even though multiple theories have been proposed, there is still no agreement on the specific molecular basis behind it (Jeong, 2017; Magalingam et al., 2018; Edwards, 2019). It is most likely that a synergistic effect might be responsible for AD's main symptom.

Neuronal loss is one of the major cellular outcome in Alzheimer's disease (Serrano-Pozo et al., 2011). AD is a complex disease and although extensive research has addressed possible mechanisms behind neurodegeneration, a consensus is yet to be reached. Formation of β-amyloid (Aβ) plaques and neurofibrillary tangles (NFTs), astrocytic activation, mitochondria impairment and synaptic degeneration are just some of the multiple toxic processes behind AD development, all of them suggested to eventually lead to a common outcome, neuronal loss (Magalingam et al., 2018). In fact, neurodegeneration is resultant from a synergistic effect between all the referred mechanisms that culminate in brain atrophy and consequently memory impairment and cognitive loss (Mukhin et al., 2017). However, some studies show that neuronal loss occurs before accumulation of toxic aggregates (Padurariu et al., 2012; Nobili et al., 2017), highlighting the need for further research.

1.2.1. Amyloid hypothesis

The formation of Aβ plaques and NFTs from the hyperphosphorylated tau are well defined elements of the AD pathophysiology. These two biological hallmarks of AD are usually used to confirm the diagnosis (Dubois et al., 2021). Aβ plaques, also called "senile plaques", arise from the deposition of neurotoxic Aβ peptides in fibrils due to an imbalance in the production and clearance pathways of Aβ. These peptides result from the abnormal proteolysis of amyloid precursor protein (APP) (O'Brien and Wong, 2011; Sadigh-Eteghad et al., 2015; DeTure and Dickson, 2019; Guo et al., 2020). The amyloid hypothesis claims that the dysregulation of Aβ levels and consequent formation Aβ

plaques leads to oxidative stress, neurotoxicity, neuroinflammation and disruption of synapses, resulting in neurodegeneration and neuronal cell death (O'Brien and Wong, 2011; Kumar et al., 2015; Sadigh-Eteghad et al., 2015; Alzheimer's Association, 2022). Moreover, Aβ also regulates the enzymes responsible for the cleavage and phosphorylation of tau protein, leading to the formation of insoluble aggregates known as NFTs of hyperphosphorylated tau (O'Brien and Wong, 2011; Kumar et al., 2015; Sadigh-Eteghad et al., 2015). However, some evidence has prompted questions related to the importance of Aβ in AD's aetiology. First, the exact order of events leading to the onset of AD is still matter of debate, with tau lesions having been observed before the formation of Aβ plaques (Braak and Del Tredici, 2014; Arnsten et al., 2021). On the other hand, the number of Aβ plaques is not directly associated with the severity of cognitive impairment, moreover plaques have been observed in healthy aged brain (Rodrigue et al., 2009). Furthermore, clinical trials targeting Aβ have revealed not entirely satisfactory results. In the last few years, these evidence has led to a shift in the focus of AD research towards tau protein (Kumar et al., 2015; Congdon and Sigurdsson, 2018; Kametani and Hasegawa, 2018; Hillen, 2019; Arnsten et al., 2021). Aggregates of hyperphosphorylated tau have been associated with synaptic dysfunction, neurodegeneration and neuroinflammation thus being hypothesized a to have a strong correlation with cognitive impairment (Giannakopoulos et al., 2003; Ballatore et al., 2007; Gong and Iqbal, 2008; Fu et al., 2017; Terada et al., 2019).

1.2.2. Hyperphosphorylation of tau protein

Tau is a microtubule-associated protein predominantly found in neurons, involved in the stabilization of microtubules and regulation of axonal transport. Post-translational modifications, like phosphorylation, regulate the correct functioning of tau (Martin et al., 2013; Kimura et al., 2018). However, upon deregulation of such mechanisms, specifically hyperphosphorylation, tau detaches from the microtubules and aggregates forming NFTs (Ittner and Götz, 2011; Iqbal et al., 2016; Guo et al., 2020). Tau has 85 residues that can be phosphorylated, with 44 having been observed to be phosphorylated in AD pathological tau. This process is mediated by kinases which have been thoroughly studied, such as cyclin dependent kinase 5 (CDK5), together with its

specific activators p35/p25, and glycogen synthase kinase-3β (GSK3β) (Martin et al., 2013; Kimura et al., 2018). Different kinases can phosphorylate the same epitope, making it a challenge to distinguish which epitope is phosphorylated at which point in AD's development and by which kinases. Nevertheless, some epitopes have attracted particular attention when referring to tau hyperphosphorylation: serine 202 (Ser202), threonine 205 (Thr205), Ser396 and Ser404 (Martin et al., 2013; Kimura et al., 2018).

Recently, tau has been proposed as the initial trigger of sporadic AD (Muralidar et al., 2020; Arnsten et al., 2021). It is thought that tau hyperphosphorylation initially occurs in more vulnerable neurons with elevated intracellular calcium (Ca^{2+}) levels. Hyperphosphorylated-tau then evades those neurons and spread causing toxicity in other cells (Katsinelos et al., 2018; Muralidar et al., 2020; Arnsten et al., 2021).

1.2.3. Vascular dysfunction

Vascular dysfunction is a trait of early AD and it has gained more relevance in recent years (Hays et al., 2016; Govindpani et al., 2019; Canepa and Fossati, 2021). Alterations in the blood vessels morphology and angiogenesis, i.e. formation of new vasculature, have been observed in the AD brain (Bennett et al., 2018). Multiple evidence has associated traits of AD with vascular impairment: deficit in Aβ clearance and Aβ-mediated toxicity (cerebral amyloid angiopathy), blood brain barrier disruption, impaired glucose metabolism, abnormal immune cell recruitment and cytokine release (Govindpani et al., 2019; Canepa and Fossati, 2021).

Recently, tau has been implicated in the development of this vascular phenotype (Canepa and Fossati, 2021). As mentioned before, hyperphosphorylation of tau could be the cellular insult responsible for early AD (Arnsten et al., 2021). It is thought that after escaping the most vulnerable neurons, it can seed to astrocytes, microglia or to the interstitial fluid (Canepa and Fossati, 2021). This might cause a toxic accumulation of hyperphosphorylated tau around vasculature causing lower cerebral blood flow (and consequentially hypoxia), rearrangement of vessels morphology with loss of integrity and finally, disruption of the blood brain barrier (Blair et al., 2015; Castillo-Carranza et al., 2017; Canepa and Fossati, 2021). Furthermore, reactive glia could induce cytokine production and initiate an immune response.

1.2.4. Astrocytic activation

Neuroinflammation is a common feature of neurodegenerative disease (Heneka et al., 2015). In specific, reactive glia such as astrocytes, is a characteristic of AD. Astrocytes have an important role in the maintenance of the correct neuronal functioning of the brain. However, given certain cellular insults, astrocytes can become reactive, changing their morphology and function and contributing to neuroinflammation, a process called astrogliosis (Wilhelmsson et al., 2006; Perez-Nievas and Serrano-Pozo, 2018; Arranz and De Strooper, 2019; Monterey et al., 2021).

Experimentally, glial fibrillary acidic protein (GFAP) is used as a standard astrocytic maker in the study of neuroinflammation (Sofroniew and Vinters, 2010; Orre et al., 2014; Heneka et al., 2015). GFAP is an intermediate filament protein that is known to be more highly expressed in astroglial cells in the aged brain, in neurodegenerative diseases and upon brain damage (Eng and Ghirnikar, 1994; Middeldorp and Hol, 2011). An increase in the levels of GFAP, accompanied by an increase in the astrocyte's protrusions in a star-shaped form are features usually associated with astrogliosis (Wilhelmsson et al., 2006).

Reactive astrocytes have been localized in more susceptible locations in the brain, such as the hippocampus (Orre et al., 2014; Pekny and Pekna, 2014; Rodríguez et al., 2014; Chun and Lee, 2018). Astrocytic activation has been observed in the area surrounding of Aβ plaques. A positive feedback mechanism has been suggested involving the activation of astrocytes and Aβ. A reduction in neuronal support function and reduced neuronal signalling gene expression has been observed in Aβ-induced activated astrocytes, suggesting a role in neuronal dysfunction and consequently in cognitive impairment (Orre et al., 2014). On the other hand, the activation of astrocytes enhances the production of Aβ plaques (Zhao et al., 2011).

More recently, astrocytic activation has been associated with the presence of aggregates of tau protein, resulting in neuronal loss (Domingues et al., 2017). Domingues *et al.* suggested this interaction is mediated by cytokines produced by the activated astrocytes (Domingues et al., 2017).

1.2.5. Dendritic and synaptic degeneration

Neurons communicate through synapses in the brain. Neurotransmitters are imported to vesicles in the presynaptic terminal, which upon stimuli, fuse with the presynaptic membrane and release the neurotransmitters into the synaptic cleft. They are then recognized by receptors located at the post density membrane, such as N-methyl-D-aspartate (NMDA) or α-amino-3-hydroxy-5-methyl-4-isoxazolepropionic acid (AMPA) receptors. These will recognize neurotransmitters and will transduce the information for the postsynaptic neuron, which is the basic process behind memory. When this process is impaired, due to pre- or postsynaptic failure or dendritic degeneration, it leads to loss of memory, the main symptom of AD (Masliah et al., 2001; Lleó et al., 2019; Colom-Cadena et al., 2020). Synaptic degeneration appears to be an early trait of AD (Barthet and Mulle, 2020). Thus, the study of neural circuits, its impairment in AD and its possible repair has become more relevant in recent years (Canter et al., 2016). However, the cellular mechanisms that connect synaptic degeneration, synaptic plasticity, memory and learning impairment and AD pathology remain unclear. Barthet *et al.* recently gathered evidence of presynaptic failure in AD (Barthet and Mulle, 2020). They exemplify how hallmarks of AD might have an important role in synaptic degeneration, further than the roles that have been extensively reported until now. A number of recent studies have begun to investigate the possibility that Aβ oligomers might interfere with synaptic function by altering synaptic proteins, such as postsynaptic density-95 (PSD-95) and glutamate receptors (Snyder et al., 2005).

Long-term potentiation (LTP) is a process of synaptic plasticity that is involved in memory formation. Briefly, an initial stimulus will lead to a long-term increase in synaptic response (Baltaci et al., 2019). Another element involved in synaptic plasticity is NMDA receptors. These are localised in the postsynaptic membrane and regulate synapses and LTP by controlling the levels of intracellular Ca^{2+} (Mota et al., 2013). These ionotropic receptors only allow Ca^{2+} into the dendrite after there is a depolarization of the postsynaptic membrane (which relieves a magnesium blockade) and after binding with glutamate. The increase of intracellular Ca^{2+} initiates a variety of the signalling cascades. Several reports have related the presence of Aβ with an increase in intracellular Ca^{2+} levels and consequently, hyperactivation of NMDA receptors and oxidative stress which ultimately results in AD pathology (Liu et al., 2019).

PSD-95 is as scaffolding protein that stabilizes and regulates membrane receptors, such as NMDA and AMPA, ion channels and signalling proteins in the postsynaptic membrane of excitatory neurons (Sheng and Kim, 2002). Furthermore, it helps maintaining NMDA receptors with subunit GluN2A in the synaptic site and reduces subunit GluN2B endocytosis (Snyder et al., 2005; Kellermayer et al., 2018). Thus it has a pivotal role in plasticity mechanisms and consequently in memory.

Dendritic impairment has also been widely studied in AD. Dendrites contain synapses, therefore dendritic degeneration might lead to synapse loss and consequently impair neural circuits that underlie cognitive impairment (Canter *et al*., 2016). It has been reported that Aβ levels might induce morphological abnormalities on dendrites, such as decrease in spine density (Grutzendler et al., 2007; Baloyannis, 2009). Curiously, dendritic abnormalities were found to be enough to alter synaptic function causing hyperexcitability in the hippocampus, which can lead to network impairment (Šišková et al., 2014; Busche and Konnerth, 2016; Zott et al., 2018). Thus, suggesting that dendritic degeneration might be an early trait of AD.

1.3. Epigenetics, neurodegeneration and Alzheimer's disease

AD is a complex and heterogenous disease, with the vast majority of cases being considered sporadic with unknown aetiology (Ferreira et al., 2018; Alzheimer's Association, 2019). In fact, only a very small percentage of AD cases are associated with genetic mutations, usually in genes associated with Aβ such as APP, presenilin 1 (PS1) and presenilin 2 (PS2). This suggest that other mechanisms might be underlying AD's development. Numerous recent studies have revealed the importance of epigenetics in normal brain function and in neurodegenerative diseases. Epigenetic regulation consists of mechanisms, such as histone post-translational modifications and DNA methylation, that change gene expression without altering the DNA sequence. (Hwang *et al.*, 2017; Berson *et al.*, 2018; Stoccoro and Coppedè, 2018; Zusso *et al.*, 2018).

Epigenetic regulation consists of three main different types of mechanisms that change gene expression without altering the DNA sequence through: 1) DNA methylation; 2) non-coding RNAs; or 3) histone post-translational modifications

(acetylation and deacetylations) (Hwang et al., 2017; Berson et al., 2018; Stoccoro and Coppedè, 2018; Sujeetha et al., 2018; Esposito and Sherr, 2019). The regulation of gene transcription, and consequently regulation of biological processes, is tightly regulated by these epigenetic mechanisms. Recently, Liu and colleagues have summarized the role of epigenetic regulation in AD's development (Liu et al., 2018).

DNA methylation is a process mediated by DNA methyltransferases (DNMTs) that consists of adding methyl groups to the nucleotide sequence, altering gene transcription. These alterations usually occur in the promoter of the target gene, repressing transcription, however it could have the opposite effect when methylation occurs within gene coding sequence (Stoccoro and Coppedè, 2018; Zusso et al., 2018; Poon et al., 2020). Overall, a reduction in DNA methylation is observed in Alzheimer's disease in humans (Chouliaras et al., 2013; Condliffe et al., 2014). However, in mice models of AD, no general conclusion can be drawn (Lardenoije et al., 2018). Feng *et al* reported memory impairment and learning deficits in mice lacking DNMT1 and/or DNMT3 in the postnatal forebrain through loss of LTP, showing that DNA methylation is associated with synaptic plasticity (Feng et al., 2010).

Another epigenetic element is non-coding RNAs (ncRNAs), which can silence gene expression by binding to the messenger RNA (mRNA) and leading to its degradation (Hove et al., 2014; Hwang et al., 2017; Stoccoro and Coppedè, 2018). Dysregulation of ncRNAs have been reported to be associated with Aβ production in AD. Also, similar to DNA methylation, it has been reported an association with synaptic plasticity (Stoccoro and Coppedè, 2018).

Histone post-translational modifications regulate gene transcription by modulating the chromatin (i.e. the complex formed by DNA and the proteins that it is packaged around, called histones) structure and controlling the access of the transcription machinery to the gene promotor. These modifications can be through acetylation, methylation or phosphorylation of the N-terminal tails of histones (Hwang et al., 2017; Narayan and Dragunow, 2017; Stoccoro and Coppedè, 2018). The effect of histone methylation is context specific, as it can stimulate or repress gene expression depending on which residue is methylated (Berson et al., 2018; Zusso et al., 2018). Phosphorylation of histones has been associated with multiple cellular mechanisms such as DNA damage response, transcriptional activation, stimulate long-term memory and regulation of

other histone modifications (Chwang et al., 2006; Rossetto et al., 2012; Cobos et al., 2019). Histone acetylation is mediated by histone acetyltransferases (HATs) and is usually associated with transcription of the target genes as it relaxes the chromatin complex. The reverse process – deacetylation – is mediated by histone deacetylases (HDACs) and leads to chromatin condensation, restraining the access of transcriptional machinery to the promotor region of the target gene thereby silencing transcription (Levenson and Sweatt, 2005; Hwang et al., 2017). This type of modification has been vastly studied in the context of neurodegenerative diseases (Beglopoulos et al., 2004; Fischer et al., 2007; Francis et al., 2009; Dubey et al., 2018).

Beglopoulos *et al.* and Saura *et al.* have studied a conditional double knock out (cDKO) mouse model lacking both *PS1* and *PS2* in the postnatal forebrain, that showed a typical neurodegenerative phenotype with neuronal loss and deficits in learning and memory. These studies demonstrated that loss of presenilins is associated with reduced expression of CREB binding protein (CBP – transcription factor with HAT activity) and affecting the respective pathway. They observed selective hippocampal reductions in NMDA receptor-mediated response and impairment of LTP. Furthermore, an increase in the levels of reactive astrocytes was observed in the cerebral cortex (Beglopoulos et al., 2004; Saura et al., 2004). Therefore it is suggested that impairment in histone acetylation is associated with a neurodegenerative phenotype with learning and memory deficits and neuroinflammation. Similar results were obtained by Francis *et al* using a double transgenic mouse model expressing human mutated *APP* and *PS1* genes (Francis et al., 2009). Although the outcome is similar – histone deacetylation is associated with memory impairment – the mechanism behind it has different intermediates. Moreover, they observed a bypass of the degenerative phenotype after using an HDAC inhibitor (Francis et al., 2009). In fact, HDAC inhibitors have strongly been suggested to have a therapeutic potential in neurodegenerative diseases (Gräff and Tsai, 2013).

CDK5 is one of the major kinases that phosphorylates tau. It has a major role in development of the central nervous system and it has also been associated with neurodegenerative diseases. In a slightly different approach, Gräff *et al.* studied a mouse model where there was conditionally overexpression of p25, a truncated version of an activator of CDK5, to clarify the mechanism behind this association (Gräff et al., 2012).

They found that chronic induction of p25 leads to neurodegenerative phenotype observing many traits of AD such as Aβ agglomerates, neuroinflammation and neuronal loss. Additionally, they discovered that AD's pathologic traits stimulated HDAC2 expression and consequently, increased levels of HDAC2 hypoacetylated genes involved in neuroplasticity (Gräff et al., 2012).

1.4. Whole-genome analysis in neurodegenerative diseases.

Neurodegenerative diseases, AD in particular, are very heterogenous diseases with multiple aetiologies, affecting various regions and pathways but with similar outcomes, loss of neurons and impairment of cerebral functions such as cognition and memory (Tsuji, 2010; Parikshak et al., 2015; Diaz-Ortiz and Chen-Plotkin, 2020). Targeted techniques, although needed to study mechanisms at a more focused perspective, might overlook important participants and connections in complex diseases. In the last 20 years, several high-throughput analyses have gained relevance in the study of these complex diseases. These allow the study of molecules, for example, DNA, RNA, proteins or methylation patterns, in a global scale and their integration in biological processes and neural circuits (Parikshak et al., 2015).

RNA-sequencing (RNA-Seq) is a high-throughput next generation sequencing of mRNA that allows the identification and quantification of global gene expression – transcriptome, i.e., all the genes expressed in a target tissue at a certain time (Wang et al., 2009). It is particularly useful to uncover aberrant gene expression in disease conditions, that then can be used in more targeted techniques (Tsuji, 2010; Diaz-Ortiz and Chen-Plotkin, 2020). Briefly, RNA-Seq has four main steps: 1) isolation of RNA; 2) conversion of RNA into complementary DNA (cDNA); 3) generation of a sequencing library and 4) sequencing in a next-generation sequencing platform (Kukurba and Montgomery, 2015).

Several studies have highlighted the advantages of screening the transcriptome of the neurodegenerative diseases. Twine and colleagues have compared gene expression in the frontal and temporal lobes of healthy individuals and AD patients. Their work revealed alternate use of promotors, different slicing patterns and identified

differentially expressed genes in AD pathology (Twine et al., 2011). In another perspective, Bennett and Keeney have researched a possible common pathological mechanism between AD and Parkinson's disease (PD) (Bennett and Keeney, 2018). Although RNA-Seq data revealed extensive heterogeneity between pathologies, they have suggested several genes that could be used as common targets in future therapies (Bennett and Keeney, 2018). Recently, Otero-Garcia *et al.* have characterized the molecular signatures of tangles using single cell RNA-Seq by comparing NFT-bearing and neighbouring NFT-free somas (Otero-Garcia et al., 2022). Thus, they concluded that NFT-bearing neurons present a set of commonly dysregulated synaptic genes. These studies highlight the versatility of RNA-Seq and the importance of studying global gene expression.

1.5. Re1-silencing transcription factor – REST

The restrictive element 1-silencing transcription factor (REST; also known as neuron restrictive silencer factor, NRSF) is a major transcriptional repressor which epigenetically silences a large cohort of neuronal genes depending, among others factors, on the stimulus, cell-type and cellular localisation (Garcia-Manteiga *et al*., 2019; Mampay and Sheridan, 2019).

REST represses genes by epigenetically remodelling the chromatin structure (**Figure 1**). First, REST binds to the *Re1* (also called neuron-restrictive silencer element – *NRSE*) sequence upstream of target genes, in the promotor region, leading to the recruitment of cofactors such as CoREST and Sin3A (Hwang and Zukin, 2018; Mampay and Sheridan, 2019). Additional silencing machinery, such as HDAC enzymes, will then be recruited, tightening the chromatin complex and thereby silencing the target gene (Hwang et al., 2017). REST-driven DNA methylation of the promotor region has also been reported (Ballas et al., 2005). Over 8,000 genomic regions in humans, and 4,000 in mice, have been identified as REST binding regions in embryonic stem cells (ESC) (Rockowitz and Zheng, 2015).

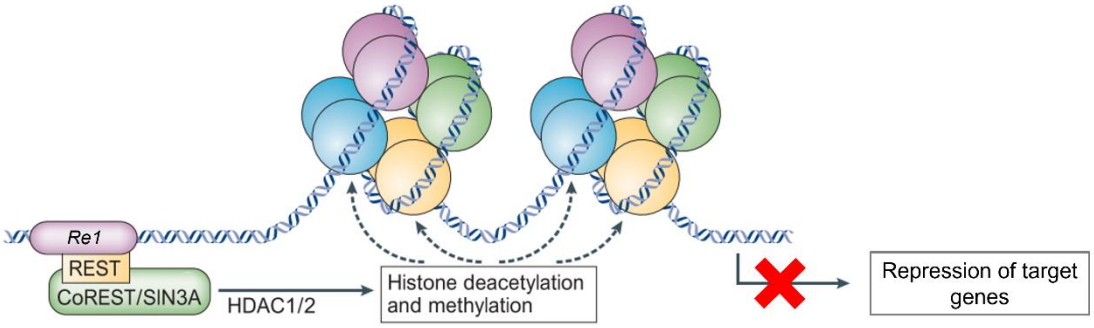

Figure 1. Mechanism of action of REST. REST binds to a *Re1* sequence located upstream of the REST-target gene in the promoter region, which will lead to the recruitment of cofactors such as CoREST and SIN3A. The REST-corepressor complex will modify the histones that compact the DNA through post-translational changes, deacetylation and methylation. This will tighten the chromatin conformation which restricts access to transcriptional machinery at promotor region, hence inhibiting the expression of the target gene. Adapted from Levenson *et al.* 2005.

1.5.1. REST structure

REST is constituted by three functional domains: two repressor domains, SIN3A and CoREST at the N- and C-terminal, respectively, and one DNA binding domain (DBD) (Chong et al., 1995; Palm et al., 1998; Ooi and Wood, 2007). The DBD comprises eight zinc-finger (ZF) C2H2 motifs (**Figure 2**) that will mediate the DNA-protein interaction. The ZF motif usually involves 28-30 residues that form a short antiparallel β-sheet and a α-helix, united by a hairpin turn. This structure is stabilized by a zinc atom that coordinates with two cysteines at one end of the β-sheet and two histidines at the end of the helix (C2H2) (Wolfe et al., 1999; Schmitges et al., 2016; Fedotova et al., 2017). The DNA-protein interaction is done by residues in specific positions, -1, +2, +3, and +6, relative to the beginning of the helix (Fedotova et al., 2017). Although the ZF C2H2 motif is conserved (i.e. involves always two cystines and two histidines coordinated with a zinc atom), the residues in the helix that bind to the DNA sequence vary and depend on the primary structure (sequence) of each protein.

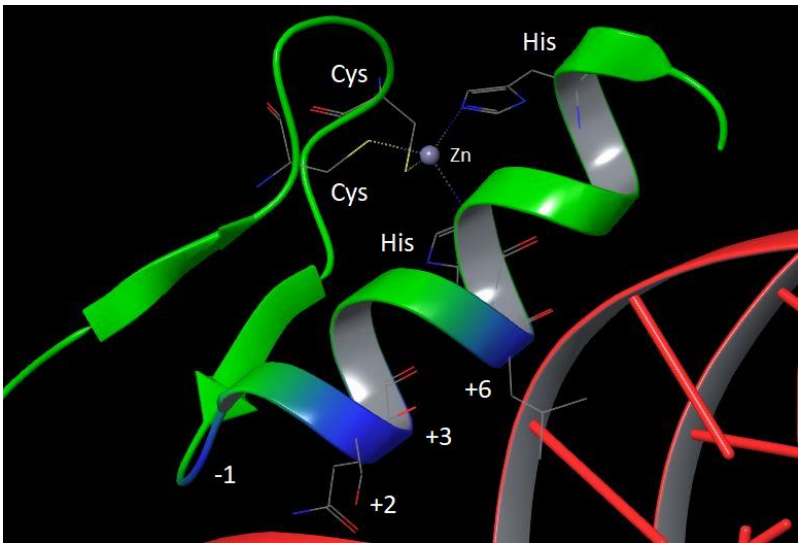

Figure 2. Zinc finger C2H2 motif protein-DNA site-specific typical recognition. The motif is stabilized by the zinc (Zn) atom that coordinates with two cysteines and two histidines. The ZF (green) interacts with the DNA sequence (red) through specific amino acids at positions -1, +2, +3 and +6 relative to the beginning of the helix (highlighted in blue) (image created by the author).

To date, REST structure hasn't been crystalized and few articles have addressed its 3D structure. In fact, there are only 3 entries in the RCSB Protein Data Bank (RCSB Protein Data Bank (PDB), 2020) that describe REST 3D structure. However, these entries only illustrate a very small fraction of the REST protein (1097 amino acids) in the form of 15 residues of the N-terminal (2CZY) and 12 residues of the C-terminal repressor domain only (6DU2 and 6DU3) (Nomura et al., 2005; Burkholder et al., 2018). Recently, the online server I-TASSER was used to obtain an automated 3D predictive structure for the REST DBD (Cortés-Sarabia et al., 2019). Cortés-Sarabia *et al.* aim was to generate monoclonal antibodies that targeted the REST DBD, so that they could be used as a diagnostic tool in cancer. They had to ensure that the antibodies would recognize peptides that would be exposed in the native structure of REST. Hence they had to propose a model of REST and Re1 sequence and docked both structures. The docked DNA didn't seem to fit completely inside REST DBD pocket, however, the 3D structures were only used to localize the epitopes to which the antibodies would bind to, and no further analysis was done involving the structures (Cortés-Sarabia et al., 2019). Furthermore, the automated modelling server used by the authors might not be the

most suitable method to do pharmacological studies. Therefore, there is a need to predict a more accurate model for the 3D structure of REST.

Protein structures are solved experimentally using techniques such as X-ray crystallography and NMR spectroscopy. However, these are time-consuming and laborious procedures which cannot always be applied (Muhammed and Aki-Yalcin, 2019). Computational chemistry emerged as an alternative to bypass those challenges allowing the prediction of molecular structures, how they will behave in the most diverse conditions and how they will interact with other molecules (Cavasotto et al., 2019; Huggins et al., 2019). One way to predict new structures is by comparing with similar structures that have already been experimentally solved – homology modelling. This comparative method has five main steps: 1) selection of homologous protein to serve as template; 2) alignment of the primary structure (amino acids sequence); 3) building the model based on the characteristics of the template; 4) refinement and optimization of the model and 5) validation of the final model (Hillisch et al., 2004; Cavasotto et al., 2019).

Recently, the AlphaFold software became available which relies on artificial intelligence to predict with high accuracy protein structures (Jumper et al., 2021; Ruff and Pappu, 2021). It resulted in the implementation of a novel protein database with more than 200 million solved proteins. David and colleagues discussed the strengths and challenges of AlphaFold through a non-expert in computational biology perspective (David et al., 2022). Apart from proposing a structure, AlphaFold also informs on the model confidence using a “per-residue confidence score” and the predicted aligned error.

Given the proposed neuroprotective role for REST, finding potential enhancers would be of utmost importance in AD therapy. Therefore, since REST structure has not been crystallized yet, it would be helpful to have the 3D structure of both REST and the DNA sequence it binds to. This project proposes a method to model the structure of REST DBD and also suggests a structure for the Re1 DNA sequence. Both structures were thoroughly studied, individually and docked together, in the following sections.

1.5.2. REST function and role in pathology

REST regulates multiple pivotal biological processes, particularly in neuronal development and tissue differentiation. In fact, germline deletion of *Rest* in mice has proved embryonically lethal (Chen et al., 1998; Aoki et al., 2012). REST has a major role in neurogenesis, both during embryogenesis and in adulthood. In ESC, REST is highly expressed to repress the expression of neural genes, regulating thousands of genomic regions, both in humans and in mice (Rockowitz and Zheng, 2015). To allow ESC to differentiate into neural progenitors and complete the acquisition of neuronal phenotype, REST expression is significantly reduced through the proteasomal pathway (**Figure 3**). However, in mature non-neural cells REST expression levels are higher, being needed to control adult neurogenesis (Ballas et al., 2005; Gao et al., 2011; McGann et al., 2021). Gao and colleagues have shown that REST expression regulates time-specific expression of genes that allow neurogenesis and differentiation of neuronal stem cells (NSC) (Gao et al., 2011). This evidences the importance of time and context-dependent expression of REST (Gao et al., 2011; Mampay and Sheridan, 2019). In fact, McGann and colleagues further investigated REST protein levels throughout the life of mice and humans (McGann et al., 2021). They observed that REST expression increased with age in humans, corroborating Lu *et al.* previous findings (Lu et al., 2014). On the other hand, they observed this was not replicated in mice, with REST levels decreasing after 4 months of age. Furthermore, these low levels were maintained throughout most of the adulthood of the mice which was also observed by Mampay and colleagues in rats (Mampay et al., 2021; McGann et al., 2021). To the best of our knowledge, only one study addressed REST expression between genders, which reported no differences (McGann et al., 2021).

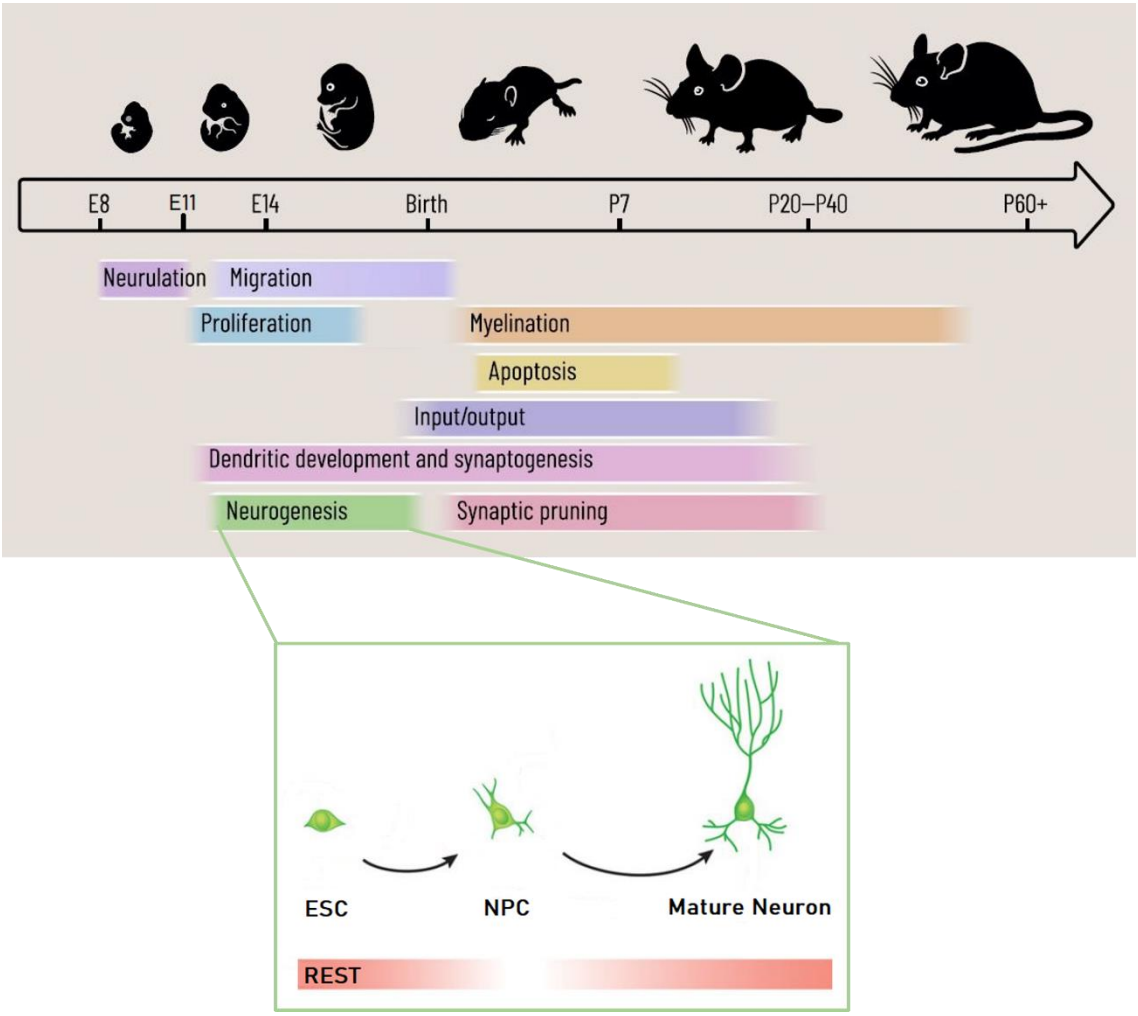

Figure 3. Timeline of the mouse neuronal development and REST expression during neurogenesis. REST is highly expressed in ESC. The expression of REST protein decreases in neural progenitor cells (NPC) and increases again when the neuron is fully matured. Adapted from Gao *et al.* (2011) and Chini and Hanganu-Opatz (2021).

REST is expressed at lower levels in differentiated neurons but it has been reported that it becomes active in response to different types of insults such as seizures, stroke and ischaemia (Liu et al., 2012; Petrosyan, 2013; Formisano et al., 2015; Hwang et al., 2017). Kaneko *et al.* observed that neuronal insults, specifically global ischemia and seizures, leads to an increase in REST due to a decrease in REST's inhibition by casein kinase 1 (Kaneko et al., 2014). Moreover, McClelland and colleagues demonstrated that an increase in REST after seizures leads to repression of pivotal genes in neuronal communication (McClelland et al., 2014). Furthermore, REST also is involved in adjusting

synaptic plasticity in early postnatal development by regulating the maturation of NMDA receptors (Rodenas-Ruano et al., 2012). This is achieved by remodelling the subunit composition ratio of NMDA receptors, containing mainly GluN2B to GluN2A. Rodenas-Ruano *et al.* studied the role of REST in this GluN2A/GluN2B ratio switch, suggesting that REST epigenetically represses *Grin2b* expression, the gene encoding GluN2B subunit, leading to a decline of GluN2B subunits and changing the NMDA receptors properties (Rodenas-Ruano et al., 2012).

REST has been associated with healthy aging and increased lifespan (Lu et al., 2014; Zullo et al., 2019). Zullo and colleagues have observed that inhibition of neural excitation leads to an increase in lifespan. Interestingly, REST appears to mediate this association by downregulating genes that mediate excitation and synaptic function in elderly population (Zullo et al., 2019). REST has also been studied in the context of multiple neurodegenerative diseases such as PD, Huntington's disease (HD) and AD, as well as other dementias (Zuccato et al., 2003; Yu et al., 2013; Lu et al., 2014; Suo et al., 2015).

HD is caused by a hereditable mutation in huntingtin protein and by reduction of brain derived neurotrophic factor (BDNF), which has a pivotal role in neuronal survival and synaptic plasticity. It has been proved that BDNF is a REST-target gene. Thus, in physiological conditions, huntingtin binds to REST maintaining it in the cytoplasm allowing the expression of BDNF. However, when huntingtin is mutated, it loses its ability to bind to REST. Consequently, REST is translocated to the nucleus, where it will inhibit BDNF and lead to neuronal degeneration (Zuccato et al., 2007; Soldati et al., 2013). On the other hand, REST has been suggested to have a neuroprotective effect in Parkinson's disease (Suo et al., 2015; Huang et al., 2019). Huang's group has demonstrated REST conditional knock-out (cKO) mice are more vulnerable to a dopaminergic toxin, MPTP, that reproduces PD's pathology. These apparent contradictory functions highlight the complexity of the role of REST, and how time-, location- and context-dependent it is.

1.5.3. REST and Alzheimer's disease

A relatively recent study has revealed the importance of REST in healthy ageing and AD (Lu et al., 2014). This study demonstrated that REST nuclear expression is a normal

feature in the aging brain, with healthy elderly individuals presenting high levels of REST. This contrasts with observations in the brain of AD patients, where REST was significantly reduced. This reduction was verified in vulnerable neuronal populations such as the prefrontal cortex and the CA1 and CA3 of the hippocampus, not only in AD but also in other types of dementia (Lu et al., 2014). Furthermore, they demonstrated that both Wnt-β-catenin signalling pathway and stress induced REST expression during ageing, which in turn downregulates a variety of genes involved in major processes such as oxidative stress (e.g. cytochrome c, mitochondrial permeability transition pore proteins), cell death (e.g. p38 MAPK, FAS, BAX), Aβ toxicity (e.g. PS2, γ-secretase) and tau phosphorylation (e.g. CDK5R1 and CDK5R2, which encode p35 and p39, respectively). On the other hand, REST enhances the expression of antioxidants (e.g. catalase, SOD1 and FOXO) as well as anti-apoptotic genes (BCL2) (Lu et al., 2014). Lu and colleagues further confirmed these findings in a human neuroblastoma cell line. They observed that when REST is inactivated in these cells, there was an upregulation of proteins encoded by the referred genes. Furthermore, they observed an upregulation of GSK3β, which lead to an upregulation of phosphorylated tau in four epitopes commonly associated with NFTs, Ser202, Thr205, Ser396 and Ser404 (Lu et al., 2014). Moreover, they concluded that in AD, REST is degraded through autophagy. This is a process characteristic of neurodegenerative diseases usually due to misfolded proteins like Aβ, α-synuclein or phosphorylated-tau. Interestingly, while REST did not colocalize with Aβ, it was colocalized with autophagosome markers, α-synuclein or phosphorylated-tau. Hence, their results suggest a neuroprotective role for REST in neurodegenerative diseases (Lu et al., 2014).

1.5.4. Novel *Rest* conditional knockout mouse model

Lu and colleagues extensively studied REST in the context of AD and proposed a neuroprotective role. A cKO mouse model was used to conditionally inhibit *Rest* in the central and peripheral nervous system (Lu et al., 2014). However, in that mouse model, *Rest* was inactivated at embryonic day 11 (E11), which raises the possibility of abnormal brain development. In mice, the brain is not fully formed until birth, with neurogenesis starting around E10 (**Figure 3**). As discussed before, REST has a pivotal role during

neuronal development, as revealed by the embryonic lethality (starting at E9.5) of germline *Rest* knockout mice (Chen et al., 1998). A question that arises is what the phenotype of *Rest* cKO mice would be if REST was inactivated in the brain only postnatally. The analysis of such a phenotype would be of particular relevance to the role of REST in AD, given that AD is a disorder that manifests at old age and is not a neurodevelopmental disorder.

To address this issue, the Director of Studies of this research project has previously generated a cKO mouse model lacking REST in the adult brain in order to bypass potential developmental abnormalities (unpublished data, also see **Sections 3.1** and **4.1**). The Cre-loxP recombination system was used allowing for recombination at *Rest* exon 2 (the first coding exon), which was flanked by loxP sites, mediated by Cre recombinase which recognizes the loxP sites and deletes the genomic content between them (**Figure 4.a**). The CaMKIIα-Cre transgene (Cre recombinase under the control of the CaMKIIα promoter), expressed specifically in excitatory neurons of the postnatal forebrain (**Figure 4.b**) (Minichiello et al., 1999), has been used for this purpose, together with a "floxed" *Rest* allele. This KO model has been validated by multiple previous studies.

Behavioural studies previously performed by the Director of Studies have identified a memory-related phenotype. An important question is whether this *Rest* cKO mouse model presents AD-associated phenotypes, such as neurodegeneration and hyperphosphorylation of tau.

REST ablation during early embryonic development in mice has been previously demonstrated to lead to a clear AD-like phenotype in mice. However, given the important role of REST in neurodevelopment, the question arises: if *Rest* is inactivated later in the mouse's life, i.e. bypassing any possible developmental abnormalities, would the results be the same? This project aims to clarify this while also addressing various biochemical mechanisms involved in the absence of REST in the adult brain.

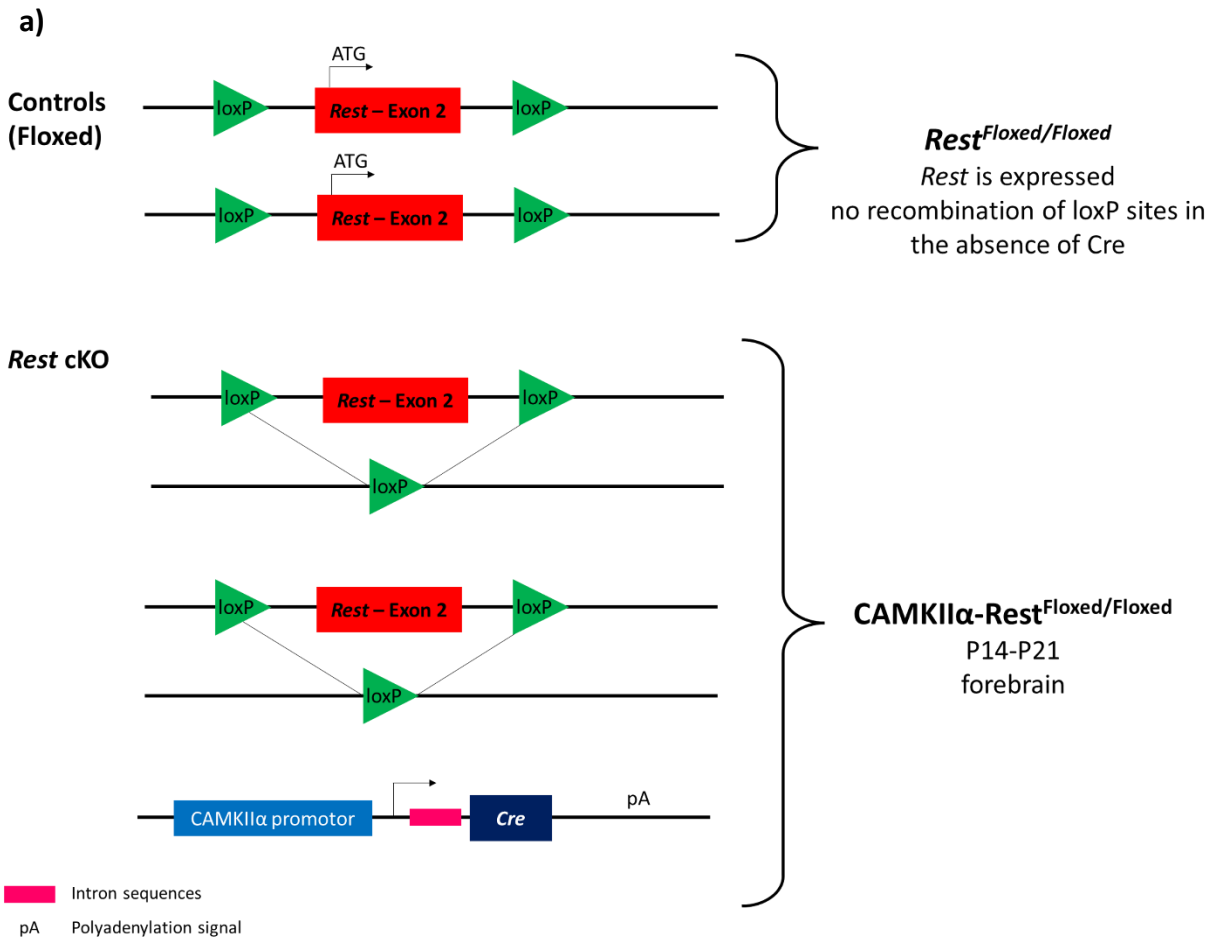

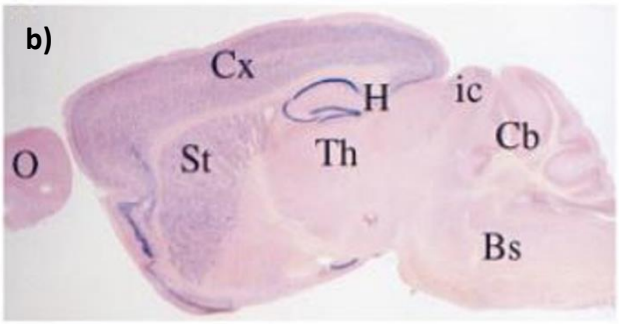

Figure 4. Strategy used for conditional ablation of REST function. **a)** A schematic drawing of the *Rest* locus in *Rest*$^{Floxed/Floxed}$ mice. Both alleles of *Rest* contain loxP sites flanking *Rest* exon 2 (the first coding exon) which is deleted upon expression of Cre recombinase due to the presence of the *CaMKIIα–CRE* transgene (pink rectangle represents intron sequences and pA represents the polyadenylation signal). Adapted from Soldati *et al*. 2012. **b)** The *CaMKIIα–CRE* transgene is expressed at P14-P21 in excitatory neurons of the forebrain (Minichiello et al. 1999). Image from Minichiello *et al.* 1999 showing Cre expression in the brain in blue by the use of a lacZ reporter system.

2. AIMS OF THE PROJECT

This project makes use of a new cKO mouse model lacking REST in the postnatal forebrain, previously generated by the first supervisor. It aims to obtain a wide understanding of the mechanisms involved in the role of REST in the brain, in particular with regard to AD-associated processes. Specifically, the aims of the project are:

1. To study whether the absence of REST in the brain in *Rest* cKO mice leads to certain AD-associated phenotypes, by:
    a. studying tau hyperphosphorylation by investigating the levels of total tau, three epitopes of phosphorylated-tau, GSK3β, p35 and p25.
    b. examining any possible morphological abnormalities in the brain associated with tau phosphorylation.
    c. assessing the possibility of neurodegeneration by examining neuronal numbers, dendritic morphology and levels of synaptic markers.
    d. studying the possibility of astrocytic activation.
2. To analyse how REST inactivation in the brain of *Rest* cKO mice affects the transcriptome, through RNA-Seq.
3. To suggest 3D structures of both the REST DNA-binding domain and its target DNA sequence, *Re1*.

3. MATERIALS AND METHODS

3.1. REST conditional knockout mice

All the experiments on this project have been performed using brain tissue from *Rest* cKO and control mice previously collected by the first supervisor. The *Rest* cKO mouse model was generated by the first supervisor and has REST inactivated only in the excitatory neurons on the postnatal forebrain of mice (**Figure 4.a**). The CAMKIIα-Cre transgene, which is expressed at 2-3 weeks postnatally, has been used for this purpose (Minichiello et al., 1999). This allowed to bypass any potential developmental abnormalities caused by the inhibition of REST too early in the mouse's neurodevelopment.

The genetic background of the mice used in this study is a hybrid of 75% C57BL/6 and 25% 129Sv. In the floxed *Rest* mouse embryonic stem cells that were used for blastocyst injections, *Rest* exon 2 (the first coding exon) is flanked by two loxP sites (**Figure 4**). These cells and the successful deletion of *Rest* in the presence of Cre recombinase, both at the DNA and protein levels have been previously described (Soldati et al., 2012). All mice were homozygous for the floxed *Rest* allele, with the control mice bearing no Cre transgene. Expression of Cre recombinase in the forebrain of the *Rest* cKO mice used in this project has been anecdotally confirmed using a green fluorescent protein reporter system (data not available due to material transfer agreement restrictions). Neuronal absence of REST protein in *Rest* cKO mice is documented in **Figure 7** (**Section 4.1**). All animals were housed in a temperature- and light-controlled environment with a 12:12h light/dark cycle, provided with food and water *ad libitum*. The same floxed *Rest* mice have been successfully used for the generation of a different *Rest* conditional knockout mouse model, in the context of studying chronic pain, using a different Cre transgene, with *Rest* specifically inactivated in peripheral sensory neurons (Zhang et al., 2019).

Rest cKO and control samples were from littermate mice. Some animals were sacrificed at the age of 14-18 months, and they were perfusion-fixed with 4% paraformaldehyde before the brains were collected and then hemispheres were frozen with cryo-embedding medium. These samples were used for histology experiments. The other mice were sacrificed at the age of 3-4 months, their non-fixed brain tissue has

been used for all other experiments. All tissue samples were stored at -80°C. All tissue collection was performed by the supervisor prior to this project.

Both the left and right hemispheres were used, always controlled between genotypes (same hemisphere for *Rest* cKO as for control). In any case, no hemisphere difference was observed throughout our entire analysis of this cKO mouse model (both in this project and in other projects), suggesting that any data variability is very unlikely to be attributed to hemisphere specificity. The same applies for the gender of the mice: both male and female mice were used, but always controlled between genotypes (same gender for *Rest* cKO as for control, for a given pair). No gender effect was observed, suggesting that any data variability is very unlikely to be attributed to gender specificity.

In order to eliminate bias, all experiments were performed blindly concerning the genotypes and all animals were identified by a unique number until all data analysis and quantification were completed.

A list of all the antibodies and suppliers name for all chemicals used in this project is presented in **Appendix 1.1** and **Appendix 1.2,** respectively. **Appendix 1.3** entails the composition of the different buffers used throughout the project. **Appendix 1.4** lists all the equipment used.

3.2. Histology

The animals used for histology experiments were sacrificed at the age of 14-18 months, to study pathology in the older brain, similar to what happens in Alzheimer's disease. The animals were perfusion-fixed with 4% paraformaldehyde before the brains were collected and then hemispheres were frozen with cryo-embedding medium. All tissue samples were stored at -80°C until ready to use.

Due to limitations to the number of samples that were available throughout the project and to the number of sections that could be collected from each brain, it was not possible to use the same number of animals for all histology experiments. Two sets of mice were used, the first only with female mice (n=3) and the second set had a ratio of 2 females and 1 male for each genotype group (n=3). Most of the results presented

in this thesis were obtained using the second set of mice. The first set was only used for the study of dendritic degeneration.

3.2.1. Cryostat Sectioning

Hemispheres were cut in sagittal sections using a cryostat at -22°C and mounted onto positively charged microscope slides. Up to 50 slides, with 30µm of thickness were collected per hemisphere, each slide contained three consecutive sections. Six *Rest* cKO mice and six controls were used. Slides were kept at -20°C, until ready to use.

3.2.2. Immunohistochemistry

Slides were hydrated and each step was intercalated with one or two 7-minute washes in phosphate-buffered saline (PBS) solution. Briefly, slides were incubated for 10 minutes in 0.5% triton, followed by a 15-minute incubation in quenching solution, 0.3% H_2O_2 in methanol. The tissue was then incubated in a blocking solution, 5% serum (goat or horse, depending on the antibodies that were going to be used), for 30 minutes. An incubation of 1 hour and a half was performed with the primary antibody diluted in block solution, followed by three washing steps and a 30-minute incubation with a biotinylated secondary antibody. The sections were then incubated in ABC solution for 30 minutes, followed by an 8-minute incubation in DAB mix. No counterstain was used, so the next step was to dehydrate the sections using 3-minute incubations in 50%, 75%, 90% and 100% ethanol and finally twice in histoclear, sequentially. Finally, using permount, a coverslip was mounted onto the slides, which then were left to air dry overnight.

3.2.3. Immunofluorescence

When using the anti-NeuN antibody, some slides were incubated with an immunofluorescence secondary antibody, Alexa 488 (ab150077), instead of the biotinylated secondary antibody previously described. The initial part of the protocol is similar to DAB immunohistochemistry protocol. However, after incubating with this particular secondary antibody, a coverslip was mounted onto the slides using

Vectashield antifade mounting media. The slides were left to air dry overnight and imaged in the following day.

3.2.4. Antigen retrieval

When using the anti-NeuN antibody, sections were subjected to the antigen retrieval procedure before the blocking step. After hydrating in PBS, the slides were immersed in the Dako PT Link instrument, that had been previously filled with 1.5L of citrate buffer 1x (pH=6.0) and warmed up until 65°C. The retrieval cycle was set to 20 minutes at 97°C. When this cycle was finished, the temperature cooled down back to 65°C and the slides were put in warm tap water and the rest of the protocol (either DAB immunohistochemistry or immunofluorescence) was followed.

3.2.5. Image acquisition and matching slides with the Mouse Brain Atlas

After immunohistochemistry protocol, a Leica DM2500 LED microscope and the Leica Application Suite X (LAS X) software were used to acquire images of the sections. The 5x magnification was used to take images of the whole hippocampus and of some regions the cortex (e.g. the cingulate, retrosplenial, prelimbic and frontal cortex). The 10x and 20x magnifications were used mainly to take images of the individual regions of the hippocampus and used for quantification purposes. The hippocampus has a well-defined structure that can be divided into 3 main subregions: CA1, CA3 and dentate gyrus (DG), which have been extensively studied in the context of AD (Hullinger and Puglielli, 2017). In some cases, the cortex was also studied under these higher magnification objectives.

Rest cKO sections were matched with their control pair using the Mouse Brain Atlas as a reference (Paxinos and Franklin, 2019). An antibody against NeuN allowed the visualization of the hippocampus and permitted the very thorough morphologic comparison of the CA1, CA3 and DG. The ventral hippocampus was also examined, when present, using both the 5x and 10x magnifications. The hippocampus morphology and size changes severely from medial to lateral planes (**Figure 5**) therefore it is really important to match slides from both genotypes to ensure that equivalent planes are being compared. To maximize the quality of the matching, six slides per mouse, evenly distributed throughout the hemisphere, were used for this purpose.

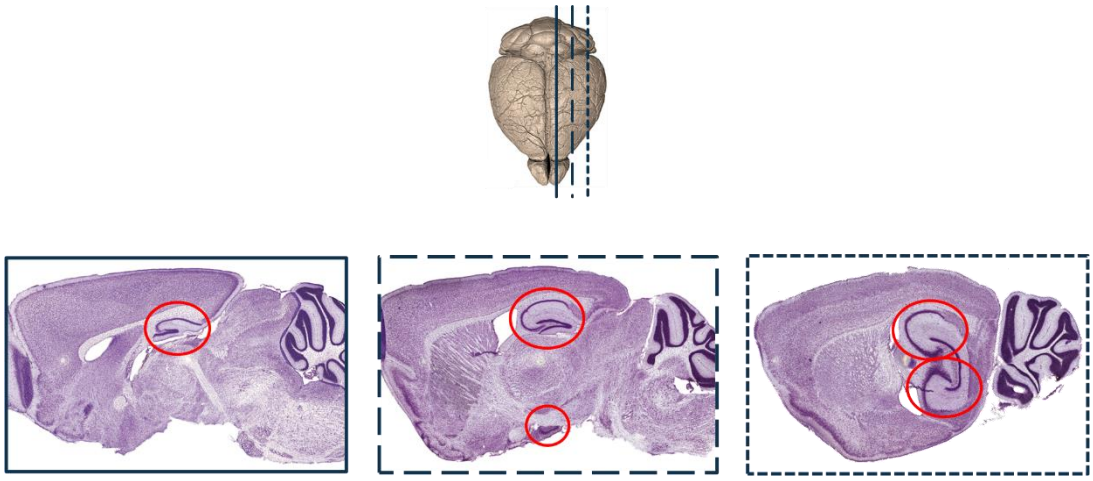

Figure 5. Matching equivalent slides. The pyramidal cell layer of the hippocampus (arrow-shaped darker lines in red circles) changes quite a lot from medial to lateral planes. Additionally, the ventral hippocampus (lower circles) is only visible on the more lateral slides. To ensure that in future experiments slides from each genotype are comparable, i.e. are in the same plane within the hemisphere, slides from controls and from *Rest* cKO mice were compared with the atlas pages of the Mouse Brain Atlas. This evaluation involved studying the morphology of the dorsal and ventral hippocampus. Images shown adapted from Paxinos and Franklin, 2019.

3.2.6. Neuronal labelling and quantification

After matching the equivalent slides, eight equivalent slides per mouse (three controls and three *Rest* cKO mice) were used for neuronal quantification to assess the possibility of a neurodegenerative phenotype in *Rest* cKO mice. The slides were subjected to the immunofluorescent assay, as described above (**Section 3.2.3**), which allowed a better distinction between nuclei and facilitated the counting of neurons.

The 20x magnification consecutive images covering the entire hippocampus were used for quantification purposes. All the neurons present in the pyramidal cell layer (CA1, CA2, CA3) and in the granular layer (DG) of the hippocampus were counted manually using a manual cell counter. The use of ImageJ software to automatically count the neurons was attempted but was not possible as the nuclei of neurons are in juxtaposition, and the software was not able to accurately distinguish the division between two different nuclei.

Since the hippocampus changes its size and morphology throughout the hemisphere, to ensure that the quantification is comparable (i.e. compare equivalent planes in different mice), each pair of slides was matched with a page of the Mouse Brain Atlas, i.e. with a sagittal plane of the hemisphere. Thus, the results were presented regarding the correspondent Mouse Brain Atlas page to each slide. Multiple planes were selected throughout the hemisphere (from medial to lateral) so that the entire hemisphere is represented in the quantification of neurons. On the other hand, to have a comprehensive evaluation of neurodegeneration in the entire hemisphere, a total neuronal count was also presented. This was done by averaging the number of neurons in each subregion of the hippocampus for the eight slides per mouse.

3.3. Biochemistry – Sample preparation

The animals used for biochemical experiments were sacrificed at an earlier stage, at the age of 3-4 months, to study the possibility of early Alzheimer's phenotypes. Their non-fixed brain tissue has been used for Western blot and RNA-Seq experiments. All tissue samples were stored at -80°C. All tissue collection was performed prior to this project and tissue samples were stored at -80°C until ready to use.

Due to their role in memory and AD pathology, both cortical and hippocampal samples were used in this project. However, due to limitations to the number of samples that were available throughout the project, it was not possible to use the same number of animals for all western blot analysis. Two sets of samples were used, the first with only female animals (n=4-6), the second set had equal gender ratio (2 male and 2 female animals in each genotypic group, n=4). In particular the study of proteins in the hippocampus, given the small concentration of samples, was done using only the second set of mice.

3.3.1. Sample preparation – total lysate preparation and nuclear extraction

To prepare samples for Western blots, total lysates were prepared using the hippocampal and neocortical region from each genotype. The protocol is equal for both

type of samples, however the volumes used were lower in hippocampal samples. Brain samples were homogenised using a motor pestle in buffer A (10 mM Tris, pH 7.5, 100 mM NaCl, 1% Triton, 0.1 mM EDTA, 0.5 mM PMSF, protease and phosphatase inhibitors). An aliquot was separated to use for nuclear extraction. To the remaining total cell lysate, a solution was added leading to final concentrations of 5 mM EDTA, 0.5% sodium deoxycholate and 1% SDS. Lysates were first rotated at 4°C for 30 minutes at 40 rpm and then vortexed for 30 seconds at 5 second interval. The samples were then centrifuged at 14,000 rpm (20,000 g) for 10 minutes at 4°C. The total cell lysate supernatant (homogenate) was then collected and stored at -80°C.

The aliquots that had been previously separated for nuclear extraction were rotated at 4°C for 20 minutes at 40 rpm and then vortexed for 30 seconds at 5 second interval. These samples were then centrifuged at 1000 g for 10 minutes at 4°C, then the non-nuclear supernatant was collected (carefully to not disturb the pellet) and stored at -80°C. Lysis buffer was then added to the remaining pellet with the same detergents and concentrations as above. The samples were first rotated at 4°C for 30 minutes at 40 rpm and then vortexed for 30 seconds at 5 second interval. Finally, the samples were centrifuged at maximum speed (20,000 g) for 10 minutes at 4°C and the nuclear supernatant was collected and stored at -80°C.

3.3.2. BCA protein assay

A Pierce BCA protein assay was used to quantitate total protein concentration in each sample for future experiments. A standard curve was prepared using serial dilutions of protein standard (BSA). The standard curve plus the samples (10µL of sample diluted in 100µL of BCA) were loaded into a 96-well plate which was incubated in the shaker for 5 minutes at room temperature before being incubated for 30 minutes at 37°C. Finally, the protein absorbance at 595nm was read using a plate reader and the total protein concentration was calculated based on the standard curve using regression.

3.4. Western blot

Protein levels were analysed using Western blot technique, which has four main steps: 1) separation of proteins through electrophoresis; 2) membrane transfer; 3) immunostaining of the blot and 4) imaging the membrane.

SDS-PAGE was used to separate protein samples by their molecular weight. Three, 10 or 15µg of each sample (depending on the cellular fraction) were mixed with 10µL of 4x Laemmli sample buffer, 4µL of NuPAGE reducing agent and RIPA Buffer, up to a final volume of 40µL. Samples were then heated for 10 minutes at 70°C in the Techne DRI-BLOCK DB3 and subsequently loaded in the wells of the gel (10-well NuPage 4-12% Bis-Tris). The Precision Plus Protein Dual Colour Standard was used as the protein standard, 3µL were loaded in the first well and 1.5µL in the last. Electrophoresis, in MOPS 1X, was then run at 200V for 35 minutes.

A polyvinylidene fluoride (PVDF) membrane was activated with a 10-seconds incubation in methanol followed by 2 minutes in dH_2O before the transfer cassette was assembled. The transfer was run at 250 mA for 2 hours at 4°C. After, the membrane was washed with PBS-Tween 1x, blocked with 5% milk for 1 hour, incubated with the primary antibody for 1 hour. Prior to a 1-hour incubation with the secondary antibody in block, membranes were washed with PBS-Tween 1x. All the three previously described incubations were done at room temperature in a VWR rocking platform. Finally, membranes were imaged using the enhanced chemiluminescence (ECL) detection method in a ChemiDoc XRS+ system with Image Lab software. This BioRad software was used for the densitometric analysis of protein band intensity in Western blots. The intensity of the signal is proportional to the quantity of protein. However, for the quantitation to be accurate , the signal from the protein bands has to be within the linear range of the imaging system. Excessive amounts of protein, high concentrations of antibodies, or prolonged exposure times can lead to saturated signals, which are identified by the software and the saturated bands are highlighted in red in these cases. These signals are no longer proportional to protein concentration and therefore should not be used for quantitation. All the images used in this project to quantify proteins were carefully selected so that the bands are not in the saturation range. Therefore, the exposure time was adjusted to each primary antibody and respective dilution, to avoid saturation and allow proper quantitation of each protein.

To properly interpret the Western blot results, a loading control should be performed. Hence, the previously described immunostaining and imaging the membrane was repeated (without re-probing), using a primary antibody specific for a protein highly expressed in a certain type of cell or cellular structure, encoded by "housekeeping genes" (**Figure 6**). Depending on the type of samples and on molecular weight of the test protein, one of these two proteins was used as loading control: β-actin and α-tubulin. One of the hallmark of Alzheimer's disease is synaptic and dendritic degeneration, which could affect the quantity of the proteins used as loading control, which are part of the cytoskeleton of neurons. To ensure that these could be used as loading control, β-actin, α-tubulin, histone H3 and NeuN (also confirmed through immunohistochemistry - see **Section 4.3.1**) were all probed on a same membrane and no difference was observed between genotypes (data not shown).

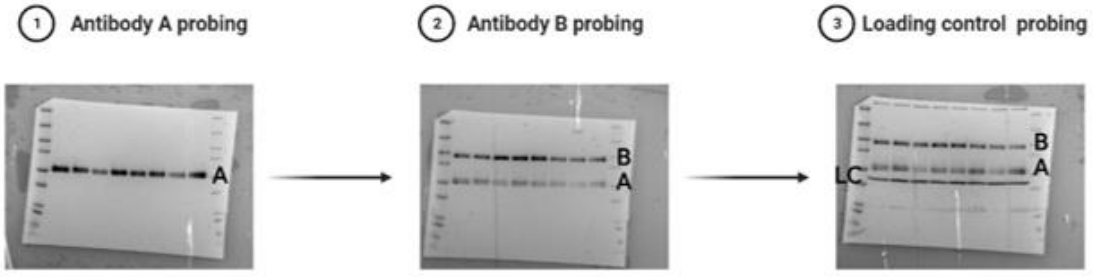

Figure 6. Membrane re-probing. Each membrane was probed with an antibody of interest (e.g. A), often re-probed with a second antibody of interest (e.g. B), without stripping, and then was re-probed with the loading control antibody (without stripping).

Finally, for quantification purposes, the abundance of the protein of interest was divided by the abundance of the loading control to obtain the normalized values. The values were then converted to percentages, with control levels mean being considered 100%, which were used to build the quantitative graphs. *Rest* cKO levels were compared with the percentage of control mean. This allowed a comparison between multiple membranes (i.e. when the of samples per group was higher than five).

3.5. Quantification and statistical analysis

Each experiment was performed blindly concerning the genotypes until all data analysis and quantification were completed in order to eliminate bias. During experimentation and analysis only the identification number of each mouse was used, and the genotypes were revealed by the Director of Studies after all analysis had been completed.

Results were shown as mean ± standard error of mean (SEM) for each group. Statistical analysis was performed using Microsoft Excel and Graph Pad Prism 9. A Student's t-test analysis was conducted to assess differences between genotypes. The level of statistical significance was set at $p < 0.05$.

Immunohistochemistry data was evaluated qualitatively, except for NeuN, where nuclei were counted manually, several slides per mouse and throughout the hemisphere.

3.6. Analysis of bioinformatics-processed RNA-seq data

Global gene expression was analysed in the neocortex of 3-4 months-old mice, using total RNA samples of both genotypes based on an equal gender ratio (2 male and 2 female animals in each genotypic group, n=4) previously prepared by the supervisor using Tri reagent.

The RNA-seq experiment was performed at the specialized facility Plateforme Genomeast, Institut de Génétique et de Biologie Moléculaire et Cellulaire (IGBMC), Strasbourg, France. The subsequent bioinformatics analysis was conducted in this facility by the collaborator Dr Celine Keime, as this required specialised software. Data were provided in the form of an Excel spreadsheet with raw and normalized read counts for each transcript, together with gene annotations, the p-value, adjusted p-value and log2 fold-change (FC) of each transcript in each of the eight samples. This data set was then used in this project to analyse and interpret differential gene expression in the transcriptome of *Rest* cKO applying multiple bioinformatic approaches.

3.7. Differential gene expression analysis

Method 1: A total 31,489 transcripts with differential expression between genotypes were observed in cortical samples. The comparison between control and *Rest* cKO was performed using the Wald, a statistical test for differential expression proposed by Love *et al*. and implemented in the Bioconductor package DESeq2 version 1.16.1 (Love et al., 2014). The Benjamini and Hochberg method was then used to adjust the p-values for multiple testing. An independent filtering step filtered out transcripts with no or little change of showing significance evidence of differential expression (without looking at their statistic), resulting in transcripts with no adjusted p-value. This analysis was performed by the collaborator Dr Celine Keime.

Method 2: The Benjamini and Hochberg method is a widely accepted approach to control false discovery rate (FDR). Nevertheless many researchers do not agree with the principle of this method (Rothman, 1990; Althouse, 2016), and it is considered by many researchers that in addition to removing false positives, the Benjamini and Hochberg method also removes some true positives. Considering that, RNA-seq data in this project were analysed both with and without this method, to obtain a broader view of the results, keeping in mind that some true positives might be removed by Method 1, whereas some false positives are likely to be present in the results of Method 2. Thus, from the initial 31,489 transcripts differentially expressed in cortical samples, a final list of statistically significant changed transcripts was created with the Wald p-value < 0.05. In Method 2, the p-value of these genes was not adjusted for multiple testing by the Benjamini and Hochberg method. This list of upregulated and downregulated transcripts/genes was then used for Gene Ontology Enrichment (GOE) analysis, through the Gene Ontology Resource powered by PANTHER database. The Protein-Protein Interaction (PPI) network and the functional enrichment in the network using STRING version 11.0 were also studied.

3.7.1. Gene ontology enrichment analysis

The list of genes obtained through the previously described Method 2 was used to perform a GOE analysis for the upregulated and downregulated genes. GOE analysis was done to enlighten which gene ontology terms are included in three aspects: 1) biological process; 2) molecular function and 3) cellular component. The names of downregulated (287) and upregulated (265) genes were submitted, separately, to the GO Consortium website (http://geneontology.org/). The gene ontology aspect and species "*Mus musculus*" were chosen and the analysis was submitted to the analysis tool from the PANTHER Classification System (Mi et al., 2019; Carbon et al., 2021). The statistical analysis and the significance of gene enrichment were calculated by Fisher's exact test with the FDR < 0.05. These analyses were done using PANTHER Overrepresentation Test. Annotation Version and Release Date: GO Ontology database DOI: 10.5281/zenodo.6799722 Released 2022-07-01.

3.7.2. Protein-protein interaction network functional enrichment analysis

A PPI network analysis was also performed using the list obtained in described Method 2 in **Section 3.7**, featuring the functional enrichments for the biological processes, molecular function, and cellular component. The analysis was done using the STRING 11.5 Database (https://string-db.org/) (Szklarczyk et al., 2021). The list of names of genes was uploaded to the STRING data base and the specie "Mus Musculus" was chosen. The "high confidence (0.700)" was selected from the advanced setting "Required score". Once a network was generated, the following setting parameters were picked: "disable structure previews inside network bubbles" and "hide disconnected nodes in the network" to simplify the interpretation of results.

3.7.3. Gene set enrichment analysis

A gene set enrichment (GSE) analysis was performed using the WEB-based Gene SeT AnaLysis Toolkit (WebGestalt – http://www.webgestalt.org/)(Liao et al., 2019). This analysis was done using the initial list with 31,489 transcripts that presented differential expression between genotypes in cortical samples. It is important to refer that the primary bioinformatics analysis, done by Dr Celine Keime, presented the fold-change results regarding the control group of mice, i.e. the quantification of each transcript in

controls was divided by the quantification in *Rest* cKO mice. Therefore, a positive log2FC value corresponded to a downregulation of the gene in *Rest* cKO mice. However, to facilitate the interpretation of the results of this analysis, the log2FC was reverted (i.e. the values were multiplied by -1) so that a downregulation was in fact associated with a negative value. The log2 was then inversed to obtain the FC. Thus, the Ensembl Gene ID and the corresponding fold-change of all the differential expressed transcripts were uploaded into the toolkit. The GSE analysis was performed to find enrichment in three aspects, biological process, cellular component and molecular function, in the geneontology functional database. A pathway analysis was also performed using the Kyoto Encyclopaedia of Genes and Genomes (KEGG) PATHWAY database. The maximum number of genes for a category was set to 32000 and the statistical significance level was set to FDR < 0.05.

3.8. Identification of a putative *Re1* site in the *Cdk5r1* (p35) promoter

The Transcription Factor Binding Site Prediction (TFBSPred) webtool (Zogopoulos et al., 2021) was used to identify putative Re1 sites in the promotor region of mouse *Cdk5r1*, the gene that encodes the activator p35 of kinase CDK5. Two transcription start sites (TSS), i.e., the location where the first DNA nucleotide is transcribed into RNA, were available. The TSS with the Ensembl Transcript stable ID 'ENSMUST00000053413', was selected to proceed on the webtool protocol. All the categories of the cell types, together with all the cell lines were selected be examined and the default transcription factor flexible model (TFFM) search threshold 0.9 was selected to run the analysis. The results were also analysed using the UCSC Genome Browser on Mouse (GRCm38/mm10) (www.genome.ucsc.edu).

3.9. Computational Details

REST has been suggested to have a neuroprotective role in the aging brain, which is lost in AD patients. Hence, an enhancer of REST could potentially be of great value for AD therapy. As usual methods are quite time-consuming and laborious, in this project an alternative method, homology modelling, was used to propose a structure for REST DBD and the *Re1* sequence.

3.9.1. REST – Sequence similarity search

In order to build a homology model, the first step is to identify similar proteins that could be used as template. The primary structure of human REST (FASTA sequence) was retrieved from NCBI Protein data base with the accession: NP_001350382.1. Then the Basic Local Alignment Search Tool (BLAST) and the algorithm protein-protein (blastp) were used to search similar sequences in the PDB database. First, a query for the entire REST sequence (1097 residues) was performed. Then the query sequence was shortened to include just the DBD region (254 residues: 159-412). The two proteins with highest query coverage and total alignment score, were Aart (PDB 2I13) and Zinc Finger Protein 568 (ZFP568) (PDB 5WJQ), but ZFP568 was used for homology modelling, with this choice explained in the results and in the discussion sections. Similar to REST, both proteins bind to the DNA through C2H2 ZF motifs.

3.9.2. Homology modelling – REST DNA binding domain structure prediction

The software Maestro 2020-4 (Schrödinger) and Prime suite were used to predict REST DBD structure using protein ZFP568 as template and "Prime Quick Start Guide – Homology modelling of a single chain" protocol was followed. Briefly, using the "Structure Prediction Wizard" in Prime, REST DBD FASTA sequence (254 amino acids: 159-412) was imported (query sequence) and the homolog protein ZFP568 (PDB ID: 5WJQ-D) was selected as template. To improve Prime's secondary structure predictions (SSPro) for the query, PSIPRED (http://bioinf.cs.ucl.ac.uk/psipred/) was used to complement the predictions and the results were imported into Prime (**Appendix 2.1**). Then both REST DBD and ZFP568 sequences were aligned using the Prime STA method

(best for low sequence identity). Some manual adjustments needed to be done in the alignment to account for the secondary structure, thus some residues in the templated were moved as follow: Gly499 was in position 122 was moved to position 118; His604-Ser608 amino acids were moved one position to the left to creating a gap in the template corresponding to Val in position 196 on the query sequence and His665 was moved one residue toward the right to align with the histidine of the query sequence to form the last zinc finger. Then, a structure was built using the energy-based method and eight zinc atoms, all except Zn701 and Zn703, were included in the REST model. The referred zinc atoms were not included as they are not needed since REST has two less zinc fingers (ZFs) than ZFP568 (**Figure 7**). The model created has four loops, and each needed to be refined (using Prime loop prediction) and then minimized (residues within 8.5Å of each loop), sequentially. The distances between residues and zinc atoms were measured to determine where constraints needed to be added in order to ensure coordination (i.e less than 3Å) within the residues that compose each ZF motif. Thus, based on the template original distances, constraints were added to all four residues that coordinate with the zinc atoms in ZF1, 2, 6, 7 and 8 (**Appendix 2.2**). The values of these constraints were defined based on the distances of equivalent residues in the template. Finally, all atoms were minimized, and residues were renumbered to match the true amino acid numeration of REST sequence.

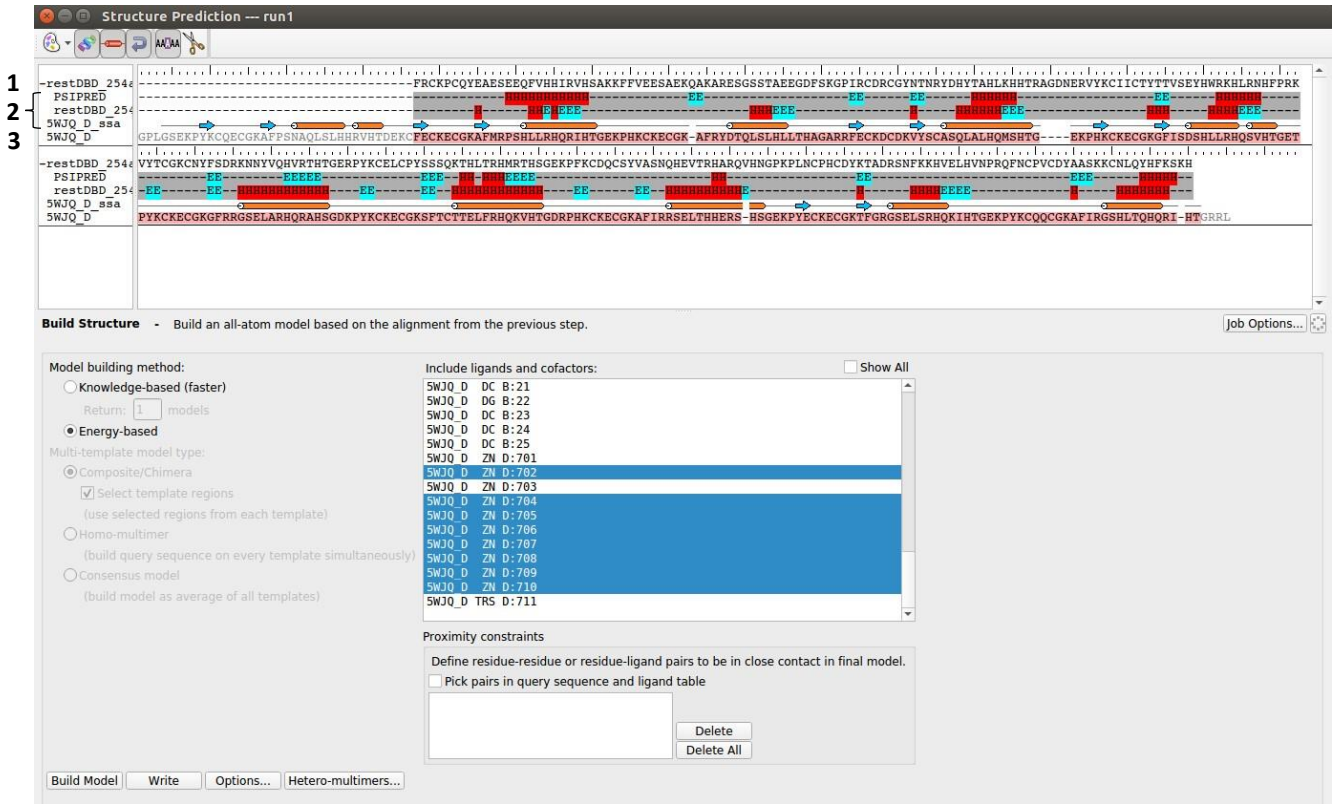

Figure 7. Final alignment of REST DBD and 5WJQ and the zinc atoms selected to build the model. The top panel shows the final alignment between REST DBD (1) and the template, ZFP568 (3), FASTA sequences. The secondary structure predicted for REST DBD are located in between the two sequences (2 – first two lines): grey lines represent loops, H (in red) represents helices and E (blue) represents strands. The secondary structure assignment (SSA) for ZFP568 is also observed (2 – third line) with blue arrows representing strands and orange cylinders representing helices. The model was built using the energy-based method and eight zinc atoms (ZN 702, 704 – 710) were included (in blue) in REST model.

This process had to be optimized, so multiple attempts were made to achieve the best final structure (data not shown) such as: try different REST sequences with different lengths, different alignment corrections, build the model with and without the zinc atoms; build the model including the DNA molecule from the template, optimize the minimization steps (decide which intermediate structures should be minimized), add constraints (optimize where to apply them and which values) or assign zero bond order to the coordination between zinc and each residue.

The final structure was then compared with the one suggested by AlphaFold (ID: Q13127) regarding several parameters such as: length, presence of zinc atoms, model confidence and secondary structure in general.

3.9.3. Re1 consensus sequence – structure prediction

Initially, the DNA double helix was predicted using the MacroMolecularBuilder (MMB) 3.2 package for Linux, through Docker. The Re1 3D structure was identified as 'DNA chain A' with the consensus sequence: 5'-TTCAGCACCATGGACAGCGCC-3'. The reverse complement sequence was represented as 'DNA chain B'. This simulation was performed in two stages. In the first stage, the defined base pairing between chains and the base stacking geometry were imposed. At the end of this stage, an initial DNA helix was structured and was almost fully folded. During stage 2, the base stacking geometry further optimized in root mean square deviation (RMSD – quantitative measure of the average distance between the atoms, the lower the better) by using nucleotide conformers (NtCs) and restraining the backbone for consecutive pair of nucleotides. (Schneider et al., 2018; Barnett et al., 2020). The dominant DNA conformer of the canonical B-DNA, NtC BB00, was manually specified for every pair of stacking bases for both chains. Thus, NtCs were sampled until the conformer with lowest potential energy for each stacking interaction was found. The simulation time of this stage was 10ps and a trajectory frame was written for every 1ps of simulation time. The trajectories were analysed using Visual Molecular Dynamics (VMD) 1.9.3 software (Humphrey et al., 1996).

A second struture of Re1 sequence was proposed after the one built initially with MMB appeared to have problems docking with the REST DBD structure. Thus, the Supercomputing Facility for Bioinformatics and Computational Biology in Indian Institute of Technology, Delhi (SCFBio IIT Delhi; http://www.scfbio-iitd.res.in/software/drugdesign/bdna.jsp) was used to create *de novo* a new basic B-DNA helix with the Re1 sequence previously described. This structure was then analysed in another web server, w3DNA 2.0 (http://web.x3dna.org/), using the option "Analysis". The subsequent file "Base-pair and base-pair step parameter" (**Appendix 2.3**) was saved and the parameters were used to rebuilt a new optimized structure with B-DNA (C2'-

endo) as backbone conformation with “Backbone geometry optimization” option selected.

3.9.4. Protein-DNA docking

In an initial protein-DNA docking test, the two proteins with highest homology obtained through the BLAST search, Aart and ZFP568, were prepared for re-docking of their native DNA. This involved: 1) pre-process the initial PDB file by filling in the missing sidechains using Prime; 2) remove artifacts of crystallization (e.g. duplicated protein chains and other molecules such as glycerol) and water molecules, keeping the protein main structure, the DNA chains and zinc atoms; 3) refine the structures; 4) minimize the structure (converging heavy atoms to RMSD 0.30Å); 5) verify the zinc finger structures; 6) save protein and DNA molecules in separate files.

The referred proteins were each submitted to HDOCK server (http://hdock.phys.hust.edu.cn/) (Lab of Biophysics and Molecular Modeling; Yan et al., 2020) to test the web server as potential docking software, more specifically, its ability to correctly re-dock its native DNA. The prepared PDB file of each template protein was uploaded as “Input Receptor Molecule”. Their respective DNA PDB structured was submitted as “Input Ligand Molecule”. The option “Template-free docking only” was selected. The docked structures and RMSD distances were analysed (**Appendix 2.4**).

Next, REST DBD structure was docked with the Re1 structures previously described. As the DNA molecule wouldn’t properly fit inside the pocket of the REST DBD, residues were removed sequentially to try to identify the problematic residues. Once the block of problematic residues was identified, those residues were mutated to Alanine and then Glycine in further trials. Ultimately the side chains of said amino acids were removed (REST DBD Δ260-265).

4. RESULTS

4.1. Absence of REST immunostaining in *Rest* conditional knockout mice

There is little evidence that anti-REST antibodies work in immunohistochemistry labelling of human samples and even less in mouse samples, and quite often high background is observed. In this project an antibody against REST (abcam, ab21635) was used to perform an immunohistochemical analysis. **Figure 8** shows a representative image of the DG region of the hippocampus stained with the referred antibody. Immunostaining was observed in the nucleus of DG granule cells in control but not in *Rest* cKO mice. No clear immunostaining in other parts of the hippocampus or in the neocortex has been observed either in control or in *Rest* cKO mice, possibly due to the lower expression of REST in these brain regions, compared to the DG, as has been previously observed in the human brain (Lu et al., 2014; McGann et al., 2021).

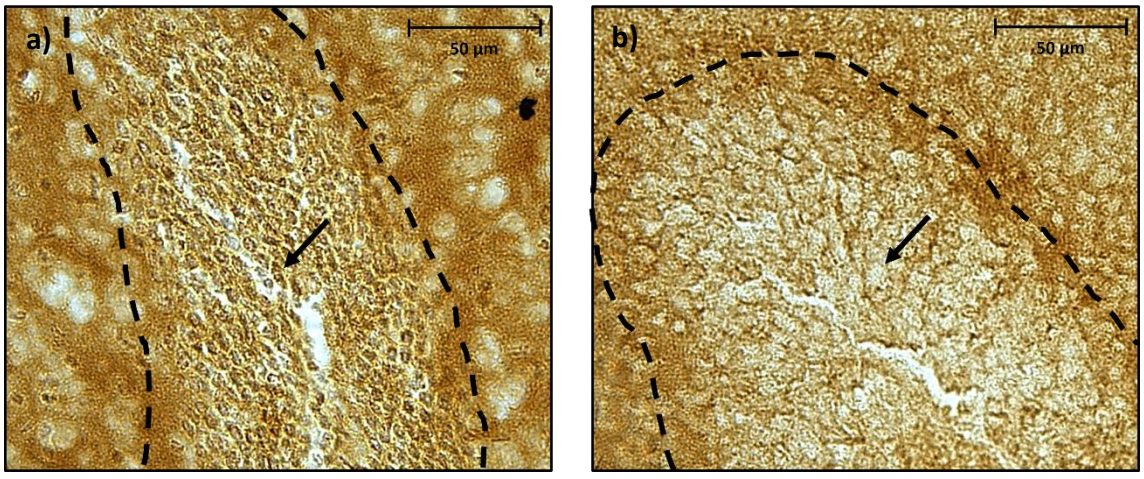

Figure 8. Representative images of anti-REST stained neurons in the DG region (delimited by the dashed line) of the hippocampus, using a 20x magnification. **a)** The nucleus of DG granule cells is stained in control but **b)** not in *Rest* cKO.

4.2. Tau phosphorylation and pathology

Hyperphosphorylation of tau protein is a hallmark of AD. Lu *et al.* showed that *Rest* knockdown in neuroblastoma cell lines leads to higher levels of total tau and in particular, higher levels of four phosphorylated tau epitopes (Lu et al., 2014). They also studied the influence of GSK3β in this increase, which they suggest might be involved in the induction of higher phosphorylation levels (Lu et al., 2014). Furthermore, they also observed an increase in the levels of p35 and p25, the activators of another kinase, CDK5, also known to participate in tau hyperphosphorylation (Lu et al., 2014).

This project wondered how inhibition of REST in the adult mouse brain would affect tau phosphorylation. Hence, levels of total tau and three phosphorylated epitopes (serine 396 (pSer396), serine 202 (pSer202) and threonine 205 (pThr205) – which have been previously implicated in AD) were evaluated in the hippocampus and neocortex of *Rest* cKO and control mice by Western blot. Furthermore, the levels of GSK3β, p35 and p25 were also evaluated to further understand their role in tau phosphorylation when REST is absent.

4.2.1. Total tau

Initially, the levels of total tau were assessed through Western blot in cortical samples (**Figure 9**) using an anti-tau antibody that recognizes both unphosphorylated and phosphorylated tau. No significant differences were observed between genotypes in the cortex ($n=8$, $t(14)=0.473$; $p=0.321$).

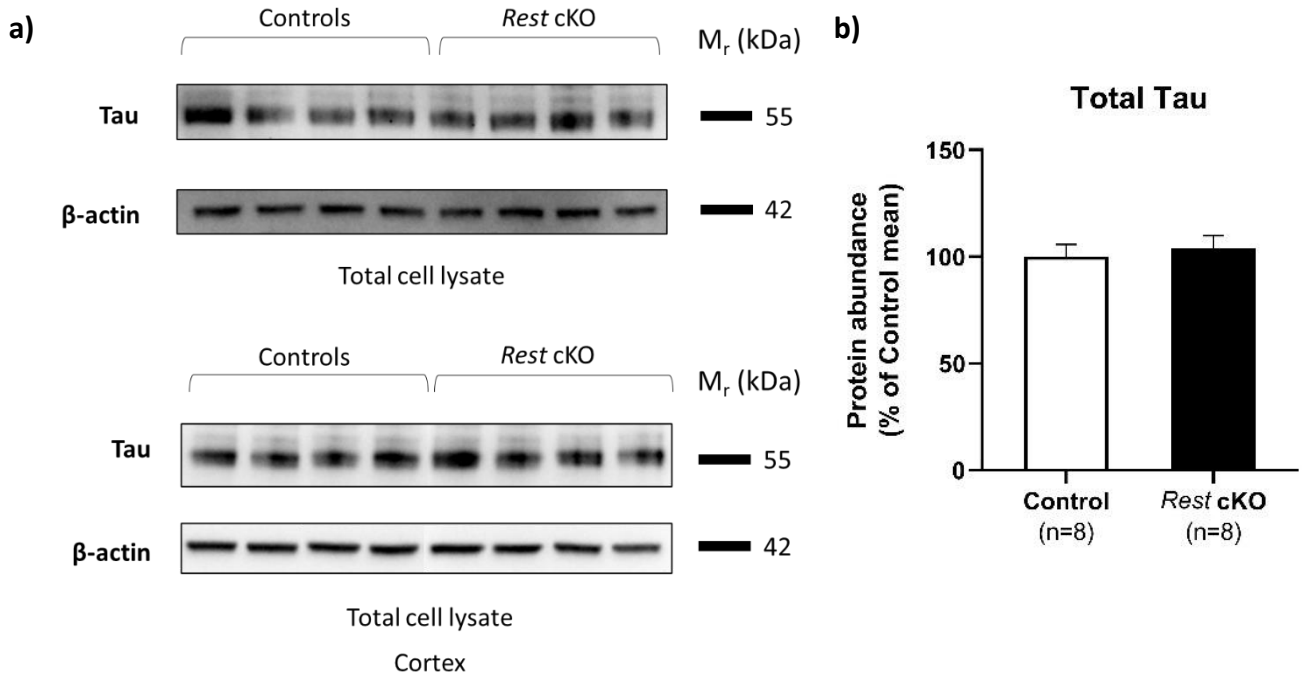

Figure 9. Levels of total tau in total cell lysates from the neocortex of eight *Rest* cKO and eight control mice. **a)** Western blot results. **b)** Quantitation of total tau levels, after normalization with β-actin as loading control. Values are represented as mean ± SEM.

The levels of total tau were also evaluated in hippocampal samples (**Figure 10**) with no difference being observed between *Rest* cKO and controls (n=4, t(6)=1.362; p=0.111).

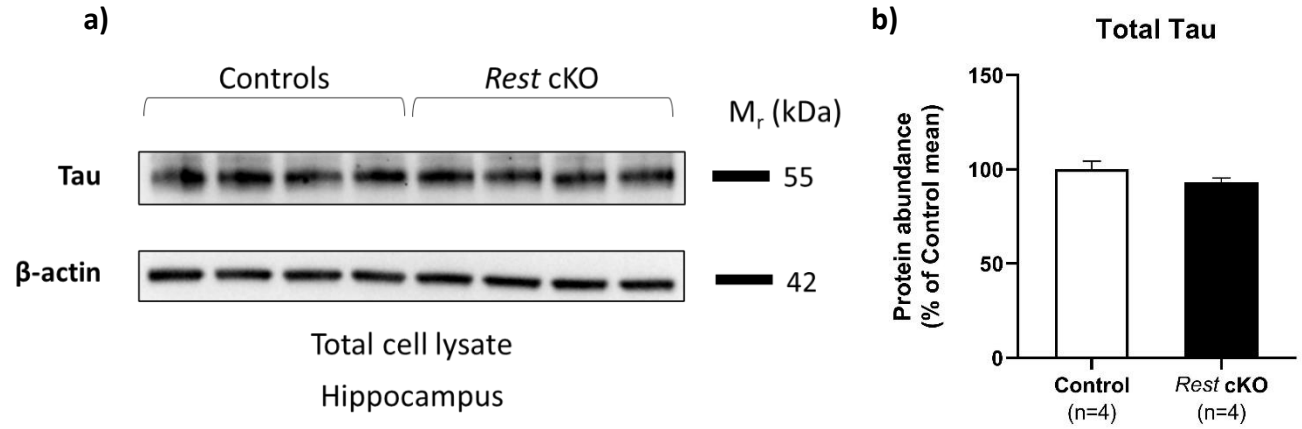

Figure 10. Levels of total tau in total cell lysates from the hippocampus of four *Rest* cKO and four control mice. **a)** Western blot results. **b)** Quantitation of total tau levels, after normalization with β-actin as loading control. Values are represented as mean ± SEM.

4.2.2. Phospho-tau pSer396

As the levels of total tau were similar between genotypes, the phosphorylation of the residue Ser396, one of the most studied in the context of AD, was then studied in the hippocampus and neocortex of *Rest* cKO and control mice by Western blot. *Rest* cKO samples were found to have slightly less tau phosphorylated in residue Ser396 in the cortex, although it was not statistically significant (**Figure 11**, n=8, t(14)=1.532; p=0.074).

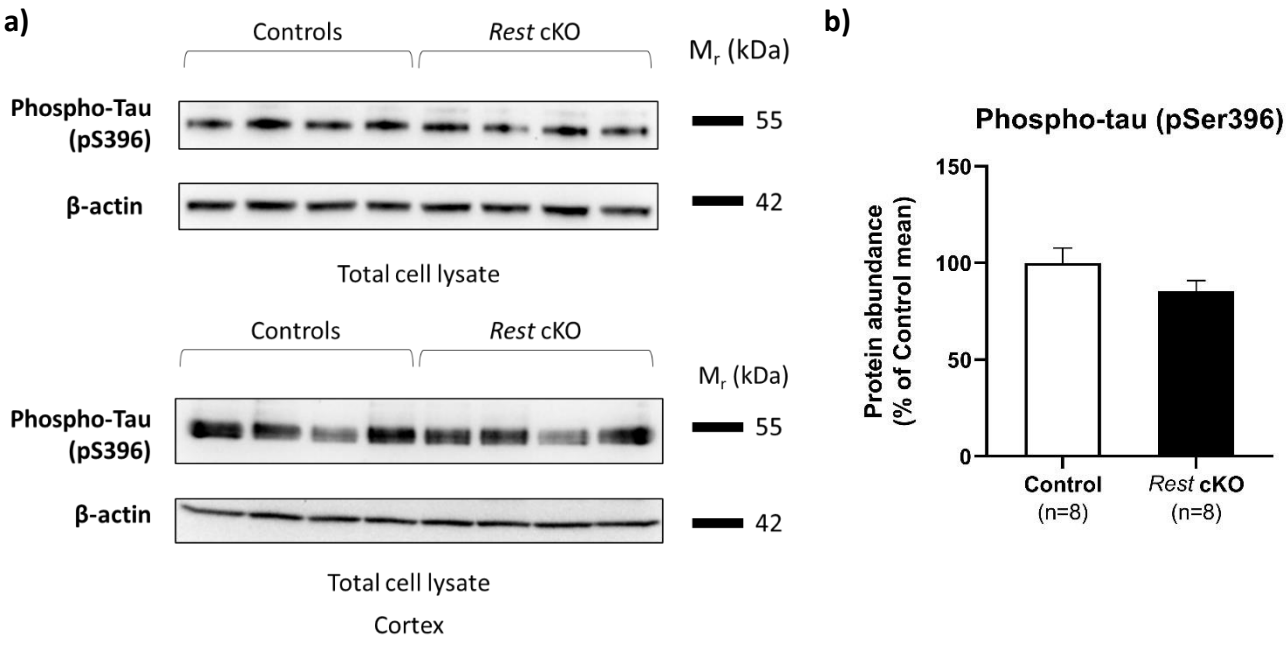

Figure 11. Levels of phospho-tau pSer396 in total cell lysates from the neocortex of eight *Rest* cKO and eight control mice. **a)** Western blot results. **b)** Quantitation of phospho-tau pSer396 levels, after normalization with β-actin as loading control. Values are represented as mean ± SEM.

Whereas in hippocampal samples there was no statistically significant difference between genotypes (**Figure 12**, n=4, t(6)=0.136; p=0.448).

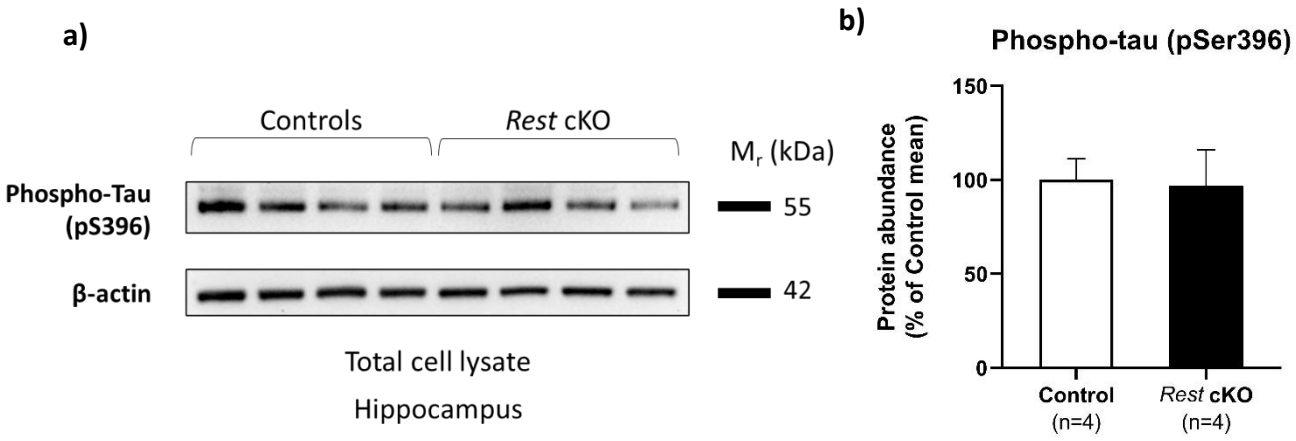

Figure 12. Levels of phospho-tau pSer396 in total cell lysates from the hippocampus of four *Rest* cKO and four control mice. **a)** Western blot results. **b)** Quantitation of phospho-tau pSer396 levels, after normalization with β-actin as loading control. Values are represented as mean ± SEM.

4.2.3. Phospho-tau pSer202 + pThr205 (AT8)

Tau protein has multiples phosphorylation sites, so another antibody against phosphorylated tau was used. The AT8 antibody detects phosphorylation on both Ser202 and Thr205 of tau protein. No differences were observed in the neocortex regarding the levels of phosphorylated tau in these epitopes (**Figure 13**, n=8, t(14)=0.139; p=0.446).

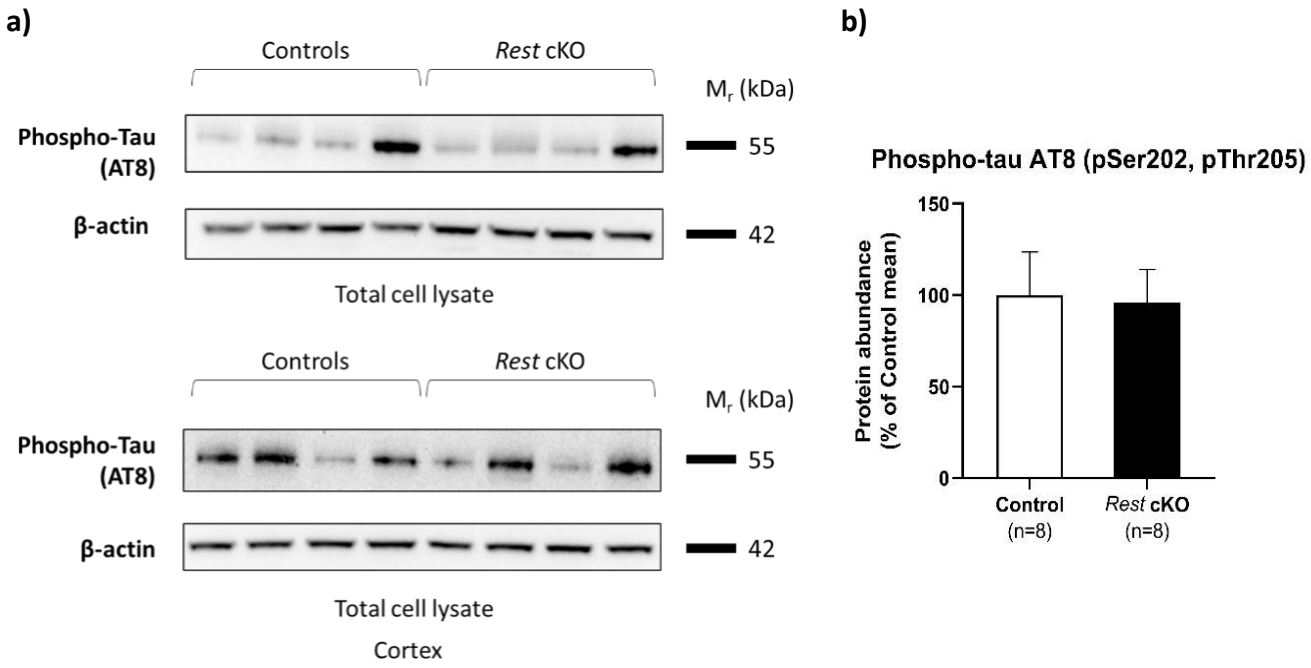

Figure 13. Levels of phospho-tau (pSer202, pThr205 – AT8) in total cell lysates from the neocortex of eight *Rest* cKO and eight control mice. **a)** Western blot results. **b)** Quantitation of phospho-tau AT8 levels, after normalization with β-actin as loading control. Values are represented as mean ± SEM.

On the other hand, *Rest* cKO levels of phosphorylated tau in residue Ser202 and Thr205 in hippocampal samples were two-times higher than the levels in control mice (**Figure 14**, n=4, t(6)=2.702; p=0.018).

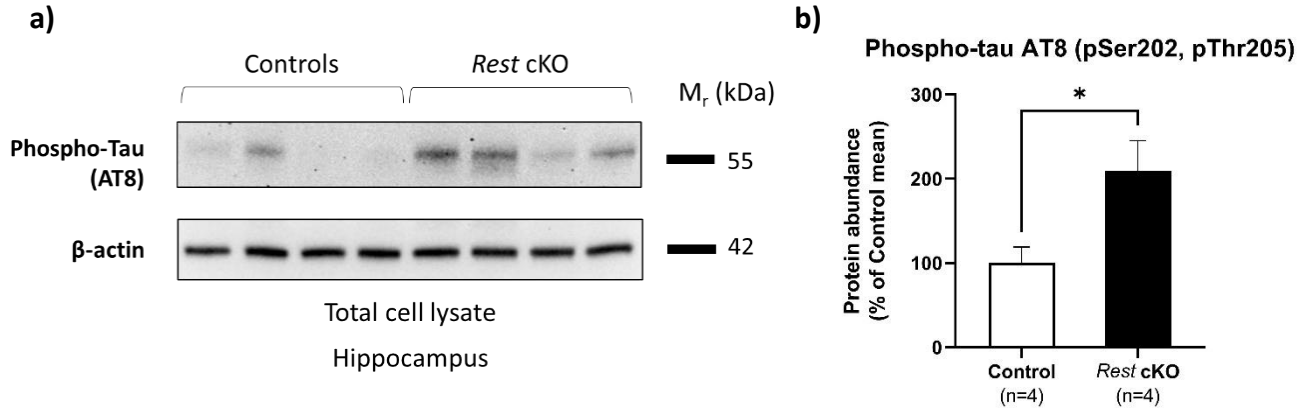

Figure 14. Levels of phospho-tau (pSer202, pThr205 – AT8) in total cell lysates from the hippocampus of four *Rest* cKO and four control mice. **a)** Western blot results. **b)** Quantitation of phospho-tau AT8 levels, after normalization with β-actin as loading control. Values are represented as mean ± SEM, *p<0.05.

Given the results obtained through Western blot, phospho-tau (pSer202, pThe205) was further studied through histology using one slide per mouse of three pairs of mice (**Figure 15-17**). In accordance with Western blot results, samples within the same genotype group present variability in the staining, nevertheless the comparison between genotypes showed the same tendency in all three pairs, with *Rest* cKO demonstrating higher levels of phosphorylated tau than control mice.

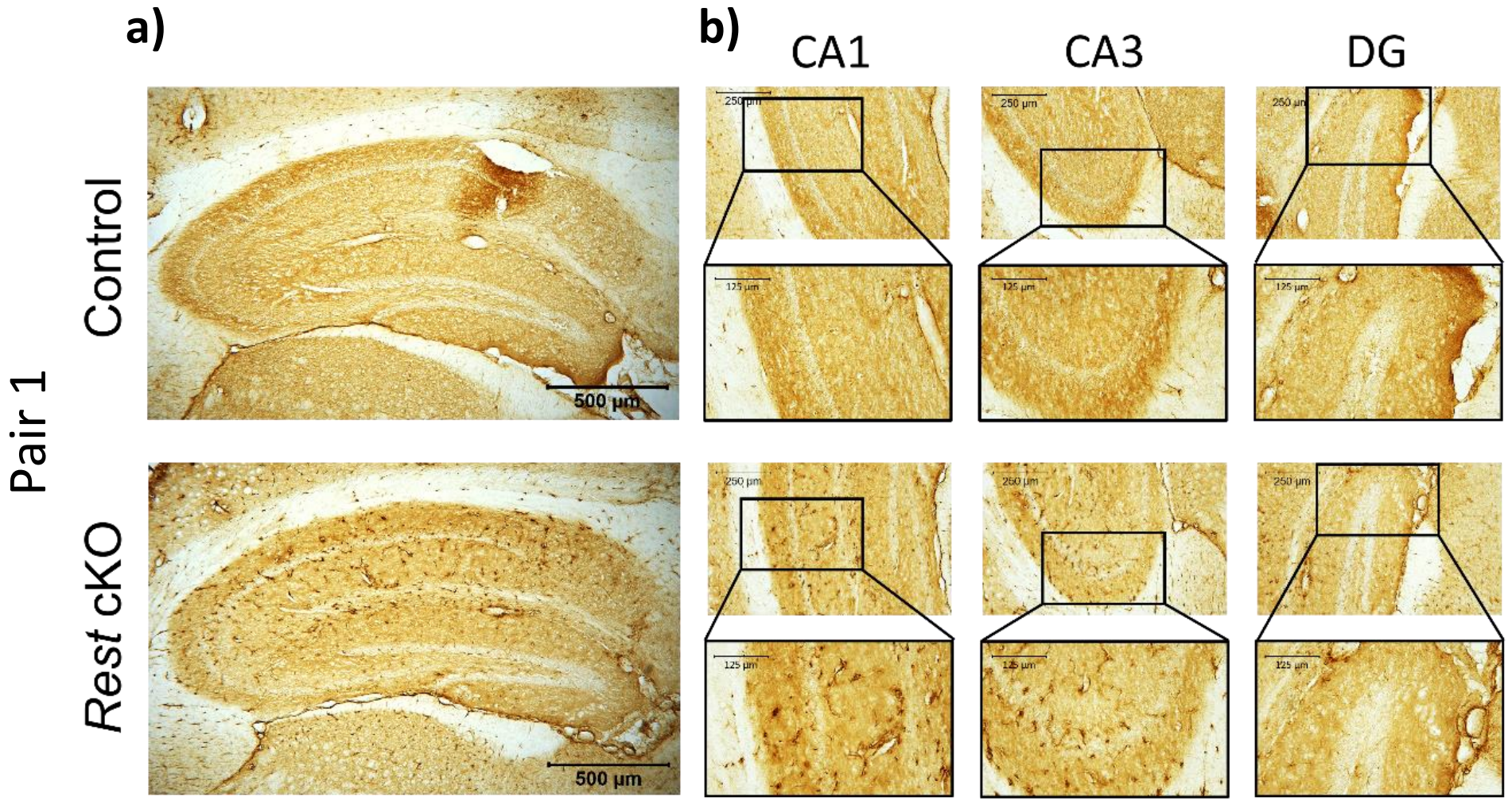

Figure 15. Representative images of equivalent slides using the antibody AT8, against phospho-tau (pSer202, pThr205) using brain sections from the first mouse pair of *Rest* cKO and control mice. **a)** The whole hippocampus was imaged using a 5x magnification. **b)** A higher magnification, 10x, was used to analyse each different region of the hippocampus. These images were then further enlarged (20x) to allow a better visualization of the staining.

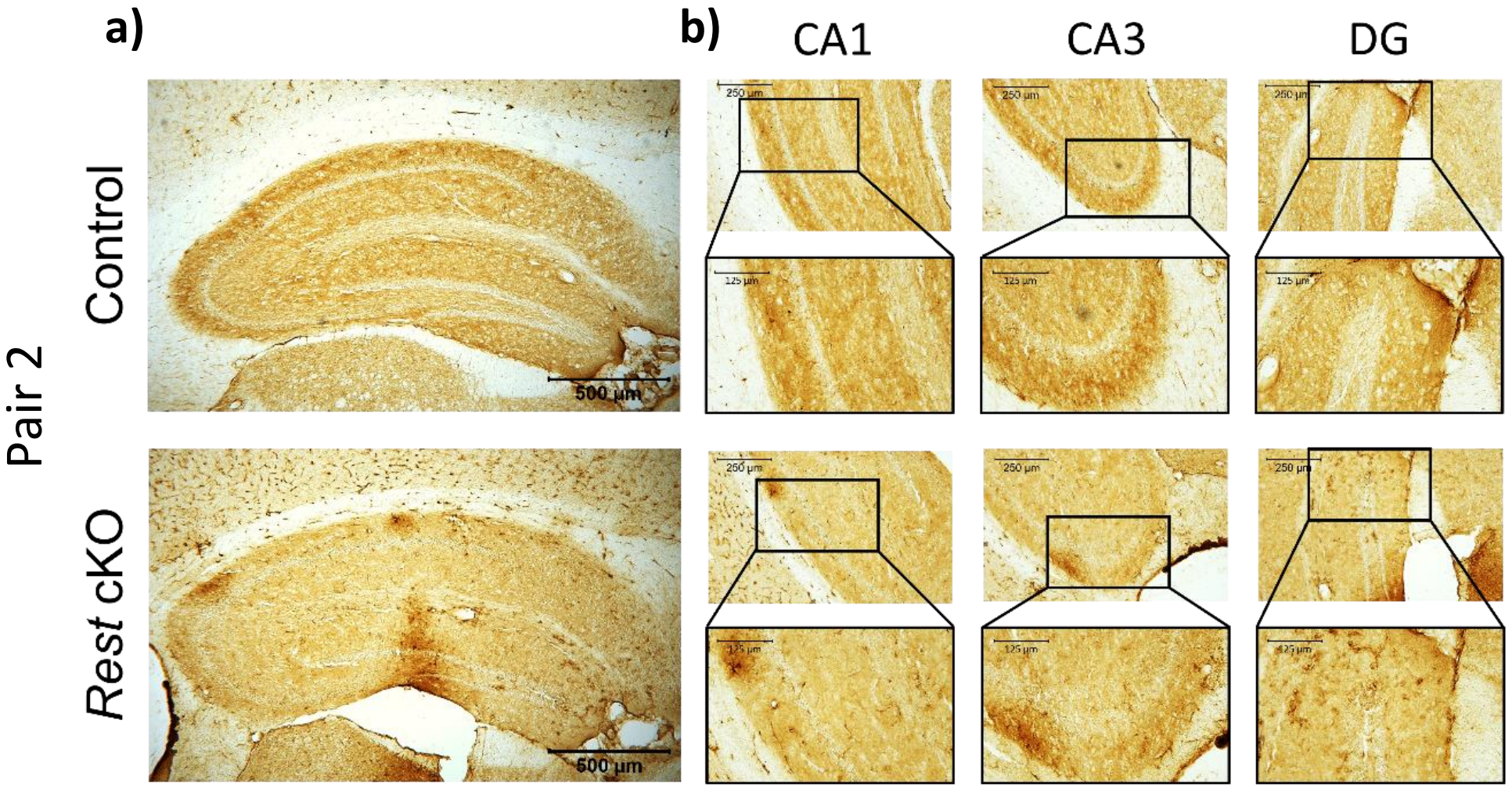

Figure 16. Representative images of equivalent slides using the antibody AT8, against phospho-tau (pSer202, pThr205) using brain sections from the second mouse pair of *Rest* cKO and control mice. Figure layout is the same as in Figure 15.

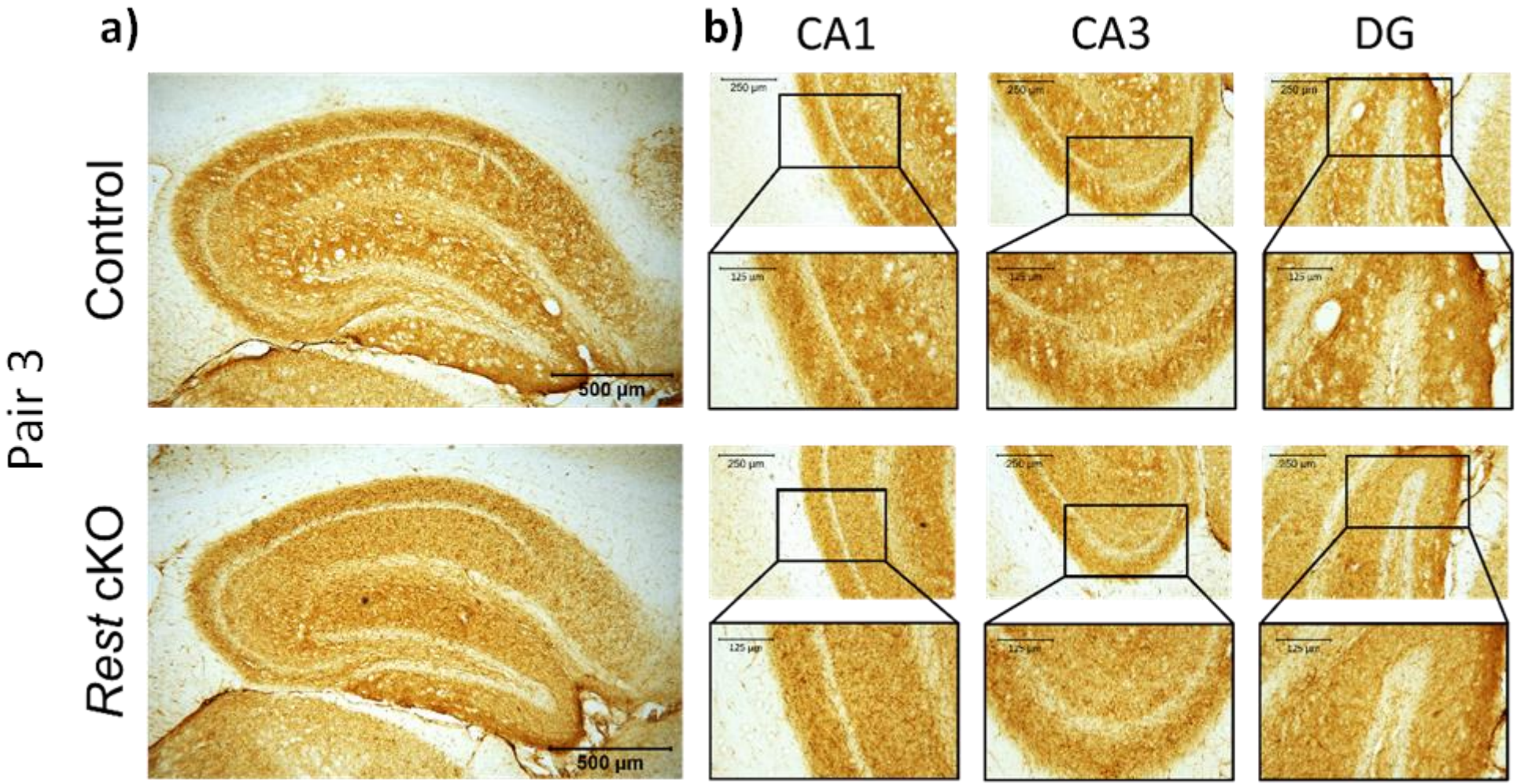

Figure 17. Representative images of equivalent slides using the antibody AT8, against phospho-tau (pSer202, pThr205) using brain sections from the third mouse pair of *Rest* cKO and control mice. Figure layout is the same as in Figure 15.

Interestingly, AT8 stained different types of well-defined structures: small puncta, bigger agglomerates structures, and filamentous morphology (typical of blood vessels) (**Figure 18**). There was also another type of structure which were characterized by dark stain, with protrusions (although not always present), surrounding a circular white region which this project hypothesizes could be pre-tangles. These different types of structures were mainly observed in two of the three pairs analyzed. In the first pair, *Rest* cKO mice was observed to have more agglomerates within the hippocampal region (**Figure 19**), whereas in the second pair, the agglomerates are mostly located in the cortex (**Figure 16**). The last pair presented very few aggregates but *Rest* cKO has overall more darker staining with more of the described puncta (**Figure 17**). Regardless of the morphology of the stain, there is a clear difference between genotypes with *Rest* cKO exhibiting evidently more of these structures than controls.

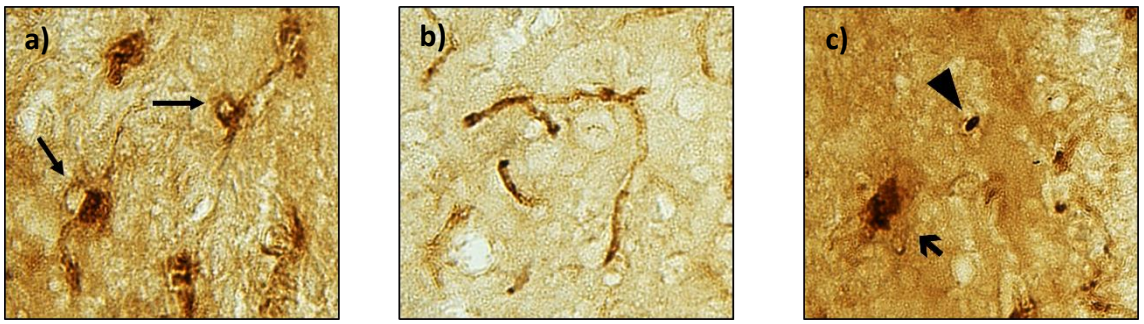

Figure 18. Representative images of different types of structures stained using the antibody AT8. A 20x magnification was zoomed in to better examine and characterize the agglomerates observed: **a)** cells with some protrusions, dark cytoplasmatic stain around a white region (→; structures resembling pretangles); **b)** filamentous structures (typical morphology of blood vessels) and **c)** small puncta (►) and as bigger agglomerates structures (➔).

These structures were observed throughout the brain in regions such as the retrosplenial cortex (**Figure 20**), the lateral parietal association cortex (**Figure 21**) or the frontal cortex (**Figure 22**). Other regions were also affected like the striatum, the *corpus callosum* (data not shown).

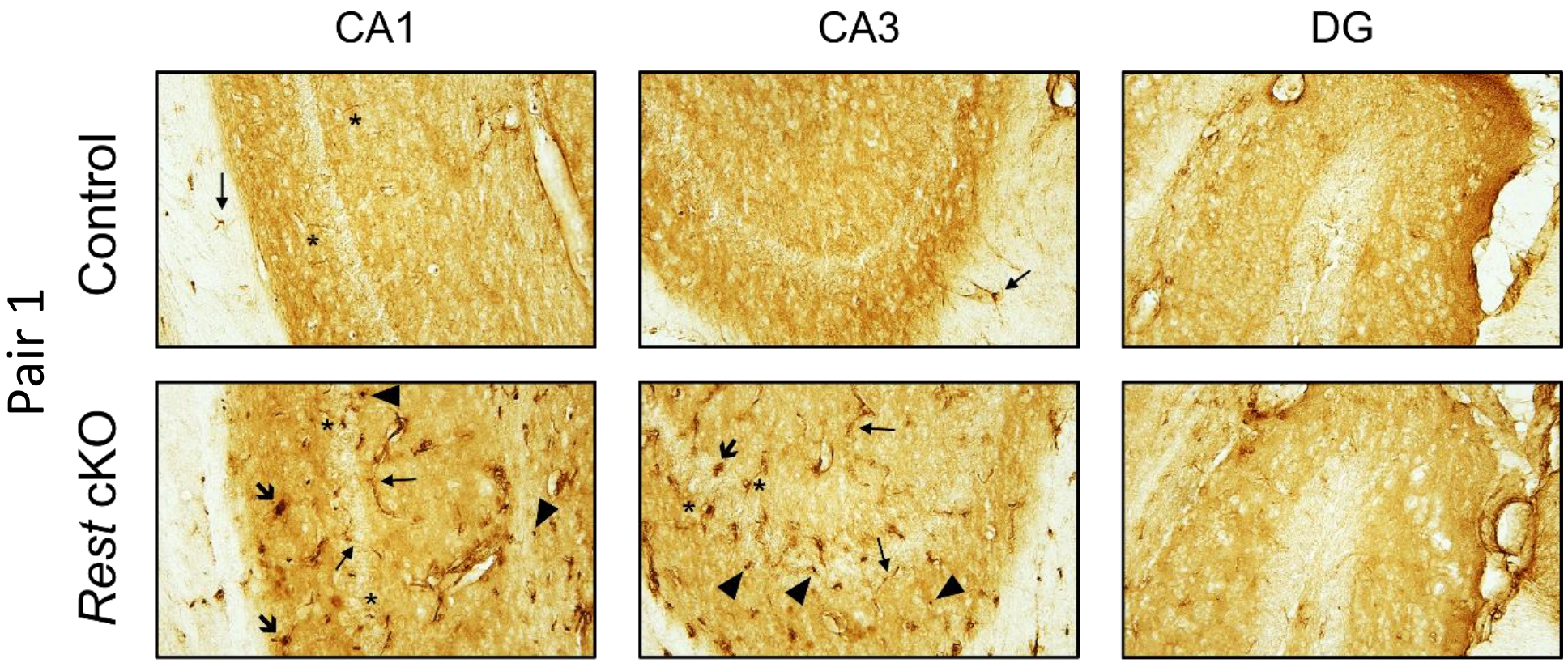

Figure 19. Representative images of equivalent slides using the antibody AT8, against phospho-tau (pSer202, pThr205) of the first pair of mice from Figure 15. A 20x magnification was used to better examine and characterize the agglomerates observed with lower magnifications. The aggregates show different types of morphology: as small puncta (►), as bigger agglomerates structures (➔) or as filamentous structures (→). There was also another type of structure which were characterized by dark puncta, some with protrusions (not always present), surrounding a circular white region (*), this project hypothesize that these could be pre-tangles.

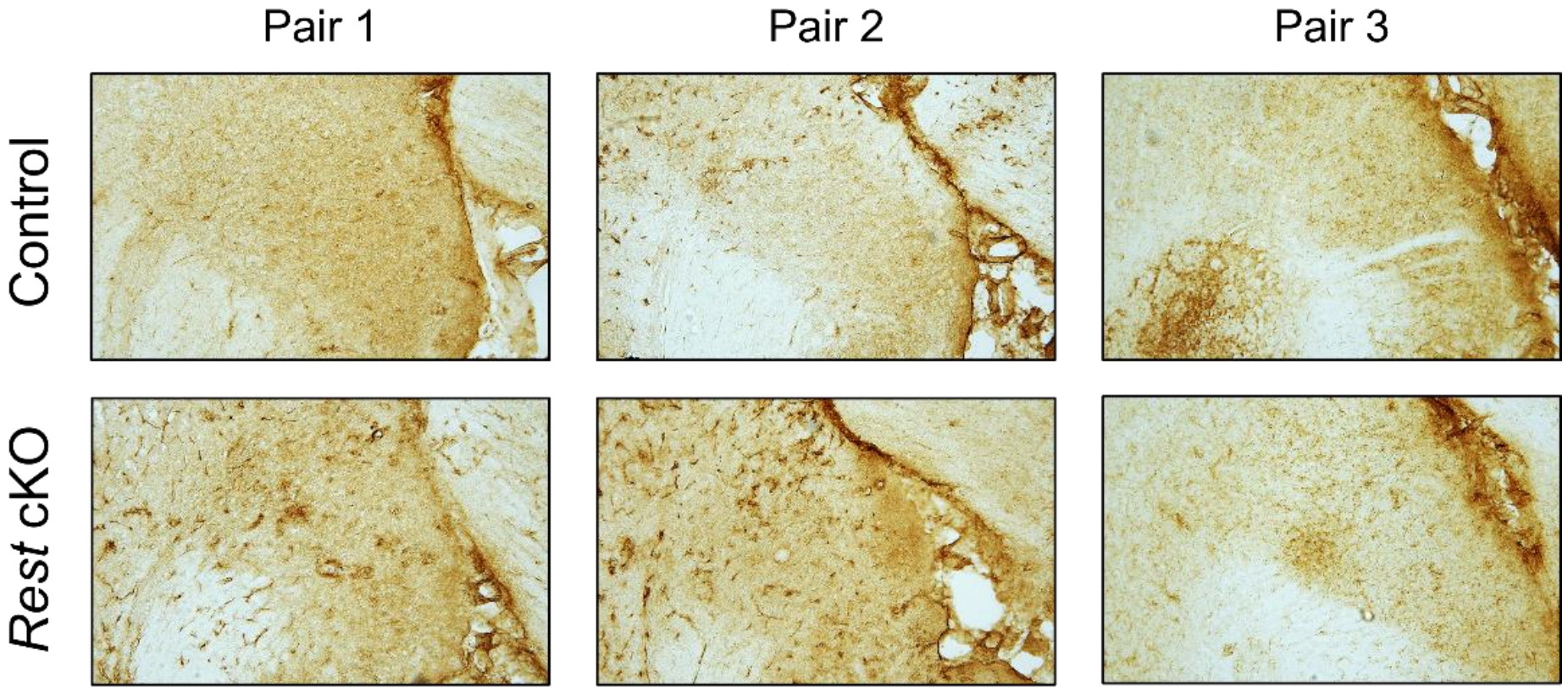

Figure 20. Representative images of phospho-tau (pSer202, pThr205) in the retrosplenial cortex. The 10x magnification was used to better analyse the stain.

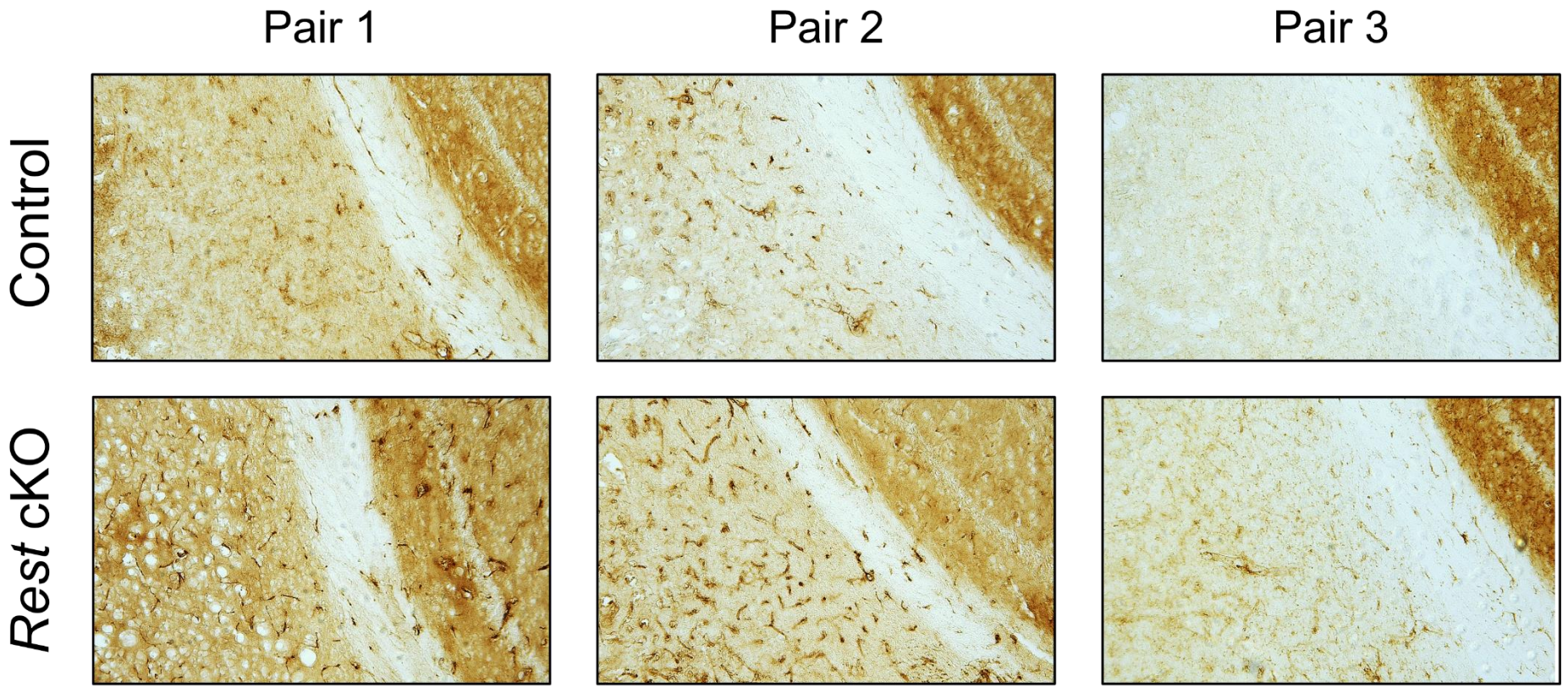

Figure 21. Representative images of phospho-tau (pSer202, pThr205) in the lateral parietal association cortex. The 10x magnification was used to better analyse the stain.

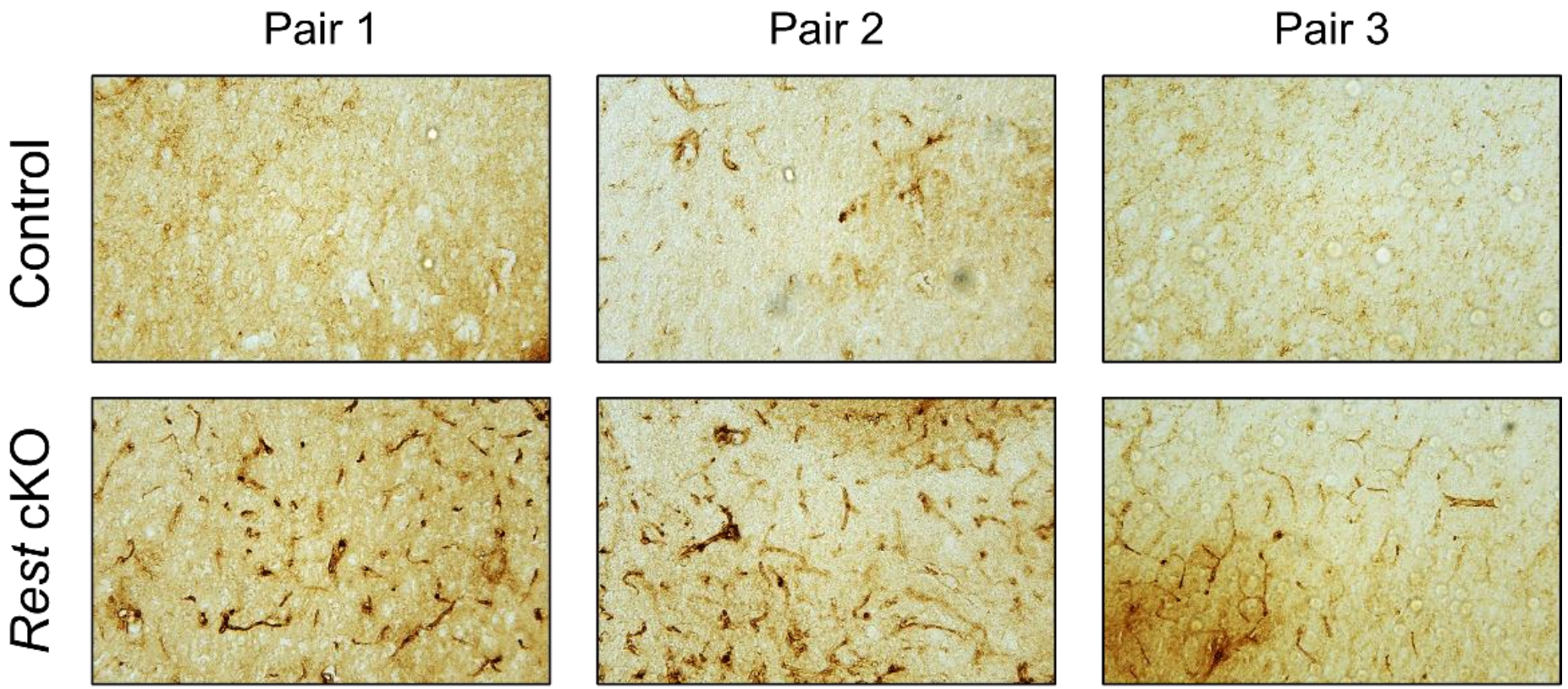

Figure 22. Representative images of phospho-tau (pSer202, pThr205) in the frontal cortex. The 20x magnification was used to better analyse the stain.

4.2.4. GSK3β

GSK3β is a kinase that phosphorylates tau, and its levels have been showed to be increased human neuronal cell lines that lack REST (Lu et al., 2014). More specifically, they observed that in the presence of an inhibitor of GSK3β, the levels of some phosphorylated epitopes decrease, suggesting the involvement of GSK3β in the phosphorylation of tau.

As an increase in tau phosphorylation was observed in *Rest* cKO mice, this project then wondered which kinases could be involved in this increase. Therefore, the levels of GSK3β were also studied and a significantly increase was observed in cortical samples of *Rest* cKO mice. In fact, these mice present levels twice as high as the ones found in controls (**Figure 23**, n=4, t(6)=5.313; p<0.001). GSK3β was also studied in hippocampal samples, however no band was observed at the expected molecular weight (data not shown).

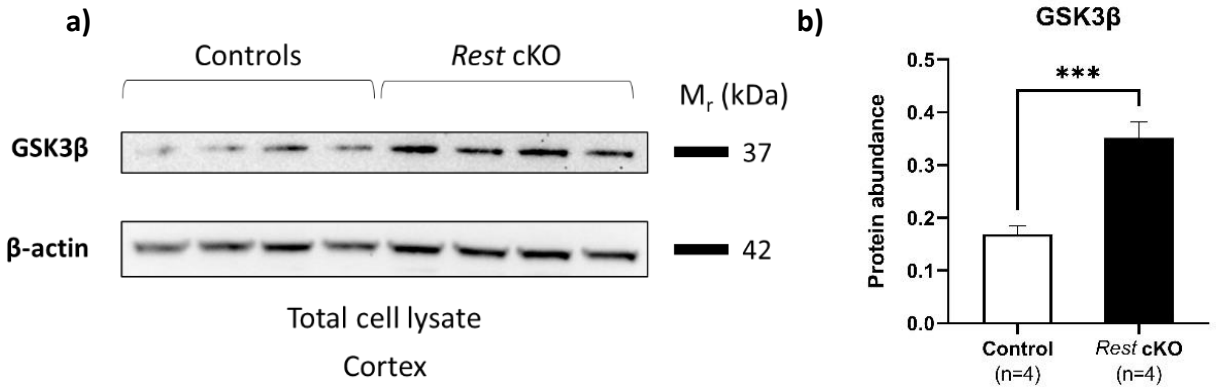

Figure 23. Levels of GSK3β in total cell lysates from the neocortex of four *Rest* cKO and four control mice. **a)** Western blot results. **b)** Quantitation of GSK3β levels, after normalization with β-actin as loading control. Values are represented as mean ± SEM, ***p<0.001.

Given the results obtained through Western blot, four slides per mouse of three pairs of mice were studied through immunohistochemistry using an antibody against kinase GSK3β to further investigate how the absence of REST affects the distribution of this protein. In the hippocampus, the antibody against GSK3β recognized well-defined

filamentous structures with typical morphology of blood vessels, similarly to what was observed with AT8, with more staining observed in *Rest* cKO than in control mice (**Figure 24-27**). These structures were also observed outside of the hippocampus, in particular in the striatum (**Figure 28**). However, no structures resembling tangles were observed with this antibody.

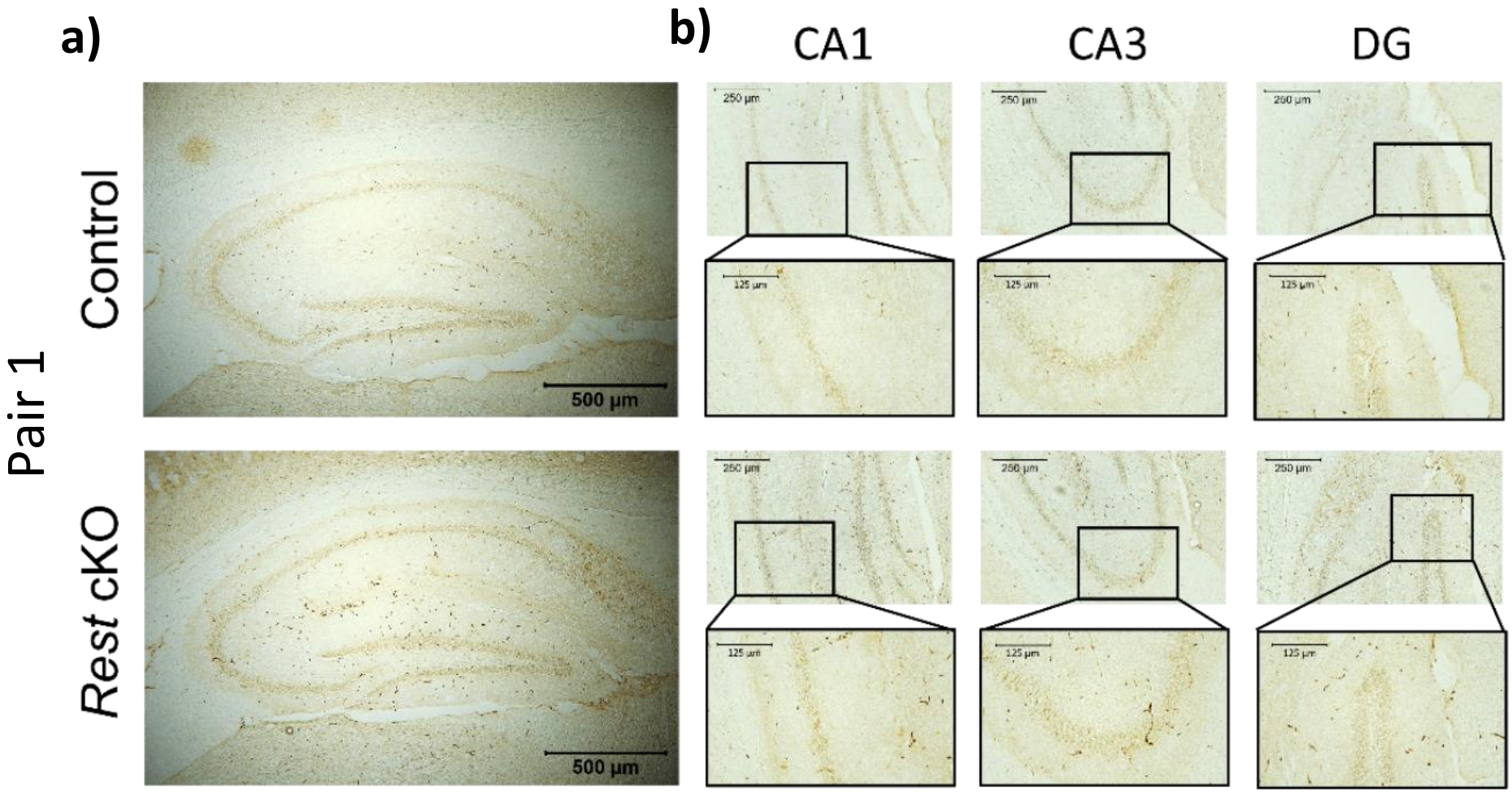

Figure 24. Representative images of equivalent slides using the antibody against GSK3β using brain sections from the first mouse pair of *Rest* cKO and control mice. **a)** The whole hippocampus was imaged using a 5x magnification. **b)** A higher magnification, 10x, was used to analyse each different region of the hippocampus. These images were then further enlarged (20x) to allow a better visualization of the staining.

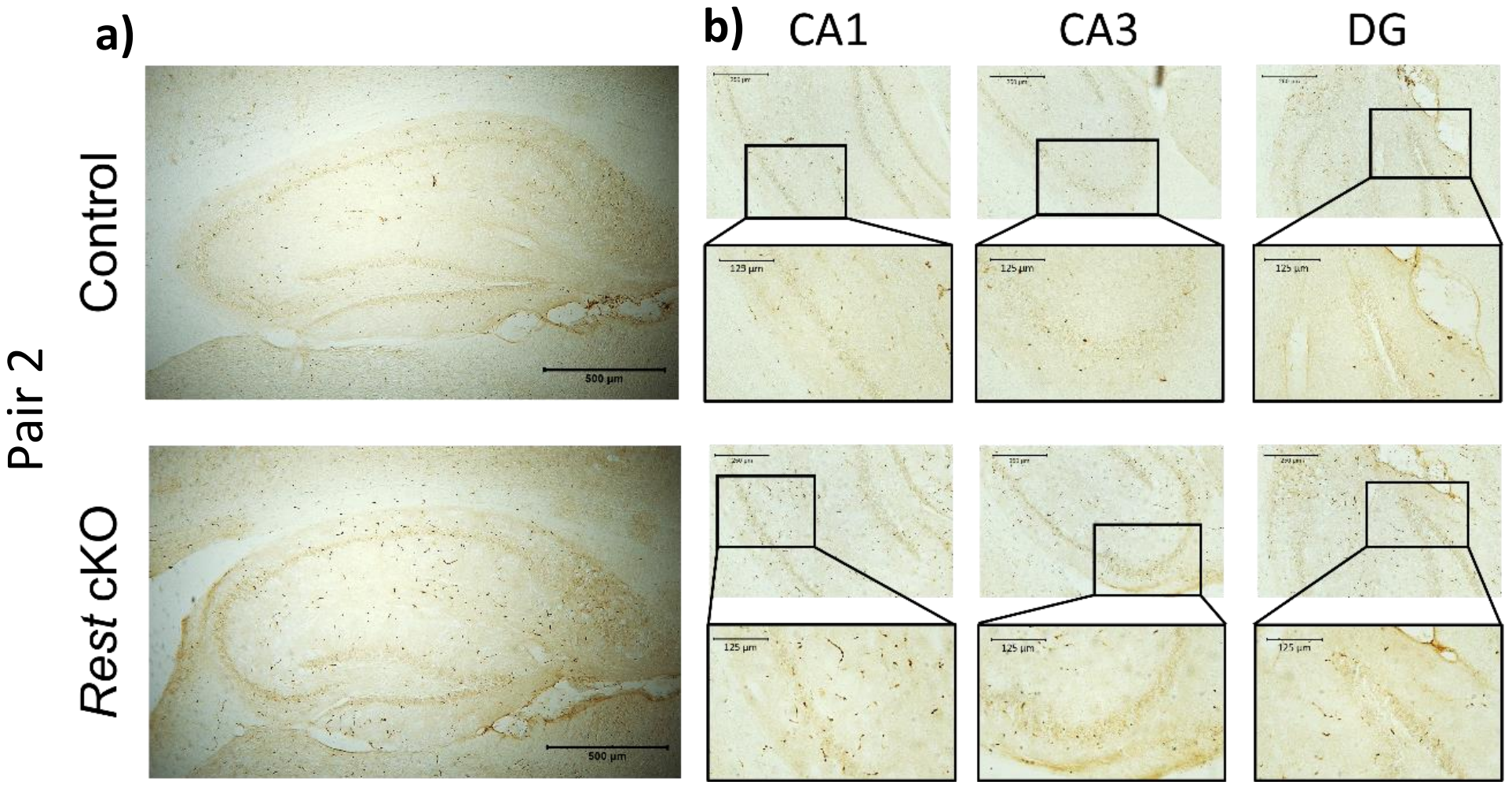

Figure 25. Representative images of equivalent slides using the antibody against GSK3β using brain sections from the second mouse pair of *Rest* cKO and control mice. Figure layout is the same as in Figure 24.

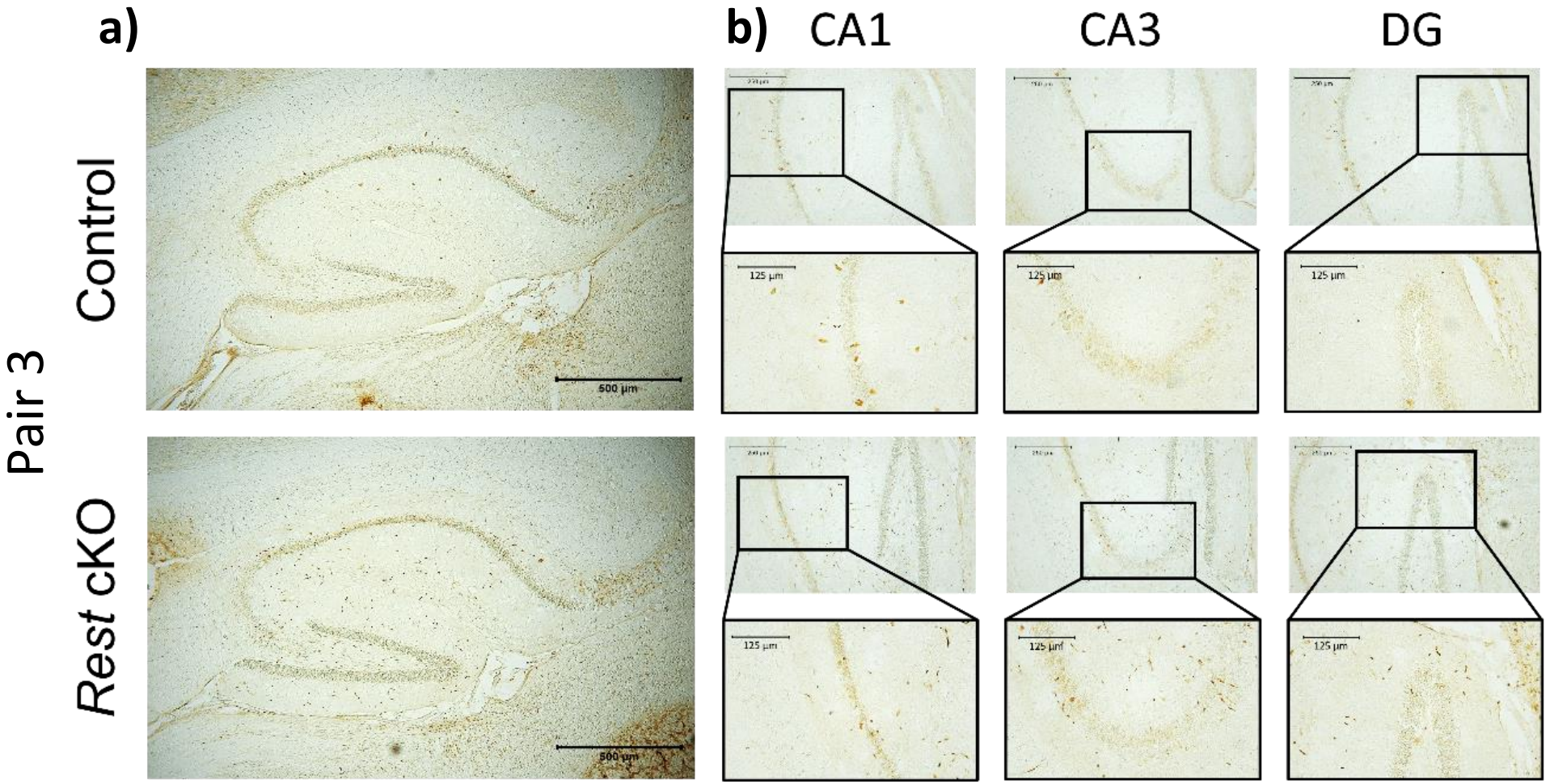

Figure 26. Representative images of equivalent slides using the antibody against GSK3β using brain sections from the third mouse pair of *Rest* cKO and control mice. Figure layout is the same as in Figure 24.

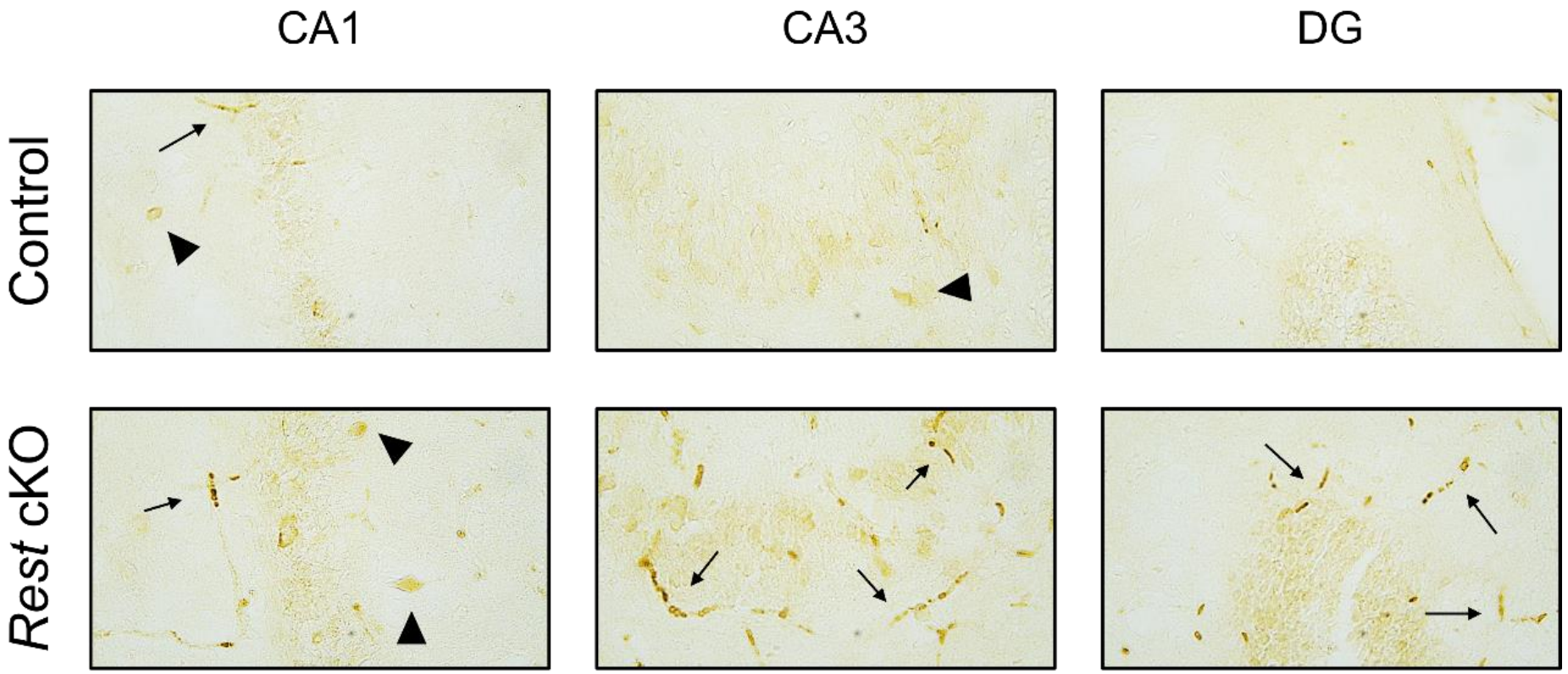

Figure 27. Representative images of equivalent slides using the antibody against GSK3β of the first pair of mice from Figure 24. A 40x magnification was used to better examine and characterize the agglomerates observed with lower magnifications. It is possible to identify stained filamentous structures (→) and whole darker cells (►).

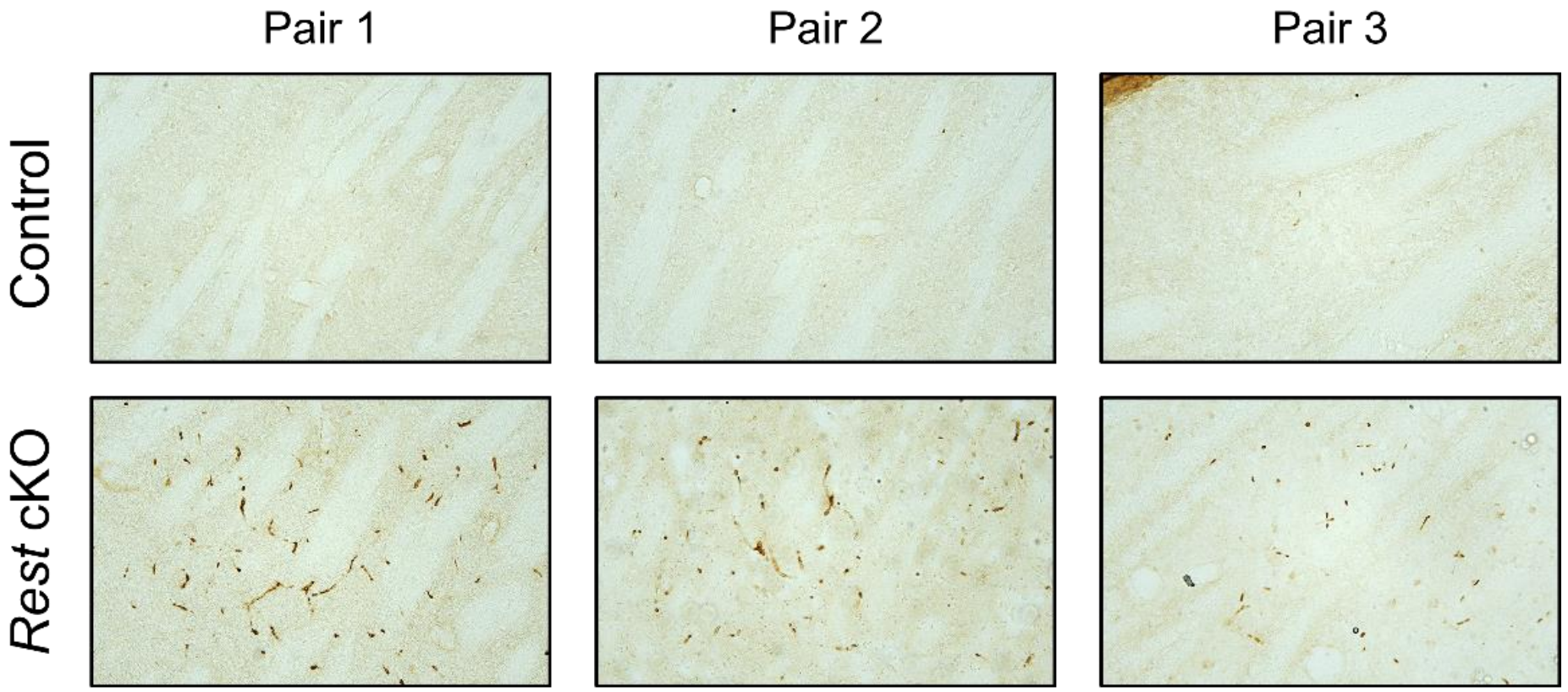

Figure 28. Representative images of GSK3β in the striatum. The 10x magnification was used to better analyse the stain.

Whole cells stained were also observed in both genotypes (**Figure 29**).

Although both types of stain are present in both genotypes, *Rest* cKO display more filamentous formations, whereas controls appear to have more stained nucleus.

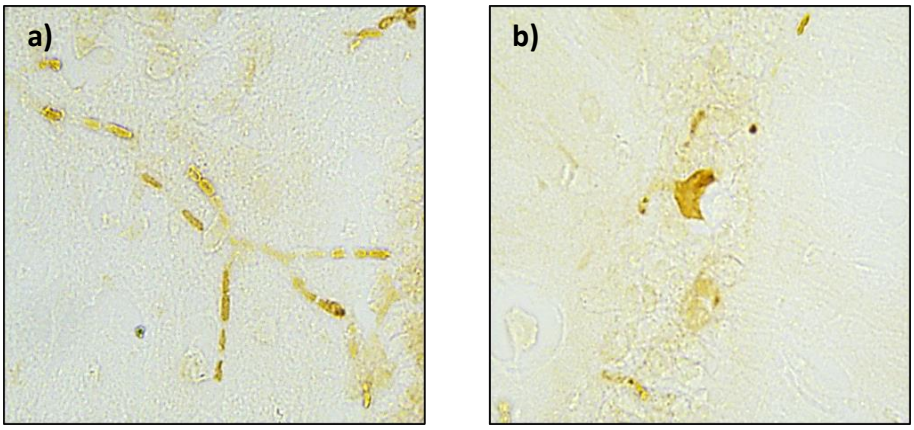

Figure 29. Representative images of different types of structures stained using the antibody GSK3β. A 40x magnification was zoomed in to better examine and characterize the types of stain observed: **a)** filamentous structures (resembling blood vessels), **b)** nucleus of cells.

4.2.5. p35/p25

Another kinase involved in tau phosphorylation is CDK5, which is activated specifically by p35 and its cleavage product, p25. Lu *et al.* also studied these activators in human neuroblastoma cell lines (Lu et al., 2014). They observed that when REST was knockdown there was an increase of the levels of p35 and p25, however, when REST was overexpressed, the levels were similar to control levels. This suggested a role for REST in the regulation of these activators and consequently CDK5.

To determine how the postnatal inhibition of REST affected p35 and p25 expression, the levels of these two activators were also evaluated through western blot in *Rest* cKO mice and in controls. The p35 activator expression is more pronounced than p25, in both the cortex (**Figure 30.a**) and the hippocampus (**Figure 31.a**).

When comparing control and *Rest* cKO mice, it was observed that the absence of REST leads to an upregulation of both activators in the two regions of the brain studied. *Rest* cKO shows about a 20% increase in the expression of p35 (**Figure 30.b**, $n=4$, $t(6)=5.754$; $p<0.001$) and p25 (**Figure 30.c**), $n=4$, $t(6)=2.082$; $p=0.041$) in cortical samples.

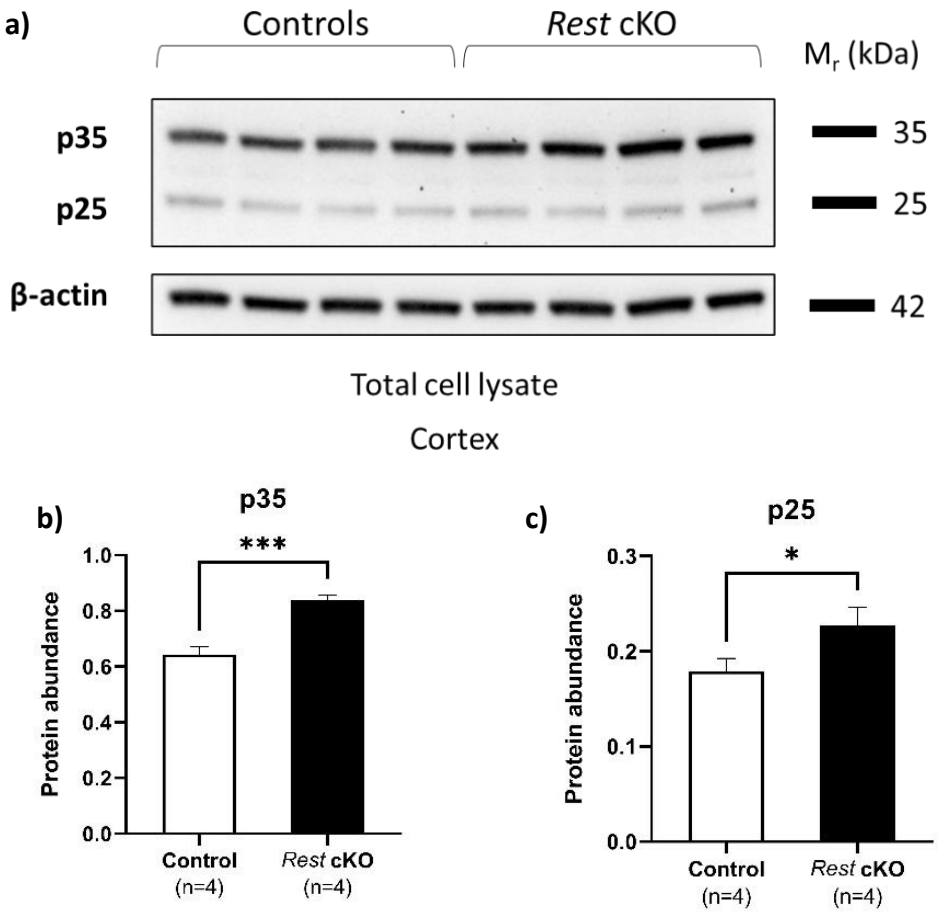

Figure 30. Levels of p35 and p25 in total cell lysates from the neocortex of four *Rest* cKO and four control mice. **a)** Western blot results. **b)** Quantitation of p35 and **c)** p25 levels, after normalization with β-actin as loading control. Values are represented as mean ± SEM, *p<0.05; ***p<0.001.

Whereas in the hippocampus the difference between genotypes was approximately 40% for both p35 (**Figure 31.b**, n=4, t(6)=3.757; p=0.005) and p25 (**Figure 31.c**, n=4, t(6)=4.290; p=0.003).

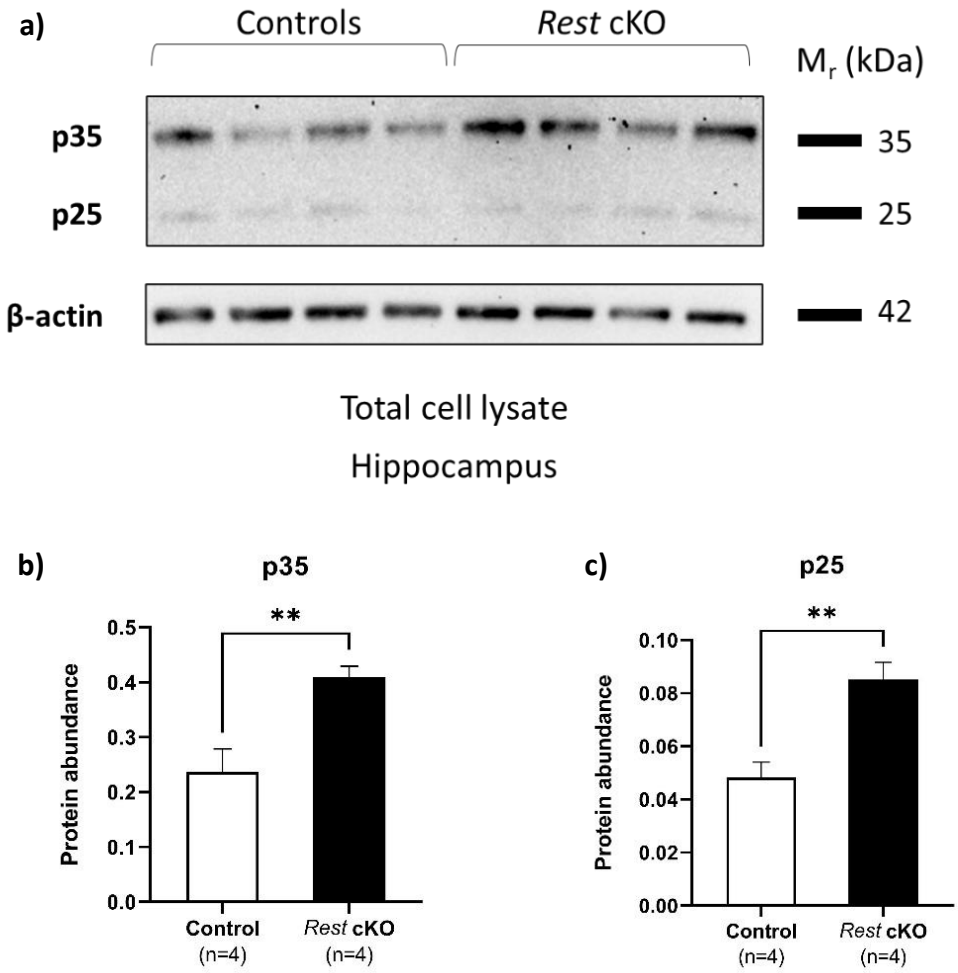

Figure 31. Levels of p35 and p25 in total cell lysates from the hippocampus of four *Rest* cKO and four control mice. **a)** Western blot results. **b)** Quantitation of p35 and c) p25 levels, after normalization with β-actin as loading control. Values are represented as mean ± SEM, **p<0.01.

4.2.6. Identification of a putative *Re1* site in the *Cdk5r1* (p35) promoter.

REST is an important gene repressor, and together with its binding site, *Re1*, is conserved across species (Mortazavi et al., 2006; McGann et al., 2021). As mentioned in **Section 1.5.2**, REST regulates time-dependent repression of certain genes, and therefore it binds to different genes throughout the lifetime of mice or humans. It also binds to

different genes depending on the different types of cells where it is located and the cellular context.

Rockowitz and Zheng have performed deep sequencing of chromatin immuno-precipitation (ChIP-Seq) to identify REST-target genes in embryonic stem cells of both humans and mice (Rockowitz and Zheng, 2015). They identified a total of 8,200 genomic regions in humans and 4,108 in mice that REST binds to. Among this vast list of genes, REST was found to bind to *CDK5R1* in human cells but there was no evidence of binding to the mouse homologous gene, *Cdk5r1* (Rockowitz and Zheng, 2015). The fact that *Cdk5r1* was not identified as a mouse REST-target gene in the study by Rockowitz and Zheng does not necessarily mean that it is not regulated by REST in the adult mouse brain. Thus, this PhD project investigated the possibility of a putative Re1 site in the *Cdk5r1* gene promoter, given the interesting results on p35/p25 and tau phosphorylation in *Rest* cKO mice.

A TFBSPred web tool was used to search putative Re1 sites in the promotor region of Cdk5r1 in the genome of mouse (GRCm38/mm10), which was aligned with the human genome (GRCh38/hg38). One putative REST-binding site, with 21bp, was find in chromosome 11 of the mouse genome, on the genomic region 80,477,031. This site aligned perfectly (100% homology) with the equivalent site in the human genome (**Figure 32**). The identified binding sequence was compared with the known *Re1* consensus sequence, presenting a 71% of identify, i.e. same nucleotides in 15 of the 21 positions. Importantly, the *Re1* nucleotides that are not shared between the consensus sequence and the identified site are the ones with the highest degree of variability, further suggesting that the identified *Re1* site is a genuine one (**Figure 32**). The identified mouse REST-binding site is located 479bp upstream of the first coding region, i.e. ATG (+1). The initial ATG (genomic location: 80,477,509) was identified using the UCSC Genome Browser on Mouse (GRCm38/mm10). Whereas in the human genome, Re1 sequence is located on the genomic region 32,486,978, which is 644bp upstream of the first coding region (genomic location: 32,487,621).

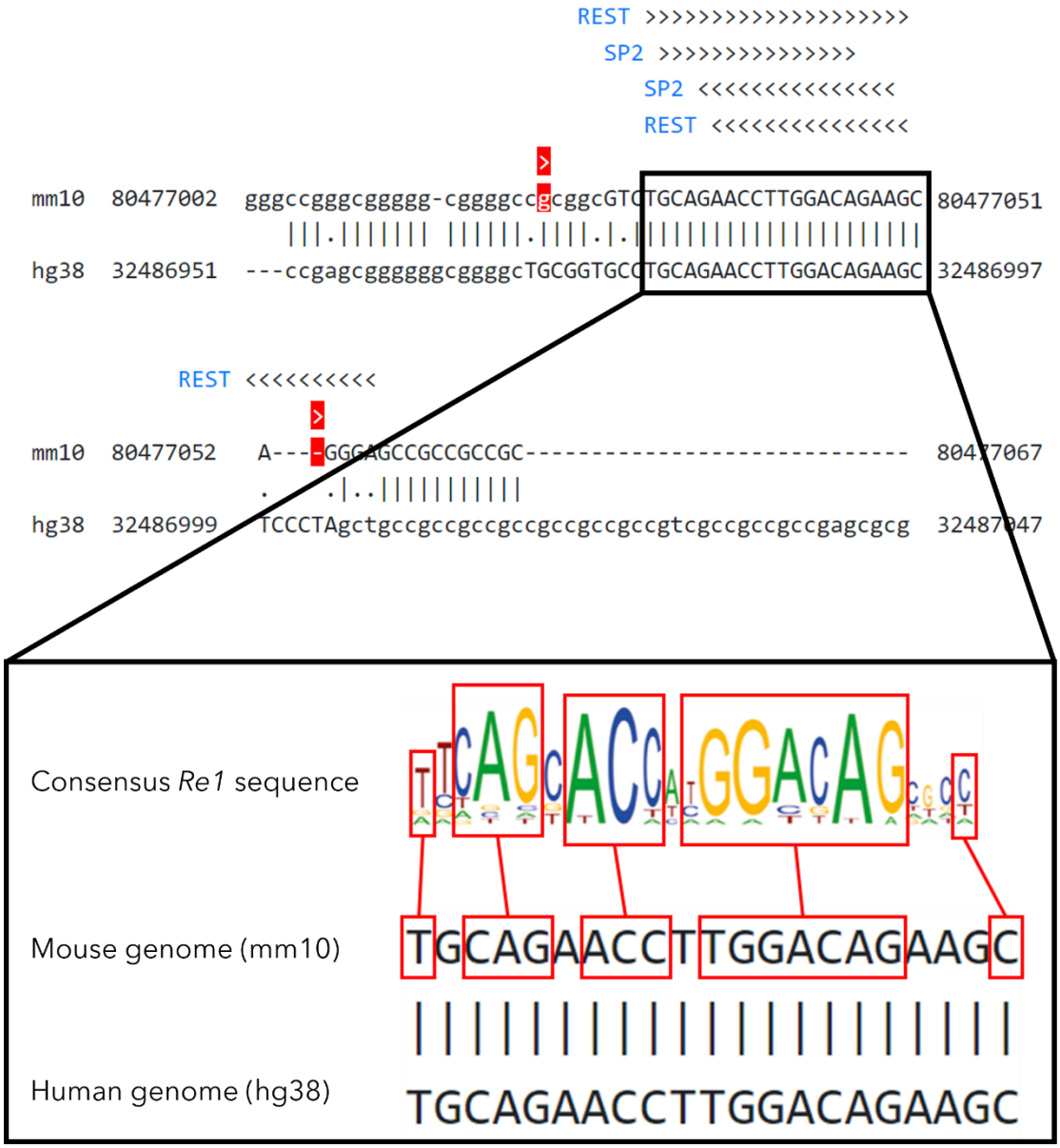

Figure 32. Pairwise alignment of the mouse (mm10) and the human genome (hg38) of the region where promoter analysis was done and comparison with the *Re1* consensus sequence. *Top image*: the TSS is coloured with a red filled box and above it, an arrow shows the orientation of the transcription. The transcription factors (light blue) predicted binding sites are signalized with black arrows. *Zoomed in box*: The consensus *Re1* sequence (coloured letters with different sizes) was compared with the predicted REST binding site. The size of the letters in the consensus sequence is proportional with the frequency of which that nucleotide occurs at a certain position. Out of the 21 nucleotides that compose the consensus *Re1* sequence, the most frequently found 15 nucleotides (around 71%) align perfectly with the identified site in both genomes.

4.3. Investigation of a possible neurodegeneration phenotype in the brain of *Rest* cKO mice

4.3.1. Neuronal labelling

The major cellular outcome of AD is the loss of neurons. One of Lu *et al.* key findings was that embryonic inhibition of REST lead to a pronounced neuronal loss in mice at 8-months of age. The mouse model used in this project has the particularity of only inhibiting REST in the postnatal forebrain to potentially avoid any developmental abnormalities. Hence, this project carefully studied the possibility of a neurodegenerative phenotype in *Rest* cKO mice using a neuronal marker, NeuN.

An antibody against the nuclear protein NeuN was used to assess the levels of this protein in cortical samples of both genotypes through Western blot (**Figure 33**). There were no major differences regarding the levels of NeuN between genotypes (n=3, t(4)=1,267; p = 0.137).

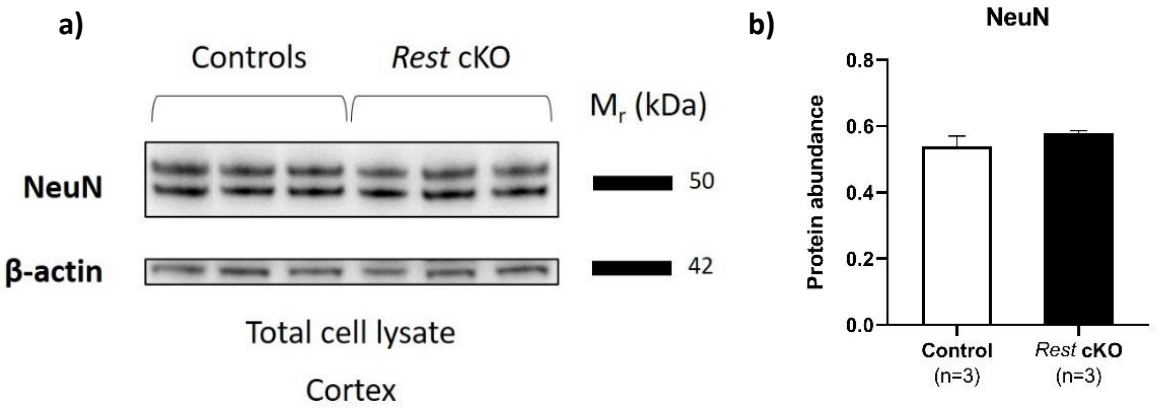

Figure 33. Levels of NeuN in total cell lysates from the neocortex of four *Rest* cKO and four control mice. **a)** Representative Western blot. **b)** Quantitation of NeuN levels, after normalization with β-actin as loading control. Values are represented as mean ± SEM.

Due to liming hippocampal sample quantities, NeuN levels were not quantified in the hippocampus through Western blot. On the other hand, the possibility of a neurodegenerative phenotype in the hippocampus of *Rest* cKO compared to control

mice was done through immunohistochemistry, using older mice, with particular focus on the pyramidal cell layer and granular cell layer.

Six slides of each *Rest* cKO mouse were used to match with their control pair. This was done very thoroughly by morphological comparison of the hippocampus with the Mouse Brain Atlas. After matching the equivalent slides, sagittal sections from *Rest* cKO mice and controls were used for neuronal quantification of the four main regions of the hippocampus, CA1, CA2, CA3 and DG. Initially three mice per genotype were studied using DAB chromogen (**Appendix 3.1**). However, to improve the quantification, immunofluorescence was used with another set of three controls and three *Rest* cKO mice (**Figure 34-36**). Immunofluorescence allowed a better contrast between the stain and the background, which facilitated the distinction between neurons. Hence, the quantification results showed here only include the second set of mice, obtained using fluorescence. The hippocampus morphology and size changes severely from medial to lateral planes therefore, to ensure that the quantification is comparable (i.e. compare equivalent planes in different mice), each pair of slides was matched with a page of the Mouse Brain Atlas, i.e. with a sagittal plane of the hemisphere. Eight equivalent slides (matched with the Mouse Brain Atlas pages 104, 107, 109, 112, 114, 117, 120 and 122) per mouse were analysed in order to cover all the hemisphere. The results are presented in **Figure 37** and **Figure 38** regarding the correspondent Mouse Brain Atlas page to each slide (Table with the counting in **Appendix 3.2**).

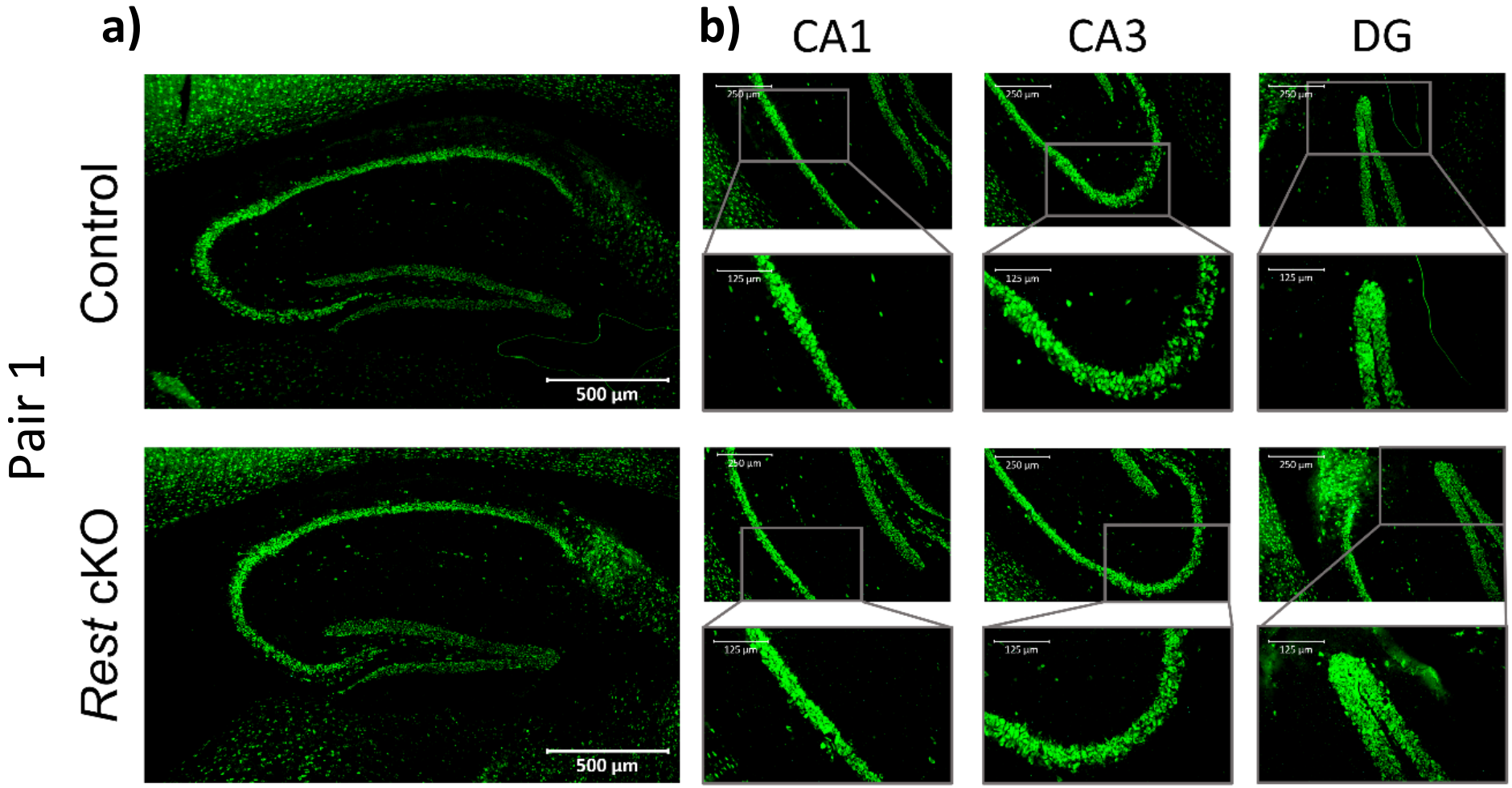

Figure 34. Representative images of neuronal labelling of equivalent slides using an anti-NeuN antibody and Alexa 488 as secondary antibody for the first pair of mice *Rest* cKO and control mice used for quantification. **a)** The whole hippocampus was imaged using a 5x magnification. **b)** A higher magnification, 10x, was used to analyse each different region of the hippocampus. These images were then further enlarged (20x) to allow a better representation of the labelled neurons.

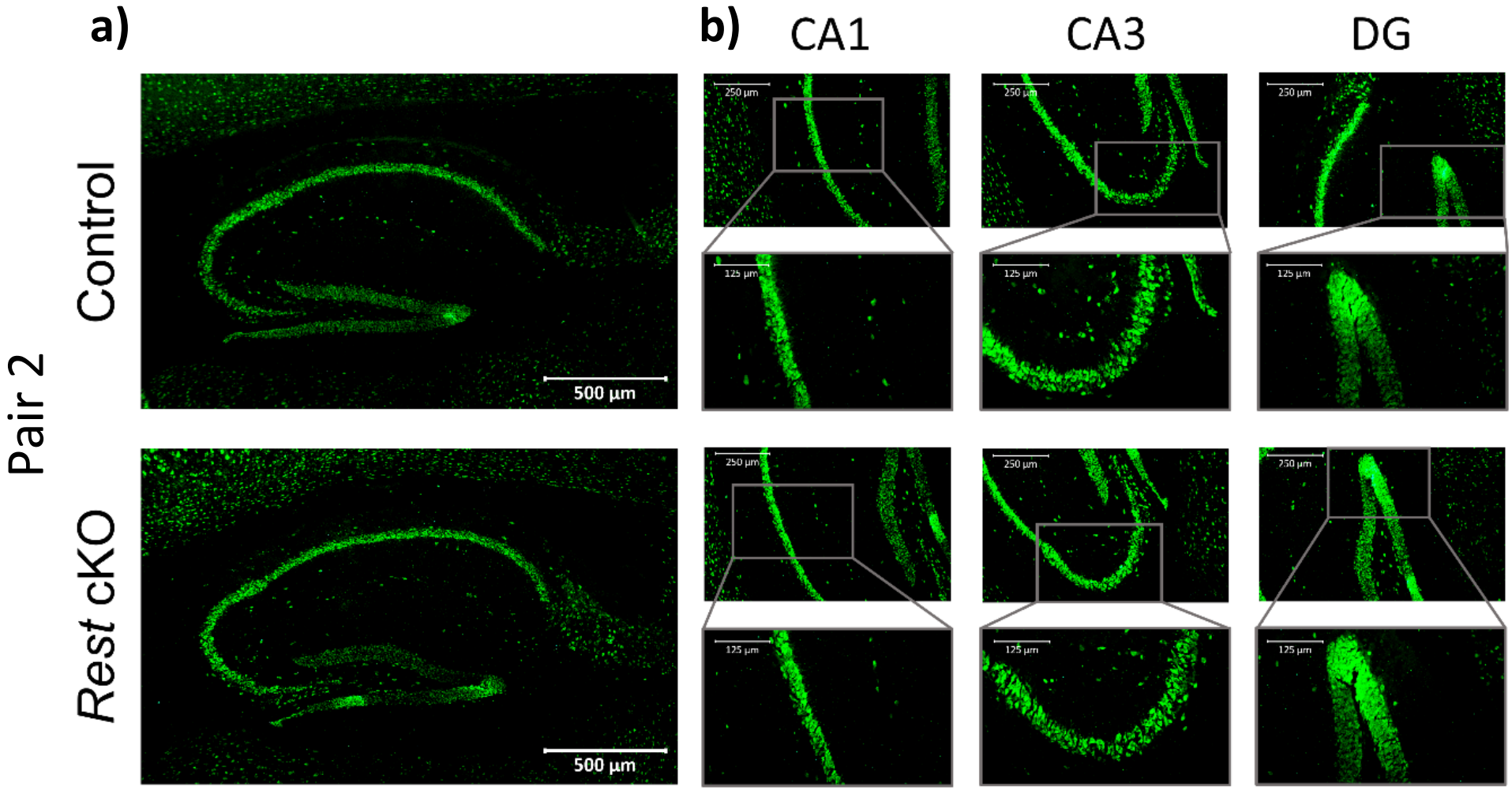

Figure 35. Representative images of neuronal labelling of equivalent slides using an anti-NeuN antibody and Alexa 488 as secondary antibody for the second pair of mice *Rest* cKO and control mice used for quantification. Figure layout is the same as in Figure 34.

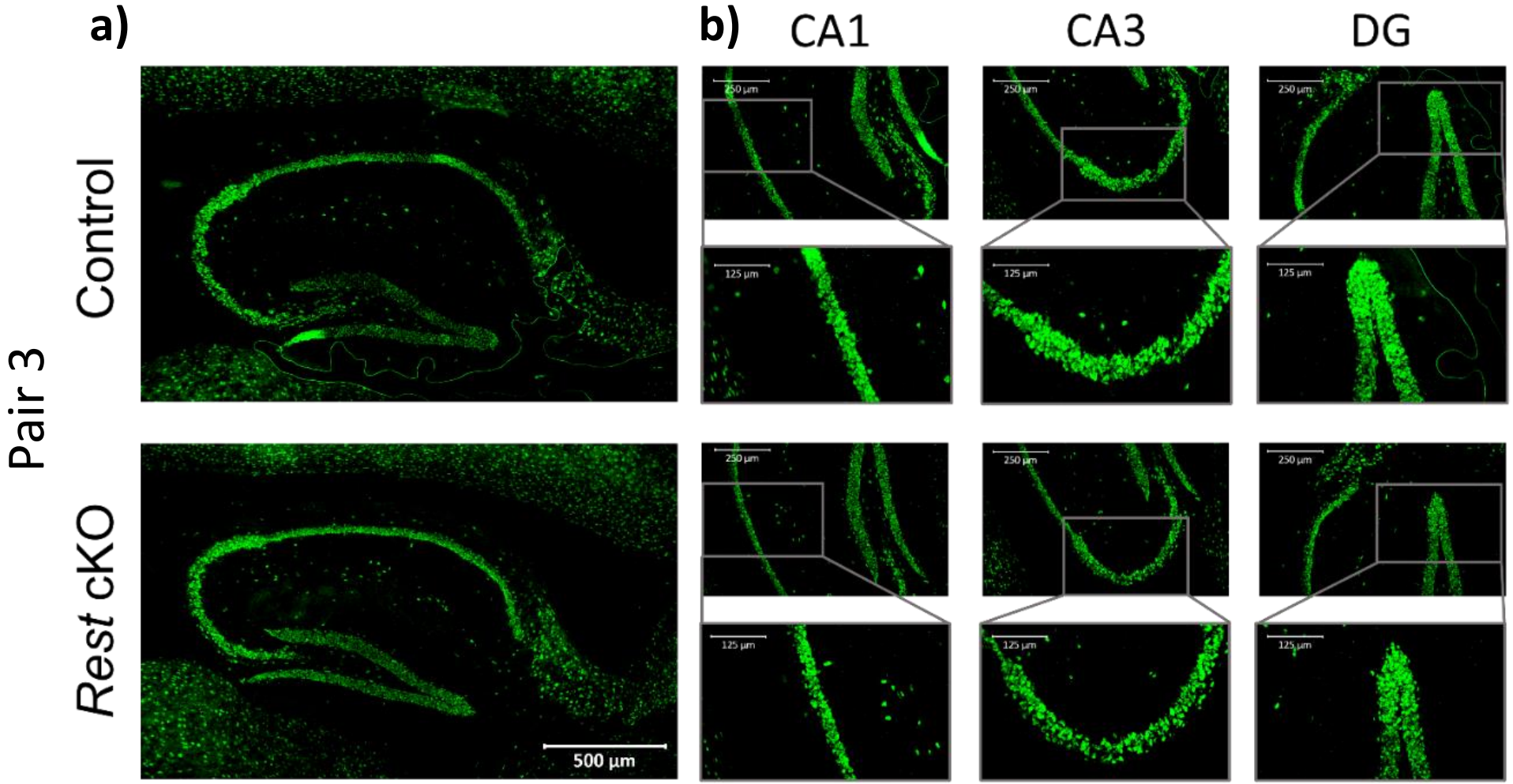

Figure 36. Representative images of neuronal labelling of equivalent slides using an anti-NeuN antibody and Alexa 488 as secondary antibody for the third pair of mice *Rest* cKO and control mice used for quantification. Figure layout is the same as in Figure 34.

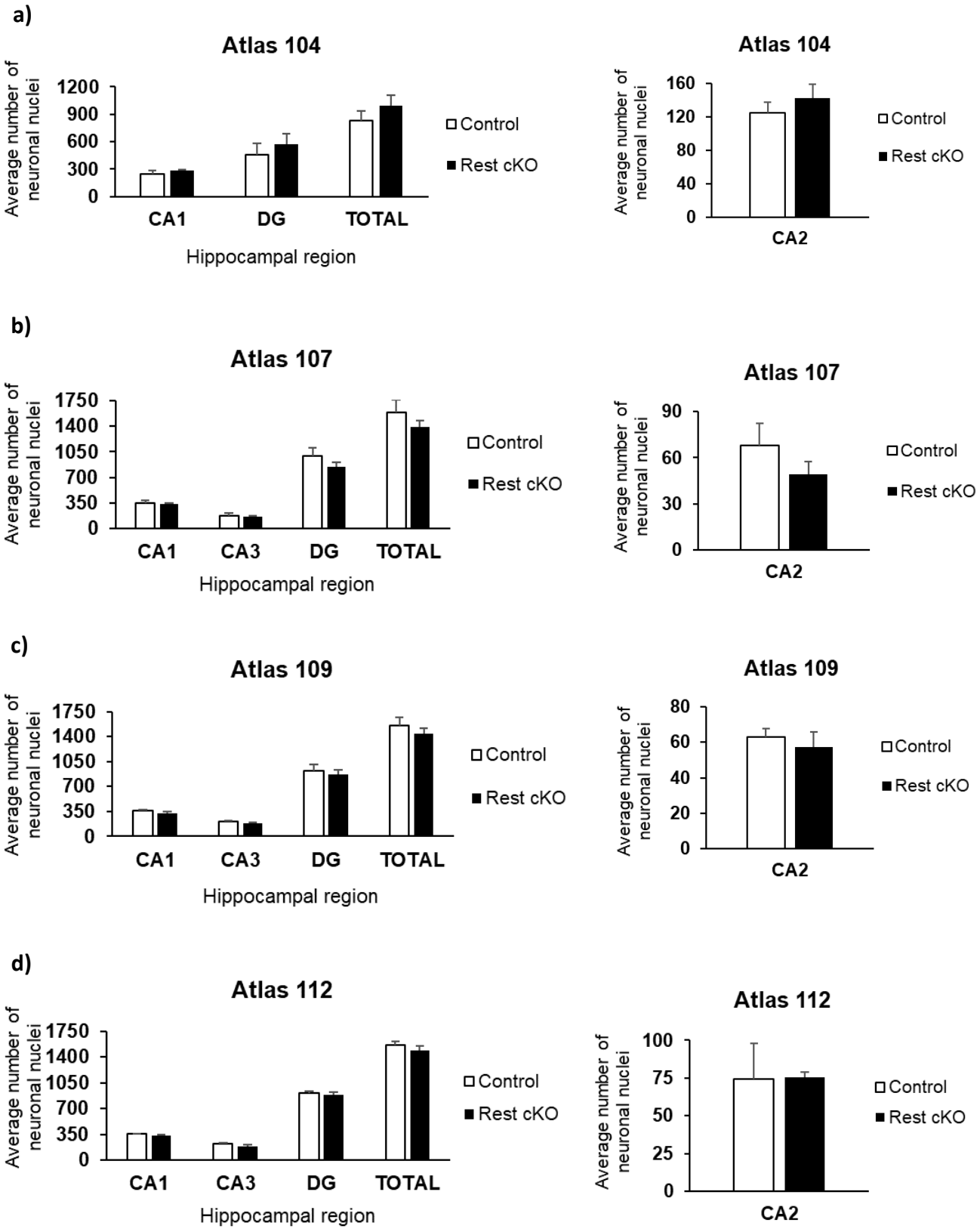

Figure 37. Neuronal counts per hippocampal region per atlas page (104 to 112) of the Mouse Brain Atlas. Values are represented as mean ± SEM.

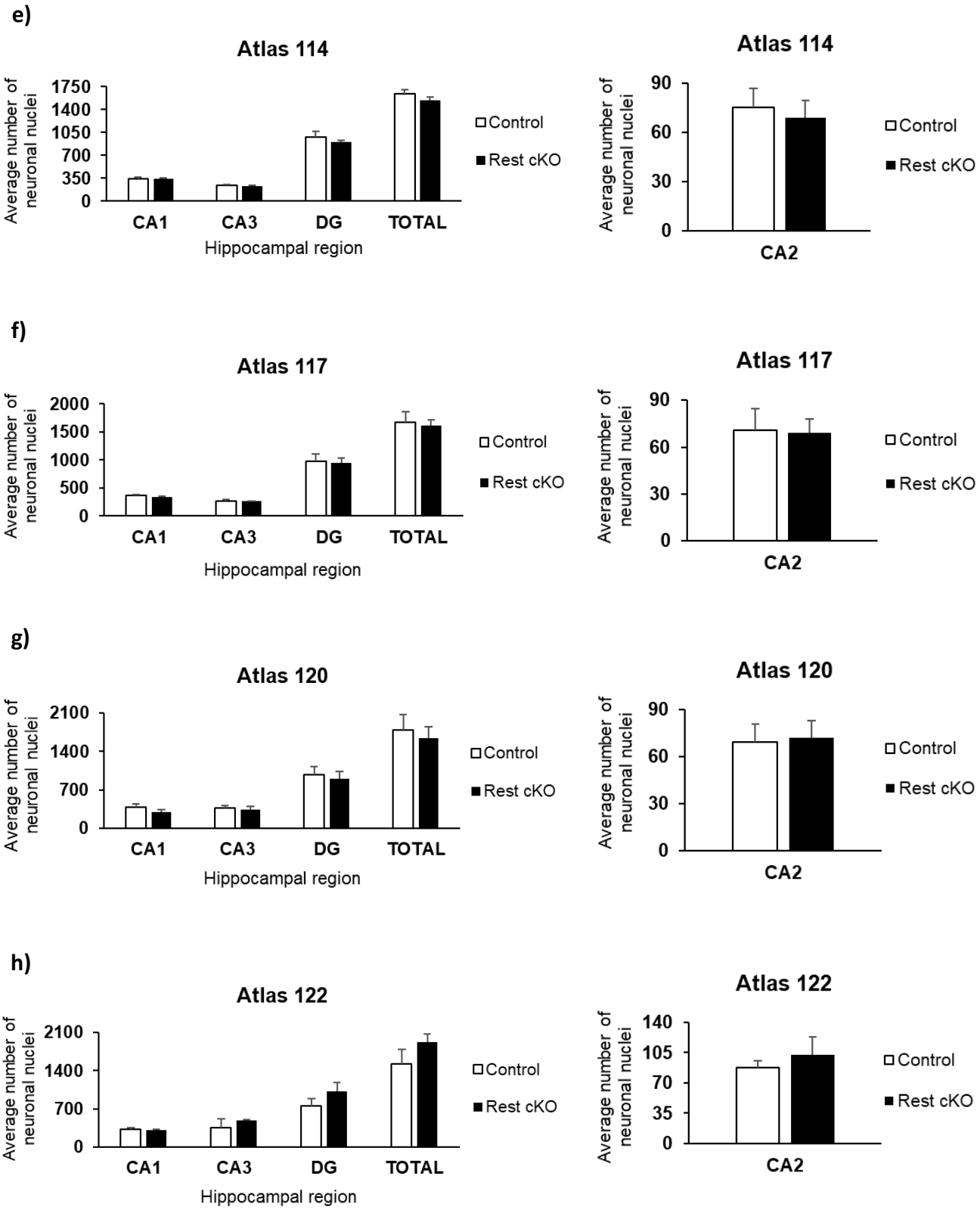

Figure 38. Neuronal counts per hippocampal region per atlas page (114 to 122) of the Mouse Brain Atlas. Values are represented as mean ± SEM.

Nonetheless, to be able to evaluate the total number of neurons per genotype, the total quantification, i.e. the average of all the eight slides per mouse, is also shown in **Figure 39** and in **Table 1**. No major reduction in neuronal count was observed in the hippocampus of *Rest* cKO mice, with the average number of neurons being very similar between the two genotypes.

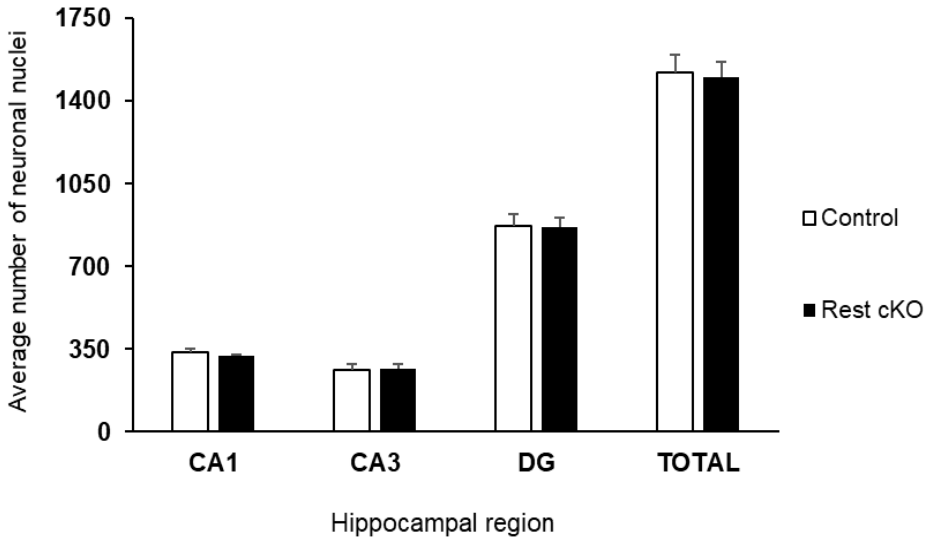

Figure 39. Total neuronal count per hippocampal region per genotype. Values are represented as mean ± SEM.

Table 1. Summary of the neuronal count per genotype, per region of the hippocampus. The results presented are the average of nuclei present in eight slides per mouse, with n=3. The third row shows the p-value of each T-test performed to evaluated.

Mouse (n=3)	**Region of the hippocampus**				
	CA1	**CA2**	**CA3**	**DG**	**TOTAL**
Control	338.83	79.13	262.86	873.29	1521.25
***Rest* cKO**	321.67	79.71	265.43	869.29	1502.92
p-value	0.1131	0.4737	0.4718	0.4744	0.4257

Apart from the three usual regions of the hippocampus, a small region between the CA1 and the CA3 – the CA2 – was also analysed. Taking the diagrams of the Mouse Brain Atlas as reference, the CA2 was identified in multiple slides per genotype (**Figure 40**). The main criteria for the delimitation of CA2 was 1) a change in the direction of the pyramidal cell layer from CA1 into CA3 and 2) an enlargement of this region.

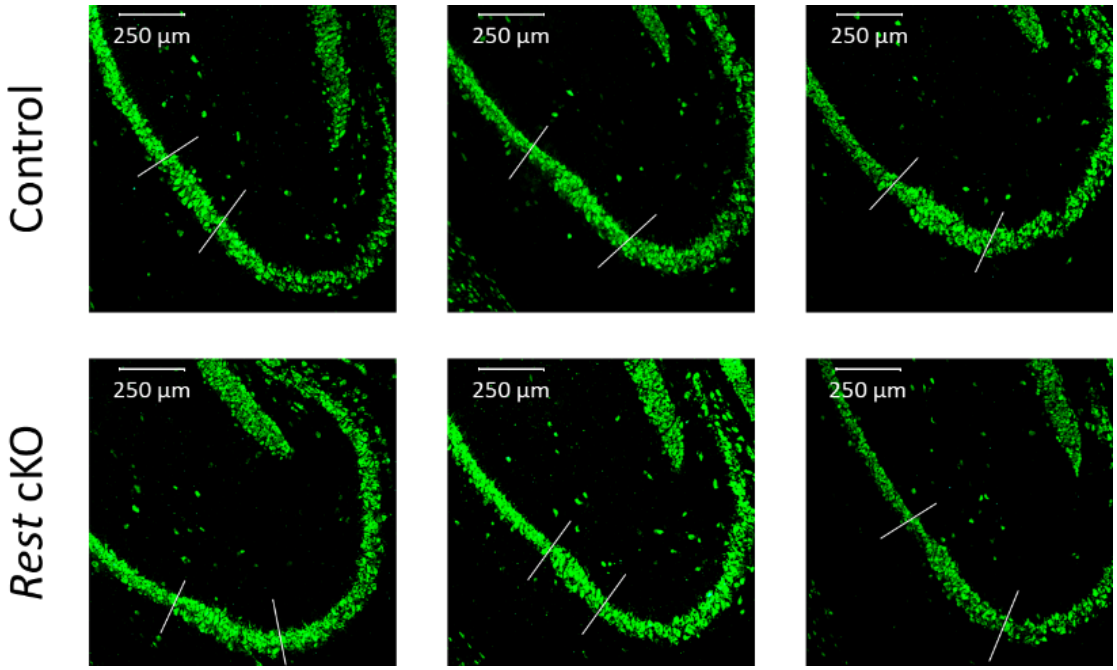

Figure 40. Representative images of the CA2 (region in between the white lines). This region was identified using the Mouse Brain Atlas.

Given the complexity in finding this region, a slight variability was observed regarding neuronal count within the same genotype group. The results observed were very similar to the other hippocampal regions with no major alterations in the number of nuclei (**Figure 41**).

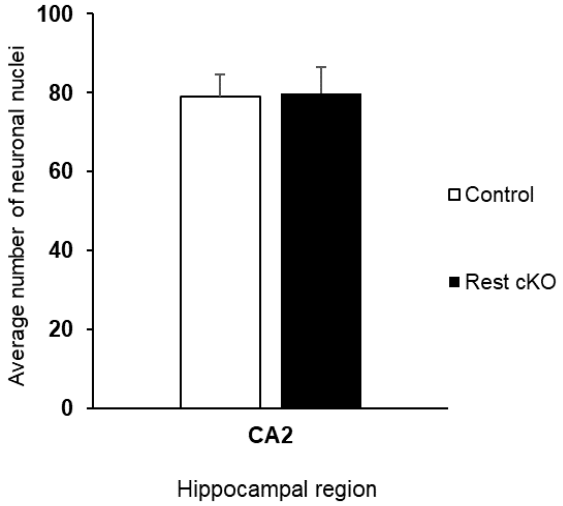

Figure 41. Total neuronal count per hippocampal region per genotype. No difference was observed between *Rest* cKO mice and controls in the CA2 region of the hippocampus. Values are represented as mean ± SEM.

4.3.2. Dendritic labelling

Another hallmark of AD is synaptic alterations, such as pre- and postsynaptic failure, which is closely related with memory loss, the main symptom of this disease. Dendrites are involved in synapses, so dendritic impairment might lead to synaptic loss and consequently, to memory impairment. Therefore this project evaluated the possibility of dendritic degeneration in the hippocampus using an antibody against microtubule-associated protein (MAP2) for this purpose (**Figure 42**).

Given the high density of dendrites (darker lines indicated by the arrows) no quantification was possible. Hence, a morphological analysis was performed, by observing and analysing multiple criteria: length, quantity, orientation and localisation of dendrites within the hippocampal region. The results are summarised in **Table 2**.

In general, both genotypes showed high variability when evaluating these criteria. Although no major morphological differences between the two genotypes were observed, minor differences in individual mice were seen, with *Rest* cKO mice appearing to have fewer and shorter dendrites.

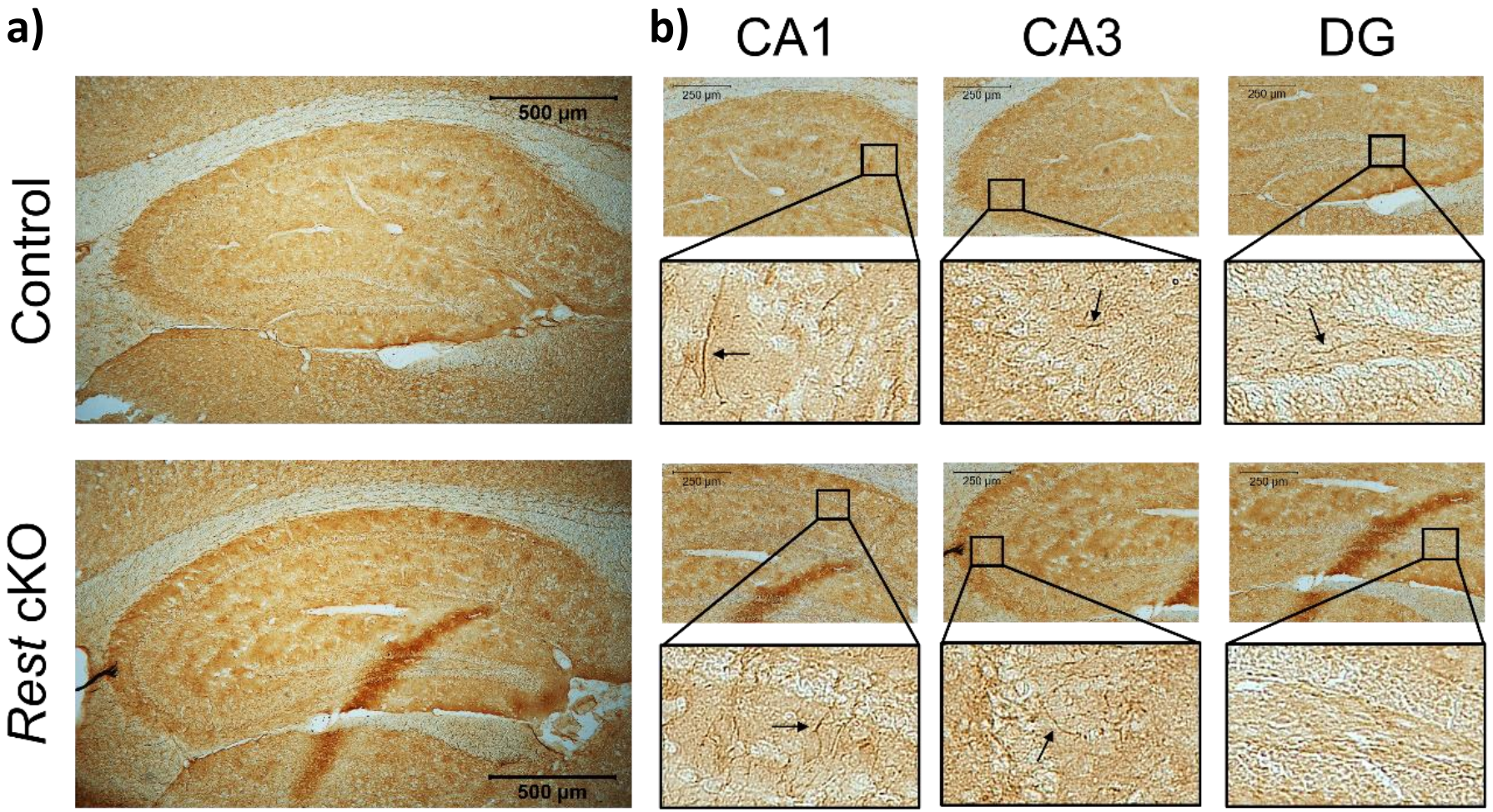

Figure 42. General representation of immunohistochemical images of MAP2. **a)** The whole hippocampus was imaged using a 5x magnification. **b)** A higher magnification, 10x, was used to analyse each different region of the hippocampus. These images were then further enlarged (20x) to allow a better representation of the labelled dendrites (→).

Table 2. Summary of the MAP2 morphological analysis performed on three matched pairs of controls and *Rest* cKO mice. Length, quantity, orientation and localisation of dendrites within the hippocampus were the analysed criteria.

	Genotype	Region	Length	Quantity	Orientation	Localisation
Pair 1	**Control**	CA1	Short	Less	No common direction	Scattered
		CA3	Long	More	No direction	Scattered
		DG	Long	more	Well defined	Scattered
	***Rest* cKO**	CA1	Long	More	Pointing towards the DG	More between CA1 and DG
		CA3	Short	Less (inner); more (outer)	Pointing towards the medial region of the hippocampus	Scattered, more outside
		DG	Short	Less	Not well defined	Scattered
Pair 2	**Control**	CA1	Long	Less but well defined	All seems to follow the same direction, more organised	More between CA1 and DG
		CA3	n/a	More defined	No common direction	Most inside of CA3, some outside (other side of the cell bodies)
		DG	n/a	Less defined	No common direction	Between the dendritic borders
	***Rest* cKO**	CA1	Short	Has more shorter dendrites	No common direction	Scattered
		CA3	n/a	Less defined	From CA3 to inside of the hippocampus	Inside the CA3
		DG	n/a	More defined	No common direction	Between the dendritic borders
Pair 3	**Control**	CA1	Long	More	No common direction	Scattered, more between CA1 and DG
		CA3	Long	More	All seems to follow the same direction, more organised (outer hippocampus)	Has more dendrites outer hippocampus in the CA3
		DG	Short	Very similar	No common direction	Between the dendritic borders
	***Rest* cKO**	CA1	Short	Less	All pointing vertically	Scattered, more between CA1 and DG
		CA3	Short	Less	No common direction	Closer to the pyramidal cell layer
		DG	Short	Very similar	No common direction	Between the dendritic borders

Western blot was used to further assess the possibility dendritic degeneration using cortical samples of both genotypes (**Figure 43.a**). Cortical samples of *Rest* cKO mice exhibited a small decrease (around 10%) in levels of MAP2 when compared with control mice (n=7, t(12)=2.000; p=0.03) (**Figure 43.b**).

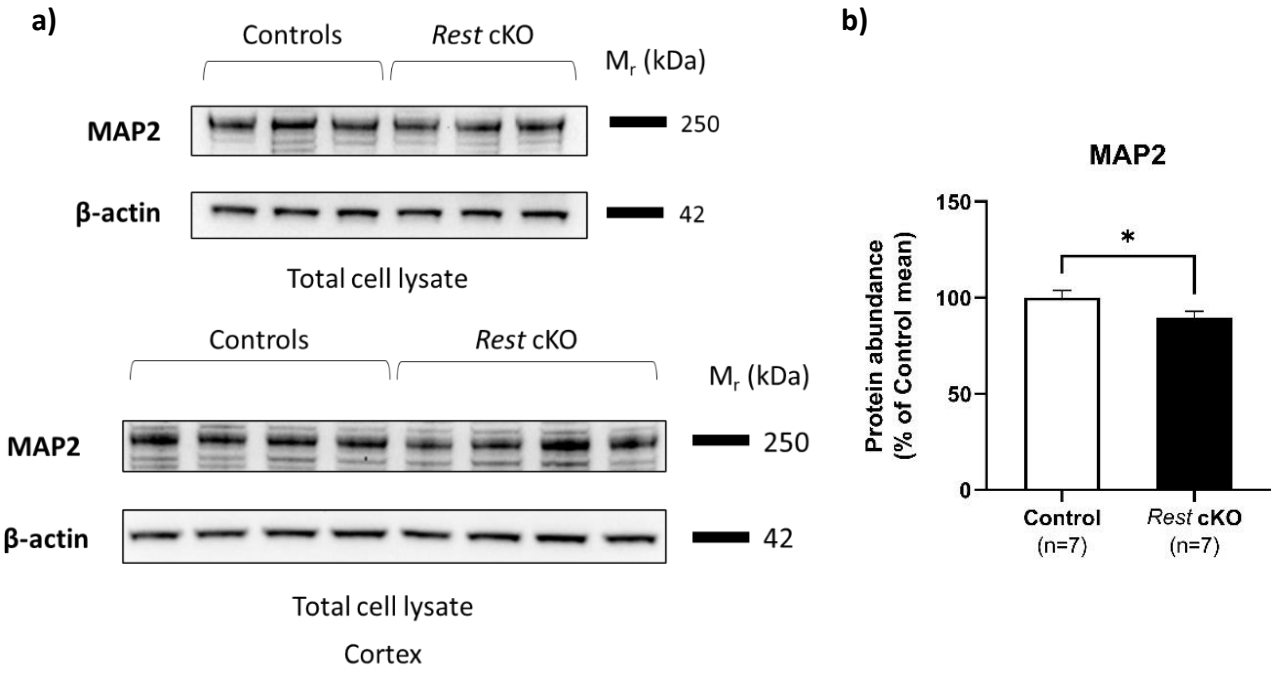

Figure 43. Levels of MAP2 in total cell lysates from the neocortex of seven *Rest* cKO and seven control mice. **a)** Representative Western blot. **b)** Quantitation of MAP2 levels, after normalization with β-actin as loading control. Values are represented as mean ± SEM, *p<0.05.

The levels of MAP2 were also assessed in the hippocampus and a significant increase was observed, with *Rest* cKO mice having a protein abundance two-times higher than controls (**Figure 44,** n=4, t(6)=3.017; p=0.012).

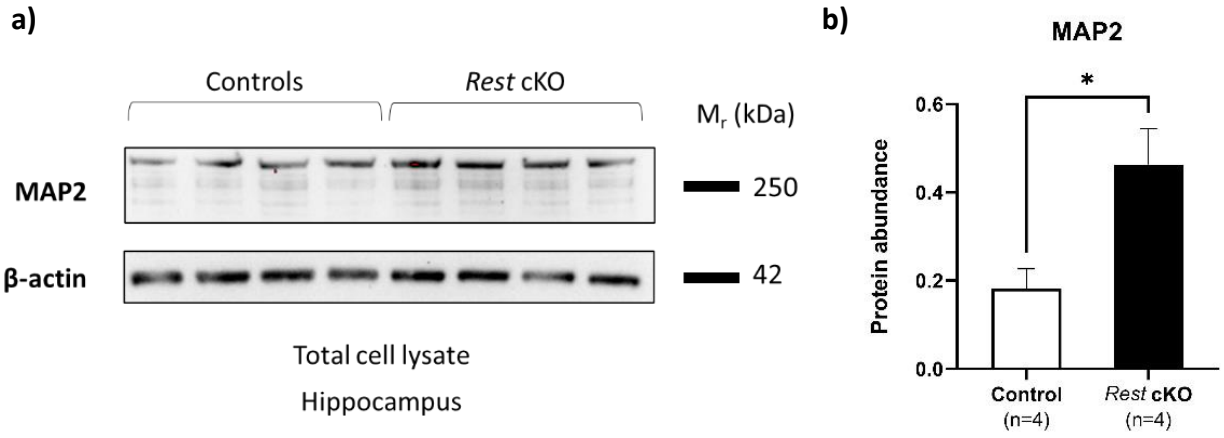

Figure 44. Levels of MAP2 in total cell lysates from the hippocampus of four *Rest* cKO and four control mice. **a)** Western blot results. **b)** Quantitation of MAP2 levels, after normalization with β-actin as loading control. Values are represented as mean ± SEM, * $p<0.05$.

4.3.3. Synaptic markers

The main symptom of AD is loss of memory, which correlates with synaptic impairment and synaptic plasticity. To further evaluate the possibility of synaptic degeneration, two proteins were evaluated: synaptophysin, to assess the presynaptic terminal, and PSD-95, a marker of postsynaptic density.

4.3.3.1. Synaptophysin

An antibody against synaptophysin, which is a major protein of the presynaptic vesicle membrane was used to evaluate the possibility of a synaptic degeneration phenotype (**Figure 45.a**). No major differences were observed between *Rest* cKO and control mice in the neocortex (**Figure 45.b**, n=5, $t(8)=1.003$; $p=0.172$).

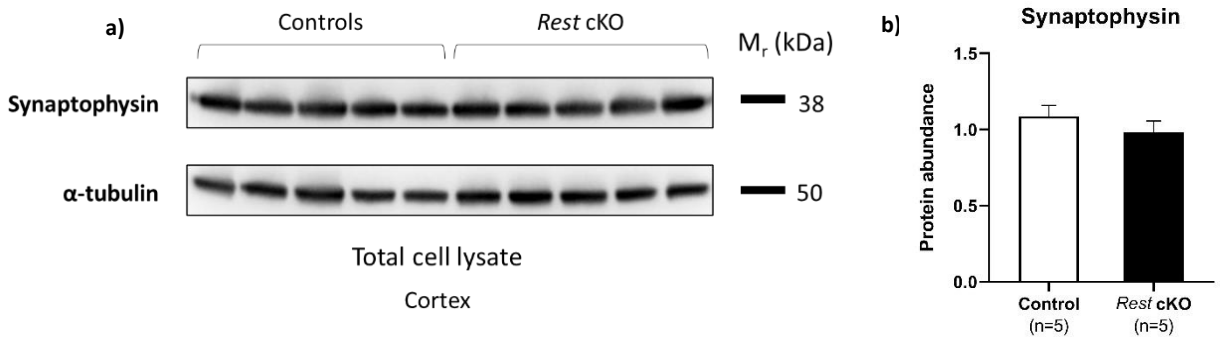

Figure 45. Levels of synaptophysin in total cell lysates from the neocortex of five *Rest* cKO and five control mice. **a)** Representative Western blot. **b)** Quantitation of synaptophysin levels, after normalization with α-tubulin as loading control. Values are represented as mean ± SEM.

Hippocampal samples were also evaluated, and no differences was observed between *Rest cKO* and controls (**Figure 46**, n=4, t(6)=0,638; p=0.275).

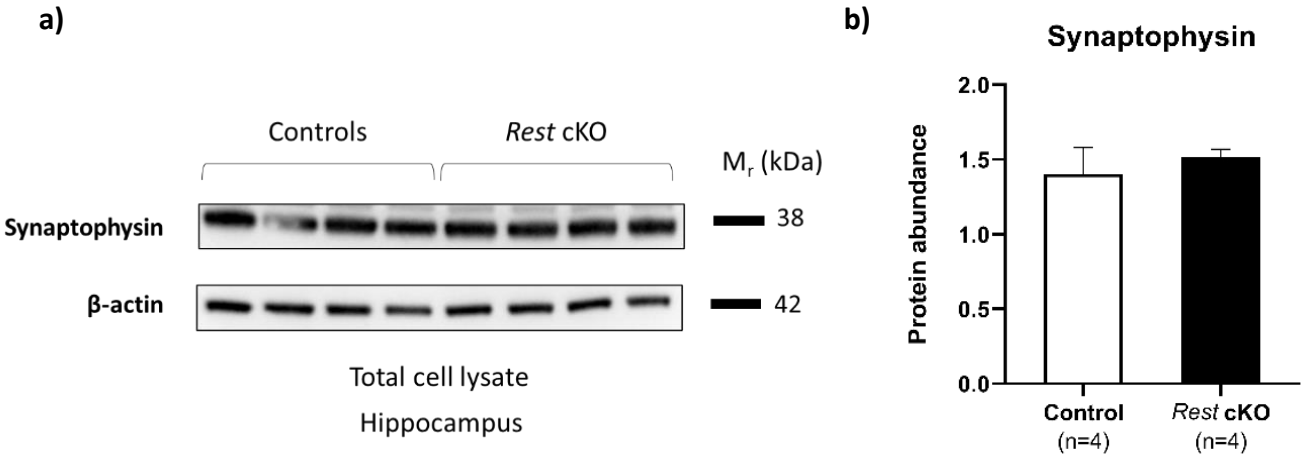

Figure 46. Levels of synaptophysin in total cell lysates from the hippocampus of four *Rest* cKO and four control mice. **a)** Western blot results. **b)** Quantitation of synaptophysin levels, after normalization with β-actin as loading control. Values are represented as mean ± SEM.

4.3.3.2. PSD-95

On the other hand, degeneration of the postsynaptic membrane was evaluated using an antibody against PSD-95, a scaffold protein pivotal in the postsynaptic density.

The levels of this protein were studied through Western blot in the neocortex (**Figure 47.a**). *Rest* cKO showed a tendency toward statistical significance (**Figure 47.b**, n=7, t(12)=1.772; p=0.051) to have lower levels (around 19%) of PSD-95 in cortical samples.

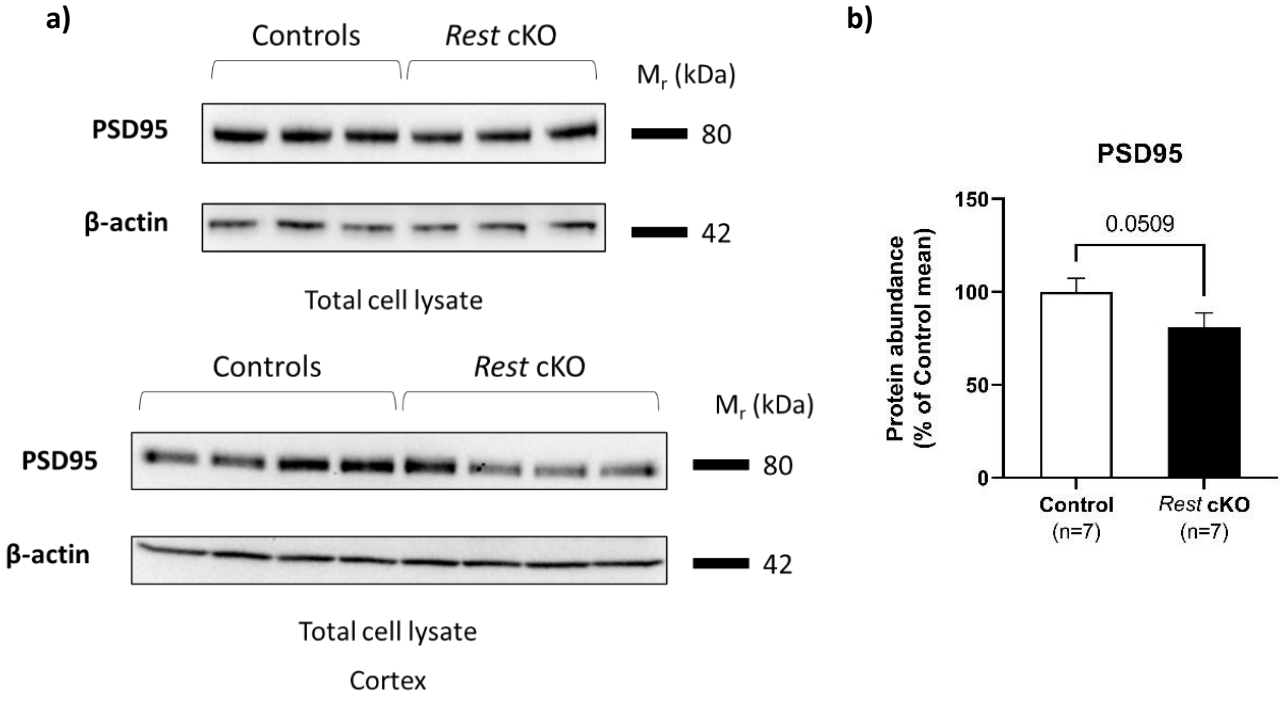

Figure 47. Levels of PSD-95 in total cell lysates from the neocortex of seven *Rest* cKO and seven control mice. **a)** Representative Western blot results. **b)** Quantitation of PSD-95 levels, after normalization with β-actin as loading control. Values are represented as mean ± SEM.

PSD-95 levels were also studied in the hippocampus (**Figure 48.a**). However, no difference was observed between genotypes (**Figure 48.b**, n=4, t(6)=0.440; p = 0.338).

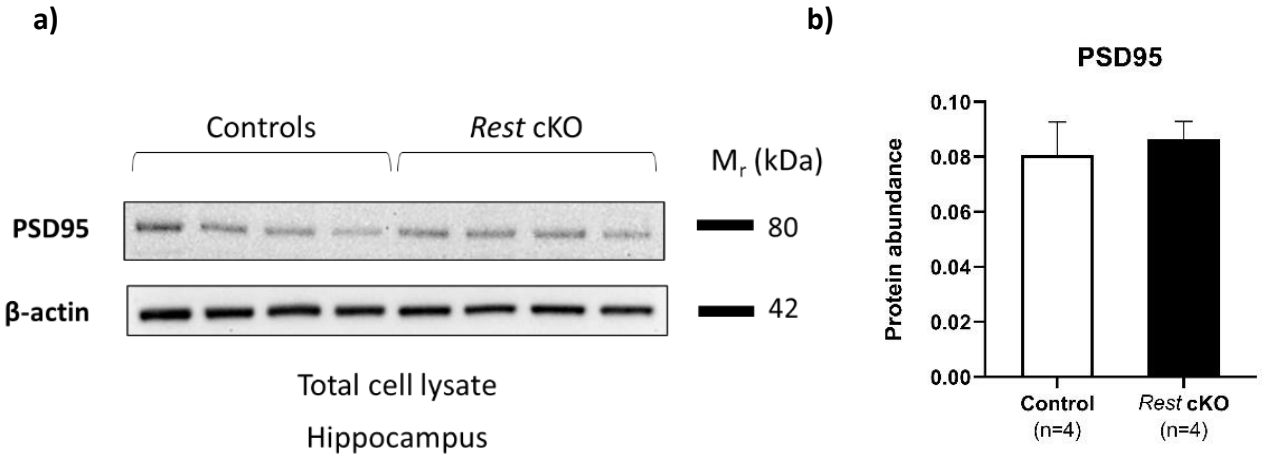

Figure 48. Levels of PSD-95 in total cell lysates from the hippocampus of four *Rest* cKO and four control mice. **a)** Western blot results. **b)** Quantitation of PSD-95 levels, after normalization with β-actin as loading control. Values are represented as mean ± SEM.

PSD-95 was also evaluated through immunohistochemistry (**Figure 49-51**). Three slides per mouse from three controls and three *Rest* cKO mice were used in this analysis. Due to the high density of the staining no quantification was possible. Hence, a qualitative analysis was performed. PSD-95 is localized in the postsynaptic density and is observed as puncta and lines. This is more easily observed in the CA1 and CA3, whereas the DG is harder to evaluate as no cell projections can be distinguishable.

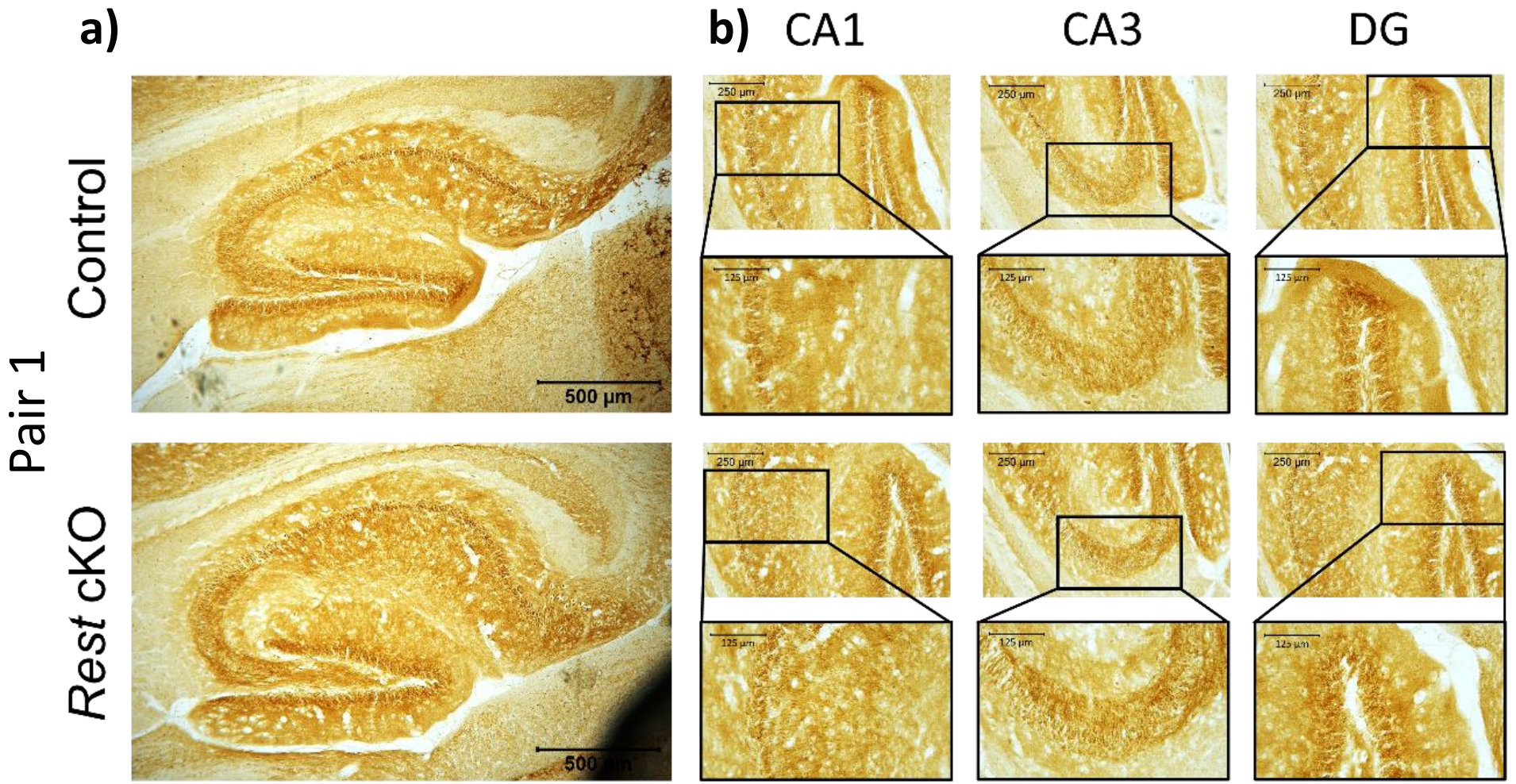

Figure 49. Representative images of equivalent slides using an antibody against PSD-95 using brain sections from the first mouse pair of *Rest* cKO and control mice. **a)** The whole hippocampus was imaged using a 5x magnification. **b)** A higher magnification, 10x, was used to analyse each different region of the hippocampus. These images were then further enlarged (20x) to allow a better visualization of the staining.

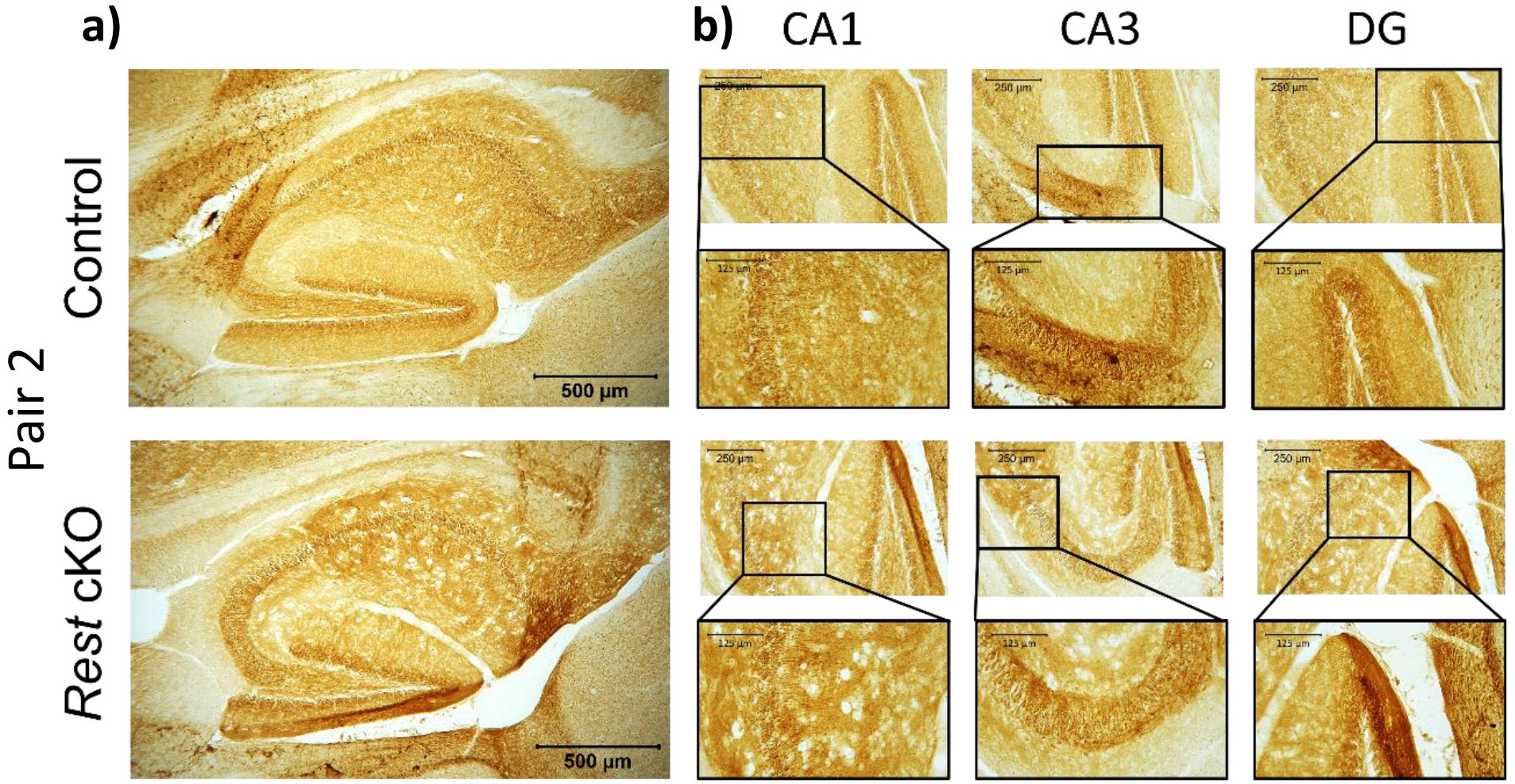

Figure 50. Representative images of equivalent slides using the antibody against PSD-95 using brain sections from the second mouse pair of *Rest* cKO and control mice. Figure layout is the same as in Figure 49.

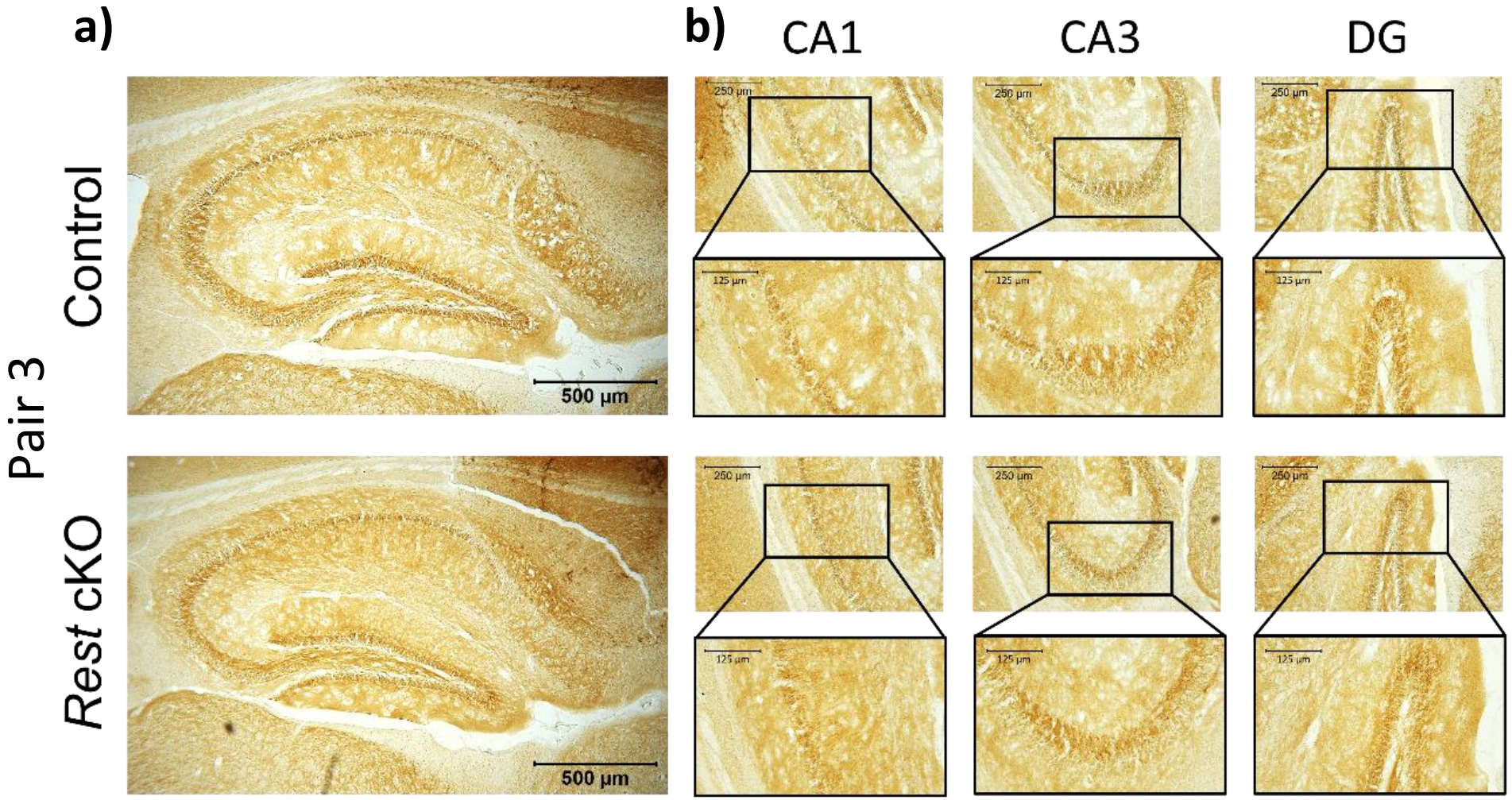

Figure 51. Representative images of equivalent slides using the antibody against PSD-95 using brain sections from the third mouse pair of *Rest* cKO and control mice. Figure layout is the same as in Figure 49.

In Pair 1, *Rest* cKO appears to have higher levels of PSD-95 in the CA1, i.e. darker cell projections and some synaptic puncta can also be observed on the pyramidal cell layer (**Figure 52**). The control also presents a lot of cell projections in the referred regions, but these are not so easily distinguishable since they are clearer. The other two pairs appear to show the reverse pattern, with controls displaying more and darker cell projections and postsynaptic densities when compared to *Rest* cKO, on the CA1 region of the hippocampus (**Figure 52**).

The cortex was very hard to evaluate since the tissue had a lot of holes, probably due to the process of antigen retrieval, which weakens the tissue making it more prone to degradation.

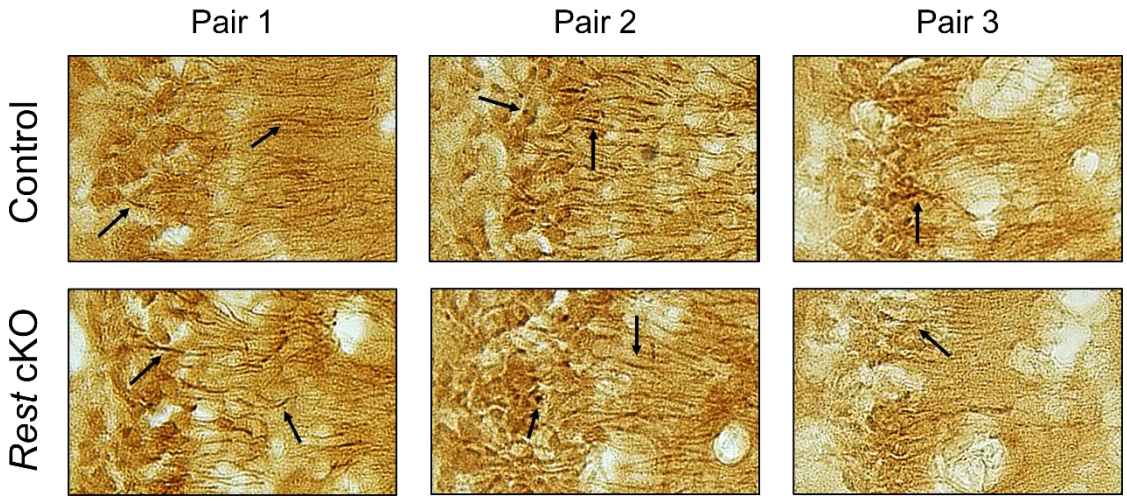

Figure 52. Representative images of the CA1 stained with an antibody against PSD-95. A 20x magnification was used to better examine the stain.

4.3.3.3. NMDA receptor – GluN2A/GluN2B switch

REST has been previously associated with the regulation of the switch between the NMDA receptor subunits GluN2B to GluN2A (Rodenas-Ruano et al., 2012). It is thought that this occurs because REST represses *Grin2b* gene which encodes GluN2B subunits. This project wondered if the postnatally inhibition of REST would affect the NMDA receptor subunits composition.

- **GluN2A**

There was no difference concerning GluN2A levels in cortical samples (**Figure 53**, n=8, t(14)=0.712; p=0.244) as revealed by Western blot.

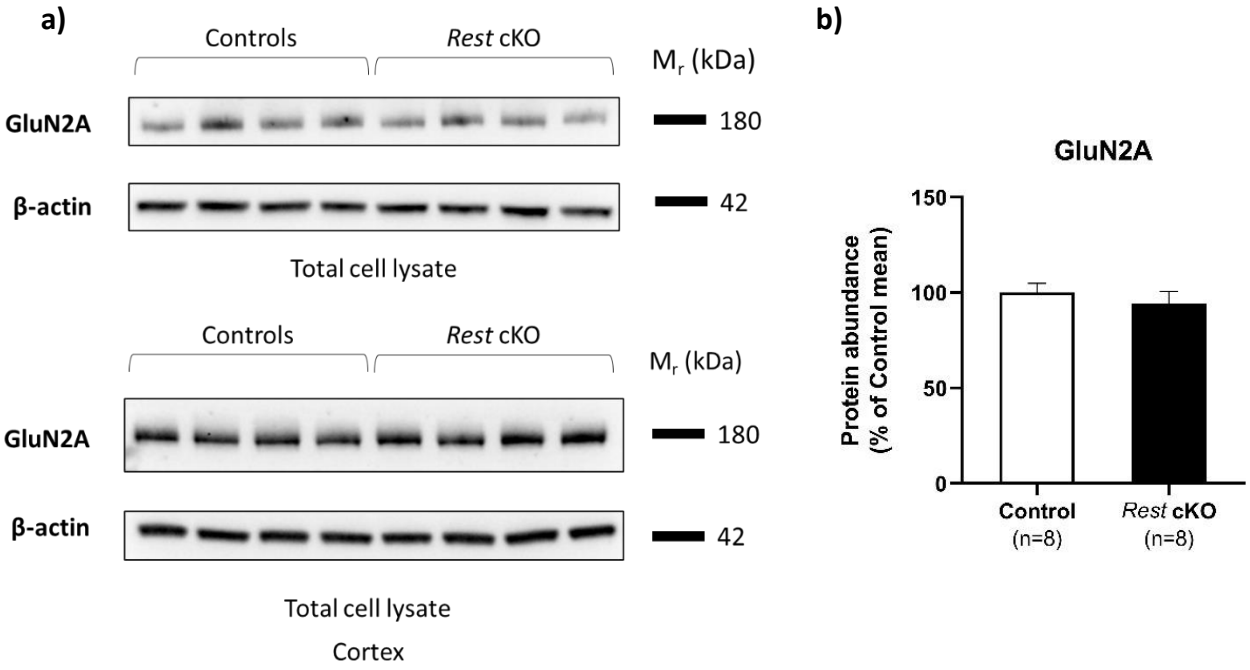

Figure 53. Levels of GluN2A in total cell lysates from the neocortex of eight *Rest* cKO and eight control mice. **a)** Western blot results. **b)** Quantitation of GluN2A levels, after normalization with β-actin as loading control. Values are represented as mean ± SEM.

The levels of GluN2A were also assessed in the hippocampus (**Figure 54**, n=4, t(6)=0.405; p=0.350) and similar levels were observed between genotypes.

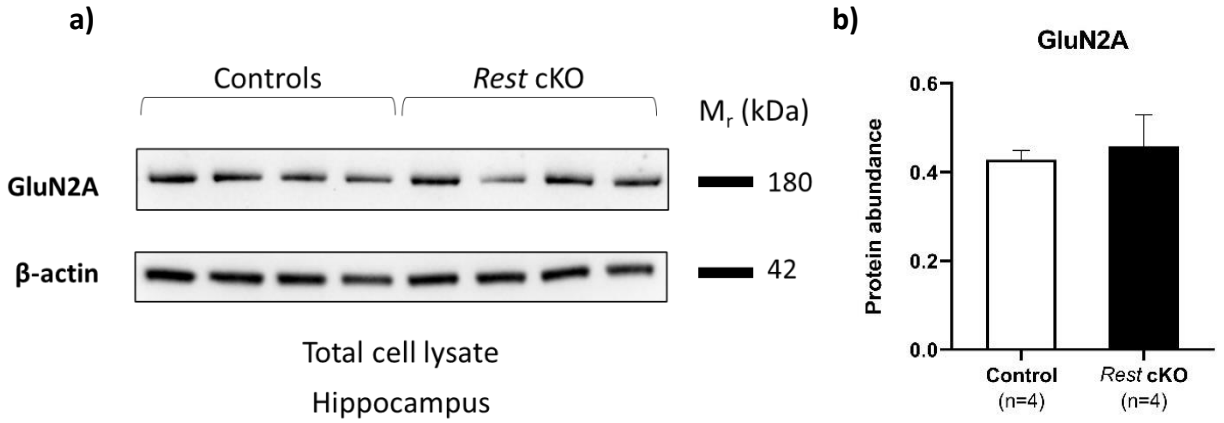

Figure 54. Levels of GluN2A in total cell lysate from the hippocampus of four *Rest* cKO and four control mice. **a)** Western blot results. **b)** Quantitation of GluN2A levels, after normalization with β-actin as loading control. Values are represented as mean ± SEM.

- **GluN2B**

Similar results were obtained for GluN2B, with no differences observed in this protein levels in cortical samples (**Figure 55**, n=4, t(6)=0.778; p=0.233).

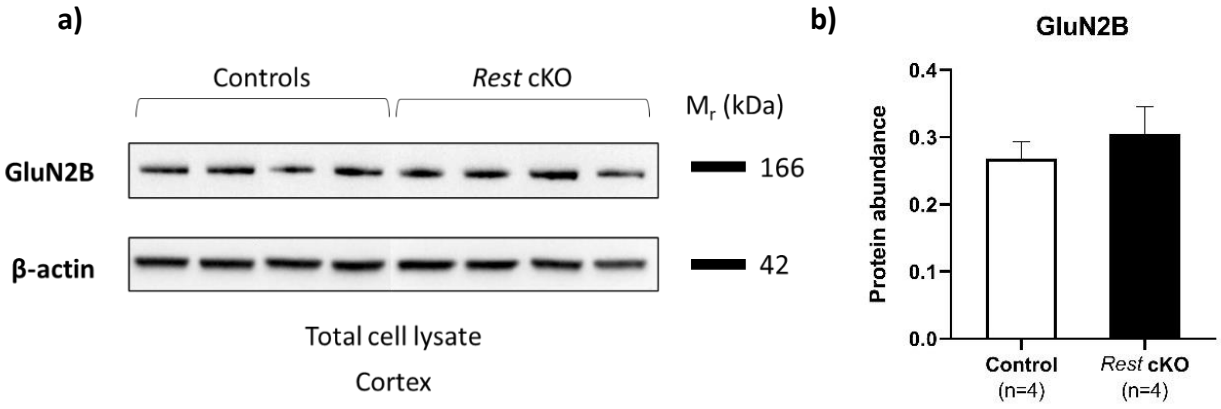

Figure 55. Levels of GluN2B in total cell lysates from the neocortex of four *Rest* cKO and four control mice. **a)** Western blot results. **b)** Quantitation of GluN2B levels, after normalization with β-actin as loading control. Values are represented as mean ± SEM.

GluN2B levels were also studied in the hippocampus (**Figure 56.a**). However, there was no difference between genotypes (**Figure 56.b** n=4, t(6)=0.672; p=0.264).

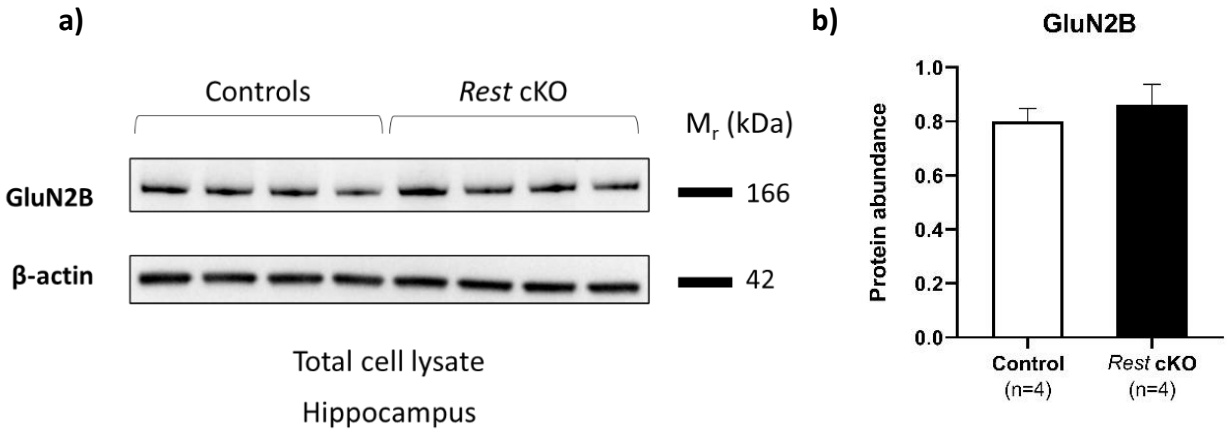

Figure 56. Levels of GluN2B in total cell lysates from the hippocampus of four *Rest* cKO and four control mice. **a)** Western blot results. **b)** Quantitation of GluN2B levels, after normalization with β-actin as loading control. Values are represented as mean ± SEM.

4.4. Astrocytic labelling

Astrocyte have an important role in the correct neuronal functioning in the brain. However, upon certain cellular insults, astrocytes can become reactive, contributing to neuroinflammation, which is another hallmark of AD. An antibody against GFAP, an astrocytic marker, was used to investigate astrocyte morphology in *Rest* cKO mice and to assess the possibility of altered astrocytic activation, which is associated with an increase in the number of protrusions, in a star-shaped form. Seven slides per mouse were used in this analysis of three pairs of mice (controls and *Rest* cKO).

Astrocytes were observed in the hippocampus (**Figure 57-59**) and the *corpus callosum* (**Figure 60**) of both genotypes. Whereas, the cortex of mice presented almost no astrocytes, in neither genotype. In the hippocampus, both genotypes present more astrocytes in the CA1 than in other hippocampal regions. In fact, there is a clear distinction between CA1 and CA3 (**Figure 61**). Although it is less pronounced in control mice, it is still visible.

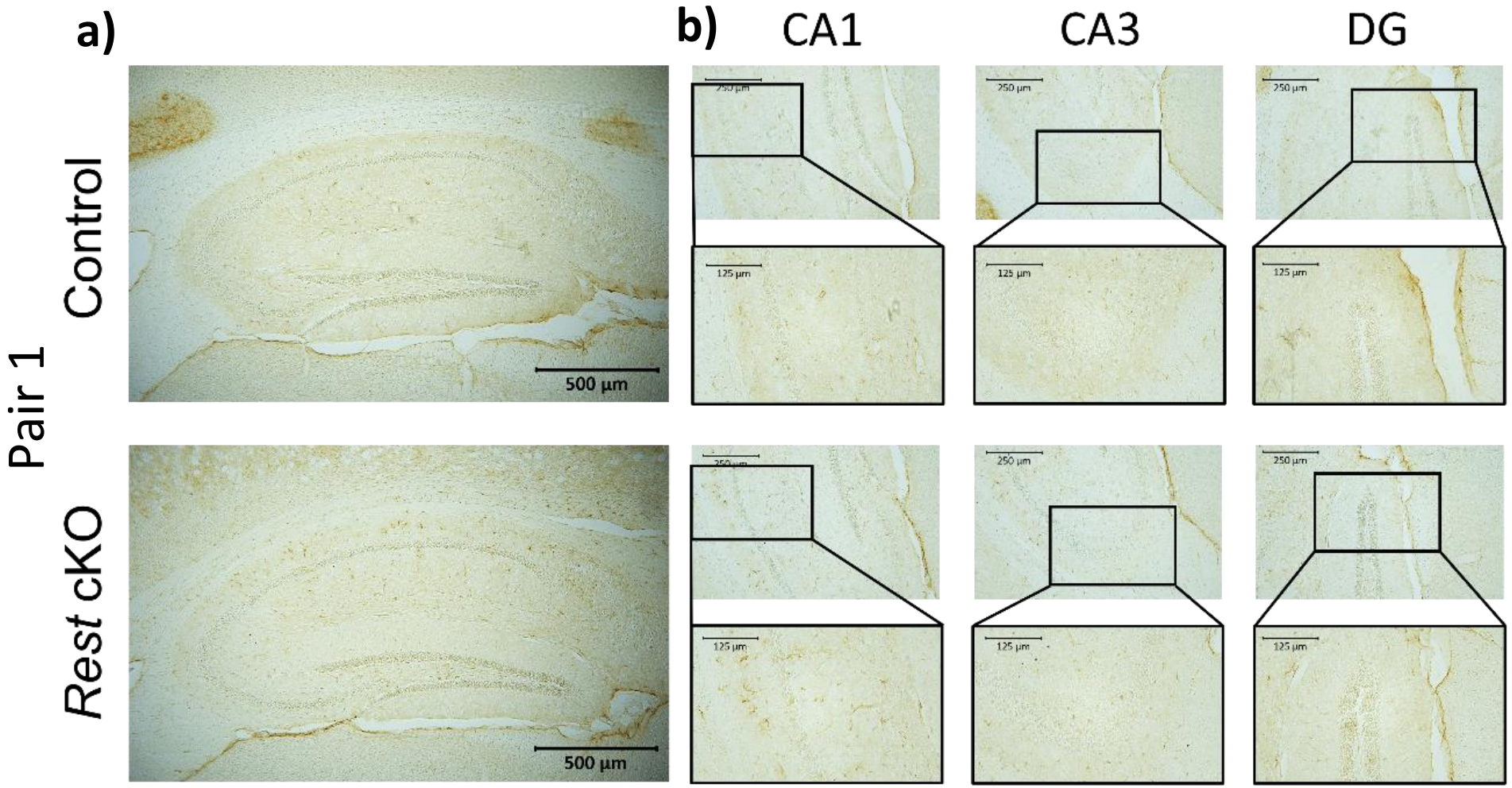

Figure 57. Representative images of equivalent slides using the antibody against GFAP using brain sections from the first mouse pair of *Rest* cKO and control mice. **a)** The whole hippocampus was imaged using a 5x magnification. **b)** A higher magnification, 10x, was used to analyse each different region of the hippocampus. These images were then further enlarged (20x) to allow a better visualization of the staining.

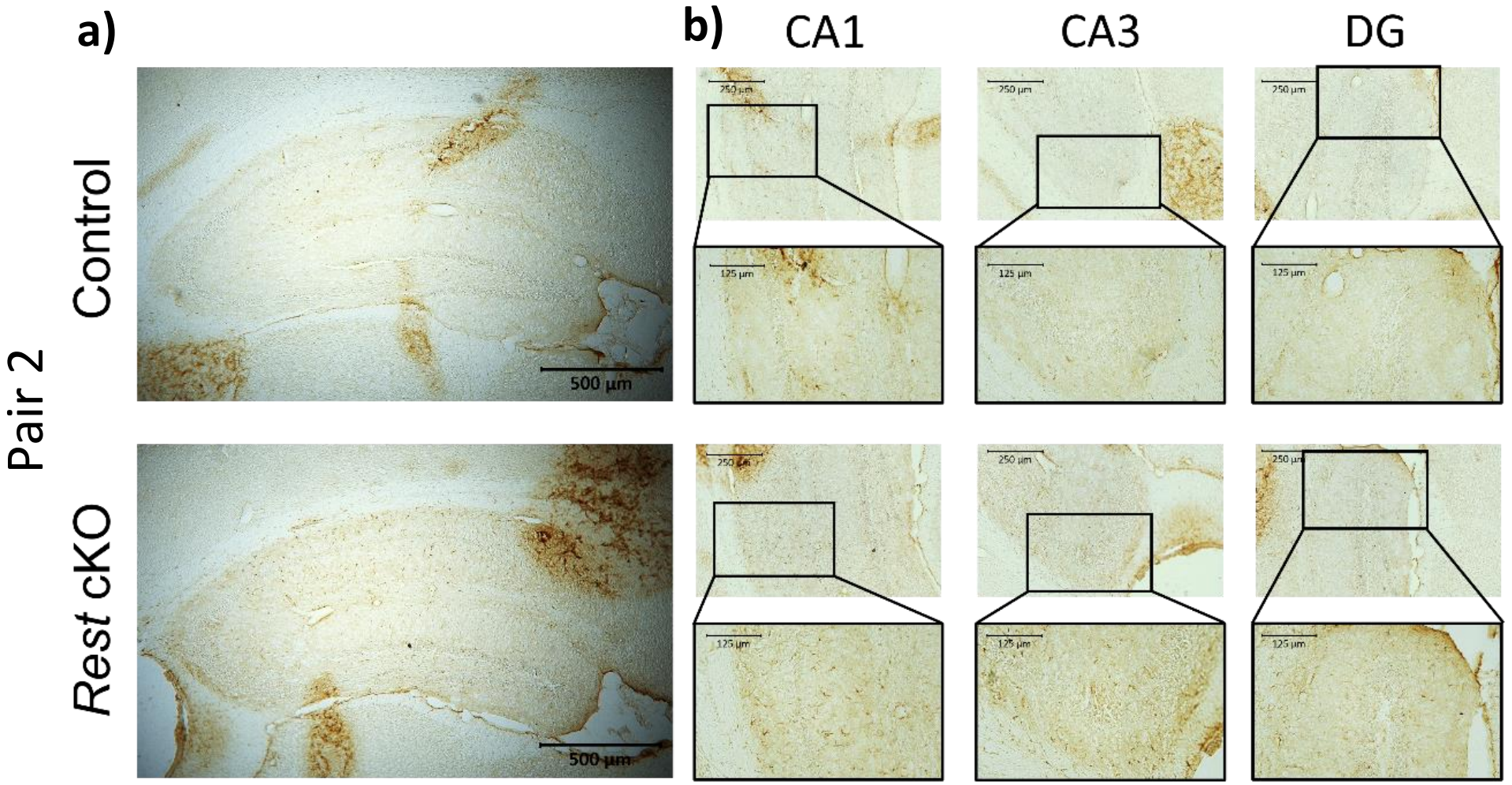

Figure 58. Representative images of equivalent slides using the antibody against GFAP using brain sections from the second mouse pair of *Rest* cKO and control mice. Figure layout is the same as in Figure 57.

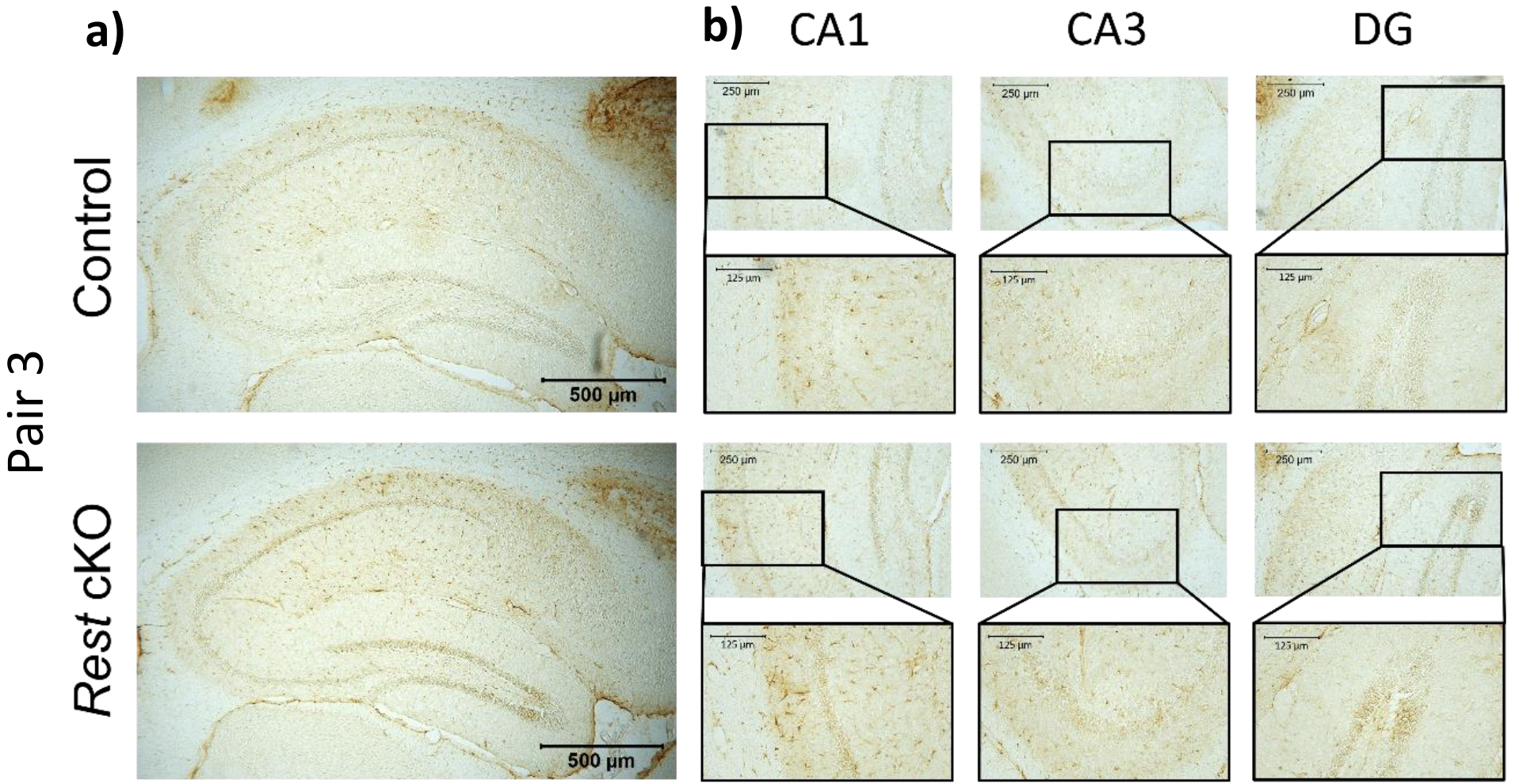

Figure 59. Representative images of equivalent slides using the antibody against GFAP using brain sections from the third mouse pair of *Rest* cKO and control mice. Figure layout is the same as in Figure 57.

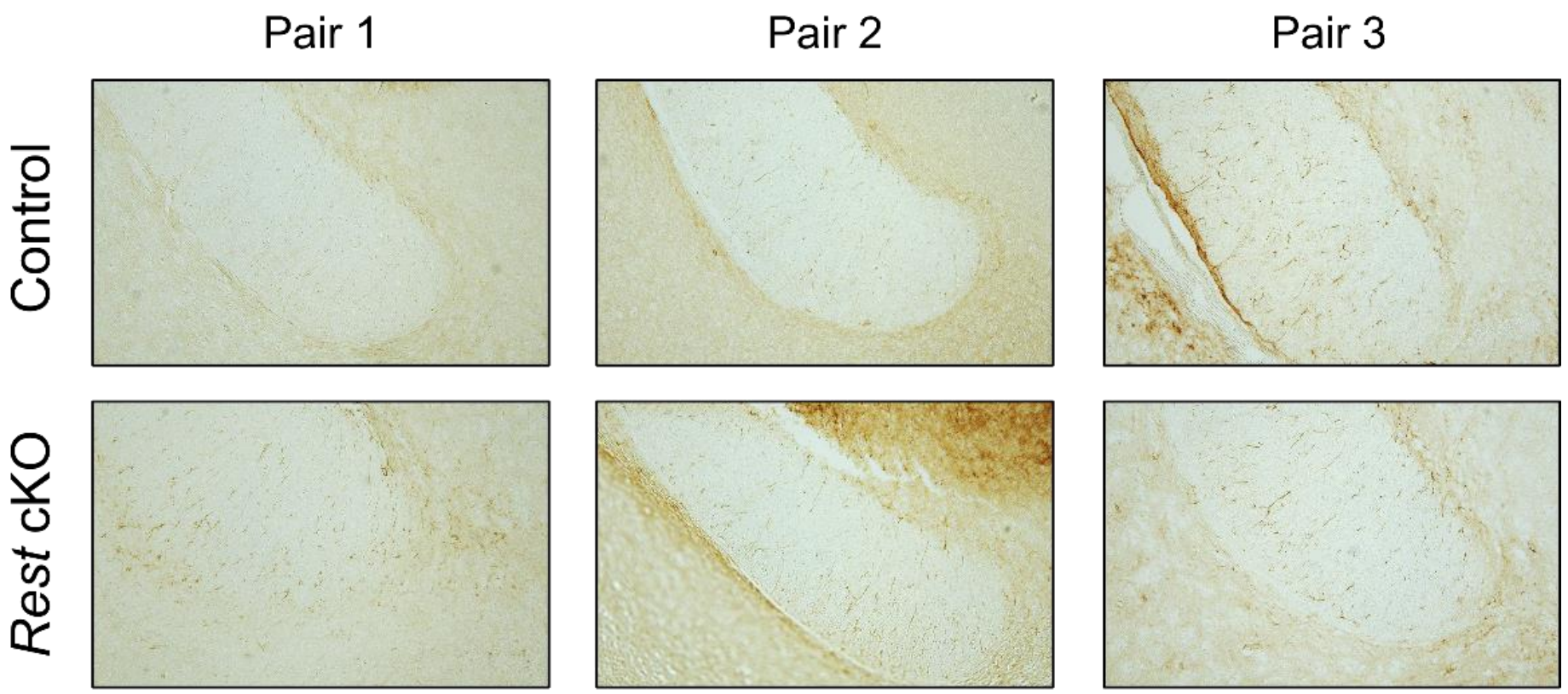

Figure 60. Representative images of GFAP in the *corpus callosum*. The 10x magnification was used to better analyse the stain.

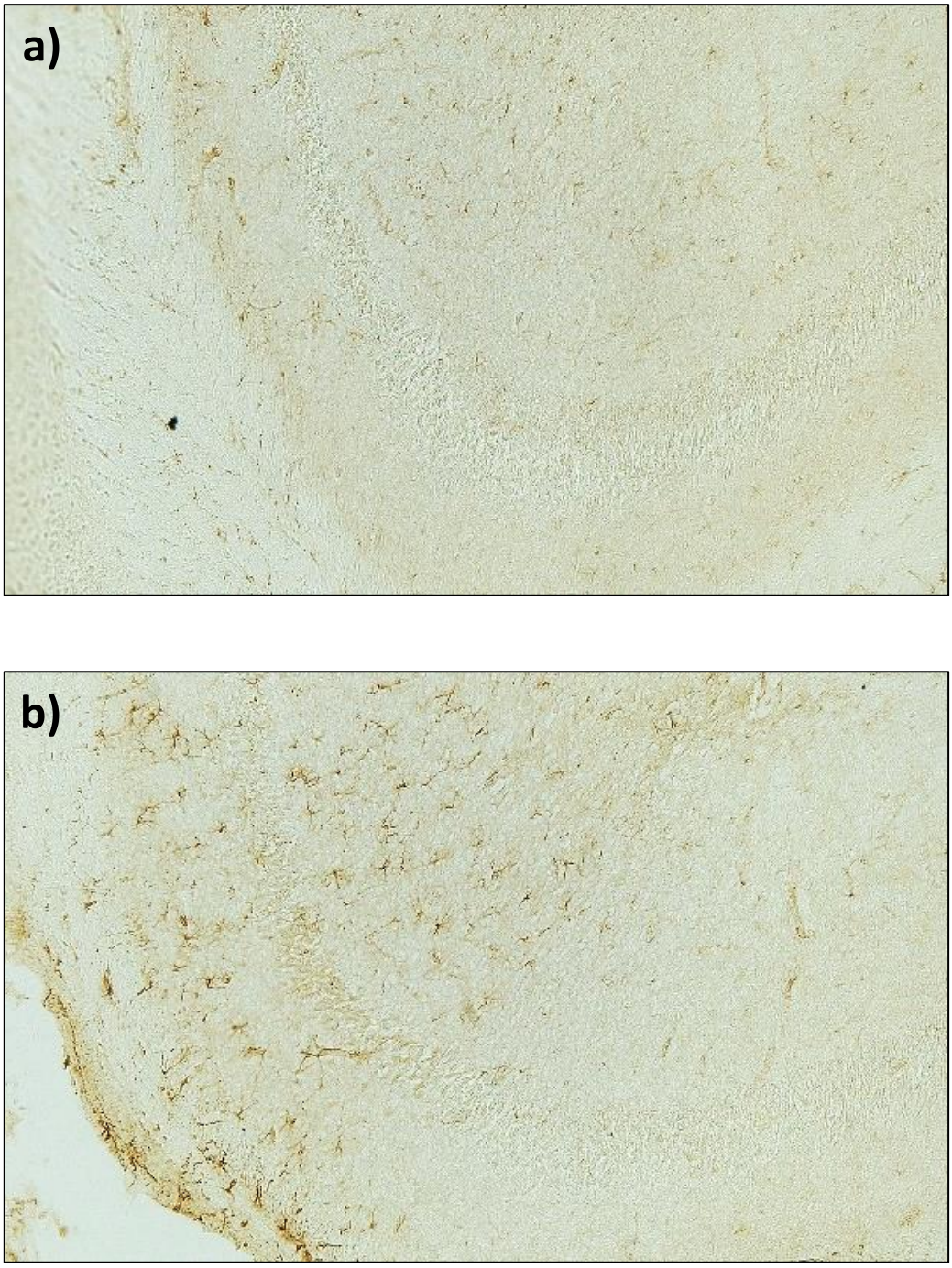

Figure 61. Representative images of the CA1 and CA3 region of the hippocampus of lateral slides of **a)** controls and **b)** *Rest* cKO mice labelled with antibody against GFAP.

The first pair of mice shows an apparent difference in the quantity of astrocytes, with *Rest* cKO mice presenting more than controls, but overall, i.e. considering all three pairs no major differences were observed regarding the number of cells.

On the other hand, when analysing the morphology of astrocytes it appears to be a difference between genotypes, with the astrocytes of *Rest* cKO displaying a higher degree of activation. Only the darker cells with 3 or more protrusions and in a star-shaped form were considered as activated astrocytes (indicated by the arrows in **Figure 62**). This difference is seen throughout the hemisphere but is more pronounced in the more lateral slides (**Figure 63**).

This data appears to indicate that *Rest* cKO presents a mild but clear astrocytic activation phenotype.

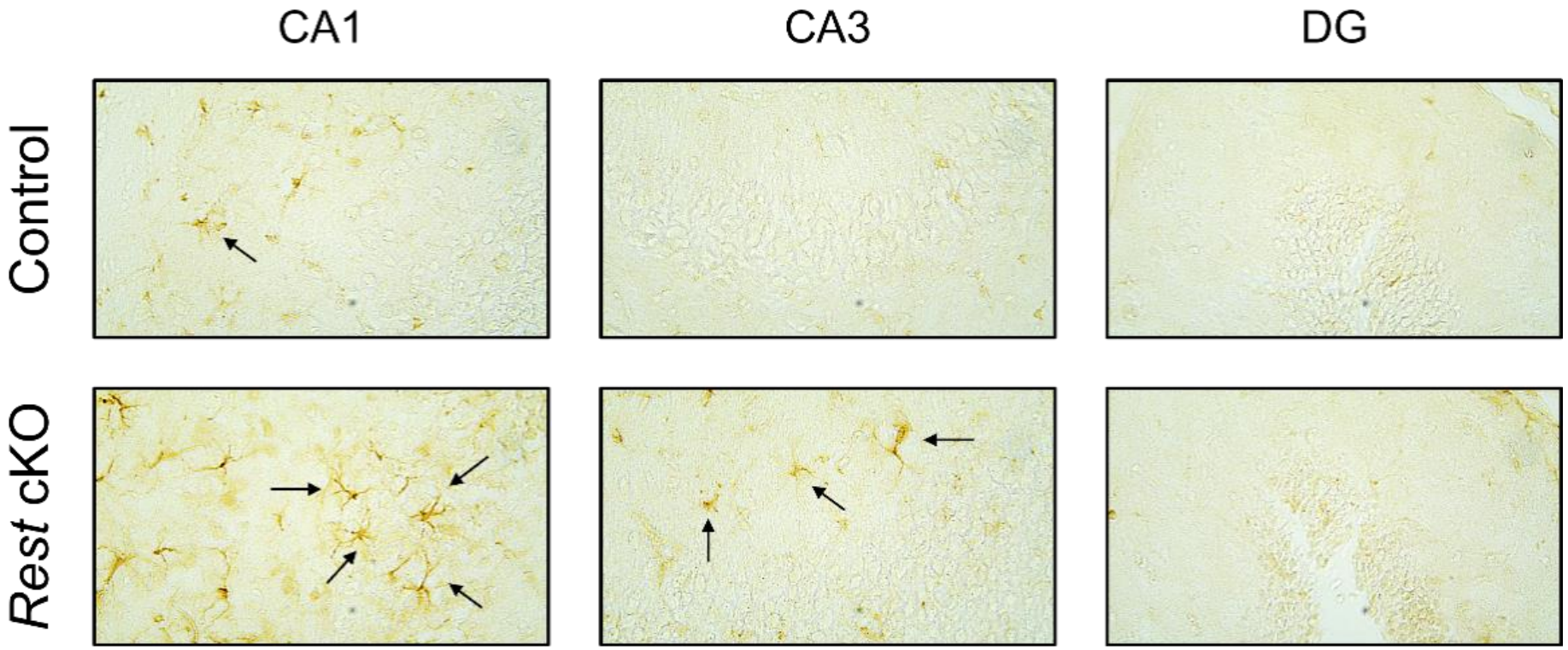

Figure 62. Representative images of astrocytes using a higher magnification. A 40x objective was used to further analyse each different region of the hippocampus and better representation of the activated astrocytes (indicated by the arrows).

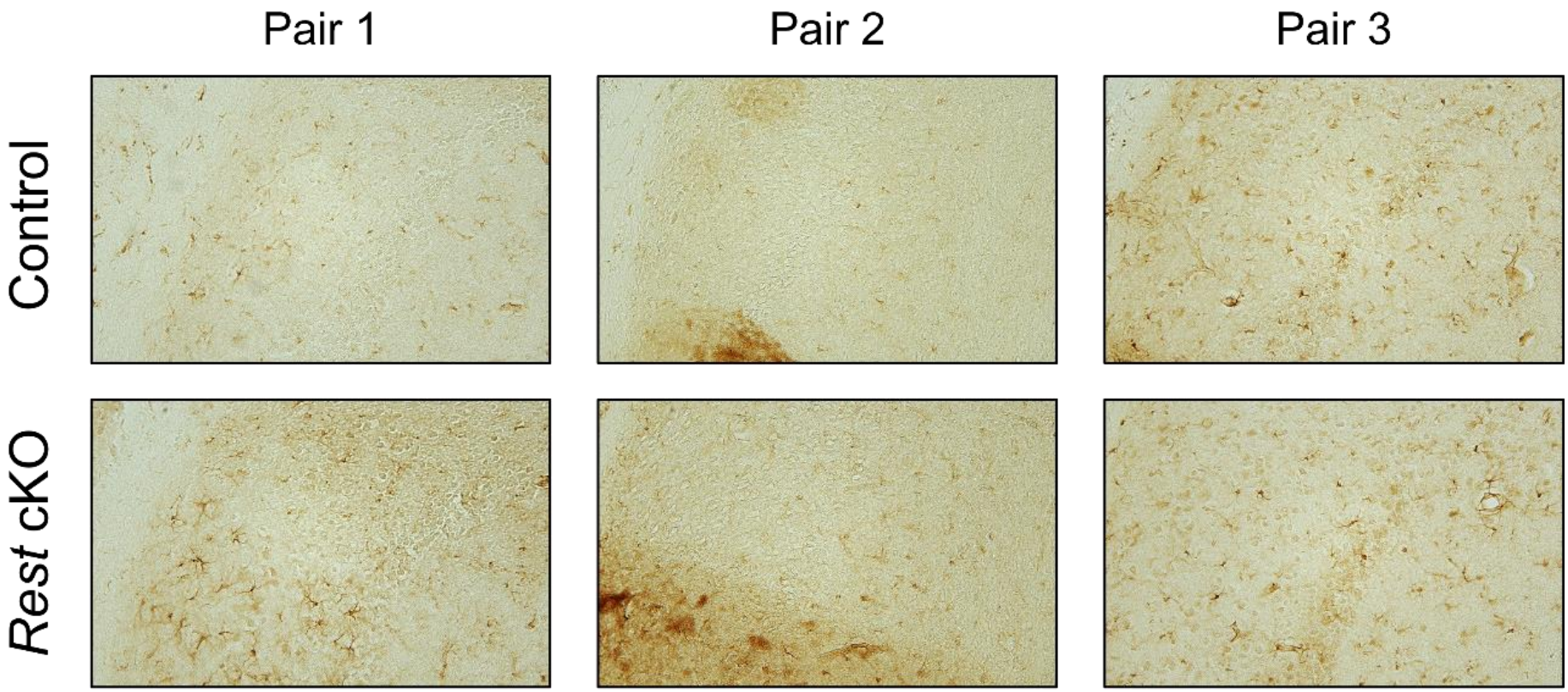

Figure 63. Representative images of the CA1 stained with an antibody against GFAP. A 20x magnification was used to better examine the astrocytes observed with smaller magnifications. Astrocytes in *Rest* cKO appear to be more activated, with the difference between genotypes being clearer in Pair 1.

Cortical samples of both genotypes were analysed through Western blot using the same antibody against GFAP (**Figure 64**). Although there is a slight decrease in the levels of GFAP in *Rest* cKO mice, there were no significant differences between genotypes (n=8, t(14)=0,5960; p=0.280).

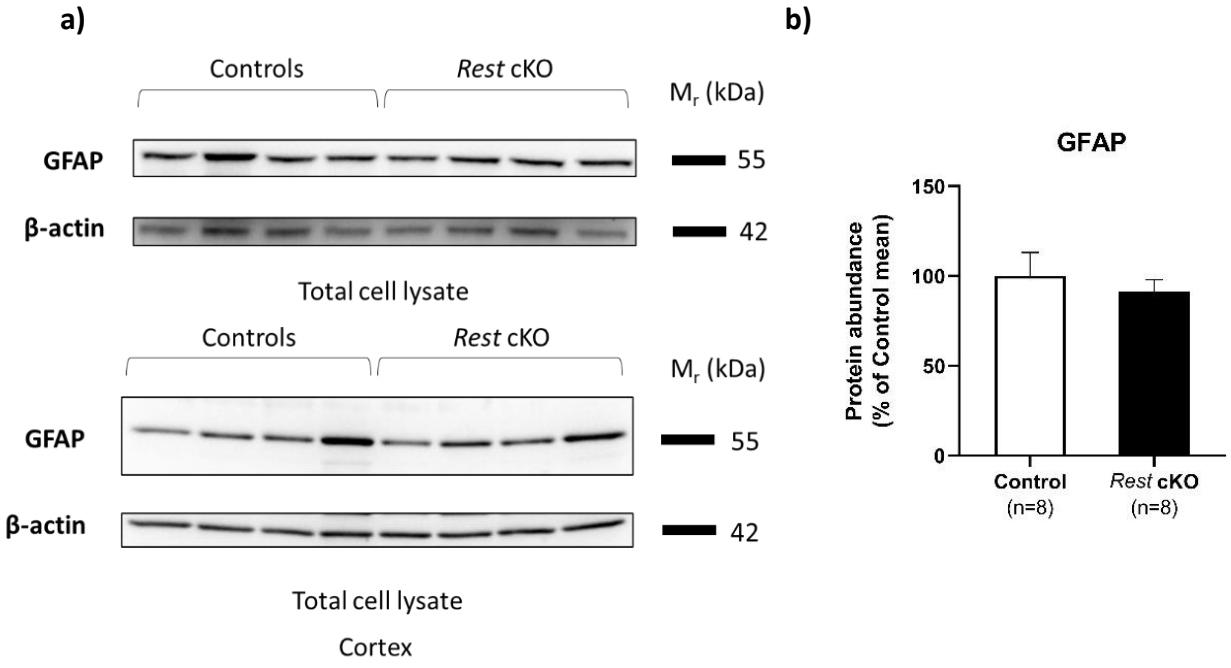

Figure 64. Levels of GFAP in total cell lysates from the neocortex of eight *Rest* cKO and eight control mice. **a)** Representative Western blot. **b)** Quantitation of GFAP levels, after normalization with β-actin as loading control. Values are represented as mean ± SEM.

Hippocampal samples were also evaluated, and no difference was observed between controls and *Rest* cKO mice (**Figure 65**, n=4, t(6)=0,160; p=0.439).

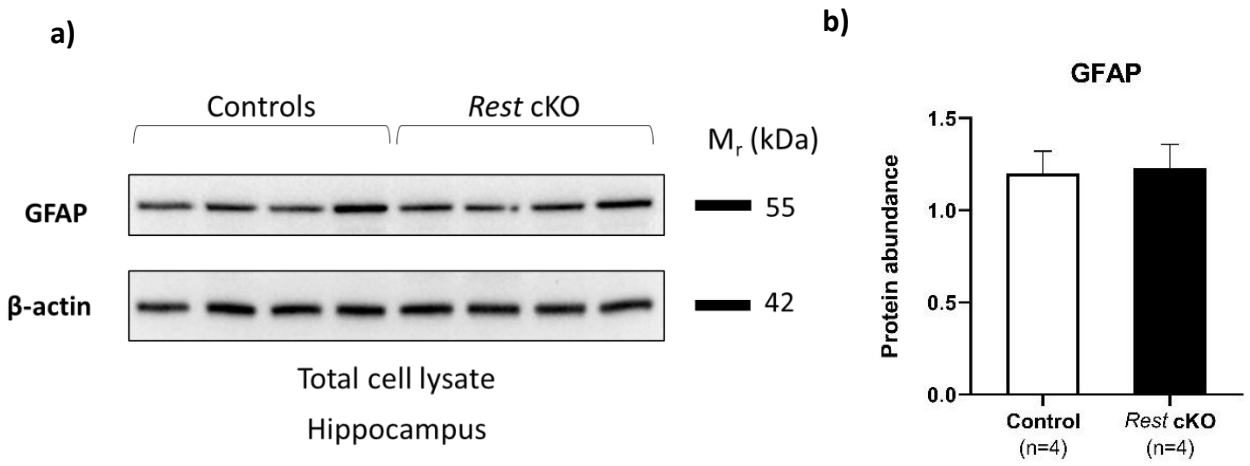

Figure 65. Levels of GFAP in total cell lysates from the hippocampus of four *Rest* cKO and four control mice. **a)** Representative Western blot. **b)** Quantitation of GFAP levels, after normalization with β-actin as loading control. Values are represented as mean ± SEM.

4.5. Analysis of bioinformatics-processed RNA-Seq data

To better understand the molecular mechanisms and pathways involved in the *Rest* cKO phenotypes and given that REST is a transcriptional factor, which regulates a vast number of genes, it is of the utmost importance to analyse global gene expression – the transcriptome – in both *Rest* cKO and control mice.

The differential gene expression analysis, using RNA from the neocortex of four *Rest* cKO and four control mice was performed by two methods described in **Section 3.7.**

4.5.1. Differential gene expression analysis by method 1

This initial analysis was performed by our collaborator Dr Celine Keime using the Wald statistical test with the Benjamini and Hochberg method to adjust the p-values for multiple testing. The primary bioinformatics analysis presented the fold-change results regarding the control group of mice, i.e. the quantification of each transcript in controls was divided by the quantification in *Rest* cKO mice. Therefore, a positive log2FC value

corresponded to a downregulation of the gene in *Rest* cKO mice. Curiously, only three genes were observed to be significantly differentially expressed between genotypes (**Figure 66**). Genes *Oxr1* and *Pop4* were found to be downregulated in *Rest* cKO, whereas *Slc2a1* was upregulated. Interestingly, in another project in our group, examining the transcriptome in the hippocampus (as opposed to the neocortex) of *Rest* cKO and control mice, O*xr1* was also found to be downregulated in *Rest* cKO mice (data not shown).

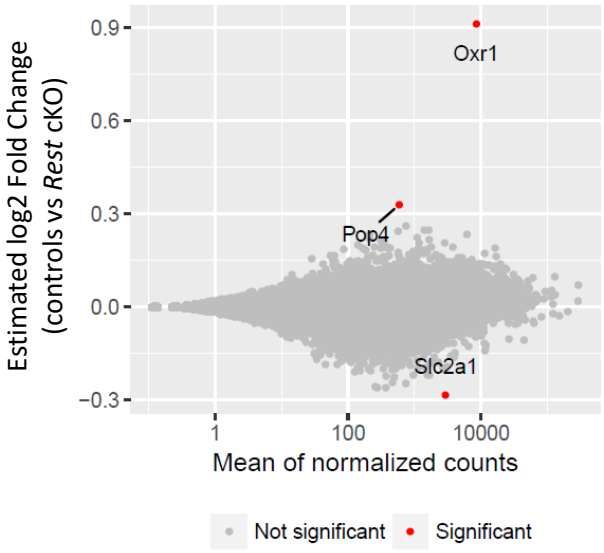

Figure 66. Differential gene expression comparison between genotypes. MA-plot of the log2FC changes (M) versus the average of normalized counts (A). Genes represented in red dots are differentially expressed in control genotype when compared with *Rest* cKO. Thus, a positive log2FC value means that the gene is downregulated in *Rest* cKO mice, i.e. is more expressed in the control than in the *Rest* cKO (False Discovery Rate < 0.05). This analysis was performed by Dr Celine Keime.

4.5.2. Differential gene expression analysis by method 2

Although the Benjamini and Hochberg method is a widely accepted approach to control false discovery rate, many researchers do not agree with the principle of this method (Rothman, 1990; Althouse, 2016), and there is a widespread belief that in addition to removing false positives, the Benjamini and Hochberg method also removes

some true positives. Therefore, in addition to using this method, RNA-seq data in this project were also analysed without this method, to obtain a broader view of the results, keeping in mind that some false positives are likely to be present in the results. Therefore, the second method applied to analyse the RNA-seq data did not involve adjusting the p-values with the Benjamini and Hochberg method. A total of 552 genes were found to be significantly differentially expressed, with Wald p-value < 0.05: 287 genes were downregulated and 265 were upregulated in *Rest* cKO mice (**Appendix 4.1 and 4.2**). These lists of up- and downregulated genes were then used for GOE analysis**,** and the functional enrichment in the PPI network.

The differentially expressed genes were also compared with previous literature to assess if they contain REST binding sites. Of the 552 differentially expressed genes in our samples, 75 (48 downregulated and 27 upregulated) have been identified as REST-binding genes in mouse embryonic stem cells (Rockowitz and Zheng, 2015). However, when compared with hippocampal samples from 5-week-old mice, REST appears to only bind to three (two downregulated and one upregulated) of the 552 differentially expressed genes (McGann et al., 2021).

4.5.3. Gene ontology enrichment analysis

The GOE analysis was performed to interpret the biological significance of the differentially expressed genes in *Rest* cKO mice. More specifically, it aims to identify what biological processes, molecular functions and cellular locations are likely to be affected by the absence of REST in the neocortex. These three aspects of gene ontology framework were analysed individually for the up- and downregulated genes, in separate. This was done through the PANTHER Overrepresentation Test, where statistical analysis and significance of gene enrichment were calculated by Fisher's exact test with an FDR < 0.05.

4.5.3.1. Upregulated genes

- **Biological Process**

The 265 upregulated genes revealed a significant enrichment in 13 root ontology terms associated mainly with immune response and angiogenesis (**Table 3**; for the complete table with root and subsequent terms, please refer to **Appendix 4.3**). More specifically, *Rest* cKO appears to have an upregulation of inflammatory response, interleukin-15 signally pathway and production of cytokines. Furthermore, data indicates that angiogenesis is increased in *Rest* CKO mice with higher vasculature development, particularly blood vessels.

Table 3. List of significant gene ontology enrichment in biological process aspect in upregulated genes in *Rest* cKO mice. Short list with only the root terms, as opposed to the complete version in the **Appendix 4.3**. The most interesting terms are highlighted.

	Mus musculus (REF)	upload_1 (▽ Hierarchy NEW!)					
GO biological process complete	#	#	expected	Fold Enrichment	+/-	raw P value	FDR
interleukin-15-mediated signaling pathway	6	3	.06	48.67	+	8.33E-05	4.53E-02
positive regulation of angiogenesis	176	10	1.81	5.53	+	2.18E-05	2.64E-02
regulation of endothelial cell migration	174	9	1.79	5.03	+	1.12E-04	4.51E-02
positive regulation of cell adhesion	512	19	5.26	3.61	+	2.33E-06	4.60E-03
positive regulation of response to external stimulus	458	16	4.71	3.40	+	3.04E-05	2.82E-02
positive regulation of cell migration	578	20	5.94	3.37	+	3.48E-06	6.10E-03
blood vessel morphogenesis	447	15	4.59	3.27	+	8.35E-05	4.39E-02
inflammatory response	512	17	5.26	3.23	+	3.19E-05	2.79E-02
regulation of cytokine production	780	22	8.01	2.75	+	2.54E-05	2.67E-02
positive regulation of immune system process	1123	27	11.54	2.34	+	5.20E-05	3.41E-02
regulation of protein modification process	1586	34	16.29	2.09	+	5.06E-05	3.47E-02
response to other organism	1513	32	15.54	2.06	+	1.11E-04	4.71E-02
sensory perception of chemical stimulus	1235	1	12.69	.08	-	5.66E-05	3.57E-02

- **Molecular Function**

Regarding the molecular function, upregulated genes seem to be associated with an enrichment in gene ontology terms related with structural integrity of the extracellular matrix, protein binding and olfactory receptor activity (**Table 4**).

Table 4. List of significant gene ontology enrichment in molecular function aspect in upregulated genes in *Rest* cKO mice. The most interesting term is highlighted.

	Mus musculus (REF)	upload_1 (▽ Hierarchy NEW!)					
GO molecular function complete	#	#	expected	Fold Enrichment	+/-	raw P value	FDR
extracellular matrix structural constituent	150	10	1.54	6.49	+	5.84E-06	9.42E-03
protein binding	9570	137	98.32	1.39	+	3.39E-07	8.19E-04
↳binding	14027	180	144.12	1.25	+	2.98E-07	1.44E-03
olfactory receptor activity	1149	0	11.80	< 0.01	-	1.19E-05	1.44E-02

- **Cellular component**

In the cellular component aspect, only one gene ontology term was statistically significantly enriched, cell surface (**Table 5**).

Table 5. List of significant gene ontology enrichment in cellular component aspect in upregulated genes in *Rest* cKO mice.

	Mus musculus (REF)	upload_1 (▽ Hierarchy NEW!)					
GO cellular component complete	#	#	expected	Fold Enrichment	+/-	raw P value	FDR
cell surface	1242	31	12.76	2.43	+	7.35E-06	1.50E-02

4.5.3.2. Downregulated genes

- **Biological Process**

Data from 287 downregulated genes revealed a strong enrichment in 40 root ontology terms (**Table 6**, for the complete table with root and subsequent terms, please refer to **Appendix 4.4**). *Rest* cKO appears to have multiple biological processes associated with neuronal structure/morphology and neuronal pathways affected. Forebrain neuron differentiation, dendrite morphogenesis and regulation of axonogenesis are some of the biological processes more affected in mice that lack REST. Neuronal pathways are also impacted by the absence of REST, with glutamate receptor

signalling pathway, positive regulation of synaptic transmission and negative regulation of neuron apoptotic process terms showing to be statistically significant enriched in the downregulated genes. Positive regulation of transcription by RNA polymerase II is the root term with more subsequent terms.

Table 6. List of significant gene ontology enrichment in biological processes aspect in downregulated genes in *Rest* cKO mice. Short list with only the root terms, as opposed to the complete version in the **Appendix 4.4**. The most interesting terms are highlighted.

	Mus musculus (REF)		upload_1 (▿ Hierarchy NEW!)				
GO biological process complete	#	#	expected	Fold Enrichment	+/-	raw P value	FDR
regulation of axon diameter	6	3	.07	42.96	+	1.20E-04	1.53E-02
intermediate filament bundle assembly	7	3	.08	36.83	+	1.70E-04	1.93E-02
regulation of postsynaptic density assembly	14	4	.16	24.55	+	4.61E-05	6.92E-03
glutamate receptor signaling pathway	40	6	.47	12.89	+	1.39E-05	2.64E-03
positive regulation of cardiac muscle tissue growth	46	5	.54	9.34	+	2.96E-04	3.11E-02
forebrain neuron differentiation	46	5	.54	9.34	+	2.96E-04	3.09E-02
tissue regeneration	53	5	.62	8.11	+	5.40E-04	4.89E-02
positive regulation of axonogenesis	98	9	1.14	7.89	+	4.12E-06	1.08E-03
dendrite morphogenesis	80	7	.93	7.52	+	6.56E-05	9.23E-03
positive regulation of protein localization to cell periphery	69	6	.80	7.47	+	2.27E-04	2.48E-02
osteoblast differentiation	107	9	1.25	7.23	+	8.01E-06	1.75E-03
chondrocyte differentiation	90	7	1.05	6.68	+	1.31E-04	1.59E-02
positive regulation of synapse assembly	80	6	.93	6.44	+	4.76E-04	4.44E-02
potassium ion transmembrane transport	146	10	1.70	5.89	+	1.37E-05	2.64E-03
positive regulation of synaptic transmission	169	9	1.97	4.58	+	2.28E-04	2.48E-02
negative regulation of neuron apoptotic process	194	10	2.26	4.43	+	1.33E-04	1.59E-02
stem cell differentiation	199	10	2.32	4.32	+	1.62E-04	1.85E-02
regulation of neuron differentiation	233	11	2.71	4.06	+	1.30E-04	1.59E-02
regulation of nervous system process	191	9	2.22	4.05	+	5.36E-04	4.89E-02
rhythmic process	263	12	3.06	3.92	+	8.82E-05	1.16E-02
positive regulation of neuron projection development	223	10	2.60	3.85	+	3.87E-04	3.72E-02
synapse organization	315	14	3.67	3.82	+	3.03E-05	4.77E-03
learning or memory	319	13	3.71	3.50	+	1.34E-04	1.59E-02
regulation of membrane potential	467	17	5.43	3.13	+	4.99E-05	7.28E-03
regulation of ion transmembrane transport	525	19	6.11	3.11	+	1.94E-05	3.43E-03
cellular chemical homeostasis	518	18	6.03	2.99	+	5.35E-05	7.74E-03
heart development	577	19	6.72	2.83	+	6.64E-05	9.26E-03
tube morphogenesis	746	22	8.68	2.53	+	8.59E-05	1.15E-02
negative regulation of cell differentiation	714	21	8.31	2.53	+	1.29E-04	1.59E-02
cell-cell signaling	894	25	10.40	2.40	+	8.37E-05	1.13E-02
animal organ morphogenesis	1057	29	12.30	2.36	+	2.54E-05	4.18E-03
positive regulation of transcription by RNA polymerase II	1249	34	14.54	2.34	+	5.23E-06	1.29E-03
cellular response to endogenous stimulus	931	25	10.83	2.31	+	1.32E-04	1.59E-02
negative regulation of protein metabolic process	1057	27	12.30	2.19	+	1.79E-04	2.00E-02
epithelium development	1161	29	13.51	2.15	+	1.27E-04	1.60E-02
embryo development	1231	30	14.33	2.09	+	1.75E-04	1.97E-02
negative regulation of macromolecule biosynthetic process	1462	33	17.01	1.94	+	3.48E-04	3.45E-02
negative regulation of cellular metabolic process	2205	47	25.66	1.83	+	5.94E-05	8.52E-03
cellular response to organic substance	1903	40	22.15	1.81	+	3.10E-04	3.19E-02
regulation of signal transduction	2924	59	34.03	1.73	+	2.66E-05	4.28E-03
sensory perception of smell	1133	1	13.19	.08	-	4.06E-05	6.22E-03

- **Molecular function**

In the molecular function aspect, voltage-gated potassium channel activity and binding of proteins such as RNA polymerase II cis-regulatory region sequence-specific DNA, chromatin and metal ions appear to be altered in the *Rest* cKO mice (**Table 7**, for the complete table with root and subsequent terms, please refer to **Appendix 4.5**).

Table 7. List of significant gene ontology enrichment in molecular function aspect in downregulated genes in *Rest* cKO mice. Short list with only the root terms, as opposed to the complete version in the **Appendix 4.5**. The most interesting terms are highlighted.

	Mus musculus (REF)	upload_1 (▽ Hierarchy NEW! ⓘ)					
GO molecular function complete	#	#	expected	Fold Enrichment	+/-	raw P value	FDR
voltage-gated potassium channel activity	95	7	1.11	6.33	+	1.79E-04	2.89E-02
chromatin binding	651	20	7.58	2.64	+	1.07E-04	2.07E-02
RNA polymerase II cis-regulatory region sequence-specific DNA binding	1143	35	13.30	2.63	+	2.61E-07	3.16E-04
DNA-binding transcription factor activity, RNA polymerase II-specific	1288	34	14.99	2.27	+	1.19E-05	3.60E-03
metal ion binding	3593	73	41.82	1.75	+	1.08E-06	4.76E-04
protein binding	9570	147	111.38	1.32	+	1.09E-05	3.52E-03
olfactory receptor activity	1149	0	13.37	< 0.01	-	2.44E-06	9.07E-04

- **Cellular component**

Regarding the cellular component aspect, downregulated genes seem to be strongly associated with changes in the synapses, as 12 of the 16 root terms statistically significant enriched are associated with different types and parts of synapses (**Table 8**, for the complete table with root and subsequent terms, please refer to **Appendix 4.6**).

Table 8. List of significant gene ontology enrichment in cellular component aspect in downregulated genes in *Rest* cKO mice. Short list with only the root terms, as opposed to the complete version in the **Appendix 4.6**. The most interesting terms are highlighted.

	Mus musculus (REF)	upload_1 (▽ Hierarchy NEW!)					
GO cellular component complete	#	#	expected	Fold Enrichment	+/-	raw P value	FDR
presynaptic intermediate filament cytoskeleton	2	2	.02	85.93	+	7.79E-04	3.88E-02
messenger ribonucleoprotein complex	15	4	.17	22.91	+	5.79E-05	5.37E-03
presynaptic cytosol	25	4	.29	13.75	+	3.24E-04	2.00E-02
hippocampal mossy fiber to CA3 synapse	49	5	.57	8.77	+	3.87E-04	2.32E-02
excitatory synapse	79	7	.92	7.61	+	6.09E-05	5.18E-03
GABA-ergic synapse	108	8	1.26	6.36	+	5.99E-05	5.31E-03
potassium channel complex	90	6	1.05	5.73	+	8.54E-04	4.15E-02
Schaffer collateral - CA1 synapse	115	7	1.34	5.23	+	5.35E-04	2.87E-02
growth cone	199	12	2.32	5.18	+	6.50E-06	8.84E-04
axon terminus	194	9	2.26	3.99	+	5.97E-04	3.12E-02
neuronal cell body	734	32	8.54	3.75	+	3.15E-10	1.61E-07
glutamatergic synapse	517	21	6.02	3.49	+	1.24E-06	1.81E-04
postsynaptic density	394	16	4.59	3.49	+	2.38E-05	2.31E-03
dendrite	740	30	8.61	3.48	+	5.92E-09	2.01E-06
intrinsic component of plasma membrane	1822	37	21.20	1.74	+	9.23E-04	4.38E-02
nucleus	7212	111	83.93	1.32	+	4.82E-04	2.81E-02

4.5.4. Protein-protein interaction network and functional enrichment analysis

The differentially expressed genes in *Rest* cKO mice were used to create PPI networks to better understand the functional and physical associations between proteins. Functional enrichment analysis of the network was done regarding the three aspects of gene ontology framework previously mentioned, biological processes, molecular function and cellular components. The confidence score, i.e. the probability that a predicted connection exists between two proteins in the same map in the Kyoto Encyclopaedia of Genes and Genomes (KEGG) database, was set to 'high'. This means that the minimum required interaction score was 0.7.

The network is composed by nodes, which represent proteins, and edges (lines that connect the node). Edges are colour coded depending on the type of interaction, i.e. if it is known or if it is a predicted interaction or other types. Proteins that are not associated with other proteins (i.e. disconnected nodes) where not displayed in the network. The size of the edges (distance between nodes) is not related with the strength of the association between proteins.

4.5.4.1. Upregulated genes

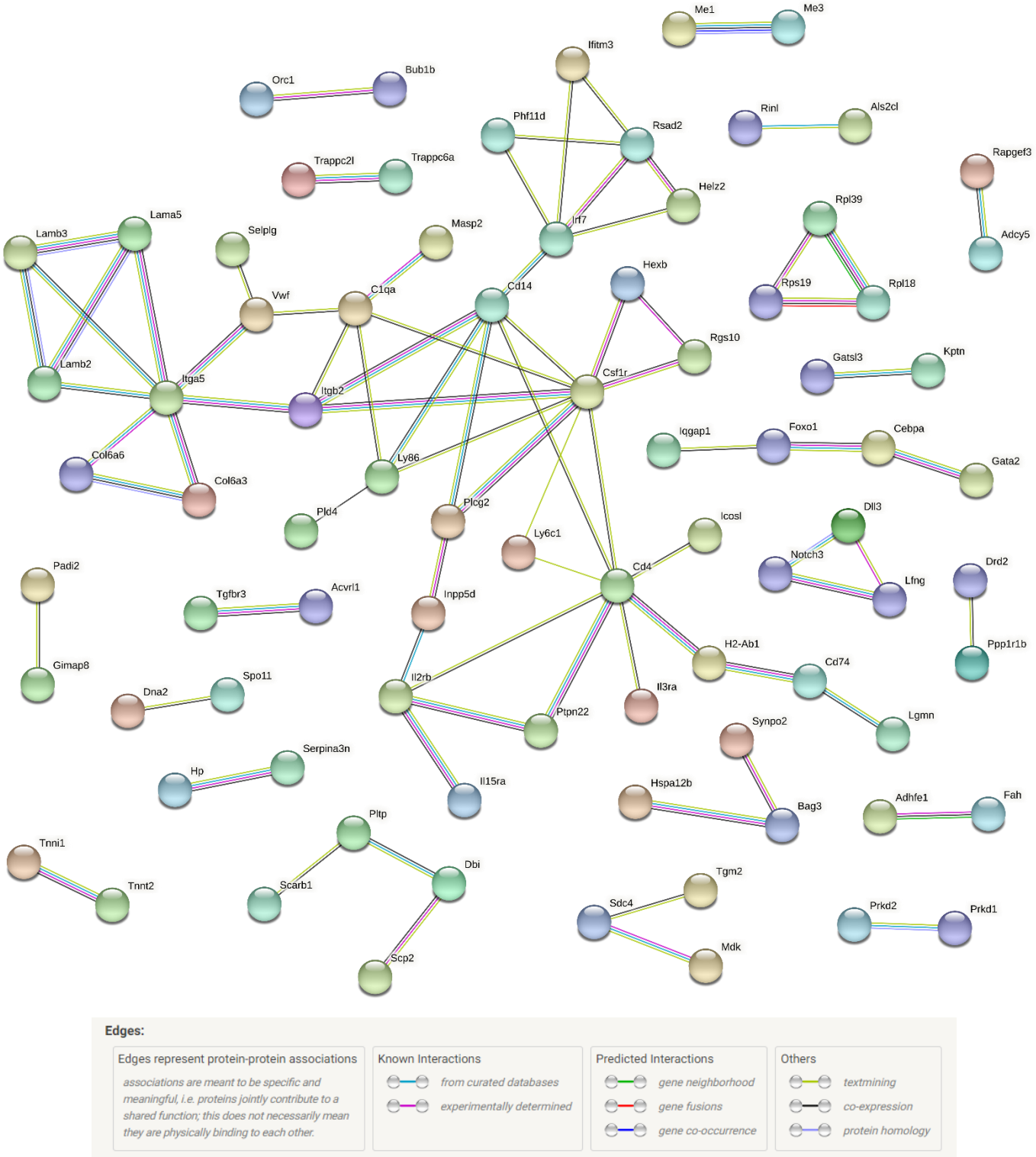

Figure 67. Overview of the PPI network of upregulated genes with high confidence (0.7) in cortical samples of *Rest* cKO mice. A total of 222 nodes and 81 edges were obtained, however, the disconnected nodes were removed from the network.

- **Biological process**

The upregulated genes revealed 84 GO-terms significantly enriched (**Table 9**). Immune response is highly affected in *Rest* cKO, either directly (**Appendix 4.7**) or indirectly (**Appendix 4.8**) . Angiogenesis is also significantly enriched in upregulated genes (**Appendix 4.9**).

- **Molecular Function**

No statistically significant enrichment was observed in molecular function regarding the upregulated genes in *Rest* cKO.

Table 9. Functional enrichment of biological processes aspect in PPI network in upregulated genes in *Rest* cKO mice. The most interesting terms are highlighted.

explain columns

Biological Process (Gene Ontology)				
GO-term	description	count in network	strength	false discovery rate
GO:0035723	interleukin-15-mediated signaling pathway	3 of 6	1.7	0.0153
GO:0010996	Response to auditory stimulus	4 of 28	1.15	0.0407
GO:0016064	Immunoglobulin mediated immune response	7 of 80	0.94	0.0081
GO:1904018	Positive regulation of vasculature development	10 of 201	0.69	0.0126
GO:0045766	Positive regulation of angiogenesis	9 of 181	0.69	0.0227
GO:0010594	Regulation of endothelial cell migration	8 of 166	0.68	0.0493
GO:0010632	Regulation of epithelial cell migration	10 of 232	0.63	0.0283
GO:1903039	Positive regulation of leukocyte cell-cell adhesion	9 of 210	0.63	0.0493
GO:0002696	Positive regulation of leukocyte activation	13 of 324	0.6	0.0102
GO:0022409	Positive regulation of cell-cell adhesion	10 of 254	0.59	0.0469
GO:0042063	Gliogenesis	10 of 255	0.59	0.0478
GO:0045785	Positive regulation of cell adhesion	16 of 425	0.57	0.0045
GO:0010038	Response to metal ion	14 of 374	0.57	0.0104
GO:1901342	Regulation of vasculature development	13 of 349	0.57	0.0150
GO:0001525	Angiogenesis	12 of 325	0.56	0.0265
GO:0006954	Inflammatory response	17 of 481	0.55	0.0049
GO:0030335	Positive regulation of cell migration	20 of 567	0.54	0.0015
GO:0048514	Blood vessel morphogenesis	15 of 433	0.54	0.0119
GO:0002252	Immune effector process	15 of 435	0.53	0.0123
GO:0001819	Positive regulation of cytokine production	15 of 436	0.53	0.0123
GO:0050778	Positive regulation of immune response	15 of 450	0.52	0.0144
GO:0032103	Positive regulation of response to external stimulus	13 of 399	0.51	0.0407
GO:0030334	Regulation of cell migration	29 of 915	0.5	0.00078
GO:0001817	Regulation of cytokine production	22 of 698	0.5	0.0023
GO:0001944	Vasculature development	18 of 562	0.5	0.0074
GO:0001568	Blood vessel development	17 of 534	0.5	0.0111
GO:0050776	Regulation of immune response	20 of 645	0.49	0.0049
GO:0010035	Response to inorganic substance	17 of 556	0.48	0.0139
GO:0045087	Innate immune response	17 of 558	0.48	0.0142
GO:0006955	Immune response	29 of 979	0.47	0.00078
GO:0002684	Positive regulation of immune system process	24 of 815	0.47	0.0023
GO:0001775	Cell activation	18 of 599	0.47	0.0123
GO:0006952	Defense response	33 of 1133	0.46	0.00078
GO:0009617	Response to bacterium	19 of 660	0.46	0.0126
GO:0045321	Leukocyte activation	15 of 511	0.46	0.0407
GO:0051270	Regulation of cellular component movement	30 of 1048	0.45	0.00078
GO:0098542	Defense response to other organism	22 of 775	0.45	0.0061
GO:0030155	Regulation of cell adhesion	20 of 705	0.45	0.0111
GO:0030097	Hemopoiesis	18 of 637	0.45	0.0198
GO:0051707	Response to other organism	32 of 1145	0.44	0.00078
GO:0035239	Tube morphogenesis	20 of 728	0.44	0.0137
GO:0048646	Anatomical structure formation involved in morphogenesis	25 of 952	0.42	0.0059
GO:0002520	Immune system development	19 of 727	0.41	0.0297
GO:0002682	Regulation of immune system process	30 of 1252	0.38	0.0049
GO:0032101	Regulation of response to external stimulus	21 of 871	0.38	0.0380
GO:0002376	Immune system process	43 of 1842	0.37	0.00078
GO:1901698	Response to nitrogen compound	25 of 1064	0.37	0.0176
GO:0051050	Positive regulation of transport	24 of 1020	0.37	0.0227
GO:0010243	Response to organonitrogen compound	23 of 975	0.37	0.0283
GO:0035295	Tube development	22 of 961	0.36	0.0485
GO:0043085	Positive regulation of catalytic activity	30 of 1341	0.35	0.0111
GO:0048584	Positive regulation of response to stimulus	45 of 2080	0.33	0.00078
GO:0009605	Response to external stimulus	47 of 2199	0.33	0.00078
GO:0007166	Cell surface receptor signaling pathway	37 of 1741	0.32	0.0057
GO:0044093	Positive regulation of molecular function	35 of 1711	0.31	0.0128
GO:0042127	Regulation of cell population proliferation	34 of 1650	0.31	0.0137
GO:0051241	Negative regulation of multicellular organismal process	27 of 1304	0.31	0.0488
GO:0006950	Response to stress	57 of 3045	0.27	0.0017
GO:0010033	Response to organic substance	52 of 2742	0.27	0.0028
GO:0070887	Cellular response to chemical stimulus	47 of 2535	0.27	0.0086

GO:0051240	Positive regulation of multicellular organismal process	36 of 1902	0.27	0.0317
GO:0031399	Regulation of protein modification process	35 of 1856	0.27	0.0407
GO:0048583	Regulation of response to stimulus	67 of 3651	0.26	0.00078
GO:0032879	Regulation of localization	52 of 2806	0.26	0.0045
GO:0009966	Regulation of signal transduction	49 of 2767	0.25	0.0134
GO:0009653	Anatomical structure morphogenesis	40 of 2244	0.25	0.0420
GO:0051239	Regulation of multicellular organismal process	56 of 3205	0.24	0.0074
GO:0042221	Response to chemical	64 of 3720	0.23	0.0036
GO:0007154	Cell communication	68 of 4179	0.21	0.0074
GO:0010646	Regulation of cell communication	53 of 3215	0.21	0.0296
GO:0023051	Regulation of signaling	53 of 3227	0.21	0.0317
GO:0048523	Negative regulation of cellular process	74 of 4672	0.2	0.0070
GO:0007165	Signal transduction	60 of 3779	0.2	0.0283
GO:0050896	Response to stimulus	108 of 6908	0.19	0.00078
GO:0048519	Negative regulation of biological process	80 of 5108	0.19	0.0049
GO:0065009	Regulation of molecular function	68 of 4379	0.19	0.0186
GO:0023052	Signaling	64 of 4065	0.19	0.0213
GO:0009893	Positive regulation of metabolic process	59 of 3767	0.19	0.0407
GO:0048522	Positive regulation of cellular process	82 of 5407	0.18	0.0086
GO:0048731	System development	67 of 4350	0.18	0.0256
GO:0048518	Positive regulation of biological process	88 of 5869	0.17	0.0064
GO:0065007	Biological regulation	143 of 10591	0.13	0.00078
GO:0050789	Regulation of biological process	136 of 9973	0.13	0.0011
GO:0050794	Regulation of cellular process	129 of 9541	0.13	0.0034

- **Cellular component**

In the cellular component aspect, membrane proteins appear to be altered in the *Rest* cKO mice (**Table 10**).

Table 10. Functional enrichment of cellular component aspect in PPI network in upregulated genes in *Rest* cKO mice.

Cellular Component (Gene Ontology)				
GO-term	*description*	*count in network*	*strength*	*false discovery rate*
GO:0009897	External side of plasma membrane	15 of 404	0.57	0.0186
GO:0098552	Side of membrane	18 of 595	0.48	0.0197
GO:0009986	Cell surface	27 of 913	0.47	0.0014
GO:0005783	Endoplasmic reticulum	29 of 1311	0.34	0.0240
GO:0110165	Cellular anatomical entity	184 of 15632	0.07	0.0186

4.5.4.2. Downregulated genes

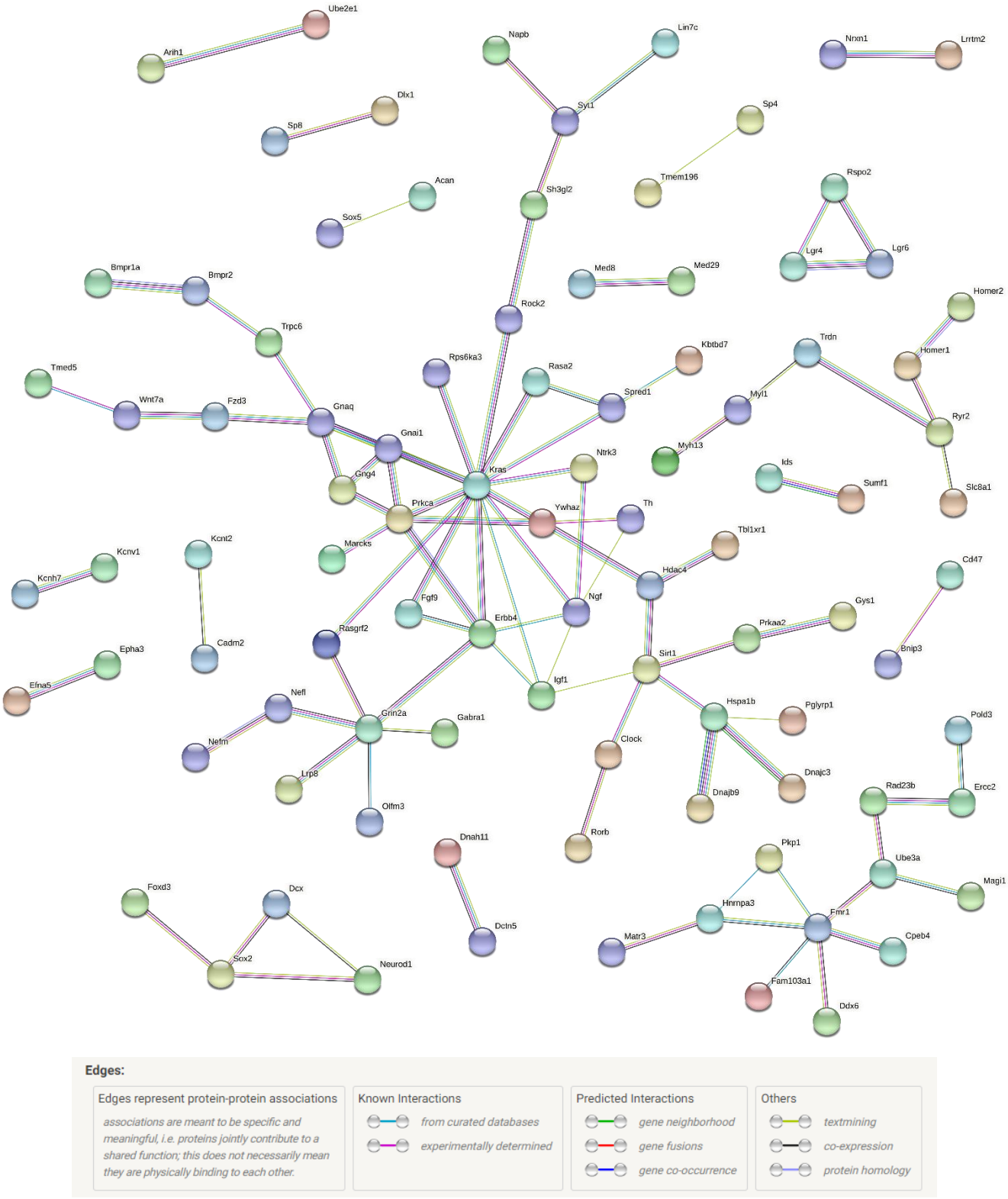

Figure 68. Overview of the PPI network of downregulated genes with high confidence (0.7) in the cortex *Rest* cKO mice. A total of 256 nodes and 97 edges were obtained, however, the disconnected nodes were removed from the network.

- **Biological process**

The downregulated genes revealed 184 GO-terms significantly enriched (**Table 11**). Neuronal pathways (**Appendix 4.10**) are highly affect in *Rest* cKO. Synapses assembly (**Appendix 4.11**) also appear to be affected in these mice.

Table 11. Functional enrichment of biological processes aspect in PPI network in downregulated genes in *Rest* cKO mice. The most interesting terms are highlighted.

explain columns

Biological Process (Gene Ontology)				
GO-term	description	count in network	strength	false discovery rate
GO:0045105	Intermediate filament polymerization or depolymerization	2 of 2	1.94	0.0484
GO:0045110	Intermediate filament bundle assembly	3 of 5	1.71	0.0077
GO:0031133	Regulation of axon diameter	3 of 6	1.63	0.0107
GO:1904889	Regulation of excitatory synapse assembly	5 of 17	1.4	0.0010
GO:0099151	Regulation of postsynaptic density assembly	4 of 14	1.39	0.0050
GO:0045109	Intermediate filament organization	4 of 25	1.14	0.0241
GO:0007215	Glutamate receptor signaling pathway	6 of 47	1.04	0.0037
GO:0021879	Forebrain neuron differentiation	7 of 58	1.02	0.0016
GO:0055023	Positive regulation of cardiac muscle tissue growth	5 of 41	1.02	0.0152
GO:0048813	Dendrite morphogenesis	7 of 73	0.92	0.0043
GO:0001754	Eye photoreceptor cell differentiation	5 of 52	0.92	0.0348
GO:0002062	Chondrocyte differentiation	8 of 86	0.9	0.0019
GO:1990090	Cellular response to nerve growth factor stimulus	5 of 55	0.89	0.0418
GO:0042461	Photoreceptor cell development	5 of 55	0.89	0.0418
GO:0042220	Response to cocaine	5 of 55	0.89	0.0418
GO:0050772	Positive regulation of axonogenesis	9 of 104	0.87	0.0012
GO:1904377	Positive regulation of protein localization to cell periphery	6 of 69	0.87	0.0185
GO:0046530	Photoreceptor cell differentiation	6 of 69	0.87	0.0185
GO:0043279	Response to alkaloid	9 of 117	0.82	0.0022
GO:0051965	Positive regulation of synapse assembly	6 of 78	0.82	0.0300
GO:0007416	Synapse assembly	6 of 81	0.8	0.0348
GO:0099175	Regulation of postsynapse organization	9 of 130	0.78	0.0039
GO:0001649	Osteoblast differentiation	7 of 100	0.78	0.0193
GO:0001678	Cellular glucose homeostasis	7 of 101	0.78	0.0199
GO:0007269	Neurotransmitter secretion	6 of 86	0.78	0.0441
GO:0016358	Dendrite development	9 of 135	0.76	0.0049
GO:0099173	Postsynapse organization	7 of 106	0.75	0.0247
GO:0021987	Cerebral cortex development	8 of 127	0.73	0.0146
GO:0050770	Regulation of axonogenesis	12 of 203	0.71	0.0013
GO:0021953	Central nervous system neuron differentiation	12 of 210	0.69	0.0017
GO:0021543	Pallium development	11 of 193	0.69	0.0032
GO:0051963	Regulation of synapse assembly	7 of 122	0.69	0.0468
GO:0006836	Neurotransmitter transport	7 of 123	0.69	0.0484
GO:0048639	Positive regulation of developmental growth	12 of 214	0.68	0.0019
GO:0010770	Positive regulation of cell morphogenesis involved in differe...	10 of 189	0.66	0.0098
GO:0023061	Signal release	10 of 194	0.65	0.0115
GO:0050808	Synapse organization	15 of 303	0.63	0.0010
GO:0043524	Negative regulation of neuron apoptotic process	9 of 182	0.63	0.0278
GO:0051216	Cartilage development	9 of 184	0.62	0.0297
GO:0045666	Positive regulation of neuron differentiation	22 of 465	0.61	3.77e-05
GO:0050807	Regulation of synapse organization	13 of 275	0.61	0.0037
GO:0050806	Positive regulation of synaptic transmission	9 of 189	0.61	0.0348
GO:0030307	Positive regulation of cell growth	9 of 192	0.61	0.0369
GO:0010976	Positive regulation of neuron projection development	17 of 366	0.6	0.00065
GO:0021537	Telencephalon development	13 of 288	0.59	0.0052
GO:0061448	Connective tissue development	11 of 244	0.59	0.0158
GO:0031346	Positive regulation of cell projection organization	21 of 474	0.58	0.00013
GO:0010769	Regulation of cell morphogenesis involved in differentiation	15 of 343	0.58	0.0025
GO:0097305	Response to alcohol	11 of 252	0.58	0.0195
GO:0051962	Positive regulation of nervous system development	28 of 651	0.57	7.18e-06
GO:0032412	Regulation of ion transmembrane transporter activity	11 of 254	0.57	0.0205
GO:0001505	Regulation of neurotransmitter levels	11 of 255	0.57	0.0209
GO:0048511	Rhythmic process	13 of 305	0.56	0.0081
GO:0050769	Positive regulation of neurogenesis	24 of 579	0.55	6.98e-05
GO:0045664	Regulation of neuron differentiation	31 of 774	0.54	5.78e-06
GO:0032990	Cell part morphogenesis	21 of 522	0.54	0.00043
GO:0034765	Regulation of ion transmembrane transport	19 of 477	0.54	0.0011
GO:0010975	Regulation of neuron projection development	24 of 607	0.53	0.00013
GO:0048812	Neuron projection morphogenesis	19 of 479	0.53	0.0011
GO:0010721	Negative regulation of cell development	15 of 384	0.53	0.0065
GO:0030900	Forebrain development	17 of 438	0.52	0.0029
GO:0050768	Negative regulation of neurogenesis	13 of 336	0.52	0.0178
GO:0051960	Regulation of nervous system development	39 of 1071	0.5	1.47e-06
GO:0050767	Regulation of neurogenesis	35 of 948	0.5	5.18e-06

GO:0120035	Regulation of plasma membrane bounded cell projection or...	29 of 788	0.5	4.54e-05
GO:0034762	Regulation of transmembrane transport	21 of 568	0.5	0.0011
GO:0050804	Modulation of chemical synaptic transmission	19 of 521	0.5	0.0024
GO:0070848	Response to growth factor	18 of 485	0.5	0.0029
GO:0040007	Growth	17 of 466	0.5	0.0051
GO:0030182	Neuron differentiation	38 of 1056	0.49	2.78e-06
GO:0032989	Cellular component morphogenesis	22 of 611	0.49	0.0010
GO:0060284	Regulation of cell development	38 of 1086	0.48	4.89e-06
GO:0034330	Cell junction organization	17 of 481	0.48	0.0069
GO:0048589	Developmental growth	16 of 458	0.48	0.0113
GO:0071363	Cellular response to growth factor stimulus	16 of 459	0.48	0.0115
GO:0007420	Brain development	26 of 759	0.47	0.00043
GO:0048667	Cell morphogenesis involved in neuron differentiation	15 of 440	0.47	0.0209
GO:0042391	Regulation of membrane potential	15 of 440	0.47	0.0209
GO:0043269	Regulation of ion transport	24 of 722	0.46	0.0012
GO:0048666	Neuron development	28 of 855	0.45	0.00042
GO:0007507	Heart development	19 of 581	0.45	0.0070
GO:0022008	Neurogenesis	57 of 1784	0.44	4.34e-08
GO:0048699	Generation of neurons	53 of 1660	0.44	1.54e-07
GO:0007417	Central nervous system development	31 of 984	0.43	0.00026
GO:0045596	Negative regulation of cell differentiation	24 of 761	0.43	0.0020
GO:0035239	Tube morphogenesis	23 of 728	0.43	0.0027
GO:0022604	Regulation of cell morphogenesis	16 of 528	0.42	0.0395
GO:0031175	Neuron projection development	21 of 697	0.41	0.0086
GO:0071495	Cellular response to endogenous stimulus	31 of 1075	0.4	0.0010
GO:0051093	Negative regulation of developmental process	30 of 1043	0.39	0.0012
GO:0072359	Circulatory system development	26 of 936	0.38	0.0052
GO:0007267	Cell-cell signaling	23 of 827	0.38	0.0115
GO:0048729	Tissue morphogenesis	18 of 646	0.38	0.0452
GO:0007399	Nervous system development	64 of 2358	0.37	4.75e-07
GO:0051094	Positive regulation of developmental process	42 of 1533	0.37	0.00011
GO:0051130	Positive regulation of cellular component organization	34 of 1236	0.37	0.00098
GO:0045597	Positive regulation of cell differentiation	30 of 1103	0.37	0.0025
GO:0009887	Animal organ morphogenesis	28 of 1038	0.37	0.0046
GO:0035295	Tube development	26 of 961	0.37	0.0072
GO:0000902	Cell morphogenesis	20 of 739	0.37	0.0352
GO:0045595	Regulation of cell differentiation	50 of 1868	0.36	2.48e-05
GO:0048468	Cell development	45 of 1730	0.35	0.00014
GO:0045944	Positive regulation of transcription by rna polymerase ii	32 of 1239	0.35	0.0032
GO:0009790	Embryo development	30 of 1165	0.35	0.0052
GO:0014070	Response to organic cyclic compound	24 of 930	0.35	0.0216
GO:2000026	Regulation of multicellular organismal development	54 of 2150	0.34	3.77e-05
GO:0045893	Positive regulation of transcription, dna-templated	39 of 1541	0.34	0.0011
GO:0043066	Negative regulation of apoptotic process	23 of 913	0.34	0.0357
GO:0009719	Response to endogenous stimulus	34 of 1370	0.33	0.0037
GO:0010628	Positive regulation of gene expression	55 of 2269	0.32	6.98e-05
GO:0009653	Anatomical structure morphogenesis	54 of 2244	0.32	0.00010
GO:0010557	Positive regulation of macromolecule biosynthetic process	45 of 1837	0.32	0.00054
GO:0051254	Positive regulation of rna metabolic process	41 of 1696	0.32	0.0013
GO:0120036	Plasma membrane bounded cell projection organization	26 of 1072	0.32	0.0291
GO:0051241	Negative regulation of multicellular organismal process	31 of 1304	0.31	0.0131
GO:0022603	Regulation of anatomical structure morphogenesis	26 of 1090	0.31	0.0350
GO:0051248	Negative regulation of protein metabolic process	26 of 1094	0.31	0.0363
GO:0071310	Cellular response to organic substance	46 of 1987	0.3	0.0012
GO:0031328	Positive regulation of cellular biosynthetic process	45 of 1940	0.3	0.0013
GO:0045935	Positive regulation of nucleobase-containing compound me...	43 of 1859	0.3	0.0019
GO:0048878	Chemical homeostasis	26 of 1124	0.3	0.0489
GO:0050793	Regulation of developmental process	61 of 2669	0.29	8.71e-05
GO:0051240	Positive regulation of multicellular organismal process	43 of 1902	0.29	0.0029
GO:0051172	Negative regulation of nitrogen compound metabolic process	51 of 2310	0.28	0.0012
GO:0051049	Regulation of transport	41 of 1862	0.28	0.0066
GO:1901700	Response to oxygen-containing compound	35 of 1585	0.28	0.0185
GO:0048869	Cellular developmental process	80 of 3731	0.27	1.80e-05
GO:0030154	Cell differentiation	79 of 3674	0.27	1.80e-05
GO:0009888	Tissue development	37 of 1720	0.27	0.0195
GO:0048731	System development	91 of 4350	0.26	5.44e-06

GO:0010605	Negative regulation of macromolecule metabolic process	56 of 2646	0.26	0.0013
GO:0070887	Cellular response to chemical stimulus	54 of 2535	0.26	0.0015
GO:0048513	Animal organ development	67 of 3230	0.25	0.00042
GO:0031324	Negative regulation of cellular metabolic process	51 of 2497	0.25	0.0053
GO:0010647	Positive regulation of cell communication	36 of 1762	0.25	0.0479
GO:0010556	Regulation of macromolecule biosynthetic process	67 of 3294	0.24	0.00070
GO:2000112	Regulation of cellular macromolecule biosynthetic process	65 of 3203	0.24	0.0010
GO:0051239	Regulation of multicellular organismal process	65 of 3205	0.24	0.0010
GO:0023051	Regulation of signaling	65 of 3227	0.24	0.0011
GO:0010646	Regulation of cell communication	65 of 3215	0.24	0.0011
GO:0051252	Regulation of rna metabolic process	61 of 3027	0.24	0.0018
GO:0032879	Regulation of localization	57 of 2806	0.24	0.0025
GO:0010033	Response to organic substance	55 of 2742	0.24	0.0045
GO:0051128	Regulation of cellular component organization	49 of 2438	0.24	0.0099
GO:0006357	Regulation of transcription by rna polymerase ii	38 of 1897	0.24	0.0484
GO:0023056	Positive regulation of signaling	36 of 1769	0.24	0.0499
GO:0007275	Multicellular organism development	97 of 4921	0.23	1.80e-05
GO:0019219	Regulation of nucleobase-containing compound metabolic ...	64 of 3265	0.23	0.0022
GO:0051173	Positive regulation of nitrogen compound metabolic process	61 of 3119	0.23	0.0034
GO:0009892	Negative regulation of metabolic process	57 of 2895	0.23	0.0050
GO:0009966	Regulation of signal transduction	54 of 2767	0.23	0.0091
GO:0010468	Regulation of gene expression	78 of 4041	0.22	0.00059
GO:0031326	Regulation of cellular biosynthetic process	67 of 3448	0.22	0.0019
GO:0009889	Regulation of biosynthetic process	68 of 3526	0.22	0.0019
GO:0031325	Positive regulation of cellular metabolic process	64 of 3320	0.22	0.0032
GO:2001141	Regulation of rna biosynthetic process	54 of 2775	0.22	0.0098
GO:0006355	Regulation of transcription, dna-templated	53 of 2720	0.22	0.0107
GO:0060255	Regulation of macromolecule metabolic process	105 of 5618	0.21	3.77e-05
GO:0048856	Anatomical structure development	100 of 5258	0.21	3.77e-05
GO:0048522	Positive regulation of cellular process	101 of 5407	0.21	6.13e-05
GO:0010604	Positive regulation of macromolecule metabolic process	66 of 3467	0.21	0.0034
GO:0048518	Positive regulation of biological process	107 of 5869	0.2	6.57e-05
GO:0032502	Developmental process	103 of 5629	0.2	9.93e-05
GO:0051171	Regulation of nitrogen compound metabolic process	94 of 5126	0.2	0.00035
GO:0048519	Negative regulation of biological process	93 of 5108	0.2	0.00049
GO:0048523	Negative regulation of cellular process	86 of 4672	0.2	0.00090
GO:0042221	Response to chemical	69 of 3720	0.2	0.0044
GO:0009893	Positive regulation of metabolic process	69 of 3767	0.2	0.0059
GO:0048583	Regulation of response to stimulus	67 of 3651	0.2	0.0071
GO:0051246	Regulation of protein metabolic process	52 of 2799	0.2	0.0318
GO:0031323	Regulation of cellular metabolic process	99 of 5479	0.19	0.00030
GO:0019222	Regulation of metabolic process	108 of 6085	0.18	0.00016
GO:0080090	Regulation of primary metabolic process	93 of 5290	0.18	0.0013
GO:0065009	Regulation of molecular function	77 of 4379	0.18	0.0071
GO:0065008	Regulation of biological quality	67 of 3822	0.18	0.0216
GO:0032501	Multicellular organismal process	107 of 6272	0.17	0.00098
GO:0051716	Cellular response to stimulus	95 of 5497	0.17	0.0019
GO:0050794	Regulation of cellular process	156 of 9541	0.15	1.43e-05
GO:0071840	Cellular component organization or biogenesis	81 of 4954	0.15	0.0348
GO:0016043	Cellular component organization	78 of 4769	0.15	0.0429
GO:0050789	Regulation of biological process	159 of 9973	0.14	3.77e-05
GO:0065007	Biological regulation	167 of 10591	0.13	2.27e-05
GO:0050896	Response to stimulus	107 of 6908	0.13	0.0219
GO:0009987	Cellular process	185 of 13330	0.08	0.0059

- **Molecular Function**

In the molecular function aspect, gene ontology term “binding” appears to be significantly enriched in downregulated genes of *Rest* cKO mice (**Table 12** and **Appendix 4.12**).

Table 12. Functional enrichment of molecular function aspect in PPI network in downregulated genes in *Rest* cKO mice.

Molecular Function (Gene Ontology)				
GO-term	*description*	*count in network*	*strength*	*false discovery rate*
GO:0046872	Metal ion binding	76 of 3513	0.27	5.18e-05
GO:0043167	Ion binding	95 of 5439	0.18	0.0049
GO:0005515	Protein binding	117 of 6764	0.17	0.00030
GO:0005488	Binding	177 of 11199	0.13	7.83e-06

- **Cellular component**

In the cellular component aspect, synaptic components appear to be altered in the *Rest* cKO mice (**Table 13** and **Appendix 4.13**).

Table 13. Functional enrichment of cellular component aspect in PPI network in downregulated genes in *Rest* cKO mice. The most interesting terms are highlighted.

Cellular Component (Gene Ontology)				
GO-term	*description*	*count in network*	*strength*	*false discovery rate*
GO:0099182	Presynaptic intermediate filament cytoskeleton	2 of 2	1.94	0.0292
GO:0099569	Presynaptic cytoskeleton	3 of 10	1.41	0.0171
GO:1990124	Messenger ribonucleoprotein complex	4 of 14	1.39	0.0035
GO:0005790	Smooth endoplasmic reticulum	4 of 36	0.98	0.0404
GO:0098686	Hippocampal mossy fiber to ca3 synapse	5 of 50	0.94	0.0173
GO:0060076	Excitatory synapse	6 of 72	0.86	0.0131
GO:0098982	GABA-ergic synapse	8 of 102	0.83	0.0033
GO:0034705	Potassium channel complex	6 of 82	0.8	0.0205
GO:0005901	Caveola	7 of 97	0.79	0.0102
GO:0098685	Schaffer collateral - CA1 synapse	7 of 113	0.73	0.0193
GO:0031234	Extrinsic component of cytoplasmic side of plasma membr...	6 of 98	0.72	0.0452
GO:0034703	Cation channel complex	11 of 207	0.66	0.0035
GO:0098984	Neuron to neuron synapse	21 of 446	0.61	2.60e-05
GO:0034702	Ion channel complex	13 of 276	0.61	0.0027
GO:0044306	Neuron projection terminus	10 of 213	0.61	0.0130
GO:0032279	Asymmetric synapse	19 of 420	0.59	0.00015
GO:0030426	Growth cone	10 of 224	0.58	0.0171
GO:0043025	Neuronal cell body	32 of 743	0.57	2.76e-07
GO:0014069	Postsynaptic density	18 of 414	0.57	0.00033
GO:0099572	Postsynaptic specialization	19 of 449	0.56	0.00029
GO:0044297	Cell body	34 of 836	0.54	2.76e-07
GO:0150034	Distal axon	16 of 399	0.54	0.0024
GO:0030425	Dendrite	28 of 753	0.51	2.60e-05
GO:0098978	Glutamatergic synapse	19 of 501	0.51	0.0011
GO:0036477	Somatodendritic compartment	40 of 1080	0.5	2.76e-07
GO:0098793	Presynapse	23 of 636	0.49	0.00030
GO:0030424	Axon	27 of 791	0.47	0.00015
GO:0045202	Synapse	48 of 1492	0.44	2.76e-07
GO:0098794	Postsynapse	24 of 761	0.43	0.0014
GO:0043005	Neuron projection	45 of 1583	0.39	1.07e-05
GO:0030054	Cell junction	53 of 2050	0.35	1.07e-05
GO:0005783	Endoplasmic reticulum	32 of 1311	0.32	0.0046
GO:0005887	Integral component of plasma membrane	28 of 1174	0.31	0.0141
GO:0031226	Intrinsic component of plasma membrane	29 of 1249	0.3	0.0164
GO:0120025	Plasma membrane bounded cell projection	48 of 2387	0.24	0.0073
GO:0042995	Cell projection	49 of 2472	0.23	0.0083
GO:0005634	Nucleus	101 of 6330	0.14	0.0083
GO:0043226	Organelle	168 of 11550	0.1	0.0014
GO:0043227	Membrane-bounded organelle	152 of 10370	0.1	0.0038
GO:0043231	Intracellular membrane-bounded organelle	139 of 9507	0.1	0.0113
GO:0043229	Intracellular organelle	159 of 11084	0.09	0.0058
GO:0005622	Intracellular	177 of 12596	0.08	0.0039
GO:0110165	Cellular anatomical entity	215 of 15632	0.07	0.00015

4.5.5. Gene set enrichment analysis

The previously described GOE analysis presents some limitations as it only takes into account the ID of the genes that were statistically significant differentially expressed genes. This might result in an overlook of some important genes involved in the observed phenotypes due to failure in reaching statistical significance. On the other hand, for GSE analysis the genes ID is complemented with quantitative information. GSE analysis attributes a specific weight to each gene in the input list and then uses statistical approaches to classify the significantly enriched genes within the quantitative information used. Therefore, GSE analysis gives a wider perspective on what gene set are involved in the phenotypes observed.

A GSE analysis was performed to study the gene sets (genes that share common biological function, location or regulation) and enlighten the pathways affected in the absence of REST. As GSE analysis does not require a cut off (such as p-value < 0.05), all the 31,489 differentially expressed genes between *Rest* cKO and controls and the respective fold change were considered.

- **Biological process**

Out of the 31,489 genes submitted, only 12,812 IDs were annotated to the biological process category and therefore only theses were used in the analysis (**Figure 69**). A total of 27 gene sets were observed to be significantly enriched. Gene ontology annotations associated with immune response are strongly significantly enriched with 13 terms related (directly or indirectly) to this biological process. On the other hand, 47 depleted gene sets, the terms more affected by ablation of REST, i.e., the gene ontology terms with lowest normalized enrichment scores, are all linked with neuronal organization and development. Additionally there is a decrease in dephosphorylation in *Rest* cKO mice.

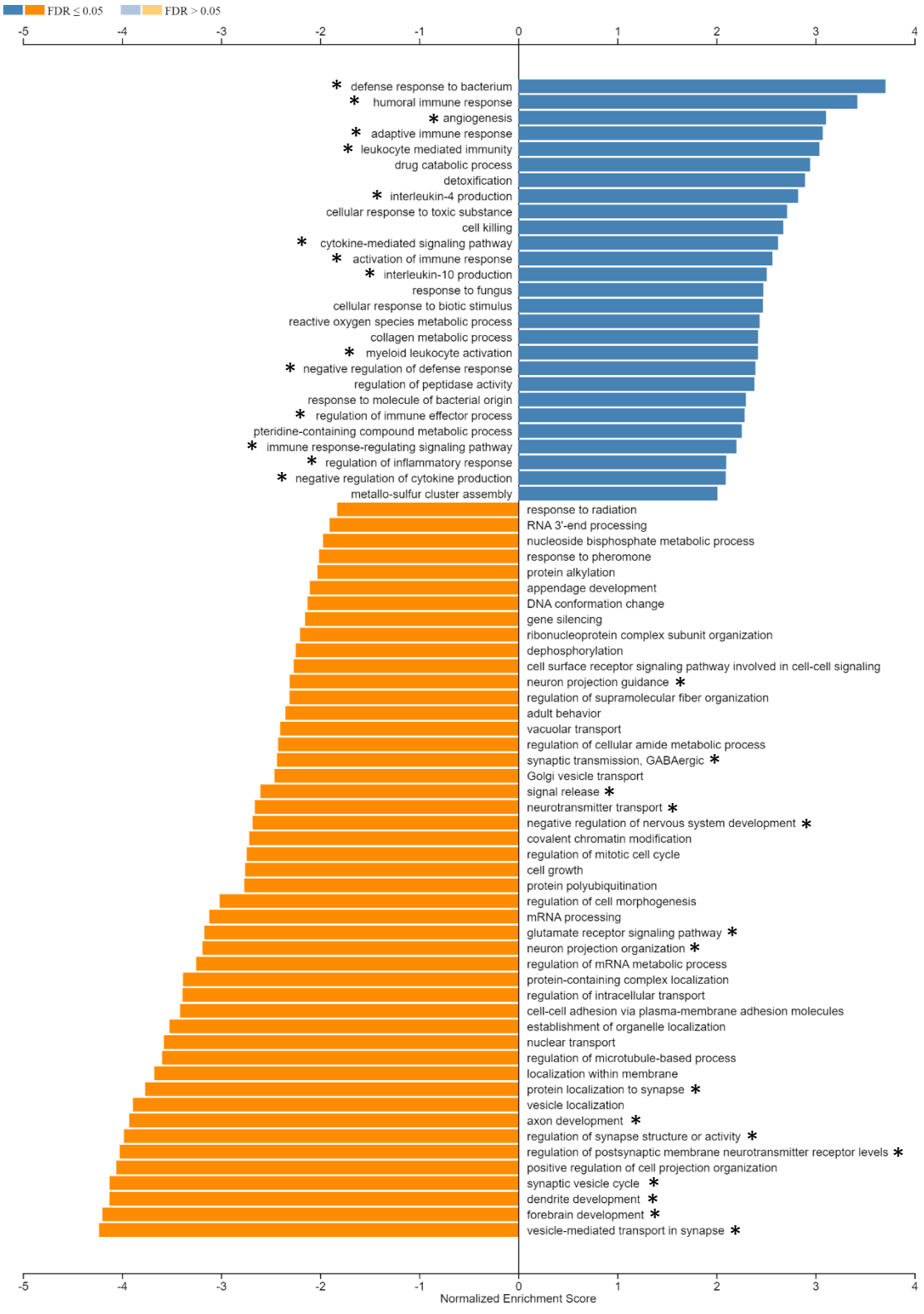

Figure 69. Overview of significantly enriched biological processes in the cortex of *Rest* cKO mice. Blue bars represent gene ontology terms that are significantly enriched whereas, orange corresponds to depleted terms. The most interesting terms are highlighted (*).

- **Molecular Function**

For the molecular function category, 10,861 IDs were annotated, from the initial list of differentially expressed genes, and used in this analysis (**Figure 70**). The data indicated that enzyme activity, such of endopeptidase, serine hydrolase, oxidoreductase and lyase, is significantly enriched in *Rest* CKO mice when compared with controls. Whereas protein binding, namely histone, glutamate receptor, appears to be impaired in the cortex of Rest cKO mice. Furthermore, phosphatase binding is also depleted in these mice.

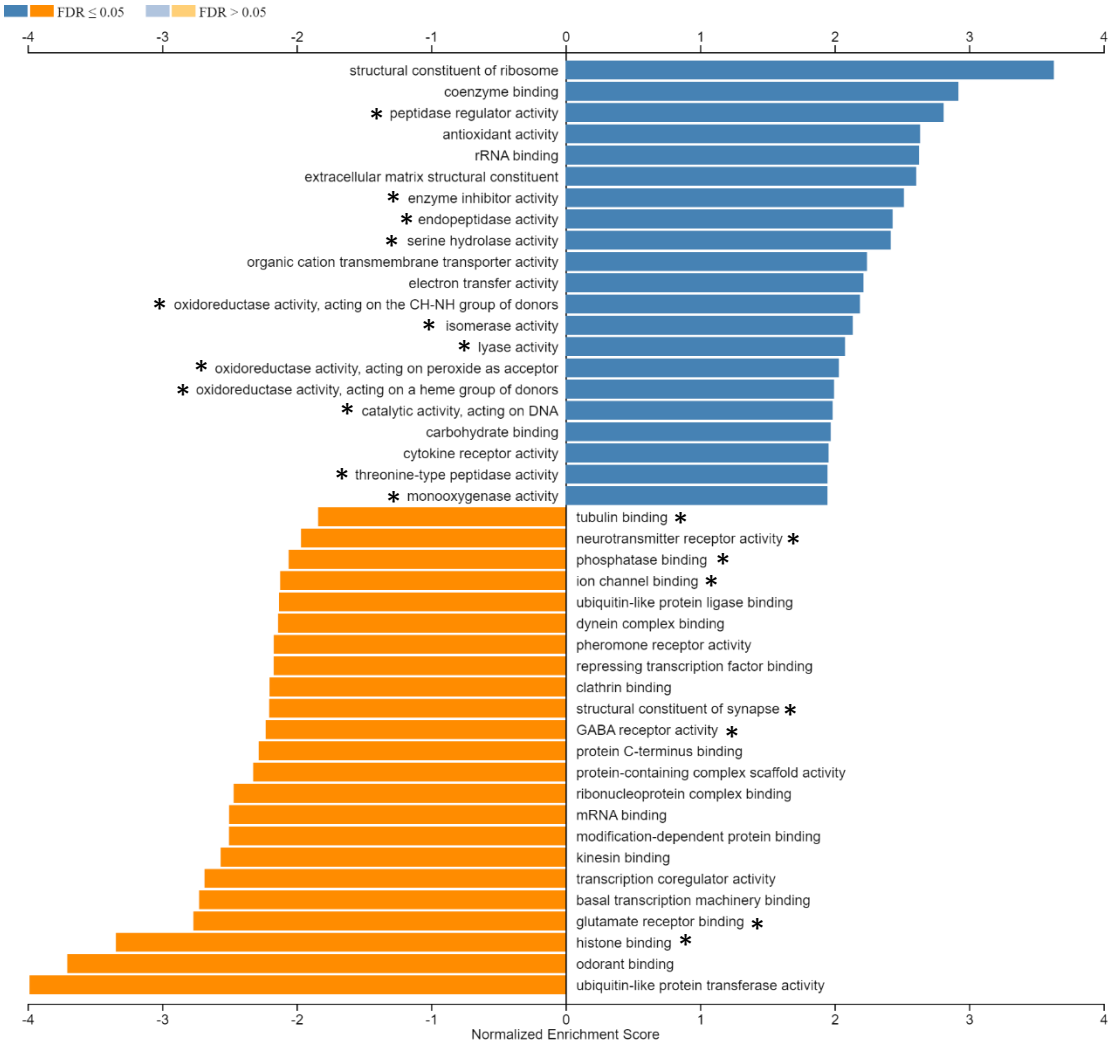

Figure 70. Overview of significantly enriched molecular functions in the cortex of *Rest* cKO mice. Blue bars represent gene ontology terms that are significantly enriched whereas, orange corresponds to depleted terms. The most interesting terms are highlighted (*).

- **Cellular component**

In the cellular component category, only 9,046 IDs were annotated in initial list of differentially expressed genes (**Figure 71**). Mitochondria gene sets are significantly enriched in the absence of REST. On the other hand, synaptic components are significantly affected in *Rest* cKO mice when compared with controls, which glutamatergic synapses being the most depleted gene ontology annotation.

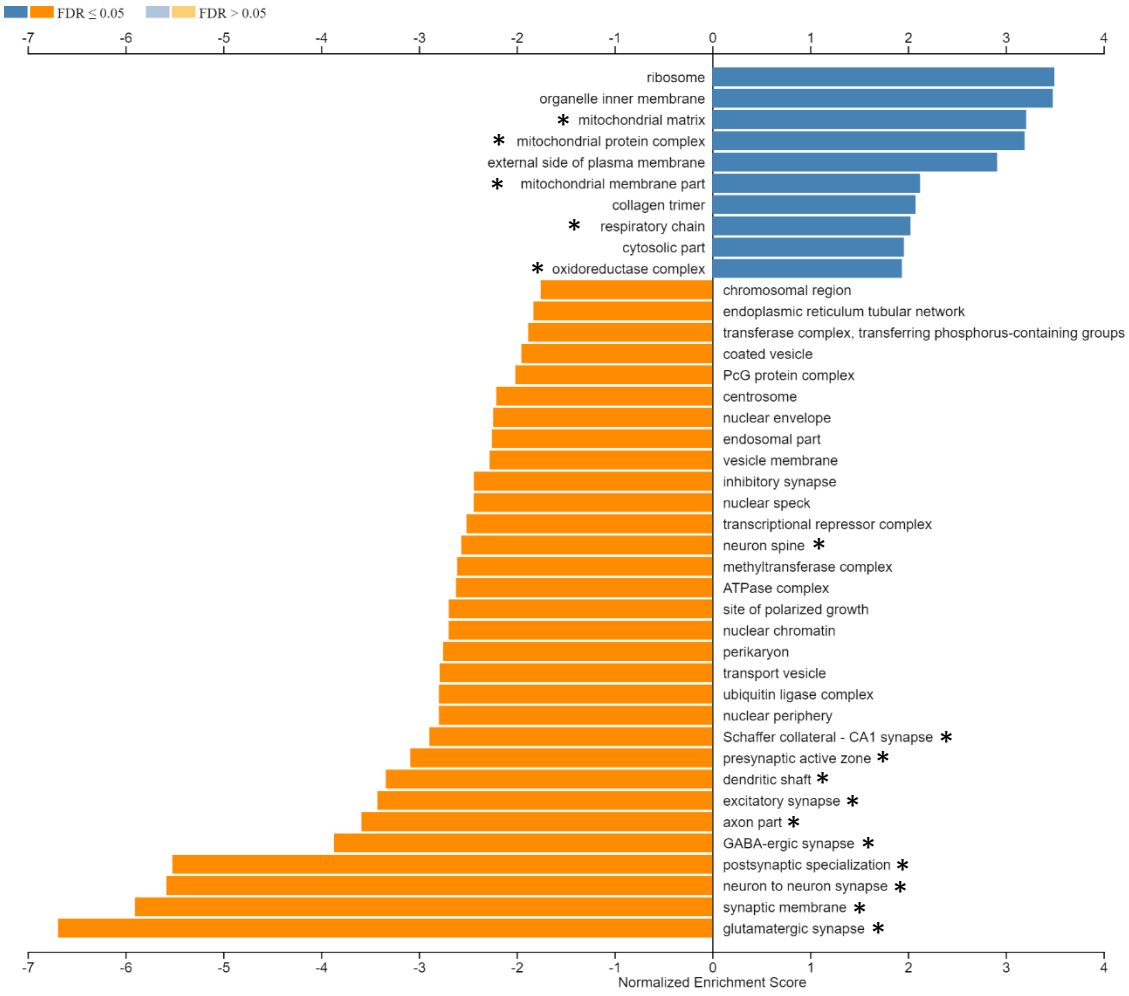

Figure 71. Overview of significantly enriched cellular components in the cortex of *Rest* cKO mice. Blue bars represent gene ontology terms that are significantly enriched whereas, orange corresponds to depleted terms. The most interesting terms are highlighted (*).

- **Pathway analysis – KEGG database**

The KEGG database is a collection of manually drawn pathway maps generated by high-throughput experimental technologies that helps to better understand which pathways and associated functions are likely to be affected in our samples.

For the pathway analysis, 6672 IDs were use for the enrichment analysis. A total of 23 pathways were found to be depleted, whereas 24 pathways were observed to be significantly enriched (**Figure 72**). Pathways associated with synaptic plasticity are negatively impacted in *Rest* cKO mice, with gene sets involved in LTP, LDP, GABAergic, dopaminergic and glutamatergic synapses being the most significantly depleted. Furthermore, FoxO signalling pathway also appears to be significantly downregulated in *Rest* cKO. On the other hand, this analysis revealed an association between REST absence and a wide range of diseases affecting the immune system.

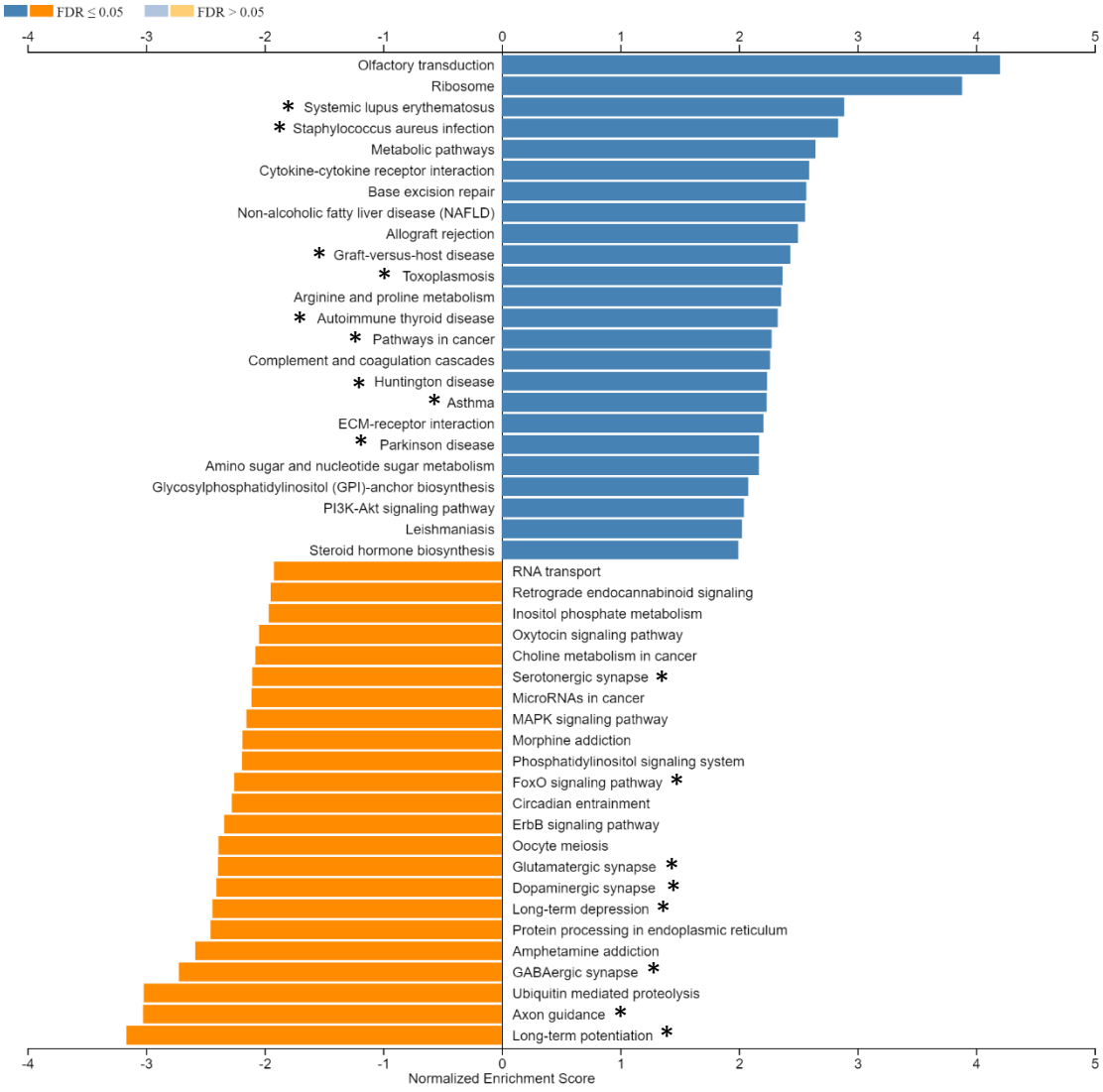

Figure 72. Overview of significantly enriched pathways in the cortex of *Rest* cKO mice. Blue bars represent gene ontology terms that are significantly enriched whereas, orange corresponds to depleted terms. The most interesting terms are highlighted (*).

4.5.6. REST and Re1 3D structure prediction

Given the proposed neuroprotective role for REST, finding potential enhancers would be of utmost importance in AD therapy. REST structure has not been crystallized yet, so it would be helpful to have the 3D structure of both REST and the DNA sequence it binds to. Hence, this project proposed a 3D structure of REST and the DNA sequence it binds to, Re1.

4.5.6.1. REST sequence similarity search

The first step was to identify similar proteins that could be used as template to build the REST DBD form (homology model). The primary structure of REST (FASTA sequence), BLAST and the algorithm blastp were used to search similar sequences in the PDB database. When querying for the entire REST protein (1097 residues, NP_001350382.1) the results showed that only the DBD region was covered by PDB entries with similar sequences, i.e. there is no protein in the PDB with a similar sequence to the entire REST protein. Another BLAST was performed in similar conditions but only querying for the DBD region (254 residues: 159-412) (**Figure 73.a**). From the results of the BLAST search, 2 proteins were selected based on query coverage and total alignment score (80-200) for further studies: ZFP568 (5WJQ) and Aart (2I13), both from *Mus musculus* (**Figure 73.b**).

Based on the percentage of identity, number of gaps and query coverage, ZFP 568 was chosen to be used as template to predict REST DBD structure with Prime. To further support this choice and also to test the docking server, both proteins were docked with their native DNA using HDOCK, i.e the DNA they were crystallized with in the PDB entry. Both proteins appear to have similar ligand RMSD values (around 0.5Å) (for more detail on these values please see **Appendix 2.4**).

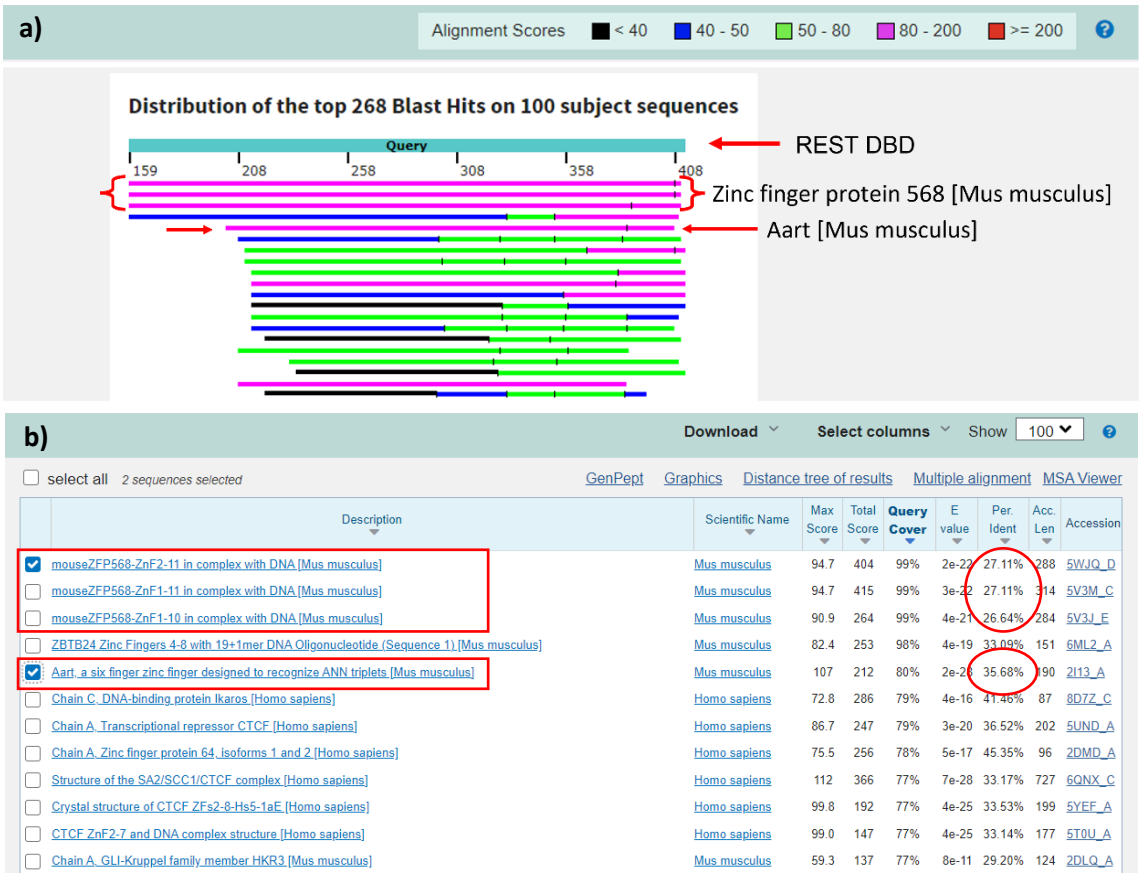

Figure 73. Protein-protein BLAST results of REST (NP_001350382.1) DBD (query length: 254 residues, 159-412). **a)** Graphic summary of the alignment. Each horizontal bar represents a match protein, with sequence similar to REST DBD. Each colour is associated with a class of alignment scores, with [80-200] (pink) being the highest score observed for this search. The proteins are vertically order by percentage of query coverage, with percentage decreasing vertically. **b)** List of proteins with similar sequences ordered by the percentage of query coverage. The entries with higher percentage of identities and total score were then selected for further studies (highlighted in red).

4.5.7. REST homology modelling and comparison with AlphaFold prediction

As described in **Section 3.9.2**, REST DBD was modelled based on the protein ZFP568 using Schrodinger software with Prime homology modelling. The final structure is depicted in **Figure 74.a.**

The REST DBD proposed in this thesis project was compared with the one predicted by AlphaFold (https://alphafold.ebi.ac.uk/entry/Q13127 - **Figure 74.b**). The superimposition of the referred two structures considering the C-α (the central point in

the backbone of every amino acid) atoms reported a RMSD of 9.82Å, which means that the two structures are quite different.

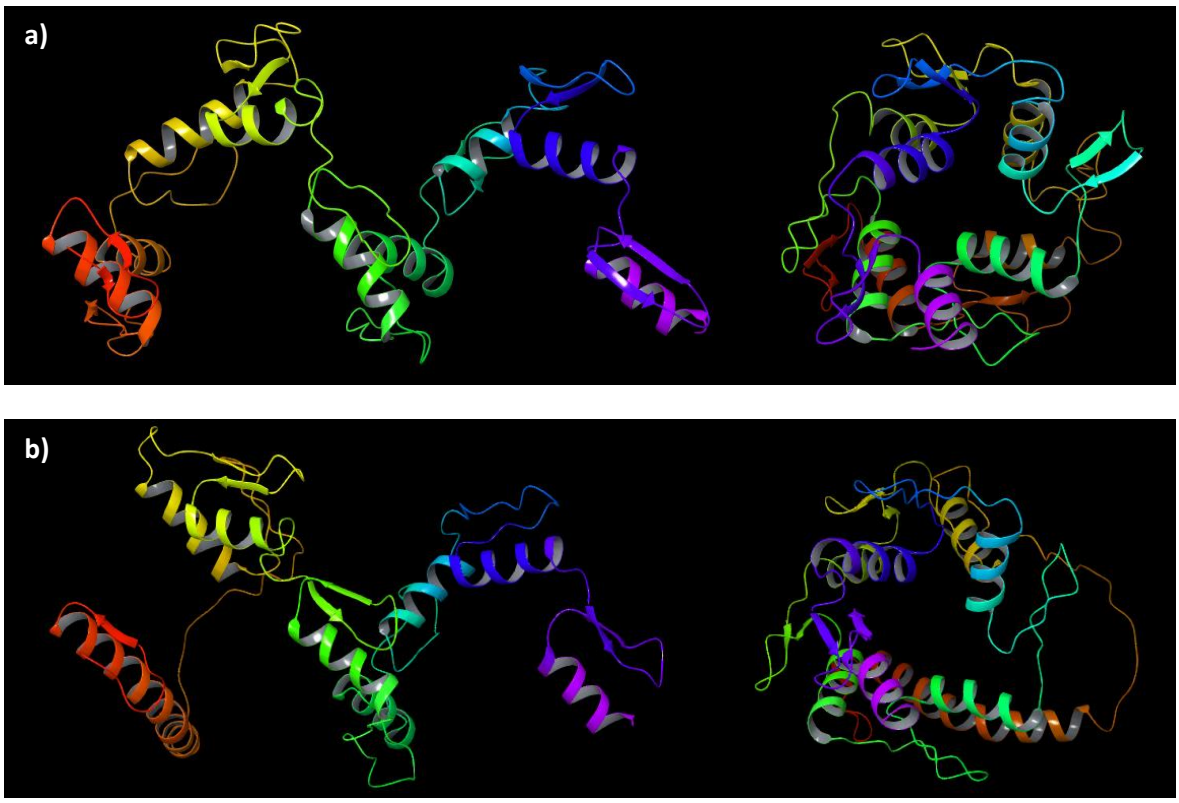

Figure 74. Predicted 3D structures of the REST DBD using **a)** Schrodinger/Prime software and **b)** AlphaFold webserver. Structures were superimposed by the C-α atoms. The two models are displayed in two different view planes: lateral view (on the left) and transversal (on the right – where the interior of the DNA-binding pocket can be seen). The residues are colour-coded by residue position to facilitate the comparison (i.e. Phe159, the first residue is coloured red and the last residue, His412, appears in purple).

The first big difference regards the structures length. The model developed in this project only has 254 residues as it was build using only the DBD sequence portion of REST, whereas AlphaFold REST shows all 1097 residues. In general, AlphaFold prediction has a "confident" (light blue) classification for the secondary structures predicted. However, when looking more carefully to the structure, the secondary structure is only defined for the DBD region, with exception for three helices comprising residues Ala43-Thr55, Glu822-Glu839 and Gly1072-Ala1093 and a β-sheet with residues Phe1060-Phe1069. The rest of the structure is predicted as loop, which is unlikely.

The second big distinction concerns zinc atoms. The ZF motifs of Schrodinger/Prime model are highlighted in **Figure 75**. The homology model proposed in this project used zinc atoms from the template, whereas the AlphaFold model doesn't present these atoms at all. These are very important in the structure stability as will be discussed in **Section 5.7**.

The third difference is with regard to the secondary structure. Overall, the structures that should form zincs motifs appear to be similar between models, varying only one or two residues in length. Likewise, the residues involved in the zinc coordination appear to be in the correct positions in both models, i.e. facing the middle, where the zinc atoms (missing for AlphaFold) should be to be able to coordinate with them. Generally, all the helices in the DBD structures involves about 12 residues (**Appendix 2.5**). However, for ZF1 AlphaFold predicts a helix with 28 amino acids (Glu171-Ala198), which differ from the 12-residue helix in the model described in this project (Glu171-Ser182). In fact, all the other helix in the structures in the DBD usually involve 12 residues. However, the AlphaFold model confidence decreases after residue Ser182, region of its 28-residue helix.

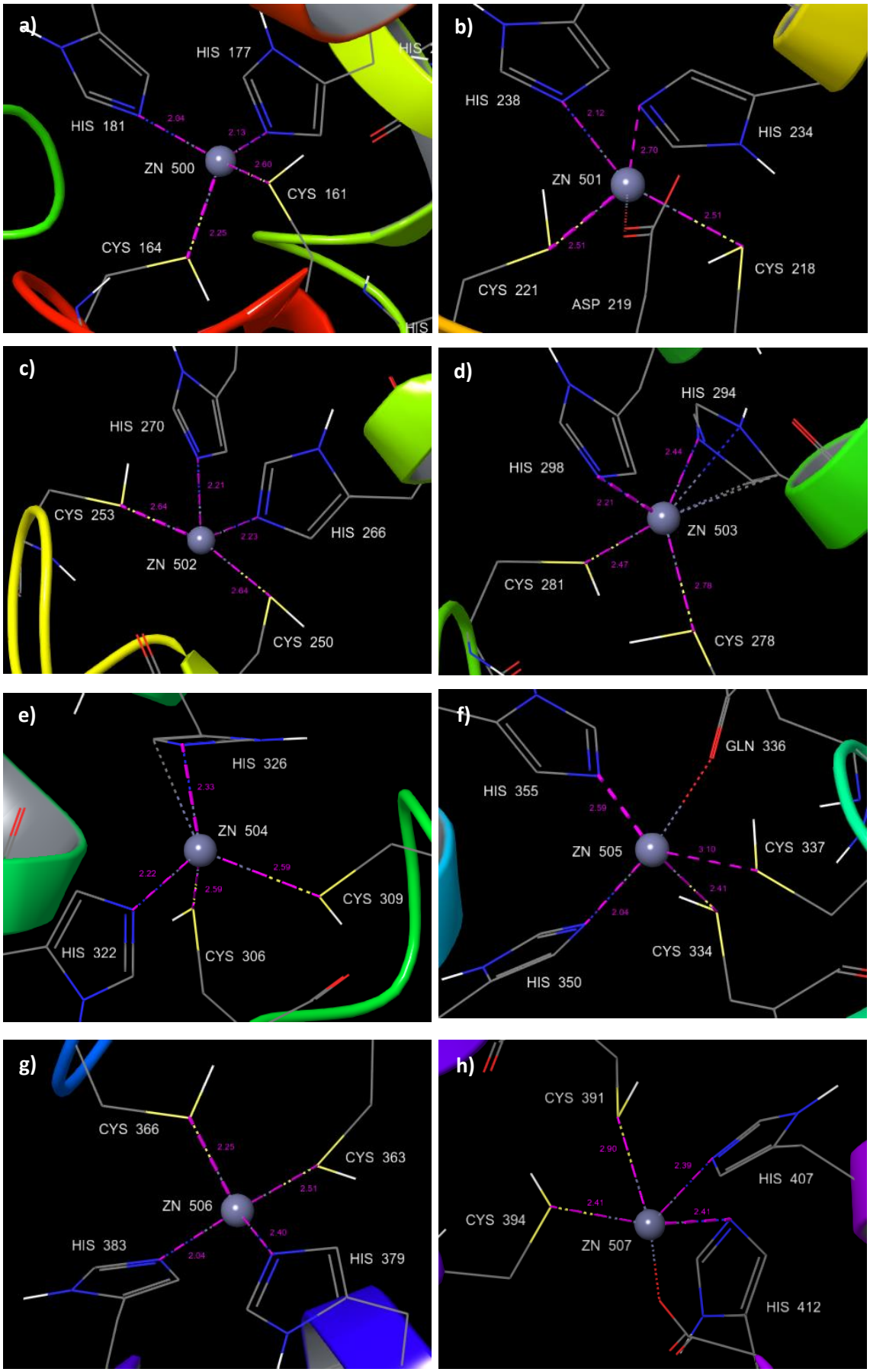
a)
HIS 177
HIS 181
2.04
2.13
ZN 500
2.60
CYS 161
2.25
CYS 164
b)
HIS 238
2.12
HIS 234
2.70
ZN 501
2.51
2.51
CYS 218
CYS 221
ASP 219
c)
HIS 270
2.21
CYS 253
2.64
2.23
HIS 266
ZN 502
2.64
CYS 250
d)
HIS 294
2.44
HIS 298
2.21
ZN 503
2.47
2.78
CYS 281
CYS 278
e)
HIS 326
2.33
ZN 504
2.22
2.59
2.59
CYS 309
HIS 322
CYS 306
f)
GLN 336
HIS 355
2.59
ZN 505
3.10
CYS 337
2.41
2.04
CYS 334
HIS 350
g)
CYS 366
2.25
CYS 363
2.51
ZN 506
2.40
HIS 383
2.04
HIS 379
h)
CYS 391
2.90
2.39
HIS 407
2.41
2.41
CYS 394
ZN 507
HIS 412

Figure 75. (previous page) Zinc coordination in the different ZFs. **a)** ZF1, **b)** ZF2, **c)** ZF3, **d)** ZF4, **e)** ZF5, **f)** ZF6, **g)** ZF7 **h)** ZF8. The zinc atoms are represented as grey spheres. The sulphur atoms from cysteines are coloured yellow, whereas the nitrogen atoms from histidines are coloured blue. Polar hydrogens are coloured white. The distances between the zinc atoms and the coordinating residues are highlighted in pink (**Appendix 2.2** – column: REST DBD Final Model).

4.5.8. Re1 3D structure

The DNA double helix of Re1 consensus sequence was predicted using the MMB 3.2 package for Linux, through Docker. MMB (previously named RNABuilder) is a modelling tool that allows the construction of 3D structural and dynamic models of nucleic acids and proteins (Flores et al., 2011; Caulfield et al., 2014). MMB uses user-specified base pairing and stacking interactions, structural constraints and internal coordinates, among other parameters, to generate 3D structures of macromolecules (Flores et al., 2011; Caulfield et al., 2019). Furthermore, MMB uses the Amber99 molecular dynamics (MD) potential to simulate the interaction between atoms and to calculate energy (Case et al., 2005). After analysing the trajectories that the software output, the last frame of the last stage was selected to proceed with future studies. However, this structure appeared to have problems docking with the Prime REST DBD (**Figure 77.a**). Thus, a new structure of Re1 was created *de novo* using the web server from SCFBio IIT Delhi and then was optimized using the w3DNA 2.0. Both structures were compared (**Figure 76**), with the DNA from w3DNA appearing to be more organized than the one built in MMB software.

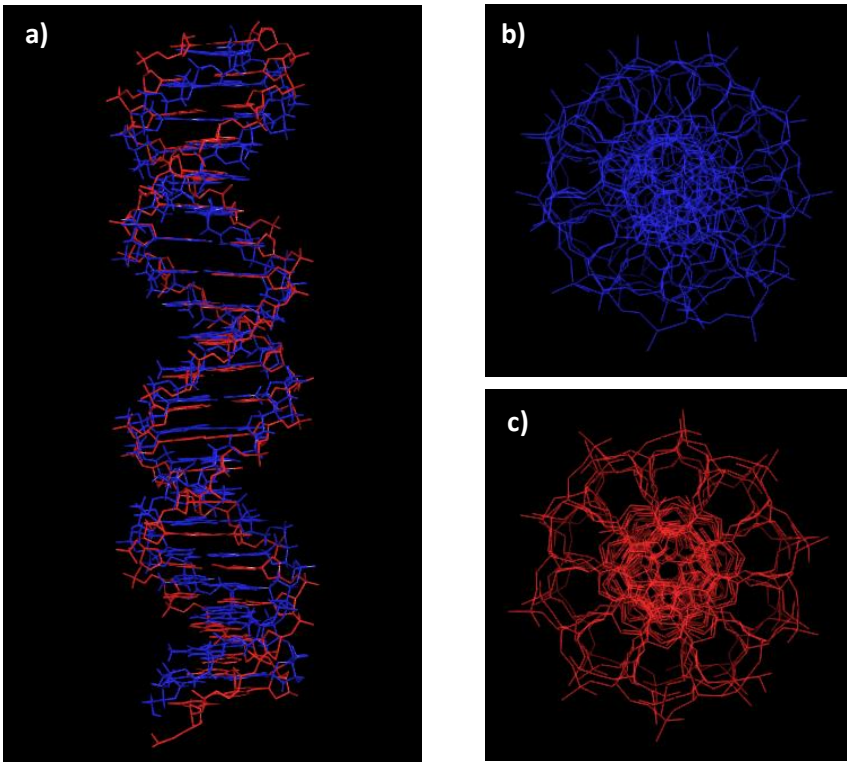

Figure 76. Predicted 3D structures of the B-DNA double helix of Re1 consensus sequence MMB software (blue) and the webserver w3DNA (red). **a)** Comparison between the two 3D structures of the Re1 consensus sequence superimposed (by the C-α atoms) in a lateral plane. **b)** and **c)** Comparison of the transversal plane.

4.5.9. Protein-DNA docking

The web server HDOCK was used to dock REST DBD from Schrödinger/Prime homology modelling with the two Re1 sequences obtained from MMB software and w3DNA (**Figure 77**).

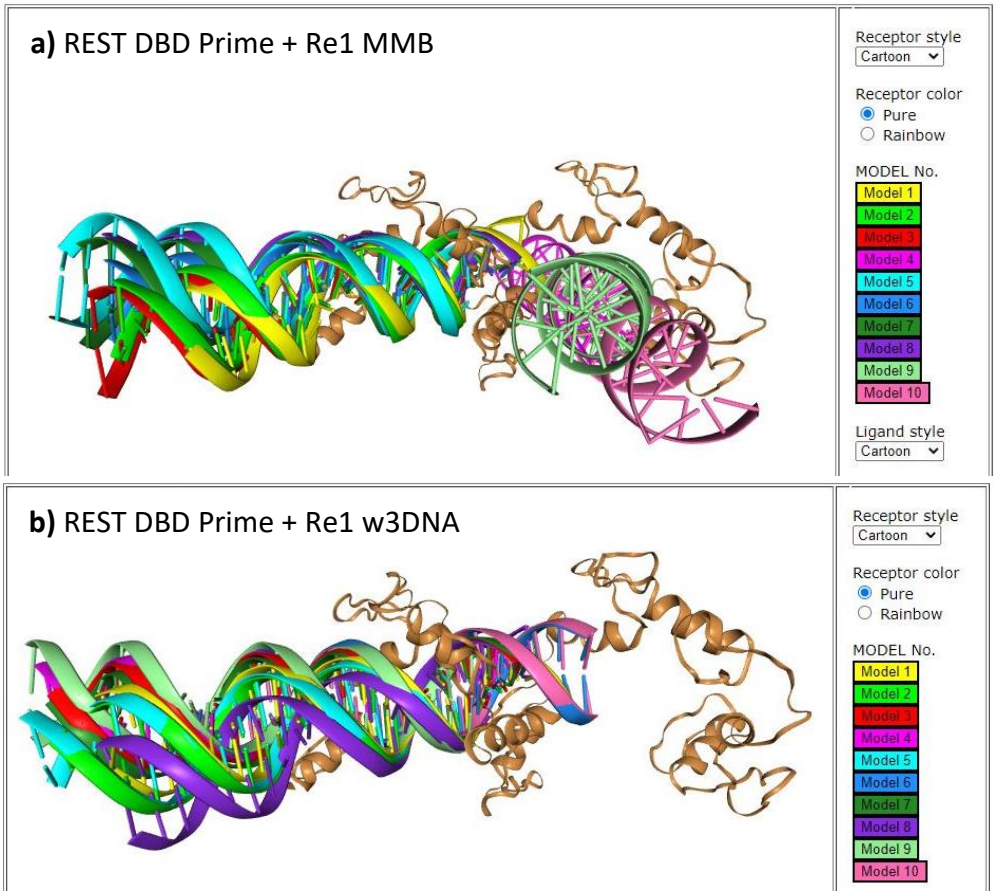

Figure 77. Docking of REST DBD from Prime homology modelling with Re1 structures built using **a)** MMB software and **b)** w3DNA. HDOCK displays the best 10 model colour coded.

It was observed that none of the DNA molecules fit completely into the protein's pocket, in any of the 10 best models. Furthermore, the Re1 DNA model built with w3DNA appears to be better as all the top 10 models are more or less inside the pocket of the protein, whereas when the docking was done with the DNA from MMB, two of the models show the DNA docked completely outside the pocket.

After careful analysis of the docked structures, it was concluded that there were six consecutive problematic residues, Glu260 to Lys265 (**Figure 78**). These residues were mutated into residues with simpler side chains, i.e. alanine and glycine (side chain is a -CH_3 and -H, respectively) to test if it was a stereochemical problem. However, that also did not work, and the problem was only bypassed when these amino acids were

completely (i.e. side chain plus the backbone) removed from the structure (REST DBD Δ260-265) and REST was docked with the DNA structure build with w3DNA 2.0.

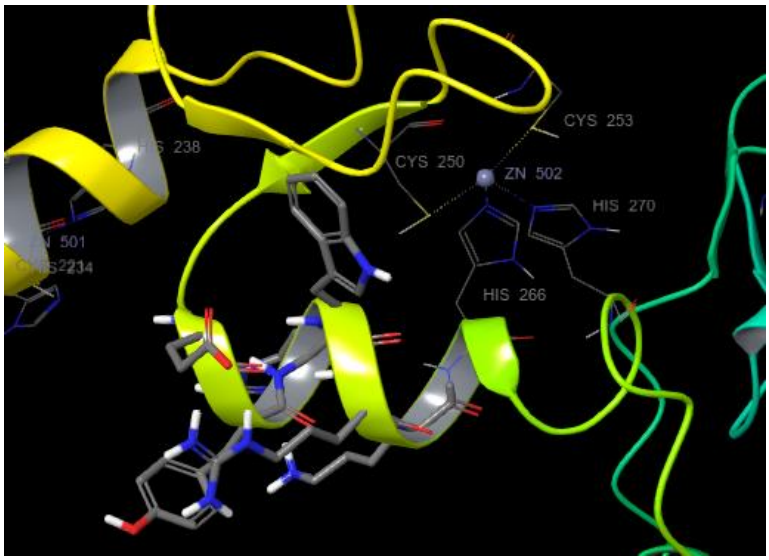

Figure 78. Residues Glu260-Lys265 that do not allow the DNA to fit perfectly in the inside of the REST DBD are located in the helix that makes ZF3. The problematic residues are represented by ball-and-stick (thicker structures), and they are coloured by atom type: oxygen (red), carbon (grey), hydrogen (white) and nitrogen (dark blue).

In fact, removing the problematic residues still did not allow Re1 from MMB software to dock fully with REST DBD (**Figure 79.a**) but this was resolved when docking with Re1 from w3DNA (**Figure 79.b**).

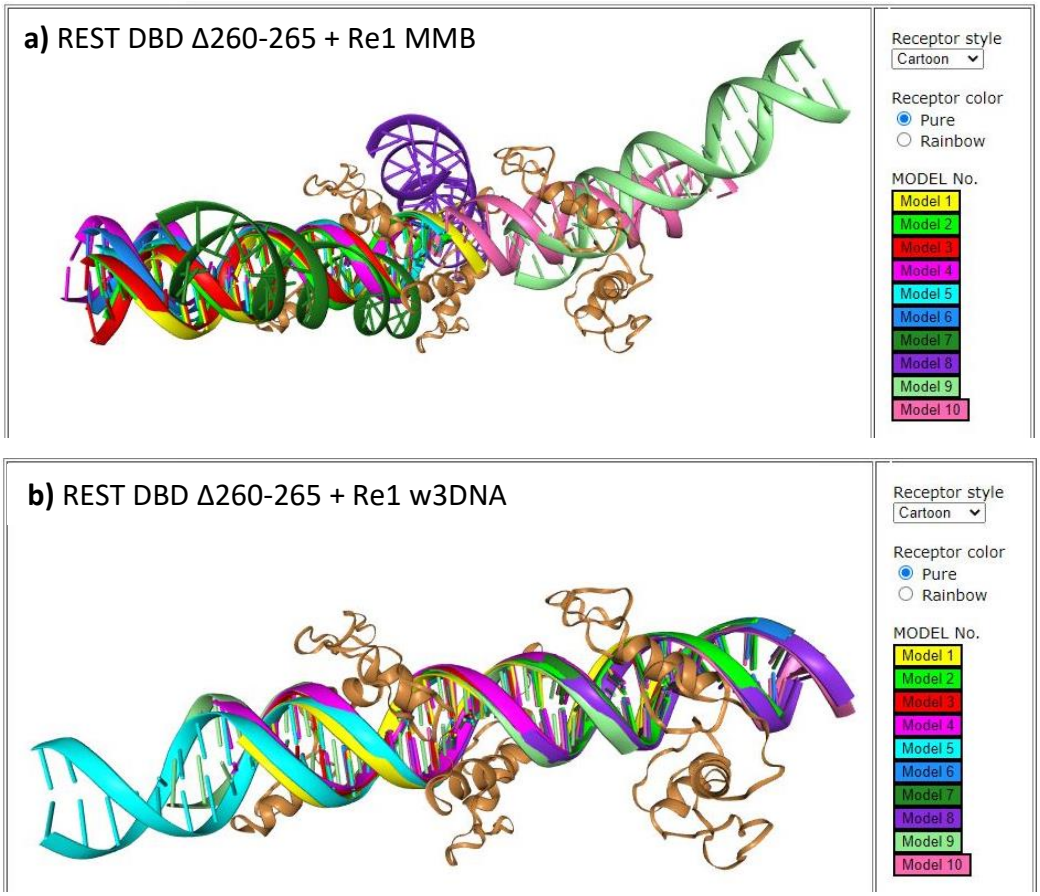

Figure 79. Docking of REST DBD from Prime homology modelling lacking the problematic residues (260-265) with Re1 structures built using **a)** MMB software and **b)** w3DNA. HDOCK displays the best 10 model colour coded.

5. DISCUSSION

REST has recently been implicated in AD, healthy ageing and longevity as neuroprotective, however the exact mechanisms mediating that role are still largely unclear. The first supervisor of this project has previously generated a genetically modified cKO mouse model with inactivation of *Rest,* specifically in the postnatal forebrain. This research project has taken the next steps in analysing this mouse model to study the role of REST in a series of AD-related characteristics in the brain. Common cellular traits of AD, like hyperphosphorylation of tau protein, neuronal, synaptic and dendritic degeneration and astrocytic activation were investigated through multiple techniques to evaluate the effects of the absence of REST. The developmental switch in synaptic NMDA receptors was also studied.

5.1. Tau phosphorylation and pathology

Tau is a microtubule-associated protein predominantly found in neurons, that has been reported to be involved in the stabilization of microtubules and regulation of axonal transport. Post-translational modifications, like phosphorylation, regulate the correct functioning of tau (Martin et al., 2013; Kimura et al., 2018). However, when there is a deregulation of such mechanisms, specifically hyperphosphorylation, tau detaches from microtubules and aggregates forming NFTs (Ittner and Götz, 2011; Iqbal et al., 2016). These NFTs are associated with multiple pathologies, also called tauopathies (Arendt et al., 2016). In fact, they represent one of the hallmarks of AD, being used in the diagnosis of this neurodegenerative disease (DeTure and Dickson, 2019). Tau has 85 residues possible of phosphorylation, with 44 having been observed to be phosphorylated in AD pathological tau. This process is mediated by kinases which have been thoroughly studied, such as CDK5 and GSK3β. Different kinases can phosphorylate the same epitope, making it a challenge to distinguish which epitope are phosphorylated at which point in AD's development and by which kinases.

Initially, this project wondered if ablation of REST affected the levels of total tau in the cortex or in the hippocampus of mice. It was observed that both genotypes presented similar levels of total tau in the two brain regions studied. However, from this analysis solely, no conclusion can be drawn about the phosphorylation state of tau, so three of the most commonly phosphorylated epitopes were also studied: pSer202, pThr205 and pSer396. The latter, Ser396, appears to be equally phosphorylated in both genotypes, with no significant differences being observed in the cortex or in the hippocampus. When considering the levels of pSer202 and pThr205 (detected by AT8 antibody), cortical samples of both genotypes presented high variability within samples of the same genotype. Yet no overall difference was observed between genotypes in the cortex. Interestingly, AT8 levels were clearly different in the hippocampus, with *Rest* cKO mice presenting as twice as much phosphorylation of residues Ser202 and Thr205 as the controls (**Figure 14**). This result has prompted further analysis of this phenotype by immunohistochemistry. In accordance with observations from Western blot technique, variability was also observed within samples of the same genotype. AT8 immunostained different types of structures: puncta, bigger agglomerate structures and filamentous structures (**Figure 18**). These structures are spread throughout the brain, in regions which have been associated with memory and AD pathology like the retrosplenial cortex, lateral parietal association cortex, the frontal cortex, striatum (Girard et al., 2013; Micotti et al., 2015; Motanis et al., 2021; Wang et al., 2022). Overall, there is a clear difference when comparing *Rest* cKO with control mice, with *Rest* cKO presenting more phosphorylated tau aggregates or puncta. This concurs with previous research in a cell culture system (SH-SY5Y cells) where the ablation of REST lead to an increase in the levels of phosphorylated tau regarding these epitopes (Lu et al., 2014).

Filamentous formations were observed throughout the sections and have similar morphology (quite often typical morphology) as blood vessels. In fact, this project hypothesizes that these are in fact blood vessels. The results observed could in theory be due to unspecific staining of peroxidase and DAB reaction with blood cells in the vasculature independently of the presence tau. This could in theory happen if perfusion of the brain has not been completely efficient. However, the immunohistochemistry (IHC) protocol was the same for all antibodies used in this project and these structures were only observed using AT8 and GSK3β (discussed further in this thesis in **section 5.1**)

antibodies, both associated directly or indirectly with phosphorylation of tau. No blood vessels were stained when the NeuN, GFAP, MAP2 and PSD-95 antibodies were used, despite the IHC protocol being the same and the fact that sections from the same mice were used. Furthermore, multiple mice were used from each genotype and the pattern in the AT8 and GSK3β IHC experiments was always the same, with *Rest* cKO mice always having a greater presence of these structures than control mice. Hence, the data in this project suggests that *Rest* cKO have a very interesting blood vessel phenotype, associated with an increase of phosphorylation of pSer202 and pThr205 of tau protein. Vasculature alterations have been reported in early AD and recently tau has been associated with these alterations (Bennett et al., 2018, 2020; Govindpani et al., 2019; Canepa and Fossati, 2021). It is thought that tau evades neurons and causes toxicity in other cells (Katsinelos et al., 2018; Canepa and Fossati, 2021). Thus, Bennett and colleagues (2020) have demonstrated angiogenesis in the brain of mice overexpressing tau and that this protein is present in AD's blood vessels (Bennett et al., 2018, 2020). That group has not studied phosphorylated tau. However, they have stained the brain of these mice with mouse IgG to observe the blood vessel morphology, and the morphology is very similar to the filamentous formations described here in this project.

Nevertheless, other types of morphologies were observed while staining sections with AT8 antibody. Apart from the filamentous structures, puncta and big agglomerates were also observed. Furthermore, some cells appear to have darker stain around a circular white region, which is hypothesized to be perinuclear staining, i.e. phospho-tau is located in the cytoplasm around the nucleus. These are characteristics usually associated with pretangles, the early stage of tangles. In fact, AT8 has been described to stain various types of structures, not only tangles and pretangles but also extracellular neuritic pathologies (extracellular accumulation of tau tangles) (Moloney et al., 2021).

As mentioned before, inhibition of REST has been previously associated with higher levels of phosphorylated tau in a cell culture system (Lu et al., 2014). This project is in agreement with previous studies, nevertheless, it takes it a step forward as the levels of phosphorylated tau are associated with structural differences. Further studies are needed to confirm this phenotype however, to the best of our knowledge this is the first time REST is proposed to be associated with any sort of tangles.

5.1.1. Tau protein kinases

As mentioned before, tau protein has 85 possible phosphorylation sites, with the same residue being able to be phosphorylated by multiple kinases. Hence it is a challenge to determine the importance of each residue phosphorylation and each kinase in AD's development. Nevertheless, two kinases have attracted particular attention when referring to tau phosphorylation: GSK3β and CDK5.

GSK3β is an important regulator of multiple physiological pathways involved in neural development, inflammation, and synaptic plasticity, for example (Llorens-Martín et al., 2014; Jaworski et al., 2019; Lauretti et al., 2020). As expected, dysregulation of GSK3β leads to many pathological events (D'mello, 2021). In fact, transgenic mice overexpressing GSK3β reproduce a typical AD phenotype, displaying the main hallmarks of AD, tau hyperphosphorylation, neurodegeneration and neuronal inflammation (Rodríguez-Matellán et al., 2020). GSK3β has been reported to phosphorylate 27 residues present in NFTs, including residues Ser202, Thr205 and Ser396 (Hanger et al., 2007; Llorens-Martín et al., 2014). Hence, here the levels of this relevant kinase were assessed in cortical samples of *Rest* cKO and control mice. Remarkably, when REST is ablated, mice present a two-fold increase in GSK3β expression in the cortex (**Figure 23**). This encouraged further studies by immunohistochemistry. Curiously, similar filamentous structures were observed by staining with an anti-GSK3β antibody as when staining the brain tissue for pSer202 and pThr205 with AT8 antibody (**Figure 27**). These structures were located not only in the hippocampus but also in regions of the cerebral cortex and in the striatum that have been mentioned before and that have been associated with memory and AD (Girard et al., 2013; Micotti et al., 2015; Motanis et al., 2021; Wang et al., 2022). Overall, there is a clear difference when comparing *Rest* cKO with control mice, with *Rest* cKO presenting more GSK3β-positive aggregates or puncta. However, no structures resembling tangles were observed with GSK3β. As it has been discussed before, this project hypothesizes that the absence of REST leads to blood vessel abnormalities associated, not only with an increase of phosphorylation of Ser202 and Thr205 but also with GSK3β. To the best of our knowledge, this is the first time a vascular phenotype has been associated with REST, phospho-tau and GSK3β.

Very few articles have addressed the role of GSK3β in angiogenesis. Kim *et al.* and Flugel *et al.* have demonstrated that inhibition of GSK3β promote angiogenesis in endothelial and HeLa cells lines (Kim et al., 2002; Flügel et al., 2012). Whereas Hoang and colleagues have demonstrated that inhibition of GSK3β improved functional neovascularization of hypoxic retina in mice (Hoang et al., 2010). To the best of our knowledge, no studies have been performed yet in the brain or in an AD context, and the results of this project identify the GSK3β structures mentioned above for the first time. Further research is clearly needed to characterise the role and importance of these structures in the brain but, given the proposed role of GSK3β in tau phosphorylation and AD, the identification of GSK3β-positive structures in the brain might prove an important neuropathological feature. Furthermore, these results provide important insights into delineating the role of REST in the brain and in AD. It would be of utmost importance to conduct in the future a similar immunohistochemical experiment using post-mortem human tissue, examining whether these GSK3β-positive structures are also present (specifically) in the brain of AD patients.

Given the brain's properties and functions, it is understandable that dysregulation of the vasculature has major impacts in the development of pathologies through events such as decrease of blood-flood which leads to hypoxia, or angiogenesis leading to faulty and leaky vasculature or even accumulation of neurotoxic components like Aβ plaques (Govindpani et al., 2019; Sweeney et al., 2019; Canepa and Fossati, 2021). This highlights the importance of the blood vessel phenotype suggested here and the need for further study.

GSK3β majorly targets substrates which have been previously phosphorylated, in a process called substrate priming. It has been widely reported a cooperation between CDK5 and GSK3β in the hyperphosphorylation of tau that leads to NFTs formation (Kimura et al., 2014, 2018; Llorens-Martín et al., 2014). Furthermore, CDK5 has been shown to indirectly regulate GSK3β through phosphatase 1 (PP1) (Morfini et al., 2004). GSK3β is constitutively activated, however phosphorylation of Ser9 by PP1 has been demonstrated to inhibit GSK3β functioning (Salcedo-Tello et al., 2011; Llorens-Martín et al., 2014; Jaworski et al., 2019).

Similar to GSK3β, CDK5 has multiple roles in important physiologic pathways in brain development, neuronal survival and memory (Liu et al., 2016; Allnutt et al., 2020; Takahashi et al., 2022). CDK5 function is tightly regulated by its activators, p35 and p39, with the quantity of these activators being a limiting factor, i.e. when the activators levels are low, CDK5 becomes inactivated (Mungenast and Tsai, 2011). Among these two activators, p35 has attracted considerably more attention than p39 in the AD field. An increase in intracellular Ca^{2+} will induce the protease calpain to cleave the N-terminal of these activators into their truncated and more stable forms, p25 and p29, respectively (Patrick et al., 1999). As the N-terminal possesses a sequence that maintains the p35/p39-CDK5 in the membrane, once cleaved, p25/p29-CDK5 will translocate to the cytoplasm and the nucleus where they will accumulate and promote neurotoxicity (Mungenast and Tsai, 2011; Liu et al., 2016; Allnutt et al., 2020). CDK5 has been reported to phosphorylate 11 residues present in NFTs, including the referred residues Ser202, Thr205 (Liu et al., 2016). Thus, this project wanted to study how REST affected this kinase. Since CDK5 is activated by binding to the activators p35/p25, an antibody against the C-terminal of p35 was used. Consequently, the truncated form, p25, will also be detected as observed in the Western blot experiments (**Figure 30** and **Figure 31**). The p35 activator expression is more pronounced in the cortex than p25, which is in agreement with previous research done using this antibody in AD's mouse models (Zhang et al., 2018). When comparing control and *Rest* cKO mice, it was observed that the absence of REST leads to an upregulation of both activators in the two regions of the brain studied.

Fischer and colleagues have shown that only a prolonged expression of p25 is pathological, with transient expression being beneficial for memory plasticity with an increase in LTP (Fischer et al., 2005). On the other hand, Shukla *et al.* have restored synaptic function in p25 transgenic mice by inhibiting p25-CDK5 complex (Shukla et al., 2017). In accordance with the results observed here, Lu *et al*. have also demonstrated that when REST is inactivated in SH-SY5Y cells there is an upregulation of p35 and p25 (Lu et al., 2014). Furthermore, *CDK5R1* is a REST-target gene in humans (Rockowitz and Zheng, 2015), and the promoter of the homologous gene in mice also has a Re1 site (perfectly aligned with the human Re1 site) to which REST can theoretically bind (further discussion on **section 5.1.2**). This further supports the hypothesis that in the absence of

REST, p25-CDK5 is upregulated and tau might be hyperphosphorylated in Ser202 and Thr205, as higher levels of these were also observed. Furthermore it strengthens the hypothesis that dysfunction in REST has a role in sporadic AD.

5.1.2. Identification of a putative *Re1* site in the *Cdk5r1* (p35) promoter.

Multiple studies have researched REST binding sites (Soldati et al., 2013; Rockowitz and Zheng, 2015; McGann et al., 2021). In particular, Rockowitz and Zheng have performed ChIP-Seq to identify REST-target genes in embryonic stem cells of both humans and mice (Rockowitz and Zheng, 2015). They identified that REST binds to 8,200 genomic regions in humans and 4,108 in mice. Among this vast list of genes, REST was found to bind to *CDK5R1* in human cells but there was no evidence of binding to the mouse homologous gene, *Cdk5r1* in that study. *CDK5R1* encodes p35, which is proteolytically cleaved by calpain, generating a p10 and p25 forms (Liu et al., 2016; Allnutt et al., 2020). The cleavage product p25 will hyperactivate CDK5 and leading consequently to hyperphosphorylation of tau (Mungenast and Tsai, 2011; Allnutt et al., 2020). Accordingly, accumulation of p25 has been observed in AD patients (Patrick et al., 1999).

The fact that *Cdk5r1* was not identified as a mouse REST-target gene in the study by Rockowitz and Zheng does not necessarily mean that *Cdk5r1* is not regulated by REST in the adult mouse brain, as a) that study was conducted in embryonic stem cells, and b) there are always false negatives in large-scale studies such as ChIP-Seq. Thus, this PhD project investigated the possibility of a putative *Re1* site in the *Cdk5r1* gene promoter, given the interesting results on p35/p25 and tau phosphorylation in *Rest* cKO mice. Using TFBSPred webtool, a REST-binding site was found in mouse chromosome 11 (**Figure 32**). This REST-binding site is located 479bp upstream of the first *Cdk5r1* coding region and is 100% conserved between humans and mice. The identification of this binding site raises the theoretical possibility that the higher levels of p35/p25 and phosphorylated tau and the tau-associated morphological abnormalities observed in *Rest* cKO mice might be due to lack of REST binding to the *Cdk5r1* promoter (REST is a transcriptional repressor). This theoretical possibility needs to be tested experimentally

in the future, e.g. by a chromatin immunoprecipitation experiment, for which the sequence flanking the identified Re1 site could be used for PCR primer design.

5.2. Neuronal labelling

Neuronal loss is one of the major cellular outcomes in Alzheimer's disease. In fact, it is resultant from a synergistic effect between multiple mechanisms that culminate in brain atrophy and consequently memory impairment and cognitive loss, AD main symptom (Mukhin et al., 2017). The hippocampus has a major role in memory and learning, plus it is highly susceptible to be affected in degenerative diseases. It can be divided into 3 main subregions: CA1, CA3 and DG, which have been extensively studied in the context of AD (Hullinger and Puglielli, 2017). A small region between the CA1 and CA3, given its location, has been overlooked until recently (Chevaleyre and Piskorowski, 2016; Pang et al., 2019). The CA2 is involved in social memory and has a distinct physiology and specific action firing patterns that allow a distinction from neighbouring neurons, having been associated with social memory (Chevaleyre and Piskorowski, 2016).

To assess the possibility of a neurodegenerative phenotype in *Rest* cKO mice, all the four subregions of the hippocampus were studied using a neuronal nuclei marker, NeuN. Initially DAB chromogen was used, however a fluorescent secondary antibody (Alexa 488) was used on the second set of mice. This allowed a better distinction between nuclei and facilitated the counting of neurons. After a detailed analysis of the hippocampus of three controls and three *Rest* cKO mice, no major differences in neuronal count were observed between genotypes, when analysing the entire hemisphere (**Figure 37** and **Figure 38**). The levels of NeuN were also analysed in cortical samples through Western blot, with no major differences being observed between genotypes. This is in agreement with the observations in the hippocampus through immunohistochemistry. The results obtained in this project appear to suggest that no major neurodegenerative phenotype is present in this new mouse model.

The findings here, although not revealing a neurodegenerative phenotype, are quite novel, as they contrast with previous findings in the literature, which however are based on analysis of mouse models with *Rest* inactivation during embryonic development (as opposed to inactivation in the adult brain in this project). Lu *et al.* studied the effect that the absence of REST has in the context of AD using a vast array of techniques. A Nestin-Cre transgenic mice was used to conditionally knock-out REST in the central and peripheral nervous system around the embryonic day (E) 11 (Lu et al., 2014; The Jackson Laboratory - Strain No. 003771, 2022). They observed a neurodegenerative phenotype in the hippocampus and in the cerebral cortex of these mice, with *Rest* cKO mice presenting at 8-months of age a neuronal loss of around 15% (Lu et al., 2014). Gao and colleagues studied REST role in neurogenesis in the adult brain and observed a decrease in the number of granule neurons in the DG when REST was inhibited (Gao et al., 2011). More recently, Wang and colleagues have studied the brain's development using a new model of *Rest* cKO, *GFAP-Cre;NRSF*$^{flox/flox}$, in which inhibition of *Rest* also happens before birth, at E13.5 (Wang et al., 2021). They observed an abnormal hippocampal structure, with lower levels of neuronal stem cells and neuronal progenitor cells, however, no conclusion was draw regarding the number of mature neurons. As discussed before in **section 1.5.2** (**Figure 3**), the brain of the mouse is still developing after birth (Chini and Hanganu-Opatz, 2021). Moreover, it has been proved that early inactivation of *Rest* causes early embryonic lethality (starting at E9.5), suggesting that this transcription factor has a major role in neural development, specifically in neurogenesis (Chen et al., 1998; Ballas et al., 2005; Gao et al., 2011). Hence, this project proposed to study a novel mouse model in which *Rest* was inactivated in the postnatal forebrain at 2-3 weeks of age, aiming to bypass any development abnormalities. Moreover, the brains used for histology experiments were from old mice, sacrificed at 14 to 18 months of age, and even at that age, no neurodegenerative phenotype was observed in *Rest* cKO mice. Although the studies that have used mouse models with inactivation of *Rest* during embryonic development are very important in exploring REST in specific contexts, the mouse model used in this project is possibly a more suitable experimental system for the study of ageing-related processes that are independent of developmental effects.

5.3. Dendritic labelling

The main symptom of Alzheimer's disease, loss of memory, is closely related with synaptic alterations such as presynaptic failure or dendritic degeneration and it appears to be an early trait of AD (Barthet and Mulle, 2020). Dendrites contain synapses, therefore dendritic degeneration might lead to synapse loss and consequently impair neural circuits that underlie cognitive impairment (Canter *et al*., 2016). It has been reported that Aβ levels might induce morphological abnormalities on dendrites, such as decrease in spine density (Grutzendler et al., 2007; Baloyannis, 2009). Curiously, dendritic abnormalities were found to be enough to alter synaptic function causing hyperexcitability in the hippocampus, which can lead to network impairment (Šišková et al., 2014; Busche and Konnerth, 2016; Zott et al., 2018). Thus, suggesting that dendritic degeneration might be an early trait of AD.

As no major neurodegeneration phenotype was observed in *Rest* cKO mice, another possibility explored by this project was a dendritic phenotype in *Rest* cKO mice. Therefore, dendritic morphology was also studied using an antibody against MAP2. This is a protein with a major role in determining and stabilizing the structure of dendrites and is not commonly found in the axon, making it a good dendritic marker.

The quantification of dendrites was not possible as a very high density of dendrites were observed. Nevertheless, a morphological analysis was performed (blindly) to evaluate length, quantity, orientation and localisation of dendrites within the hippocampal regions. Even though both genotypes demonstrated high variability between samples, there are some minor differences in individual mice that should be noted. In general, control mice appear to have more dendrites, which are longer than in *Rest* cKO mice, in accordance with a possible mild dendritic degeneration phenotype (Cochran *et al.,* 2014; Šišková *et al.*, 2014).

This possibility was further investigated by Western blot to study MAP2 levels in cortical and hippocampal samples. The cortex of *Rest* cKO mice appears to have lower levels of MAP2. Intriguingly, MAP2 appears to be overexpressed in the hippocampus. These results are rather inconclusive and are difficult to be interpreted without further investigation.

The limited quantity of literature available on REST and dendrites focuses on the regulation of REST by microRNAs and its consequences on dendrites (Giusti et al., 2014). So, these results are a step towards a better the understanding of REST role in dendritic function.

5.4. Synaptic degeneration

Neurons communicate through synapses in the brain. Neurotransmitters are released into the synaptic cleft, where they are recognized by receptors located at the post density membrane. These will recognize the neurotransmitters and will transduce the information for the postsynaptic neuron. Synaptic plasticity is considered a cellular correlate of memory loss which is a hallmark of Alzheimer's disease (Masliah et al., 2001; Lleó et al., 2019; Colom-Cadena et al., 2020). Lower levels of the presynaptic protein synaptophysin have been associated with loss of synapses and consequently cognitive decline (Sze et al., 1997; Scheff et al., 2006; Hong et al., 2016; Mampay et al., 2021).

As no major neurodegeneration phenotype was observed in *Rest* cKO mice, the possibility of evidence of a milder, synaptic degeneration phenotype in *Rest* cKO mice was explored. Therefore, the levels of synaptophysin, a major component of the presynaptic vesicle membrane, were analysed through Western blot. Levels of synaptophysin were studied in the cortex and in the hippocampus of *Rest* cKO and control mice. No significant differences were observed in any of the two brain regions, appearing to suggest that *Rest* cKO mice do not present synaptic degeneration phenotype, at least at a young age (3-4 months old). This contrasts with a previous study in neuroblastoma cells, where ablation of *Rest* led to altered levels of synaptophysin (Xu et al., 2021), the difference possibly being due to the different experimental system. The gene that encodes synaptophysin, *SP1*, is a REST-target gene (Lietz et al., 2003; Rockowitz and Zheng, 2015). However, even though *SP1* can be targeted by REST, it is not clear whether this takes place in the adult brain (as with many other REST target genes). Moreover, given the relatively young age of the mice used for Western blot it might be possible that an age-dependent synaptic degenerative phenotype is present in *Rest* cKO mice but not yet developed at the age of 3-4 months. It would be very

interesting to explore in the future a possible age-dependent decrease in synaptophysin levels in *Rest* cKO mice (currently not possible due to tissue unavailability).

To fully study the possibility of synaptic degeneration, this project also studied PSD-95, a postsynaptic marker. PSD-95 is as scaffolding protein that stabilizes and regulates membrane receptors, such as NMDA and AMPA, ion channels and signalling proteins in the postsynaptic membrane of excitatory neurons (Sheng and Kim, 2002). Furthermore, it helps maintaining GluN2A receptors in the synaptic site and reduces GluN2B endocytosis (Snyder et al., 2005; Kellermayer et al., 2018). Thus it has a pivotal role in plasticity mechanisms and consequently in memory. Initially, the levels of PSD-95 were compared between *Rest* cKO and control mice, in the both the cortex and in the hippocampus. There was no difference between genotypes in the hippocampus, although PSD-95 showed a tendency to be downregulated in cortical samples of *Rest* cKO mice. This was further evaluated through immunohistochemistry. Overall, control mice appear to have higher levels of PSD-95 in the CA1, with darker cell projections and postsynaptic densities. Nevertheless, in Pair 1 the pattern is the opposite, with Rest cKO appearing to have higher levels of PSD-95. In the literature, PSD-95 expression has been demonstrated to be both up- and downregulated in the context of AD. One possible explanation for this difference lays in different studies using different models of mice, at different ages, with different severities of AD-associated phenotypes (Savioz et al., 2014). Altogether, the PSD-95 Western blot and IHC results do not provide conclusive evidence about a possible regulation of PSD-95 by REST (PSD-95 is a REST-target gene but with no proven binding of REST in the adult brain), and further studies need to be conducted. For example, it would be important to simultaneous study the presence of PDS95 and synaptophysin through immunofluorescence to further address the possibility of a synaptic degeneration phenotype in *Rest* cKO mice.

Another element involved in synaptic plasticity is NMDA receptors. These are localised in the postsynaptic membrane and regulate synapses and LTP by controlling the levels of intracellular Ca^{2+} (Mota et al., 2013). These ionotropic receptors only allow Ca^{2+} into the dendrite after there is a depolarization of the postsynaptic membrane (which relieves a magnesium blockade) and after binding with glutamate. The increase of intracellular Ca^{2+} initiates a variety of the signalling cascades. Functional NMDA

receptors are heterotetramers commonly composed of two GluN1 and two GluN2 subunits, with different subunit compositions being associated with different NMDA receptors properties and therefore different expression levels and localizations (Rodenas-Ruano et al., 2012; Vieira et al., 2020). During embryogenesis, GluN2B subunits are vastly expressed throughout the brain. With adulthood, the expression decreases and becomes restricted to the forebrain. On the other hand, expression of GluN2A subunits increase through postnatal development in the central nervous system (Vieira et al., 2020). REST has been demonstrated to regulate this switch in the constitution of NMDA receptors' subunits in early postnatal development, between P15-P17 (Rodenas-Ruano et al., 2012). It has been proposed that REST, together with cellular prion protein, epigenetically represses the gene encoding GluN2B subunit, *Grin2b*, which will alter NMDA receptor properties through decline of GluN2B and consequently switch for GluN2A subunits (Rodenas-Ruano et al., 2012; Song et al., 2018). To further study REST role in this postnatal developmental switch, both GluN2A and GluN2B protein levels were assessed in the cortex and in the hippocampus of *Rest* cKO and control mice. No major differences were observed in any condition. This appears to confirm one of the points made by Rodenas-Ruano and colleagues on the resilience of the switch, i.e. once the switch has been triggered, REST inhibition does not increase GluN2B expression.

5.5. Astrocytic activation

Astrocytes have an important role in the maintenance of the correct neuronal functioning of the brain. However, given certain cellular insults, astrocytes can become reactive, changing their morphology and function and contributing to neuroinflammation, another characteristic of AD (Perez-Nievas and Serrano-Pozo, 2018; Arranz and De Strooper, 2019; Monterey et al., 2021). Thus, in order to analyse the possibility of astrocytic activation, an antibody against GFAP, an astrocytic marker, was used. This protein composes the intermediate filaments and is known to be highly expressed in the aged brain, in neurodegenerative diseases and upon brain damage. Since GFAP is not specific for activated astrocytes, only darker brown cells with three or

more protrusions in a star-shaped form were considered as reactive astrocytes in this project.

Astrocytes were mostly observed in the hippocampus and the *corpus callosum* but were scarcely observed in the neocortex. This is in agreement with Zhang and colleagues, who have discussed the different astrocytic markers usually used in research. They concluded that GFAP is a better maker to use in the study of the hippocampus and the *corpus callosum*, whereas N-Myc downstream-regulated gene 2 (NDRG2) is more suitable to study the cortex (Zhang et al., 2019). In the future it would be interesting to use NDRG2 to further study the astrocytic activation in the cortex.

The CA1 in *Rest* cKO mice appears to have more reactive astrocytes than control mice, which could suggest a mild neuroinflammation phenotype. This difference is seen throughout the hemisphere but is more pronounced in the more lateral slides. In this plane of the hemisphere, the CA1 of the dorsal hippocampus is located very closely to the auditory cortex. Curiously, REST has been previously associated with deafness (Nakano et al., 2018). Furthermore, an increase in astrocytic activation has been observed in this region of the brain when they replicated tinnitus, a hearing disorder where there is a perception of sound even without external stimulus (Xia et al., 2020). Thus, the increase in inflammation in this region observed in the absence of REST could be associated with hearing impairment.

In a different approach, the levels of GFAP were assessed in cortical and hippocampal samples of *Rest* cKO and controls, through Western blot technique. Supporting the evidence observed through histology, no major differences were observed in the expression of GFAP in the cortex or in the hippocampus. However, it should be taken into consideration that GFAP levels, as an astrocytic marker, can be associated with the quantity of astrocytes in general but no inference regarding reactive astrocytes can be done just by evaluating GFAP levels.

Astrocytic activation and neuroinflammation has been extensively studied in AD context. As astrocytes are activated, usually due to the deposition of Aβ plaques, they lose their regular function to support the neurons and acquire neurotoxic properties that contribute to the further development of AD (Perez-Nievas and Serrano-Pozo, 2018; Monterey et al., 2021; Preman et al., 2021). It has been shown that reduced levels of REST leads to more reactive astrocytes on Parkinson's disease mouse models, which

were associated with an aggravated progression of the disease (Li et al., 2020). Furthermore, recent studies have suggested REST neuroprotective function to be mediated by astrocytes, as the ablation of this transcription factor in astrocytes lead to an increase in manganese-induced neuroinflammation (Pajarillo et al., 2022). This role appears to be mediated by the upregulation of glutamate transporter 1 expression (Pajarillo et al., 2021). Lu *et al.* also studied astrocytic activation in the CA1 of 8-month-old mice with *Rest* inactivation during embryonic development. They observed that in the absence of REST, astrocytes were considerably bigger and more branched, i.e. more reactive (Lu et al., 2014). Data presented in this thesis are in agreement with the Lu *et al*. observations, even though if to a lesser degree. Thus, when REST is inactivated postnatally, a mild astrocytic phenotype can be observed.

5.6. RNA-Seq

RNA-Seq is a high-throughput next generation of mRNA sequencing method that allows the identification and quantification of global gene expression – transcriptome, i.e., all the genes expressed in a target tissue at a certain time (Wang et al., 2009; Stark et al., 2019). Since REST is a transcriptional factor that regulates a vast number of genes, it is of the utmost importance to analyse the transcriptome in *Rest* cKO compared to control mice. In this project, the initial RNA-Seq bioinformatic analysis was performed as a collaboration by Dr Celine Keime at the IGBMC, France, as this required specialised software. This first analysis used the Benjamini and Hochberg method to control false discovery rate and culminated in a list of three differentially expressed genes in *Rest* cKO: *Oxr1* and *Pop4* were found to be downregulated, whereas *Slc2a1* was upregulated when compared to control samples. *Oxr1* has not been previously studied specifically in the context of AD, but it has been proposed to be protective against oxidative stress and thus prevent neurodegeneration (Volkert and Crowley, 2020). *Pop4* encodes a subunit of the small nucleolar ribonucleoprotein complexes (proteins responsible for RNA splicing) and has seen observed to be included in a cluster of genes downregulated in AD associated with mitochondrial electron transport, the proteosome and ribosomes (Lanke et al., 2018). *Slc2a1* encodes GLUT1, a glucose transporter that mediates glucose

to the brain through the blood-brain barrier. Winkler and colleagues have shown that a ablation of GLUT1 induce early AD-like degeneration in mice with vascular degeneration (Winkler et al., 2015). Additionally it has been reported that *Slc2a1* is associated with angiogenesis and hypoxia in glioblastomas (Komaki et al., 2019).

Although the Benjamini and Hochberg method is a widely accepted approach to control false discovery rate, i.e., limit the number of false positives that are reported as significant, many researchers do not agree with the principle of this method (Rothman, 1990; Althouse, 2016). As far as it is known, the mouse model used in this project is the first whereby *Rest* is specifically inactivated in the postnatal mouse brain, thus it is important to get a full perspective of all the genes that might be affected and avoid some important genes to be overlooked. Therefore, a second analysis of the normalized read counts was performed without the FDR adjustment to the p-value, and a total of 552 genes were found to be differentially expressed: 287 genes were downregulated and 265 were upregulated in *Rest* cKO mice.

Upregulated genes were consistently associated with immune response and angiogenesis. Upregulation of inflammatory response, interleukin-15 signally pathway and production of cytokines were biological processes that were enriched in all three types of analysis. These were accompanied with an upregulation of protein binding and enzymatic activity, although in the PPI network, no molecular function terms were statistically significantly enriched. Regarding the cellular components, cell surface was also enriched in GOE and PPI, whereas GSE revealed an enrichment in terms associated with the mitochondria. Furthermore, pathways associated with diseases affecting the immune system appear to be upregulated in *Rest* cKO mice.

These results suggest that there is a strong immune response in *Rest* cKO mice. Curiously both types, innate and adaptive immune responses appeared to be associated with the lack of REST. Immune response has been extensively related with AD (Zhang et al., 2013; Heavener and Bradshaw, 2022). Lu *et al.* have also demonstrated that inhibition of REST leads to gliosis (Lu et al., 2014). Furthermore, genes related with cytokine production and protein binding were also upregulated which strengthen the hypothesis of inflammatory response (Rubio-Perez and Morillas-Ruiz, 2012). On the other hand, the mild astrocytic activation observed in the brain of *Rest* cKO in this project further supports the RNA-Seq data. However, it is still unclear what is behind this

phenotype. Is this response caused by the absence of REST directly, that stops repressing detrimental pathways, or is this some sort of compensatory mechanism of the brain to deal with the absence of REST?

RNA-Seq data revealed another strong upregulated process in *Rest* cKO, angiogenesis, with higher vasculature development and morphogenesis, particularly blood vessels (**Table 9** and **Appendix 4.9**). Additionally, as mentioned before, the only upregulated gene with FDR correction was *Slc2a1,* which has been previously associated with angiogenesis and blood-brain barrier leaks (Winkler et al., 2015; Komaki et al., 2019). This concurs with the immunohistochemistry results observed in this project when staining for GSK3β and phospho-tau. RNA-Seq results support the hypothesis that the filamentous structures in *Rest* cKO mice observed when staining sections for phospho-tau (pSer202 and pThr205) and GSK3β could be indeed blood vessels. Nevertheless, this hypothesis needs to be confirmed with the use of an endothelial marker (endothelial cells that line the vasculature). Moreover, they strengthen the conclusion that the blood vessel alterations revealed by these experiments in *Rest* cKO mice are indeed a consequence of the absence of REST and are not the outcome of unspecific staining. These are very interesting results as, to the best of our knowledge, this is the first time that a vascular phenotype is proposed to be associated with REST, and in addition, this appears to be related to proteins with important roles in AD. Vasculature alterations have been reported in early AD and recently, tau has been associated with these alterations (Bennett et al., 2018, 2020; Govindpani et al., 2019; Canepa and Fossati, 2021). Nevertheless, this project presents for the first time evidence of a possible association between GSK3β and blood vessels. It would be interesting the investigate in the future whether GSK3b-positive blood vessels are also found in human post-mortem brain tissue from AD patients, possibly to a greater extent than in control subjects.

Furthermore, an enrichment in mitochondria cellular components might suggest hypermetabolism, which has been associated with early stages of AD as compensatory mechanism (Ashraf et al., 2015; Rubinski et al., 2020). Interestingly, a hypermetabolic phenotype has also been observed in mice with *Rest* inactivation during embryonic development by monitoring glucose utilisation (Zullo et al., 2019).

On the other hand, ablation of REST downregulated the expression of genes associated with synaptic activity and neuronal pathways, suggesting a possible synaptic dysfunction in *Rest* cKO mice. Synaptic activity-associated genes are suggested to be affected in *Rest* cKO mice in all three aspects studied as well as in the pathway analysis. Excitatory synapse assembly, post synapse structure and function and vesicle-mediated transport were found consistently present in the multiple analyses. Moreover, neuronal pathways appear to be strongly associated with downregulated genes, in particular glutamate receptor signalling pathway is found to be affected in all the three aspects of each type of analysis. Although we didn't observe any differences in the GluN2A/GluN2B ratio regarding NMDA receptors, these receptors can be affected in multiple ways by the various proteins that interact with them, such as PSD-95, which has been observed to be slightly decreased in this project in *Rest* cKO. Moreover, there are other types of receptors that might be affected. In fact, RNA-Seq data suggests that GABAergic, dopaminergic and serotonergic synapses are also affected by the absence of REST. Synaptic degeneration has been vastly associated with AD with Aβ and tau pointed as major culprits (Chen et al., 2019; Jackson et al., 2019). Chen and colleagues have summarized the role of hyperphosphorylated tau, GSK3β, CDK5 and PSD-95 in synaptic degeneration (Chen et al., 2019). Additionally learning and memory are also terms significantly enriched in *Rest* cKO downregulated genes, with LTP and LDP pathways being also strongly affected.

Overall, the transcriptome data support some of the results observed in this project through targeted techniques. In addition, the upregulation of pathways involved in immune responses in *Rest* cKO mice and the downregulation of pathways involved in synaptic activity further support an important role for REST in AD and provide interesting insights into the associated neurobiological mechanisms.

To further understand REST molecular mechanisms in the development of AD, it would be of utmost importance to identify which of the differentially expressed genes are REST-target genes in the adult brain of mice. This could be done through a ChIP-Seq analysis and subsequent comparison of the ChIP-Seq patterns between control and *Rest* cKO mice. Unfortunately, due to time-constrictions, it wasn't possible to perform ChIP-Seq with these samples. Nevertheless, the list of differently expressed genes obtained

in this project was compared with the previously described literature to further explore how the absence of REST affects those genes, i.e. if the difference in expression was due to REST direct or indirect regulation.

Rockowitz and Zheng have studied REST-binding sites embryonic stem cells from both humans and mice (Rockowitz and Zheng, 2015). As expected, given the importance of REST in neurodevelopment, they found that it binds to 8199 genomic regions in the human genome and 4107 in the mouse genome. On the other hand, McGann and colleagues, studied REST-binding profile in postnatal hippocampal samples of humans and mice. Interestingly, they observed that REST attaches to 2125 genomic regions in humans and 221 in mice.

The list of differently expressed genes obtained in this project was compared with the previously described literature to further explore how the absence of REST affects those genes, i.e. if the difference in expression was due to REST direct or indirect regulation. Around 13.6% of the differentially expressed genes in our samples have been identified as REST-binding genes in mouse embryonic stem cells (Rockowitz and Zheng, 2015). However, when compared with hippocampal samples from 5-week-old mice, REST appears to only bind to three genes, around 0.5% of all the differentially expressed genes (McGann et al., 2021).

REST is a major transcription factor that regulates time-dependent repression of certain genes by binding to a Re1 sequence. Hence, REST-binding profile genes changes throughout life and is dependent on the different types of cells where it is located and the cellular context. This highlights the need to clarify the link between the phenotypes observed and the transcriptome data from our *Rest* cKO mice, where REST was inhibited only in adulthood, to fully understand the mechanisms behind REST involvement in AD.

5.7. REST DBD and *Re1* 3D structure – Molecular modelling

Computational chemistry arose to complement to the time-consuming experimental approaches (Cavasotto et al., 2019; Huggins et al., 2019). Nowadays, using an array of different types of simulations techniques, we can predict molecular

structures, how they will behave in the most diverse conditions and how they will interact with other molecules using a computer.

REST has been suggested to have a neuroprotective role in the aging brain and is lost in AD patients. Hence, an enhancer of REST could potentially be of great value for AD therapy. The 3D structures of both REST and the *Re1* sequence would be very useful in this direction as they would enable a computational screen of potential molecules using chemical libraries.

Few articles have addressed the 3D structure of REST. The three entries that refer to REST in the PDB only describe very small portions of the protein either on the N-terminal (2CYZ) or on the C-terminal (6DU2 and 6DU3). Recently the online server I-TASSER was used to obtain an automated 3D predictive structure for the REST DBD with the aim to produce monoclonal antibodies against the DBD (Cortés-Sarabia et al., 2019). However, the automated modelling server used by the authors might not be the most suitable method to do pharmacological studies. Therefore, there is a need to predict a more accurate model for the 3D structure of REST.

After using BLAST to search for similar protein sequences in the PBD, it was concluded that there is no protein in the PDB that has a sequence similar to the entire REST protein (1097 residues). Therefore, this project focused on the DBD (254 residues: 159-412), as it is responsible for binding to a recognition sequence, Re1, situated on the promotor region of target genes and therefore inhibiting their transcription (Mampay and Sheridan, 2019).

The 3D structure of both REST DBD and Re1 sequence were suggested using two different methods. Homology modelling allowed the proposition of a structure for REST based on the protein with highest similarity, ZPF568. Whereas the DNA sequence was initially designed *de novo* using MMB software package but as it was showing some problems docking with REST DBD, a new model was built using a different strategy, *de novo* build using the web server from SCFBio IIT Delhi and then optimized using the w3DNA 2.0.

As rule of thumb, for homology modelling purposes, proteins need to have at least 30% of sequence identity, although some authors suggest a higher percentage (Madhusudhan et al., 2005; Xiang, 2006). Below this threshold, the accuracy of the proposed model becomes uncertain. However, nowadays computer programmes rely

on other parameters beside sequence identity to validate the final structure (Hillisch et al., 2004; Madhusudhan et al., 2005; Xiang, 2006). The proteins with highest query coverage and percentage of identify obtained through BLAST search were Aart (2I13) and ZFP568 (5WJQ) with, respectively, 35.68% and 27.11%. So, this particular aim was predicted to be a challenge since the beginning of the project.

Aart (2I12) is a protein with six ZF motifs crystallized by Segal and colleagues to study this group of protein-DNA recognition domain (Segal et al., 2006). Whereas Patel *et al.* studied ZFP568, a protein with the same ZF motifs, that has a very important role in embryonic development in mice. Due to difficulties in the crystallization process, ZFP568 has three entries in the PDB (5V3J, 5V3M and 5WJQ) that, although refer to the same protein, have slight differences regarding the number and which of the 11 zinc fingers are crystallized in the structure. The length of the DNA sequence that is bound to the protein also differs from entries (Patel et al., 2018). Given that ZF1 does not bind to the DNA sequence and ZF11 does, the PDB 5WJQ was selected to be used as template to predict REST DBD structure with Prime.

Since Aart only has six ZF, it would have been very difficult to model the two extra ZFs that REST possesses, as there wouldn't be a template. On the other hand, ZFP568 has more ZFs than REST so it's easier to use in homology modelling. Additionally, as a way to test the software that we would use later in the project, both the referred proteins were submitted to the HDOCK software to be docked with their native DNA (Yan et al., 2020). The small ligand RMSD obtained were very good indicators that the server works well which gives confidence in the HDOCK server (**Appendix 2.4**).

Of the ten ZFs crystallized in 5WJQ, the first ZF did not align with REST, having the alignment suggested by Prime started with the second motif. Moreover, this alignment suggested some problems that needed to be fixed. As the software aligned residue Gly499 (of the template) in position 122 (of the query – REST), a gap in the helix was created, so this residue was moved four positions backwards so that the helix was fully structured. The block His604–Ser608 (template) was moved one residue to the left in order to create a gap on Val196 (query). This means that the software is forced to build a valine instead of an arginine (residue suggested in the initial alignment). As valine has a shorter side chain, it would be easier to fit inside the helix.

The ZF motif (**Figure 2**) is composed by a zinc atom that is tetrahedrally coordinated with two cysteines located in a β-sheet and two histidines in the C-terminal portion of the α-helix. So, the last two residues (of the template), His665 and Thr666 were moved one position to the right, to align the histidine on both sequences so that the ZF8 motif can be correctly formed in the final structure.

The zinc atoms were chosen according with which ZF of the template were going to be used in the homology model. After carefully analysis of the final alignment (**Figure 7**), it was concluded that all the helices from the template will form ZF motifs on REST, except for the second helix. This helix is located in a region of the REST sequence where there are no cysteines or histidines, so it's not possible to form a ZF C2H2 motif. Therefore, and because the first ZF is left out of the template, only zinc atoms 702, 704-710, were chosen to build REST model. However, after building the final structure of REST, some of the zinc atoms were not coordinating with the surrounding residues as the minimization's steps required before had relaxed the structure and distanced the zinc atom from their coordinating groups. Hence, constraints had to be added to the structure to ensure that the sulphur (from cysteines) and nitrogen (from histidines) atoms were less than 3Å from the zinc atom, to ensure coordination. The values of the constraints were decided based on the template distances. Additionally, zero order bonds were assigned to each ZF to keep the structure of the motifs intact.

Regarding the DNA sequence, the Re1 structure was built using MMB software and was then initially docked directly to ZFP568 and Aart. The docking wasn't successful for either protein, with the DNA not fitting completely inside the pocket of the proteins, which was somewhat expected as Re1 is not the native DNA. Once REST DBD Schrödinger/Primer homology model structure was finalized it was submitted to HDOCK to be docked with Re1. Logically, the results were very similar to ZFP568 docking with Re1. At this point, a new DNA structure was build *de novo* using a different method and was then optimized using the w3DNA 2.0. This new structure was also docked with the REST DBD homology model.

After analysing the docked structures, it was identified a region of the protein that tightened the pocket, not allowing the DNA molecules to fit completely inside. The six residues, Glu260 to Lys265 were identified as causing this problem (**Figure 78**). Multiple attempts were made to identify the reason of this behaviour, like replacing the side

chains for simpler ones. However, the DNA would only fit inside the protein if these amino acids were completely removed from the structure. This would only happen if the REST DBD was docked with the Re1 obtained from w3DNA, suggesting that this DNA model is better than the one proposed with MMB. Furthermore, this suggests that the problem was on the backbone of the protein itself (positioning of residues) and not the side chains of the residues. Of these six residues, only one was created using all the coordinates from the template, the remaining five were created using only the coordinates from the backbone, which further supports the previously suggested theory. Furthermore, these residues are part of the helix that constitutes ZF3 which should be responsible to interact with the DNA, so it would be extremely difficult to improve the structure without affecting the protein-DNA interaction.

In 2021, a new database of protein structures, AlphaFold became available (Jumper et al., 2021; Ruff and Pappu, 2021). This is a new computational method which relies on artificial intelligence to predict with high accuracy protein structure. AlphaFold resulted in the implementation of a novel protein database with more than 200 million proteins with suggested structure. David *et al.* discussed brilliantly the strengths and challenges of AlphaFold through a non-expert in computational biology perspective (David et al., 2022). Apart from proposing a structure, AlphaFold also informs on the model confidence using a "per-residue confidence score" and the predicted aligned error.

As described before in **Section 4.5.7**, there are some discrepancies between REST DBD predicted using Schrodinger/Prime and AlphaFold. The major difference being the absence of zinc atoms in the AlphaFold model, which will have a major impact in future studies. Zinc atoms have a key role in maintaining protein structure and stability and consequently, function. Additionally, there are some differences concerning the secondary structure, although the residues involved show a decrease in the model confidence in AlphaFold. This strengthens the model predicted in this project using Prime.

Given the docking results, it became clear that the structure build is not optimal and cannot be used for further studies. This was expected to be a challenge since, as referred before, building proteins through homology modelling using sequences with less than 30% of sequence similarity is really difficult, with the accuracy of the final model decreasing considerably below this percentage (Madhusudhan et al., 2005). On the

other hand, there is still no clear answer as if it is the protein that adapts to the optimal conformation to interact with the DNA molecule or if it is the DNA that bends to fit the protein. Hence, it is extremely difficult to predict accurately DNA structure and study its dynamics binding to proteins (Huggins et al., 2019).

6. CONCLUSIONS

AD is a neurodegenerative condition affecting predominantly older populations, being the major form of dementia. Given the rise of life-expectancy globally, AD's prevalence is increasing, making it an important global health concern. No cure is currently available and clinical trials have not been able to halt the progress of AD. Therefore, there is a clear need to investigate further the underlying brain mechanisms in order to develop more effective therapeutical approaches. This research project has aimed to contribute to this effort by analysing *Rest* cKO mice for the presence or absence of a series of AD-associated phenotypes in the brain (**Figure 80**).

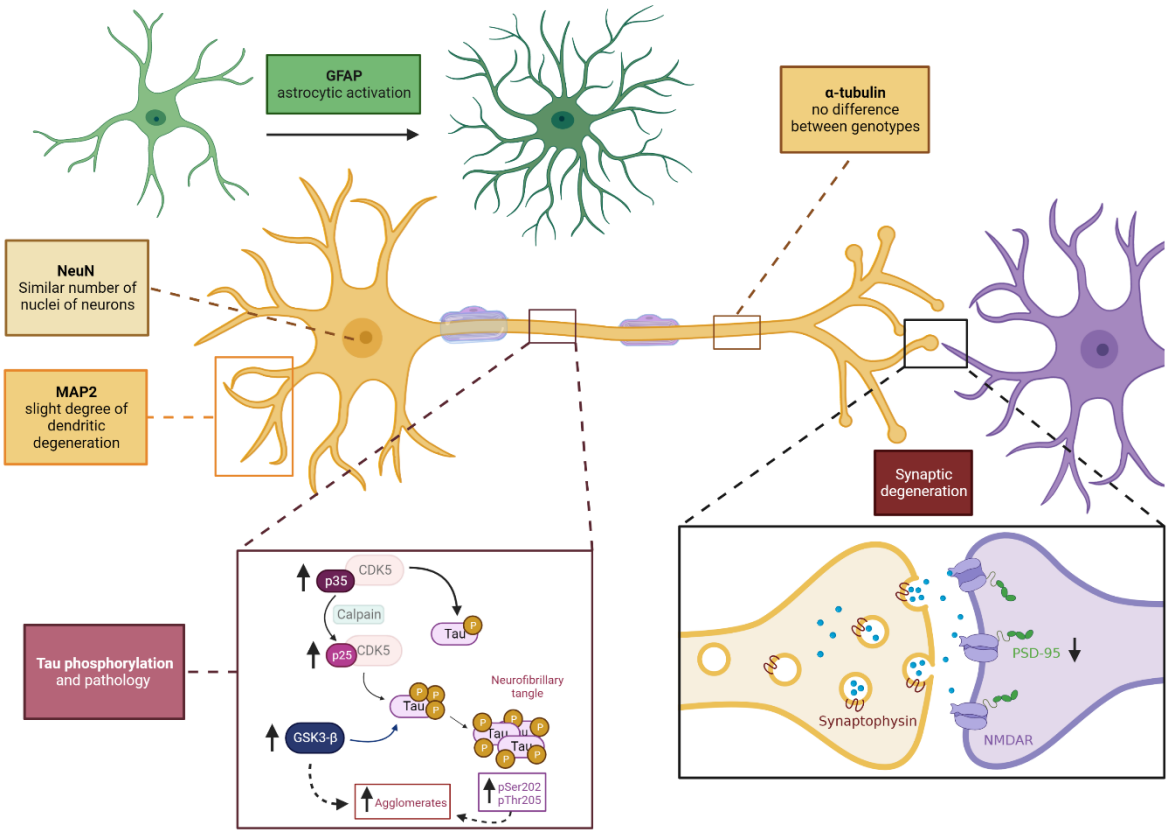

Figure 80. Overview of potential REST effects on the hallmarks of AD. Diagram created with BioRender.com

Hyperphosphorylation of tau protein is a hallmark of AD. This project studied how ablation of REST affects the levels of total tau and of three phosphorylated tau epitopes, pSer202, pThr205 and pSer396. Although no difference was observed regarding total tau and pSer396 levels, *Rest* cKO mice showed an increase of phosphorylation of residues Ser202 and Thr205 in the hippocampus, when compared with control mice, two residues that have attracted a great deal of attention in the context of AD (Martin et al., 2013). This result has prompted further analysis of this phenotype by phospho-tau (Ser202 and Thr205) immunohistochemistry, which suggested a very interesting blood vessel phenotype together with structures resembling pre-tangles in *Rest* cKO mice present both in the neocortex and in the hippocampus. Next, this project wondered which kinases were likely to be responsible for phosphorylation of tau in the referred epitopes. The levels of the thoroughly studied kinase GSK3β and CDK5, activators p35 and its truncated form p25, were also investigated. Remarkably, all these three proteins were found at higher levels in the neocortex of *Rest* cKO mice, whereas p35/p25 levels were also increased in the hippocampus. Curiously, filamentous structures, possibly representing blood vessels were observed both in the neocortex and in the hippocampus of *Rest* cKO mice when staining with an anti-GSK3β antibody that appeared similar to some of the structures observed with phospho-tau (pSer202 and pThr205) immunohistochemistry. Moreover, RNA-Seq data supported the hypothesis that the filamentous structures in *Rest* cKO mice observed are indeed blood vessels, with some of the *Rest* cKO upregulated genes being associated with angiogenesis and blood vessel morphology. Thus, this project presents for the first time evidence that GSK3β is associated with blood vessels and, in addition, that the quantity of GSK3β-positive blood vessels seems to be regulated by REST. Altogether these very interesting observations (phospho-tau and GSK3β immunohistochemistry, and RNA-Seq) suggest for the first time, to the best of our knowledge, an association between REST and a vascular phenotype, and in addition, this appears to involve proteins with important roles in AD.

A neurodegenerative phenotype has been previously demonstrated when *Rest* was inactivated during embryonic development. This project wanted to investigate if the absence of REST, when inactivated postnatally and without an effect on development (therefore with stronger relevance to AD), would reproduce a similar phenotype. This is of particular significance given the very important role of REST during development

(Chen et al., 1998). The analysis of a possible neurodegenerative phenotype was conducted blindly and very thoroughly, paying particular attention to matching *Rest* cKO and control sections in terms of medial-to-lateral position, and analysing multiple slides per mouse representative of the entire hemisphere. All four main subregions of the hippocampus were studied individually. The results obtained in this project appear to suggest that this new mouse model presents no major difference regarding the number of neurons between genotypes. The findings here, although not revealing a neurodegenerative phenotype, are quite novel, as they contrast with previous findings in the literature (Lu et al., 2014), which have been based on analysis of mouse models with *Rest* inactivation during embryonic development (as opposed to inactivation in the postnatal brain in this project).

The possibility of dendritic and synaptic degeneration was also studied through multiple techniques with results cautiously suggesting the possible presence of mild degeneration phenotypes in *Rest* cKO mice. Nevertheless, analysis of the transcriptome revealed that ablation of REST downregulated genes which are strongly associated with synaptic activity and neuronal pathways. Genes associated with glutamate receptor signalling pathway appear to be particularly affected in *Rest* cKO, though the GluN2A/GluN2B subunit ratio in NMDA receptors does not appear to be altered in these mice as revealed by Western blot analysis.

Neuroinflammation is another hallmark of AD and was also studied in this project through the analysis of astrocytic activation. Results suggest that when REST is inactivated postnatally, a mild astrocytic phenotype can be observed. This is in agreement with the Lu *et al.* (2014) observations (with inactivation of *Rest* during embryonic development), even though if to a lesser degree in this project. Furthermore, RNA-Seq data have suggested a strong immune response in *Rest* cKO mice, concurring with the immunohistochemistry observations. However, it is still unclear what is behind this phenotype.

Throughout this project the importance of REST in the aged brain has been highlighted. The possibility of contributing to the future design of REST enhancers has also been discussed, and how homology modelling could have a major role in that process. This project suggested a 3D structure for the REST DBD and for the *Re1* DNA sequence. The docked models of both structures were also studied, which highlighted

six problematic residues. Moreover, the structure was thoroughly compared with other available models that were created applying different methods, which point out the strengths of the Prime model. As stated before in **Section 5.7**, trying to purpose a structure for REST was quite an ambitious aim with obvious limitations. Even though the REST DBD 3D structure proposed in this project has a major fault that prevented further studies, it also has some useful aspects that cannot be overlooked. Although there is still no validated 3D structural model of REST, hopefully in the future it will be possible to predict the REST structure using the method described in this project with a template with higher sequence identity with REST.

Overall, postnatal ablation of REST appears to present a phenotype resembling several aspects of early mild AD, with pivotal mechanisms appearing affected in Rest cKO mice. Nevertheless, this study harbours some limitations, namely the use of different aged mice for distinctive techniques, which restricted a direct comparison of results obtained through immunohistochemistry. Also, time constraints did not allow the identification of REST-binding genes through ChIP-Seq, which could enlighten the relationship between the differentially expressed genes and REST regulation. Furthermore, the use of an endothelial marker would have greatly enhanced this project as it would confirm the hypothesis of a vascular phenotype associated with tau phosphorylation and GSK3β. Finally, the highest percentage of sequence identity with REST sequence was only of 30% which hindered the generation of the homology model.

7. FUTURE PERSPECTIVES

As far as it is known, the mouse model used in this project is the first whereby *Rest* is specifically inactivated in the postnatal mouse brain. It is fair to suggest that this mouse model is possibly a more suitable experimental system for the study of ageing-related processes, when compared with mouse models with early *Rest* inactivation. Overall, postnatal ablation of REST appears to present a phenotype resembling features of mild AD, with pivotal mechanisms appearing affected in *Rest* cKO mice but without (possibly before) major neurodegeneration, possibly reminiscent of early, pre-diagnosed stages of AD. Nevertheless, further research is needed to further investigate the phenotypes observed here. It would be very interesting to study the immunohistochemistry results with more powerful microscopy, to characterise the observed structures in more detail. Also, it is essential to use a marker of the endothelial cells that line the vasculature to confirm that filamentous structures observed are in fact, blood-vessels.

Additionally, it would be good to study the role of REST in regulating other epitopes of phosphorylated tau, like Ser404, and other kinases that are also involved in tau-phosphorylation, like p38 mitogen-activated protein kinase (MAPK). On the other hand, it would be very interesting to study the possible presence of Aβ plaques in the brain of *Rest* cKO mice and the levels of soluble Aβ. Also, it would be important to simultaneous study the presence of PDS95 and synaptophysin through immunofluorescence to further address the possibility of synaptic degeneration. Finally, having studied global gene expression, it would be good to identify REST-target genes in the adult brain of control mice through a ChIP-Seq analysis and to compare with the ChIP-Seq pattern in *Rest* cKO mice. Given the p35/p25 and phospho-tau results in this project and the identification of an *Re1* site in the p35 promoter, it would be of particular interest to study the possible binding of REST to the p35 promoter in the adult brain of control mice and whether this is absent in *Rest* cKO mice.

This projected characterised for the first time the role of REST in the brain in a mouse model in which the important functions of REST during development are not disturbed. Furthermore, it provided interesting clues on the regulation of certain AD-associated phenotypes by REST that need further investigation.

8. REFERENCES

Allnutt, A.B., Waters, A.K., Kesari, S. and Yenugonda, V.M., (2020) Physiological and Pathological Roles of Cdk5: Potential Directions for Therapeutic Targeting in Neurodegenerative Disease. *ACS Chemical Neuroscience*, 119, pp.1218–1230.

Althouse, A.D., (2016) Adjust for Multiple Comparisons? It's Not That Simple. *Annals of Thoracic Surgery*, [online] 1015, pp.1644–1645. Available at: http://dx.doi.org/10.1016/j.athoracsur.2015.11.024.

Alzheimer's Association, (2019) 2019 Alzheimer's Disease Facts and Figures. *Alzheimer's and Dementia*, [online] pp.1–88. Available at: https://www.alz.org/alzheimers-dementia/10_signs.

Alzheimer's Association, (2022) 2022 Alzheimer's disease facts and figures. *Alzheimer's and Dementia*, 184, pp.700–789.

Anon (2020) *RCSB Protein Data Bank (PDB)*. [online] Available at: https://www.rcsb.org/ [Accessed 23 Jun. 2020].

Anon (2022) *The Jackson Laboratory - Strain No. 003771*. [online] Available at: https://www.jax.org/strain/003771.

Aoki, H., Hara, A., Era, T., Kunisada, T. and Yamada, Y., (2012) Genetic ablation of Rest leads to in vitro-specific derepression of neuronal genes during neurogenesis. *Development*, 1394, pp.667–677.

Arendt, T., Stieler, J.T. and Holzer, M., (2016) Tau and tauopathies. *Brain Research Bulletin*, 126, pp.238–292.

Arnsten, A.F.T., Datta, D., Del Tredici, K. and Braak, H., (2021) Hypothesis: Tau pathology is an initiating factor in sporadic Alzheimer's disease. *Alzheimer's and Dementia*, 171, pp.115–124.

Arranz, A.M. and De Strooper, B., (2019) The role of astroglia in Alzheimer's disease: pathophysiology and clinical implications. *The Lancet Neurology*, [online] 184, pp.406–414. Available at: http://dx.doi.org/10.1016/S1474-4422(18)30490-3.

Ashraf, A., Fan, Z., Brooks, D.J. and Edison, P., (2015) Cortical hypermetabolism in MCI subjects: a compensatory mechanism? *European Journal of Nuclear Medicine and Molecular Imaging*, 423, pp.447–458.

Ballas, N., Grunseich, C., Lu, D.D., Speh, J.C. and Mandel, G., (2005) REST and its corepressors mediate plasticity of neuronal gene chromatin throughout neurogenesis. *Cell*, [online] 1214, pp.645–657. Available at: http://dx.doi.org/10.1016/j.cell.2005.03.013.

Ballatore, C., Lee, V.M.Y. and Trojanowski, J.Q., (2007) Tau-mediated neurodegeneration in Alzheimer's disease and related disorders. *Nature Reviews Neuroscience*, 89, pp.663–672.

Baloyannis, S.J., (2009) Dendritic pathology in Alzheimer's disease. *Journal of the Neurological Sciences*, [online] 2831–2, pp.153–157. Available at: http://dx.doi.org/10.1016/j.jns.2009.02.370.

Baltaci, S.B., Mogulkoc, R. and Baltaci, A.K., (2019) Molecular Mechanisms of Early and Late LTP.

Neurochemical Research, [online] 442, pp.281–296. Available at: http://dx.doi.org/10.1007/s11064-018-2695-4.

Barnett, C., Senapathi, T. and Bray, S., (2020) *Analysis of molecular dynamics simulations (Galaxy Training Materials).* [online] Available at: https://galaxyproject.github.io/training-material/topics/computational-chemistry/tutorials/analysis-md-simulations/tutorial.html#rmsd [Accessed 10 Jul. 2020].

Barthet, G. and Mulle, C., (2020) Presynaptic failure in Alzheimer's disease. *Progress in Neurobiology*. [online] Available at: https://doi.org/10.1016/j.pneurobio.2020.101801.

Beglopoulos, V., Sun, X., Saura, C.A., Lemere, C.A., Kim, R.D. and Shen, J., (2004) Reduced β-amyloid production and increased inflammatory responses in presenilin conditional knock-out mice. *Journal of Biological Chemistry*, 27945, pp.46907–46914.

Bennett, J.P. and Keeney, P.M., (2018) RNA-Sequencing Reveals Similarities and Differences in Gene Expression in Vulnerable Brain Tissues of Alzheimer's and Parkinson's Diseases. *Journal of Alzheimer's Disease Reports*, 21, pp.129–137.

Bennett, R.E., Hu, M., Fernandes, A., Perez-Rando, M., Robbins, A., Kamath, T., Dujardin, S. and Hyman, B.T., (2020) Tau reduction in aged mice does not impact Microangiopathy. *Acta Neuropathologica Communications*, 81, pp.1–17.

Bennett, R.E., Robbins, A.B., Hu, M., Cao, X., Betensky, R.A., Clark, T., Das, S. and Hyman, B.T., (2018) Tau induces blood vessel abnormalities and angiogenesis-related gene expression in P301L transgenic mice and human Alzheimer's disease. *Proceedings of the National Academy of Sciences of the United States of America*, 1156, pp.E1289–E1298.

Berson, A., Nativio, R., Berger, S.L. and Bonini, N.M., (2018) Epigenetic Regulation in Neurodegenerative Diseases. *Trends in Neurosciences*, [online] 419, pp.587–598. Available at: http://dx.doi.org/10.1016/j.tins.2018.05.005.

Blair, L.J., Frauen, H.D., Zhang, B., Nordhues, B.A., Bijan, S., Lin, Y.C., Zamudio, F., Hernandez, L.D., Sabbagh, J.J., Selenica, M.L.B. and Dickey, C.A., (2015) Tau depletion prevents progressive blood-brain barrier damage in a mouse model of tauopathy. *Acta neuropathologica communications*, 3, p.8.

Braak, H. and Del Tredici, K., (2014) Are cases with tau pathology occurring in the absence of Aβ deposits part of the AD-related pathological process? *Acta Neuropathologica*, 1286, pp.767–772.

Burkholder, N.T., Mayfield, J.E., Yu, X., Irani, S., Arce, D.K., Jiang, F., Matthews, W.L., Xue, Y. and Zhang, Y.J., (2018) Phosphatase activity of small C-terminal domain phosphatase 1 (SCP1) controls the stability of the key neuronal regulator RE1-silencing transcription factor (REST). *Journal of Biological Chemistry*, 29343, pp.16851–16861.

Busche, M.A. and Konnerth, A., (2016) Impairments of neural circuit function in Alzheimer's disease. *Philosophical Transactions Royal Society B*, 371, pp.1–10.

Canepa, E. and Fossati, S., (2021) Impact of Tau on Neurovascular Pathology in Alzheimer's Disease. *Frontiers in Neurology*, 11January, pp.1–19.

Canter, R.G., Penney, J. and Tsai, L.H., (2016) The road to restoring neural circuits for the

treatment of Alzheimer's disease. *Nature*, 5397628, pp.187–196.

Carbon, S., Douglass, E., Good, B.M., Unni, D.R., Harris, N.L., Mungall, C.J., Basu, S., Chisholm, R.L., Dodson, R.J., Hartline, E., Fey, P., Thomas, P.D., Albou, L.P., Ebert, D., Kesling, M.J., Mi, H., Muruganujan, A., Huang, X., Mushayahama, T., LaBonte, S.A., Siegele, D.A., Antonazzo, G., Attrill, H., Brown, N.H., Garapati, P., Marygold, S.J., Trovisco, V., dos Santos, G., Falls, K., Tabone, C., Zhou, P., Goodman, J.L., Strelets, V.B., Thurmond, J., Garmiri, P., Ishtiaq, R., Rodríguez-López, M., Acencio, M.L., Kuiper, M., Lægreid, A., Logie, C., Lovering, R.C., Kramarz, B., Saverimuttu, S.C.C., Pinheiro, S.M., Gunn, H., Su, R., Thurlow, K.E., Chibucos, M., Giglio, M., Nadendla, S., Munro, J., Jackson, R., Duesbury, M.J., Del-Toro, N., Meldal, B.H.M., Paneerselvam, K., Perfetto, L., Porras, P., Orchard, S., Shrivastava, A., Chang, H.Y., Finn, R.D., Mitchell, A.L., Rawlings, N.D., Richardson, L., Sangrador-Vegas, A., Blake, J.A., Christie, K.R., Dolan, M.E., Drabkin, H.J., Hill, D.P., Ni, L., Sitnikov, D.M., Harris, M.A., Oliver, S.G., Rutherford, K., Wood, V., Hayles, J., Bähler, J., Bolton, E.R., de Pons, J.L., Dwinell, M.R., Hayman, G.T., Kaldunski, M.L., Kwitek, A.E., Laulederkind, S.J.F., Plasterer, C., Tutaj, M.A., Vedi, M., Wang, S.J., D'Eustachio, P., Matthews, L., Balhoff, J.P., Aleksander, S.A., Alexander, M.J., Cherry, J.M., Engel, S.R., Gondwe, F., Karra, K., Miyasato, S.R., Nash, R.S., Simison, M., Skrzypek, M.S., Weng, S., Wong, E.D., Feuermann, M., Gaudet, P., Morgat, A., Bakker, E., Berardini, T.Z., Reiser, L., Subramaniam, S., Huala, E., Arighi, C.N., Auchincloss, A., Axelsen, K., Argoud-Puy, G., Bateman, A., Blatter, M.C., Boutet, E., Bowler, E., Breuza, L., Bridge, A., Britto, R., Bye-A-Jee, H., Casas, C.C., Coudert, E., Denny, P., Es-Treicher, A., Famiglietti, M.L., Georghiou, G., Gos, A.N., Gruaz-Gumowski, N., Hatton-Ellis, E., Hulo, C., Ignatchenko, A., Jungo, F., Laiho, K., Le Mercier, P., Lieberherr, D., Lock, A., Lussi, Y., MacDougall, A., Ma-Grane, M., Martin, M.J., Masson, P., Natale, D.A., Hyka-Nouspikel, N., Orchard, S., Pedruzzi, I., Pourcel, L., Poux, S., Pundir, S., Rivoire, C., Speretta, E., Sundaram, S., Tyagi, N., Warner, K., Zaru, R., Wu, C.H., Diehl, A.D., Chan, J.N., Grove, C., Lee, R.Y.N., Muller, H.M., Raciti, D., van Auken, K., Sternberg, P.W., Berriman, M., Paulini, M., Howe, K., Gao, S., Wright, A., Stein, L., Howe, D.G., Toro, S., Westerfield, M., Jaiswal, P., Cooper, L. and Elser, J., (2021) The Gene Ontology resource: Enriching a GOld mine. *Nucleic Acids Research*, 49D1, pp.D325–D334.

Case, D.A., Cheatham, T.E., Darden, T., Gohlke, H., Luo, R., Merz, K.M., Onufriev, A., Simmerling, C., Wang, B. and Woods, R.J., (2005) The Amber Biomolecular Simulation Programs. *J Comput Chem*, 26, pp.1668–1688.

Castillo-Carranza, D.L., Nilson, A.N., Van Skike, C.E., Jahrling, J.B., Patel, K., Garach, P., Gerson, J.E., Sengupta, U., Abisambra, J., Nelson, P., Troncoso, J., Ungvari, Z., Galvan, V. and Kayed, R., (2017) Cerebral microvascular accumulation of tau oligomers in Alzheimer's disease and related tauopathies. *Aging and Disease*, 83, pp.257–266.

Caulfield, T., Coban, M., Tek, A. and Flores, S.C., (2019) Molecular dynamics simulations suggest a non-doublet decoding model of –1 frameshifting by tRNAser3. *Biomolecules*, 911, pp.1–14.

Caulfield, T.R., Fiesel, F.C., Moussaud-Lamodière, E.L., Dourado, D.F.A.R., Flores, S.C. and Springer, W., (2014) Phosphorylation by PINK1 Releases the UBL Domain and Initializes the Conformational Opening of the E3 Ubiquitin Ligase Parkin. *PLoS Computational Biology*, 1011.

Cavasotto, C.N., Aucar, M.G. and Adler, N.S., (2019) Computational chemistry in drug lead discovery and design. *International Journal of Quantum Chemistry*, 1192, pp.1–19.

Chen, Y., Fu, A.K.Y. and Ip, N.Y., (2019) Synaptic dysfunction in Alzheimer's disease: Mechanisms and therapeutic strategies. *Pharmacology and Therapeutics*, [online] 195, pp.186–198. Available at: https://linkinghub.elsevier.com/retrieve/pii/S0163725818302031 [Accessed 25 Mar. 2020].

Chen, Z.F., Paquette, A.J. and Anderson, D.J., (1998) NRSF/REST is required in vivo for repression of multiple neuronal target genes during embryogenesis. *Nature Genetics*, 202, pp.136–142.

Chevaleyre, V. and Piskorowski, R.A., (2016) Hippocampal Area CA2: An Overlooked but Promising Therapeutic Target. *Trends in Molecular Medicine*, [online] 228, pp.645–655. Available at: http://dx.doi.org/10.1016/j.molmed.2016.06.007.

Chini, M. and Hanganu-Opatz, I.L., (2021) Prefrontal Cortex Development in Health and Disease: Lessons from Rodents and Humans. *Trends in Neurosciences*, [online] 443, pp.227–240. Available at: https://doi.org/10.1016/j.tins.2020.10.017.

Chong, J.A., Tapia-Ramirez, J., Kim, S., Toledo-Aral, J.J., Zheng, Y., Boutros, M.C., Altshuller, Y.M., Frohman, M.A., Kraner, S.D. and Mandel, G., (1995) REST: A mammalian silencer protein that restricts sodium channel gene expression to neurons. *Cell*, 806, pp.949–957.

Chouliaras, L., Mastroeni, D., Delvaux, E., Grover, A., Kenis, G., Hof, P.R., Steinbusch, H.W.M., Coleman, P.D., Rutten, B.P.F. and Hove, D.L.A. Van Den, (2013) Consistent decrease in global DNA methylation and hydroxymethylation in the hippocampus of Alzheimer's disease patients. *Neurobiology of Aging*, [online] 349, pp.2091–2099. Available at: http://dx.doi.org/10.1016/j.neurobiolaging.2013.02.021.

Chun, H. and Lee, C.J., (2018) Reactive astrocytes in Alzheimer's disease: A double-edged sword. *Neuroscience Research*, [online] 126, pp.44–52. Available at: http://dx.doi.org/10.1016/j.neures.2017.11.012.

Chwang, W.B., Riordan, K.J.O., Levenson, J.M. and Sweatt, J.D., (2006) ERK / MAPK regulates hippocampal histone phosphorylation following contextual fear conditioning. *Learning & Memory*, 13, pp.322–328.

Cobos, S.N., Bennett, S.A. and Torrente, M.P., (2019) The impact of histone post-translational modifications in neurodegenerative diseases. *BBA - Molecular Basis of Disease*, [online] 18658, pp.1982–1991. Available at: https://doi.org/10.1016/j.bbadis.2018.10.019.

Cochran, J.N., Hall, A.M. and Roberson, E.D., (2014) The dendritic hypothesis for Alzheimer's disease pathophysiology. *Brain Research Bulletin*, [online] 103, pp.18–28. Available at: http://dx.doi.org/10.1016/j.brainresbull.2013.12.004.

Colom-Cadena, M., Spires-Jones, T., Zetterberg, H., Blennow, K., Caggiano, A., Dekosky, S.T., Fillit, H., Harrison, J.E., Schneider, L.S., Scheltens, P., De Haan, W., Grundman, M., Van Dyck, C.H., Izzo, N.J. and Catalano, S.M., (2020) The clinical promise of biomarkers of synapse damage or loss in Alzheimer's disease. *Alzheimer's Research and Therapy*, 121, pp.1–12.

Condliffe, D., Wong, A., Troakes, C., Proitsi, P., Patel, Y., Chouliaras, L., Fernandes, C., Cooper, J., Lovestone, S., Schalkwyk, L., Mill, J. and Lunnon, K., (2014) Cross-region reduction in 5-hydroxymethylcytosine in Alzheimer's disease brain. *Neurobiology of Aging*, [online] 358, pp.1850–1854. Available at: http://dx.doi.org/10.1016/j.neurobiolaging.2014.02.002.

Congdon, E.E. and Sigurdsson, E.M., (2018) Tau-targeting therapies for Alzheimer disease. *Nature Reviews Neurology*, [online] 147, pp.399–415. Available at: http://dx.doi.org/10.1038/s41582-018-0013-z.

Cortés-Sarabia, K., Medina-Flores, Y., Alarcón-Romero, L.D.C., Mata-Ruíz, O., Vences-Velázquez, A., Rodríguez-Ruíz, H.A., Valdés, J. and Ortuño-Pineda, C., (2019) Production and

characterization of monoclonal antibodies against the DNA binding domain of the RE1-silencing transcription factor. *Journal of biochemistry*, 1665, pp.393–402.

D'mello, S.R., (2021) When good kinases go rogue: GSK3, p38 MAPK and CDKs as therapeutic targets for Alzheimer's and Huntington's disease. *International Journal of Molecular Sciences*, 2211.

David, A., Islam, S., Tankhilevich, E. and Sternberg, M.J.E., (2022) The AlphaFold Database of Protein Structures: A Biologist's Guide. *Journal of Molecular Biology*, [online] 4342, p.167336. Available at: https://doi.org/10.1016/j.jmb.2021.167336.

DeTure, M.A. and Dickson, D.W., (2019) The neuropathological diagnosis of Alzheimer's disease. *Molecular Neurodegeneration*, 141, pp.1–18.

Diaz-Ortiz, M.E. and Chen-Plotkin, A.S., (2020) Omics in Neurodegenerative Disease: Hope or Hype? *Trends in Genetics*, [online] 363, pp.152–159. Available at: https://doi.org/10.1016/j.tig.2019.12.002.

Domingues, C., da Cruz e Silva, O.A.B. and Henriques, A.G., (2017) Impact of Cytokines and Chemokines on Alzheimer's Disease Neuropathological Hallmarks. *Current Alzheimer Research*, 148, pp.870–882.

Dubey, H., Gulati, K. and Ray, A., (2018) Recent studies on cellular and molecular mechanisms in Alzheimer's disease: focus on epigenetic factors and histone deacetylase. *Reviews in Neurosciences*, 293, pp.1–20.

Dubois, B., Villain, N., Frisoni, G.B., Rabinovici, G.D., Sabbagh, M., Cappa, S., Bejanin, A., Bombois, S., Epelbaum, S., Teichmann, M., Habert, M.O., Nordberg, A., Blennow, K., Galasko, D., Stern, Y., Rowe, C.C., Salloway, S., Schneider, L.S., Cummings, J.L. and Feldman, H.H., (2021) Clinical diagnosis of Alzheimer's disease: recommendations of the International Working Group. *The Lancet Neurology*, 206, pp.484–496.

Edwards, F.A., (2019) A Unifying Hypothesis for Alzheimer's Disease: From Plaques to Neurodegeneration. *Trends in Neurosciences*, [online] 425, pp.310–322. Available at: https://doi.org/10.1016/j.tins.2019.03.003.

Eng, L.F. and Ghirnikar, R.S., (1994) GFAP and Astrogliosis. *Brain Pathology*, 43, pp.229–237.

Esposito, M. and Sherr, G.L., (2019) Epigenetic modifications in Alzheimer's neuropathology and therapeutics. *Frontiers in Neuroscience*, 13MAY, pp.1–12.

Fedotova, A.A., Bonchuk, A.N., Mogila, V.A. and Georgiev, P.G., (2017) C2H2 zinc finger proteins: The largest but poorly explored family of higher eukaryotic transcription factors. *Acta Naturae*, 92, pp.47–58.

Feng, J., Zhou, Y., Campbell, S.L., Le, T., Li, E., Sweatt, J.D., Silva, A.J. and Fan, G., (2010) Dnmt1 and Dnmt3a maintain DNA methylation and regulate synaptic function in adult forebrain neurons. *Nature Neuroscience*, 134, pp.423–432.

Ferreira, D., Wahlund, L. and Westman, E., (2018) The heterogeneity within Alzheimer's disease. *Aging*, 1011, pp.3058–3060.

Fischer, A., Sananbenesi, F., Pang, P.T., Lu, B. and Tsai, L.H., (2005) Opposing roles of transient

and prolonged expression of p25 in synaptic plasticity and hippocampus-dependent memory. *Neuron*, 485, pp.825–838.

Fischer, A., Sananbenesi, F., Wang, X., Dobbin, M. and Tsai, L., (2007) Recovery of learning and memory is associated with chromatin remodelling. *Nature*, 447, pp.178–183.

Flores, S.C., Sherman, M.A., Bruns, C.M., Eastman, P. and Altman, R.B., (2011) Fast flexible modeling of RNA structure using internal coordinates. *IEEE/ACM Transactions on Computational Biology and Bioinformatics*, 85, pp.1247–1257.

Flügel, D., Görlach, A. and Kietzmann, T., (2012) GSK-3β regulates cell growth, migration, and angiogenesis via Fbw7 and USP28-dependent degradation of HIF-1α. *Blood*, 1195, pp.1292–1301.

Formisano, L., Guida, N., Valsecchi, V., Cantile, M., Cuomo, O., Vinciguerra, A., Laudati, G., Pignataro, G., Sirabella, R., Di Renzo, G. and Annunziato, L., (2015) Sp3/REST/HDAC1/HDAC2 complex represses and Sp1/HIF-1/p300 complex activates ncx1 gene transcription, in brain ischemia and in ischemic brain preconditioning, by Epigenetic mechanism. *Journal of Neuroscience*, 3519, pp.7332–7348.

Francis, Y.I., Fà, M., Ashraf, H., Zhang, H., Staniszewski, A., Latchman, D.S. and Arancio, O., (2009) Dysregulation of Histone Acetylation in the APP/PS1 Mouse Model of Alzheimer's Disease. *Journal of Alzheimer's Disease*, 18, pp.131–139.

Fu, H., Rodriguez, G.A., Herman, M., Emrani, S., Nahmani, E., Barrett, G., Figueroa, H.Y., Goldberg, E., Hussaini, S.A. and Duff, K.E., (2017) Tau Pathology Induces Excitatory Neuron Loss, Grid Cell Dysfunction, and Spatial Memory Deficits Reminiscent of Early Alzheimer's Disease. *Neuron*, [online] 933, pp.533-541.e5. Available at: http://dx.doi.org/10.1016/j.neuron.2016.12.023.

Gao, Z., Ure, K., Ding, P., Nashaat, M., Yuan, L., Ma, J., Hammer, R.E. and Hsieh, J., (2011) The master negative regulator REST/NRSF controls adult neurogenesis by restraining the neurogenic program in quiescent stem cells. *Journal of Neuroscience*, 3126, pp.9772–9786.

Garcia-Manteiga, J.M., D'Alessandro, R. and Meldolesi, J., (2019) News about the Role of the Transcription Factor REST in Neurons: From Physiology to Pathology. *International journal of molecular sciences*, 211.

Giannakopoulos, P., Herrmann, F.R., Bussière, T., Bouras, C., Kövari, E., Perl, D.P., Morrison, J.H., Gold, G. and Hof, P.R., (2003) Tangle and neuron numbers, but not amyloid load, predict cognitive status in Alzheimer's disease. *Neurology*, 609, pp.1495–1500.

Girard, S.D., Baranger, K., Gauthier, C., Jacquet, M., Bernard, A., Escoffier, G., Marchetti, E., Khrestchatisky, M., Rivera, S. and Roman, F.S., (2013) Evidence for early cognitive impairment related to frontal cortex in the 5XFAD mouse model of Alzheimer's disease. *Journal of Alzheimer's Disease*, 333, pp.781–796.

Giusti, S.A., Vogl, A.M., Brockmann, M.M., Vercelli, C.A., Rein, M.L., Trümbach, D., Wurst, W., Cazalla, D., Stein, V., Deussing, J.M. and Refojo, D., (2014) MicroRNA-9 controls dendritic development by targeting REST. *eLife*, 3, pp.1–22.

Gong, C.-X. and Iqbal, K., (2008) Hyperphosphorylation of Microtubule-Associated Protein Tau: A Promising Therapeutic Target for Alzheimer Disease. *Current Medicinal Chemistry*, 1523,

pp.2321–2328.

Govindpani, K., McNamara, L.G., Smith, N.R., Vinnakota, C., Waldvogel, H.J., Faull, R.L.M. and Kwakowsky, A., (2019) Vascular dysfunction in Alzheimer's disease: A prelude to the pathological process or a consequence of it? *Journal of Clinical Medicine*, 85, pp.1–57.

Grutzendler, J., Helmin, K., Tsai, J. and Gan, W.B., (2007) Various dendritic abnormalities are associated with fibrillar amyloid deposits in Alzheimer's disease. *Annals of the New York Academy of Sciences*, 1097, pp.30–39.

Gräff, J., Rei, D., Guan, J., Wang, W., Seo, J., Hennig, K.M., Nieland, T.J.F., Fass, D.M., Kao, P.F., Kahn, M., Su, S.C., Samiei, A., Joseph, N., Haggarty, S.J., Delalle, I. and Tsai, L., (2012) An epigenetic blockade of cognitive functions in the neurodegenerating brain. *Nature*, 482, pp.222–228.

Gräff, J. and Tsai, L., (2013) The Potential of HDAC Inhibitors as Cognitive Enhancers. *Annual Review of Pharmacology and Toxicology*, 53, pp.311–330.

Guo, T., Zhang, D., Zeng, Y., Huang, T.Y., Xu, H. and Zhao, Y., (2020) Molecular and cellular mechanisms underlying the pathogenesis of Alzheimer's disease. *Molecular Neurodegeneration*, 151, pp.1–37.

Hanger, D.P., Byers, H.L., Wray, S., Leung, K.Y., Saxton, M.J., Seereeram, A., Reynolds, C.H., Ward, M.A. and Anderton, B.H., (2007) Novel phosphorylation sites in Tau from Alzheimer brain support a role for casein kinase 1 in disease pathogenesis. *Journal of Biological Chemistry*, [online] 28232, pp.23645–23654. Available at: http://dx.doi.org/10.1074/jbc.M703269200.

Hays, C.C., Zlatar, Z.Z. and Wierenga, C.E., (2016) The Utility of Cerebral Blood Flow as a Biomarker of Preclinical Alzheimer's Disease. *Cellular and Molecular Neurobiology*, 362, pp.167–179.

Heavener, K.S. and Bradshaw, E.M., (2022) The aging immune system in Alzheimer's and Parkinson's diseases. *Seminars in Immunopathology*, [online] 0123456789. Available at: https://doi.org/10.1007/s00281-022-00944-6.

Heneka, M.T., Carson, M.J., Khoury, J. El, Landreth, G.E., Brosseron, F., Feinstein, D.L., Jacobs, A.H., Wyss-Coray, T., Vitorica, J., Ransohoff, R.M., Herrup, K., Frautschy, S.A., Finsen, B., Brown, G.C., Verkhratsky, A., Yamanaka, K., Koistinaho, J., Latz, E., Halle, A., Petzold, G.C., Town, T., Morgan, D., Shinohara, M.L., Perry, V.H., Holmes, C., Bazan, N.G., Brooks, D.J., Hunot, S., Joseph, B., Deigendesch, N., Garaschuk, O., Boddeke, E., Dinarello, C.A., Breitner, J.C., Cole, G.M., Golenbock, D.T. and Kummer, M.P., (2015) Neuroinflammation in Alzheimer's disease. *The Lancet Neurology*, 144, pp.388–405.

Hillen, H., (2019) The Beta Amyloid Dysfunction (BAD) Hypothesis for Alzheimer's Disease. *Frontiers in Neuroscience*, 13November, pp.1–10.

Hillisch, A., Pineda, L.F. and Hilgenfeld, R., (2004) Utility of homology models in the drug discovery process. *DDT*, 9January.

Hoang, M. V., Smith, L.E.H. and Senger, D.R., (2010) Moderate GSK-3β inhibition improves neovascular architecture, reduces vascular leakage, and reduces retinal hypoxia in a model of ischemic retinopathy. *Angiogenesis*, 133, pp.269–277.

Hong, S., Beja-Glasser, V.F., Nfonoyim, B.M., Frouin, A., Li, S., Ramakrishnan, S., Merry, K.M., Shi, Q., Rosenthal, A., Barres, B.A., Lemere, C.A., Selkoe, D.J. and Stevens, B., (2016) Complement and microglia mediate early synapse loss in Alzheimer mouse models. *Science*, 3526286, pp.712–716.

Hove, D.L. Van Den, Kompotis, K., Lardenoije, R., Kenis, G., Mill, J., Steinbusch, H.W., Lesch, K., Fitzsimons, C.P., Strooper, B. De and Rutten, B.P.F., (2014) Epigenetically regulated microRNAs in Alzheimer's disease. *Neurobiology of Aging*, [online] 354, pp.731–745. Available at: http://dx.doi.org/10.1016/j.neurobiolaging.2013.10.082.

Huang, D., Li, Q., Wang, Y., Liu, Z., Wang, Z., Li, H., Wang, J., Su, J., Ma, Y., Yu, M., Fei, J. and Huang, F., (2019) Brain-specific NRSF deficiency aggravates dopaminergic neurodegeneration and impairs neurogenesis in the MPTP mouse model of Parkinson's disease. *Aging*, 1110, pp.3280–3297.

Huggins, D.J., Biggin, P.C., Dämgen, M.A., Essex, J.W., Harris, S.A., Henchman, R.H., Khalid, S., Kuzmanic, A., Laughton, C.A., Michel, J., Mulholland, A.J., Rosta, E., Sansom, M.S.P. and van der Kamp, M.W., (2019) Biomolecular simulations: From dynamics and mechanisms to computational assays of biological activity. *Wiley Interdisciplinary Reviews: Computational Molecular Science*, 93, pp.1–23.

Hullinger, R. and Puglielli, L., (2017) Molecular and cellular aspects of age-related cognitive decline and Alzheimer's disease. *Behavioural Brain Research*, [online] 322, pp.191–205. Available at: http://dx.doi.org/10.1016/j.bbr.2016.05.008.

Humphrey, W., Dalke, A. and Schulten, K., (1996) VMD: Visual Molecular Dynamics. *Journal of Molecular Graphics*, [online] 14October 1995, pp.33–38. Available at: http://www.ks.uiuc.edu/Research/vmd/.

Hwang, J.Y., Aromolaran, K.A. and Zukin, R.S., (2017) The emerging field of epigenetics in neurodegeneration and neuroprotection. *Nature Reviews Neuroscience*, [online] 186, pp.347–361. Available at: http://dx.doi.org/10.1038/nrn.2017.46.

Hwang, J.Y. and Zukin, R.S., (2018) REST, a master transcriptional regulator in neurodegenerative disease. *Current Opinion in Neurobiology*, [online] 48, pp.193–200. Available at: http://dx.doi.org/10.1016/j.conb.2017.12.008.

Iqbal, K., Liu, F. and Gong, C.X., (2016) Tau and neurodegenerative disease: The story so far. *Nature Reviews Neurology*, 121, pp.15–27.

Ittner, L.M. and Götz, J., (2011) Amyloid-β and tau — a toxic pas de deux in Alzheimer's disease. *Nature Reviews Neuroscience*, [online] 12February, pp.67–72. Available at: http://dx.doi.org/10.1038/nrn2967.

Jackson, J., Jambrina, E., Li, J., Marston, H., Menzies, F., Phillips, K. and Gilmour, G., (2019) Targeting the synapse in Alzheimer's disease. *Frontiers in Neuroscience*, 13JUL, pp.1–8.

Jaworski, T., Banach-Kasper, E. and Gralec, K., (2019) GSK-3β at the intersection of neuronal plasticity and neurodegeneration. *Neural Plasticity*, 2019.

Jeong, S., (2017) Molecular and cellular basis of neurodegeneration in alzheimer's disease. *Molecules and Cells*, 409, pp.613–620.

Jumper, J., Evans, R., Pritzel, A., Green, T., Figurnov, M., Ronneberger, O., Tunyasuvunakool, K., Bates, R., Žídek, A., Potapenko, A., Bridgland, A., Meyer, C., Kohl, S.A.A., Ballard, A.J., Cowie, A., Romera-Paredes, B., Nikolov, S., Jain, R., Adler, J., Back, T., Petersen, S., Reiman, D., Clancy, E., Zielinski, M., Steinegger, M., Pacholska, M., Berghammer, T., Bodenstein, S., Silver, D., Vinyals, O., Senior, A.W., Kavukcuoglu, K., Kohli, P. and Hassabis, D., (2021) Highly accurate protein structure prediction with AlphaFold. *Nature*, [online] 5967873, pp.583–589. Available at: http://dx.doi.org/10.1038/s41586-021-03819-2.

Kametani, F. and Hasegawa, M., (2018) Reconsideration of amyloid hypothesis and tau hypothesis in Alzheimer's disease. *Frontiers in Neuroscience*, 1225, pp.1–11.

Kaneko, N., Hwang, J.Y., Gertner, M., Pontarelli, F. and Suzanne Zukin, R., (2014) Casein Kinase 1 suppresses activation of REST in insulted hippocampal neurons and halts ischemia-induced neuronal death. *Journal of Neuroscience*, 3417, pp.6030–6039.

Katsinelos, T., Zeitler, M., Dimou, E., Karakatsani, A., Müller, H.M., Nachman, E., Steringer, J.P., Ruiz de Almodovar, C., Nickel, W. and Jahn, T.R., (2018) Unconventional Secretion Mediates the Trans-cellular Spreading of Tau. *Cell Reports*, 237, pp.2039–2055.

Kellermayer, B., Ferreira, J.S., Dupuis, J., Levet, F., Grillo-Bosch, D., Bard, L., Linarès-Loyez, J., Bouchet, D., Choquet, D., Rusakov, D.A., Bon, P., Sibarita, J.B., Cognet, L., Sainlos, M., Carvalho, A.L. and Groc, L., (2018) Differential Nanoscale Topography and Functional Role of GluN2-NMDA Receptor Subtypes at Glutamatergic Synapses. *Neuron*, 1001, pp.106-119.e7.

Kim, H.S., Skurk, C., Thomas, S.R., Bialik, A., Suhara, T., Kureishi, Y., Birnbaum, M., Keaney, J.F. and Kenneth Walsh, S., (2002) Regulation of angiogenesis by glycogen synthase kinase-3β. *Journal of Biological Chemistry*, [online] 27744, pp.41888–41896. Available at: http://dx.doi.org/10.1074/jbc.M206657200.

Kimura, T., Ishiguro, K. and Hisanaga, S.I., (2014) Physiological and pathological phosphorylation of tau by Cdk5. *Frontiers in Molecular Neuroscience*, 7JULY, pp.1–10.

Kimura, T., Sharma, G., Ishiguro, K. and Hisanaga, S.I., (2018) Phospho-tau bar code: Analysis of phosphoisotypes of tau and its application to tauopathy. *Frontiers in Neuroscience*, 12FEB, pp.1–9.

Komaki, S., Sugita, Y., Furuta, T., Yamada, K., Moritsubo, M., Abe, H., Akiba, J., Miyagi, N., Nakamura, H., Miyoshi, H., Ohshima, K. and Morioka, M., (2019) Expression of GLUT1 in pseudopalisaded and perivascular tumor cells is an independent prognostic factor for patients with glioblastomas. *Journal of Neuropathology and Experimental Neurology*, 785, pp.389–397.

Kukurba, K.R. and Montgomery, S.B., (2015) RNA sequencing and analysis. *Cold Spring Harbor Protocols*, 201511, pp.951–969.

Kumar, A., Singh, A. and Ekavali, (2015) A review on Alzheimer's disease pathophysiology and its management: An update. *Pharmacological Reports*, [online] 672, pp.195–203. Available at: http://dx.doi.org/10.1016/j.pharep.2014.09.004.

Kumar, A. and Tsao, J.W., (2019) *Alzheimer Disease*. [online] StatPearls Publishing, Treasure Island (FL). Available at: http://europepmc.org/books/NBK499922.

Lab of Biophysics and Molecular Modeling, (n.d.) *HDOCK Server*. [online] Available at: http://hdock.phys.hust.edu.cn.

Lanke, V., Moolamalla, S.T.R., Roy, D. and Vinod, P.K., (2018) Integrative analysis of hippocampus gene expression profiles identifies network alterations in aging and Alzheimer's disease. *Frontiers in Aging Neuroscience*, 10MAY, pp.1–14.

Lardenoije, R., van den Hove, D., Havermans, M., Casteren, A. van, Le, K.X., Palmour, R., Lemere, C.A. and Rutten, B.P.F., (2018) Age-related epigenetic changes in hippocampal subregions of four animal models of Alzheimer's disease. *Molecular and Cellular Neuroscience*, [online] 86October 2017, pp.1–15. Available at: https://doi.org/10.1016/j.mcn.2017.11.002.

Lauretti, E., Dincer, O. and Praticò, D., (2020) Glycogen synthase kinase-3 signaling in Alzheimer's disease. *BBA - Molecular Cell Research*, [online] 18675, p.118664. Available at: https://doi.org/10.1016/j.bbamcr.2020.118664.

Levenson, J.M. and Sweatt, J.D.D., (2005) Epigenetic Mechanisms in Memory Formation. *Nature Reviews Neuroscience*, 6February, pp.108–118.

Li, H., Liu, Z., Wu, Y., Chen, Y., Wang, J., Wang, Z., Huang, D., Wang, M., Yu, M., Fei, J. and Huang, F., (2020) The deficiency of NRSF/REST enhances the pro-inflammatory function of astrocytes in a model of Parkinson's disease. *Biochimica et Biophysica Acta - Molecular Basis of Disease*, 18661.

Liao, Y., Wang, J., Jaehnig, E.J., Shi, Z. and Zhang, B., (2019) WebGestalt 2019: gene set analysis toolkit with revamped UIs and APIs. *Nucleic Acids Research*, 47W1, pp.W199–W205.

Lietz, M., Hohl, M. and Thiel, G., (2003) RE-1 silencing transcription factor REST regulates human synaptophysin.pdf. *European Journal of Biochemistry*, 270, pp.2–9.

Liu, J., Chang, L., Song, Y., Li, H. and Wu, Y., (2019) *The role of NMDA receptors in Alzheimer's disease*. *Frontiers in Neuroscience*, .

Liu, M., Sheng, Z., Cai, L., Zhao, K., Tian, Y. and Fei, J., (2012) Neuronal conditional knockout of NRSF decreases vulnerability to seizures induced by pentylenetetrazol in mice. *Acta Biochimica et Biophysica Sinica*, 446, pp.476–482.

Liu, S.L., Wang, C., Jiang, T., Tan, L., Xing, A. and Yu, J.T., (2016) The Role of Cdk5 in Alzheimer's Disease. *Molecular Neurobiology*, [online] 537, pp.4328–4342. Available at: http://dx.doi.org/10.1007/s12035-015-9369-x.

Liu, X., Jiao, B. and Shen, L., (2018) The Epigenetics of Alzheimer's Disease: Factors and Therapeutic Implications. *Frontiers in Genetics*, 9November, pp.1–10.

Lleó, A., Núñez-Llaves, R., Alcolea, D., Chiva, C., Balateu-Paños, D., Colom-Cadena, M., Gomez-Giro, G., Muñoz, L., Querol-Vilaseca, M., Pegueroles, J., Rami, L., Lladó, A., Molinuevo, J.L., Tainta, M., Clarimón, J., Spires-Jones, T., Blesa, R., Fortea, J., Martínez-Lage, P., Sánchez-Valle, R., Sabidó, E., Bayés, À. and Belbin, O., (2019) Changes in synaptic proteins precede neurodegeneration markers in preclinical Alzheimer's disease cerebrospinal fluid*. *Molecular and Cellular Proteomics*, 183, pp.546–560.

Llorens-Martín, M., Jurado, J., Hernández, F. and Ávila, J., (2014) GSK-3β, a pivotal kinase in Alzheimer disease. *Frontiers in Molecular Neuroscience*, 7MAY, pp.1–11.

Love, M.I., Huber, W. and Anders, S., (2014) Moderated estimation of fold change and dispersion for RNA-seq data with DESeq2. *Genome Biology*, 1512, pp.1–21.

Lu, T., Aron, L., Zullo, J., Pan, Y., Kim, H., Chen, Y., Yang, T.H., Kim, H.M., Drake, D., Liu, X.S., Bennett, D.A., Colaiácovo, M.P. and Yankner, B.A., (2014) REST and stress resistance in ageing and Alzheimer's disease. *Nature*, 5077493, pp.448–454.

Madhusudhan, M.S., Marti-Renom, M.A., Eswar, N., John, B., Pieper, U., Karchin, R., Shen, M.-Y. and Sali, A., (2005) Comparative Protein Structure Modeling. In: *The Proteomics Protocols Handbook*. pp.831–860.

Magalingam, K.B., Radhakrishnan, A., Ping, N.S. and Haleagrahara, N., (2018) Current Concepts of Neurodegenerative Mechanisms in Alzheimer's Disease. *BioMed Research International*, pp.1–13.

Mampay, M. and Sheridan, G.K., (2019) REST: An epigenetic regulator of neuronal stress responses in the young and ageing brain. *Frontiers in Neuroendocrinology*, [online] 53April, p.100744. Available at: https://doi.org/10.1016/j.yfrne.2019.04.001.

Mampay, M., Velasco-Estevez, M., Rolle, S.O., Chaney, A.M., Boutin, H., Dev, K.K., Moeendarbary, E. and Sheridan, G.K., (2021) Spatiotemporal immunolocalisation of REST in the brain of healthy ageing and Alzheimer's disease rats. *FEBS Open Bio*, 111, pp.146–163.

Martin, L., Latypova, X., Wilson, C.M., Magnaudeix, A., Perrin, M.L., Yardin, C. and Terro, F., (2013) Tau protein kinases: Involvement in Alzheimer's disease. *Ageing Research Reviews*, [online] 121, pp.289–309. Available at: http://dx.doi.org/10.1016/j.arr.2012.06.003.

Masliah, E., Mallory, M., Alford, M., DeTeresa, R., Hansen, L.A., McKeel, D.W. and Morris, J.C., (2001) Altered expression of synaptic proteins occurs early during progression of Alzheimer's disease. *Neurology*, 561, pp.127–129.

McClelland, S., Brennan, G.P., Dubé, C., Rajpara, S., Iyer, S., Richichi, C., Bernard, C. and Baram, T.Z., (2014) The transcription factor NRSF contributes to epileptogenesis by selective repression of a subset of target genes. *eLife*, 3, p.e01267.

McGann, J.C., Spinner, M.A., Garg, S.K., Mullendorff, K.A., Woltjer, R.L. and Mandel, G., (2021) The genome-wide binding profile for human RE1 silencing transcription factor unveils a unique genetic circuitry in hippocampus. *Journal of Neuroscience*, 4131, pp.6582–6595.

Mi, H., Muruganujan, A., Ebert, D., Huang, X. and Thomas, P.D., (2019) PANTHER version 14: More genomes, a new PANTHER GO-slim and improvements in enrichment analysis tools. *Nucleic Acids Research*, 47D1, pp.D419–D426.

Micotti, E., Paladini, A., Balducci, C., Tolomeo, D., Frasca, A., Marizzoni, M., Filibian, M., Caroli, A., Valbusa, G., Dix, S., O'Neill, M., Ozmen, L., Czech, C., Richardson, J.C., Frisoni, G.B. and Forloni, G., (2015) Striatum and entorhinal cortex atrophy in AD mouse models: MRI comprehensive analysis. *Neurobiology of Aging*, [online] 362, pp.776–788. Available at: http://dx.doi.org/10.1016/j.neurobiolaging.2014.10.027.

Middeldorp, J. and Hol, E.M., (2011) GFAP in health and disease. *Progress in Neurobiology*, [online] 933, pp.421–443. Available at: http://dx.doi.org/10.1016/j.pneurobio.2011.01.005.

Minichiello, L., Korte, M., Wolfer, D., Kühn, R., Unsicker, K., Cestari, V., Rossi-Arnaud, C., Lipp, H.-P., Bonhoeffer, T. and Klein, R., (1999) Essential Role for TrkB Receptors in Hippocampus-Mediated Learning below a certain threshold before behavioral defects become apparent. *Neuron*, 24, pp.401–414.

Moloney, C.M., Lowe, V.J. and Murray, M.E., (2021) Visualization of neurofibrillary tangle maturity in Alzheimer's disease: A clinicopathologic perspective for biomarker research. *Alzheimer's and Dementia*, 179, pp.1554–1574.

Monterey, M.D., Wei, H., Wu, X. and Wu, J.Q., (2021) The Many Faces of Astrocytes in Alzheimer's Disease. *Frontiers in Neurology*, 12August, pp.1–12.

Morfini, G., Szebenyi, G., Brown, H., Pant, H.C., Pigino, G., DeBoer, S., Beffert, U. and Brady, S.T., (2004) A novel CDK5-dependent pathway for regulating GSK3 activity and kinesin-driven motility in neurons. *EMBO Journal*, 2311, pp.2235–2245.

Mortazavi, A., Thompson, E.C.L., Garcia, S.T., Myers, R.M. and Wold, B., (2006) Comparative genomics modeling of the NRSF/REST repressor network: From single conserved sites to genome-wide repertoire. *Genome Research*, 1610, pp.1208–1221.

Mota, S.I., Ferreira, I.L. and Rego, A.C., (2013) Dysfunctional synapse in Alzheimer's disease - A focus on NMDA receptors. *Neuropharmacology*, [online] 76PART A, pp.16–26. Available at: http://dx.doi.org/10.1016/j.neuropharm.2013.08.013.

Motanis, H., Khorasani, L.N., Giza, C.C. and Harris, N.G., (2021) Peering into the Brain through the Retrosplenial Cortex to Assess Cognitive Function of the Injured Brain. *Neurotrauma Reports*, 21, pp.564–580.

Muhammed, M.T. and Aki-Yalcin, E., (2019) Homology modeling in drug discovery: Overview, current applications, and future perspectives. *Chemical Biology and Drug Design*, 931, pp.12–20.

Mukhin, V.N., Pavlov, K.I. and Klimenko, V.M., (2017) Mechanisms of Neuron Loss in Alzheimer's Disease. *Neuroscience and Behavioral Physiology*, 475, pp.508–516.

Mungenast, A.E. and Tsai, L.H., (2011) Addressing the complex etiology of Alzheimers disease: The role of p25/Cdk5. *Future Neurology*, 64, pp.481–496.

Muralidar, S., Ambi, S.V., Sekaran, S., Thirumalai, D. and Palaniappan, B., (2020) Role of tau protein in Alzheimer's disease: The prime pathological player. *International Journal of Biological Macromolecules*, [online] 163, pp.1599–1617. Available at: https://doi.org/10.1016/j.ijbiomac.2020.07.327.

Nakano, Y., Kelly, M.C., Rehman, A.U., Boger, E.T., Morell, R.J., Kelley, M.W., Friedman, T.B. and Bánfi, B., (2018) Defects in the Alternative Splicing-Dependent Regulation of REST Cause Deafness. *Cell*, 1743, pp.536-548.e21.

Narayan, P. and Dragunow, M., (2017) Alzheimer's Disease and Histone Code Alterations. In: *Neuroepigenomics in Aging and Disease - Chapter 17*. pp.321–336.

National Institute of Ageing, (2017) *What Happens to the Brain in Alzheimer's Disease?* [online] Available at: https://www.nia.nih.gov/health/what-happens-brain-alzheimers-disease [Accessed 27 Jul. 2020].

Nobili, A., Latagliata, E.C., Viscomi, M.T., Cavallucci, V., Cutuli, D., Giacovazzo, G., Krashia, P., Rizzo, F.R., Marino, R., Federici, M., De Bartolo, P., Aversa, D., Dell'Acqua, M.C., Cordella, A., Sancandi, M., Keller, F., Petrosini, L., Puglisi-Allegra, S., Mercuri, N.B., Coccurello, R., Berretta, N. and D'Amelio, M., (2017) Dopamine neuronal loss contributes to memory and reward

dysfunction in a model of Alzheimer's disease. *Nature Communications*, 8.

Nomura, M., Uda-Tochio, H., Murai, K., Mori, N. and Nishimura, Y., (2005) The neural repressor NRSF/REST binds the PAH1 domain of the Sin3 corepressor by using its distinct short hydrophobic helix. *Journal of Molecular Biology*, 3544, pp.903–915.

O'Brien, R.J. and Wong, P.C., (2011) Amyloid Precursor Protein Processing and Alzheimer's Disease. *Annual Review of Neuroscience*, 34, pp.185–204.

Ooi, L. and Wood, I.C., (2007) Chromatin crosstalk in development and disease: Lessons from REST. *Nature Reviews Genetics*, 87, pp.544–554.

Orre, M., Kamphuis, W., Osborn, L.M., Jansen, A.H.P., Kooijman, L., Bossers, K. and Hol, E.M., (2014) Isolation of glia from Alzheimer's mice reveals inflammation and dysfunction. *Neurobiology of Aging*, 3512, pp.2746–2760.

Otero-Garcia, M., Mahajani, S.U., Wakhloo, D., Tang, W., Xue, Y.Q., Morabito, S., Pan, J., Oberhauser, J., Madira, A.E., Shakouri, T., Deng, Y., Allison, T., He, Z., Lowry, W.E., Kawaguchi, R., Swarup, V. and Cobos, I., (2022) Molecular signatures underlying neurofibrillary tangle susceptibility in Alzheimer's disease. *Neuron*, [online] pp.1–20. Available at: https://doi.org/10.1016/j.neuron.2022.06.021.

Padurariu, M., Ciobica, A., Mavroudis, I., Fotiou, D. and Baloyannis, S.J., (2012) Hippocampal neuronal loss in the CA1 and CA3 areas of Alzheimer's disease patients. *Psychiatria Danubina*, 242, pp.152–8.

Pajarillo, E., Demayo, M., Digman, A., Nyarko-Danquah, I., Son, D.-S., Aschner, M. and Lee, E., (2022) Deletion of RE1-silencing transcription factor in striatal astrocytes exacerbates manganese-induced neurotoxicity in mice. *Glia*, 70, pp.1886–1901.

Pajarillo, E., Digman, A., Nyarko-Danquah, I., Son, D.S., Soliman, K.F.A., Aschner, M. and Lee, E., (2021) Astrocytic transcription factor REST upregulates glutamate transporter EAAT2, protecting dopaminergic neurons from manganese-induced excitotoxicity. *Journal of Biological Chemistry*, [online] 2976, p.101372. Available at: https://doi.org/10.1016/j.jbc.2021.101372.

Palm, K., Belluardo, N., Metsis, M. and Timmusk, T., (1998) Neuronal expression of zinc finger transcription factor REST/NRSF/XBR gene. *Journal of Neuroscience*, 184, pp.1280–1296.

Pang, C.C.C., Kiecker, C., O'Brien, J.T., Noble, W. and Chang, R.C.C., (2019) Ammon's Horn 2 (CA2) of the Hippocampus: A Long-Known Region with a New Potential Role in Neurodegeneration. *Neuroscientist*, 252, pp.167–180.

Parikshak, N.N., Gandal, M.J. and Geschwind, D.H., (2015) Systems biology and gene networks in neurodevelopmental and neurodegenerative disorders. *Nature Reviews Genetics*, [online] 168, pp.441–458. Available at: http://dx.doi.org/10.1038/nrg3934.

Patel, A., Yang, P., Tinkham, M., Pradhan, M., Sun, M.A., Wang, Y., Hoang, D., Wolf, G., Horton, J.R., Zhang, X., Macfarlan, T. and Cheng, X., (2018) DNA Conformation Induces Adaptable Binding by Tandem Zinc Finger Proteins. *Cell*, [online] 1731, pp.221-233.e12. Available at: http://dx.doi.org/10.1016/j.cell.2018.02.058.

Patrick, G.N., Zukerberg, L., Nikolic, M., De La Monte, S., Dikkes, P. and Tsai, L.H., (1999) Conversion of p35 to p25 deregulates Cdk5 activity and promotes neurodegeneration. *Nature*,

4026762, pp.615–622.

Paxinos, G. and Franklin, K.B.J., (2019) *Paxinos and Franklin's The Mouse Brain in Stereotaxic Coordinates*. 5th ed. San Diego: Elsevier Academic Press.

Pekny, M. and Pekna, M., (2014) Astrocyte reactivity and reactive astrogliosis: Costs and benefits. *Physiological Reviews*, 944, pp.1077–1098.

Perez-Nievas, B.G. and Serrano-Pozo, A., (2018) Deciphering the astrocyte reaction in Alzheimer's disease. *Frontiers in Aging Neuroscience*, 10APR, pp.1–23.

Petrosyan, R., (2013) Binding of NRSF to the HCN1 Gene Represses Expression after Seizures. *Cureus*, 51, pp.1–8.

Piaceri, I., Nacmias, B. and Sorbi, S., (2013) Genetics of familial and sporadic Alzheimer's disease. *Frontiers in Bioscience*, Elite5, pp.167–177.

Poon, C.H., Tse, L.S.R. and Lim, L.W., (2020) DNA methylation in the pathology of Alzheimer's disease: from gene to cognition. *Annals of the New York Academy of Sciences*, pp.1–19.

Preman, P., Alfonso-Triguero, M., Alberdi, E., Verkhratsky, A. and Arranz, A.M., (2021) Astrocytes in alzheimer's disease: Pathological significance and molecular pathways. *Cells*, 103, pp.1–19.

Rasmussen, J. and Langerman, H., (2019) Alzheimer's Disease – Why We Need Early Diagnosis . *Degenerative Neurological and Neuromuscular Disease*, Volume 9, pp.123–130.

Rockowitz, S. and Zheng, D., (2015) Significant expansion of the REST/NRSF cistrome in human versus mouse embryonic stem cells: Potential implications for neural development. *Nucleic Acids Research*, 4312, pp.5730–5743.

Rodenas-Ruano, A., Chávez, A.E., Cossio, M.J., Castillo, P.E. and Zukin, R.S., (2012) REST-dependent epigenetic remodeling promotes the developmental switch in synaptic NMDA receptors. *Nature Neuroscience*, [online] 1510, pp.1382–1390. Available at: http://dx.doi.org/10.1038/nn.3214.

Rodrigue, K.M., Kennedy, K.M. and Park, D.C., (2009) Beta-amyloid deposition and the aging brain. *Neuropsychology Review*, 194, pp.436–450.

Rodríguez-Matellán, A., Avila, J. and Hernández, F., (2020) Overexpression of GSK-3β in Adult Tet-OFF GSK-3β Transgenic Mice, and Not During Embryonic or Postnatal Development, Induces Tau Phosphorylation, Neurodegeneration and Learning Deficits. *Frontiers in Molecular Neuroscience*, 13September, pp.1–11.

Rodríguez, J.J., Yeh, C.Y., Terzieva, S., Olabarria, M., Kulijewicz-Nawrot, M. and Verkhratsky, A., (2014) Complex and region-specific changes in astroglial markers in the aging brain. *Neurobiology of Aging*, [online] 351, pp.15–23. Available at: http://dx.doi.org/10.1016/j.neurobiolaging.2013.07.002.

Rossetto, D., Avvakumov, N., Côté, J., Rossetto, D., Avvakumov, N. and Côté, J., (2012) A chromatin modification involved in diverse nuclear events Histone phosphorylation. *Epigenetics*, 710, pp.1098–1108.

Rothman, K.J., (1990) No Adjustments Are Needed for Multiple Comparisons. *Epidemiology*,

1January, pp.43–46.

Rubinski, A., Franzmeier, N., Neitzel, J. and Ewers, M., (2020) FDG-PET hypermetabolism is associated with higher tau-PET in mild cognitive impairment at low amyloid-PET levels. *Alzheimer's Research and Therapy*, 121, pp.1–12.

Rubio-Perez, J.M. and Morillas-Ruiz, J.M., (2012) A review: Inflammatory process in Alzheimer's disease, role of cytokines. *The Scientific World Journal*, 2012.

Ruff, K.M. and Pappu, R. V., (2021) AlphaFold and Implications for Intrinsically Disordered Proteins. *Journal of Molecular Biology*, [online] 43320, p.167208. Available at: https://doi.org/10.1016/j.jmb.2021.167208.

Sadigh-Eteghad, S., Sabermarouf, B., Majdi, A., Talebi, M., Farhoudi, M. and Mahmoudi, J., (2015) *Amyloid-beta: A crucial factor in Alzheimer's disease*. *Medical Principles and Practice*, .

Salcedo-Tello, P., Ortiz-Matamoros, A. and Arias, C., (2011) GSK3 function in the brain during development, neuronal plasticity, and neurodegeneration. *International Journal of Alzheimer's Disease*, 2011, pp.7–10.

Saura, C.A., Choi, S.Y., Beglopoulos, V., Malkani, S., Zhang, D., Rao, B.S.S., Chattarji, S., Kelleher, R.J., Kandel, E.R., Duff, K., Kirkwood, A. and Shen, J., (2004) Loss of presenilin function causes impairments of memory and synaptic plasticity followed by age-dependent neurodegeneration. *Neuron*, 421, pp.23–36.

Savioz, A., Leuba, G. and Vallet, P.G., (2014) A framework to understand the variations of PSD-95 expression in brain aging and in Alzheimer's disease. *Ageing Research Reviews*, [online] 18, pp.86–94. Available at: http://dx.doi.org/10.1016/j.arr.2014.09.004.

Scheff, S.W., Price, D.A., Schmitt, F.A. and Mufson, E.J., (2006) Hippocampal synaptic loss in early Alzheimer's disease and mild cognitive impairment. *Neurobiology of Aging*, 2710, pp.1372–1384.

Schmitges, F.W., Radovani, E., Najafabadi, H.S., Barazandeh, M., Campitelli, L.F., Yin, Y., Jolma, A., Zhong, G., Guo, H., Kanagalingam, T., Dai, W.F., Taipale, J., Emili, A., Greenblatt, J.F. and Hughes, T.R., (2016) Multiparameter functional diversity of human C2H2 zinc finger proteins. *Genome Research*, 2612, pp.1742–1752.

Schneider, B., Božíková, P., Nečasová, I., Čech, P., Svozil, D. and Černý, J., (2018) A DNA structural alphabet provides new insight into DNA flexibility. *Acta Crystallographica Section D: Structural Biology*, 74, pp.52–64.

Segal, D.J., Crotty, J.W., Bhakta, M.S., Barbas, C.F. and Horton, N.C., (2006) Structure of Aart, a Designed Six-finger Zinc Finger Peptide, Bound to DNA. *Journal of Molecular Biology*, 3632, pp.405–421.

Serrano-Pozo, A., Frosch, M.P., Masliah, E. and Hyman, B.T., (2011) Neuropathological alterations in Alzheimer disease. *Cold Spring Harbor Perspectives in Medicine*, 1a006189.

Sheng, M. and Kim, M.J., (2002) Postsynaptic signaling and plasticity mechanisms. *Science*, 2985594, pp.776–780.

Shukla, V., Seo, J., Binukumar, B.K., Amin, N.D., Reddy, P., Grant, P., Kuntz, S., Kesavapany, S.,

Steiner, J., Mishra, S.K., Tsai, L.H. and Pant, H.C., (2017) TFP5, a peptide inhibitor of aberrant and hyperactive Cdk5/p25, attenuates pathological phenotypes and restores synaptic function in CK-p25Tg mice. *Journal of Alzheimer's Disease*, 561, pp.335–349.

Šišková, Z., Justus, D., Kaneko, H., Friedrichs, D., Henneberg, N., Beutel, T., Pitsch, J., Schoch, S., Becker, A., vonderKammer, H. and Remy, S., (2014) Dendritic structural degeneration is functionally linked to cellular hyperexcitability in a mouse model of alzheimer's disease. *Neuron*, 845, pp.1023–1033.

Snyder, E.M., Nong, Y., Almeida, C.G., Paul, S., Moran, T., Choi, E.Y., Nairn, A.C., Salter, M.W., Lombroso, P.J., Gouras, G.K. and Greengard, P., (2005) Regulation of NMDA receptor trafficking by amyloid-β. *Nature Neuroscience*, 88, pp.1051–1058.

Sofroniew, M. V. and Vinters, H. V., (2010) Astrocytes: Biology and pathology. *Acta Neuropathologica*, 1191, pp.7–35.

Soldati, C., Bithell, A., Johnston, C., Wong, K.Y., Stanton, L.W. and Buckley, N.J., (2013) Dysregulation of REST-regulated coding and non-coding RNAs in a cellular model of Huntington's disease. *Journal of Neurochemistry*, 1243, pp.418–430.

Soldati, C., Bithell, A., Johnston, C., Wong, K.Y., Teng, S.W., Beglopoulos, V., Stanton, L.W. and Buckley, N.J., (2012) Repressor element 1 eilencing transcription factor couples loss of pluripotency with neural induction and neural differentiation. *Stem Cells*, 303, pp.425–434.

Song, Z., Yang, W., Cheng, G., Zhou, X., Yang, L. and Zhao, D., (2018) Prion protein is essential for the RE1 silencing transcription factor (REST)-dependent developmental switch in synaptic NMDA receptors. *Cell Death and Disease*, [online] 95. Available at: http://dx.doi.org/10.1038/s41419-018-0576-z.

Stark, R., Grzelak, M. and Hadfield, J., (2019) RNA sequencing: the teenage years. *Nature Reviews Genetics*, [online] 2011, pp.631–656. Available at: http://dx.doi.org/10.1038/s41576-019-0150-2.

Stoccoro, A. and Coppedè, F., (2018) Role of epigenetics in Alzheimer's disease pathogenesis. *Neurodegenerative disease management*, 83, pp.181–193.

Sujeetha, P., Cheerian, J., Basavaraju, P., Moorthi, P.V. and Anand, A.V., (2018) The role of epigenetics in Alzheimer's disease. *Journal of Geriatric Mental Health*, 52, pp.94–98.

Suo, H., Wang, P., Tong, J., Cai, L., Liu, J., Huang, D., Huang, L., Wang, Z., Huang, Y., Xu, J., Ma, Y., Yu, M., Fei, J. and Huang, F., (2015) NRSF is an essential mediator for the neuroprotection of trichostatin A in the MPTP mouse model of Parkinson's disease. *Neuropharmacology*, [online] 99, pp.67–78. Available at: http://dx.doi.org/10.1016/j.neuropharm.2015.07.015.

Sweeney, M.D., Montagne, A., Sagare, A.P., Nation, D.A., Schneider, L.S., Chui, H.C., Harrington, M.G., Pa, J., Law, M., Wang, D.J.J., Jacobs, R.E., Doubal, F.N., Ramirez, J., Black, S.E., Nedergaard, M., Benveniste, H., Dichgans, M., Iadecola, C., Love, S., Bath, P.M., Markus, H.S., Salman, R.A., Allan, S.M., Quinn, T.J., Kalaria, R.N., Werring, D.J., Carare, R.O., Touyz, R.M., Williams, S.C.R., Moskowitz, M.A., Katusic, Z.S., Lutz, S.E., Lazarov, O., Minshall, R.D., Rehman, J., Davis, T.P., Wellington, C.L., González, H.M., Yuan, C., Lockhart, S.N., Hughes, T.M., Chen, C.L.H., Sachdev, P., O'Brien, J.T., Skoog, I., Pantoni, L., Gustafson, D.R., Biessels, G.J., Wallin, A., Smith, E.E., Mok, V., Wong, A., Passmore, P., Barkof, F., Muller, M., Breteler, M.M.B., Román, G.C., Hamel, E., Seshadri, S., Gottesman, R.F., van Buchem, M.A., Arvanitakis, Z., Schneider, J.A., Drewes, L.R.,

Hachinski, V., Finch, C.E., Toga, A.W., Wardlaw, J.M. and Zlokovic, B. V., (2019) Vascular dysfunction—The disregarded partner of Alzheimer's disease. *Alzheimer's and Dementia*, 151, pp.158–167.

Sze, C.-I., Troncoso, J.C., Kawas, C., Mouton, P., Price, D.L. and Martin, L.J., (1997) Loss of the presynaptic vesicle protein synaptophysin in hippocampus correlates with cognitive decline in Alzheimer disease. *J Neuropathol Exp Neurol*, 568, pp.933–944.

Szklarczyk, D., Gable, A.L., Nastou, K.C., Lyon, D., Kirsch, R., Pyysalo, S., Doncheva, N.T., Legeay, M., Fang, T., Bork, P., Jensen, L.J. and von Mering, C., (2021) The STRING database in 2021: Customizable protein-protein networks, and functional characterization of user-uploaded gene/measurement sets. *Nucleic Acids Research*, 49D1, pp.D605–D612.

Takahashi, M., Nakabayashi, T., Mita, N., Jin, X., Aikawa, Y., Sasamoto, K., Miyoshi, G., Miyata, M., Inoue, T. and Ohshima, T., (2022) Involvement of Cdk5 activating subunit p35 in synaptic plasticity in excitatory and inhibitory neurons. *Molecular Brain*, [online] 151, pp.1–9. Available at: https://doi.org/10.1186/s13041-022-00922-x.

Terada, T., Yokokura, M., Obi, T., Bunai, T., Yoshikawa, E., Ando, I., Shimada, H., Suhara, T., Higuchi, M. and Ouchi, Y., (2019) In vivo direct relation of tau pathology with neuroinflammation in early Alzheimer's disease. *Journal of Neurology*, [online] 2669, pp.2186–2196. Available at: https://doi.org/10.1007/s00415-019-09400-2.

Tsuji, S., (2010) Genetics of neurodegenerative diseases: Insights from high-throughput resequencing. *Human Molecular Genetics*, 19R1, pp.65–70.

Twine, N.A., Janitz, K., Wilkins, M.R. and Janitz, M., (2011) Whole transcriptome sequencing reveals gene expression and splicing differences in brain regions affected by Alzheimer's disease. *PLoS ONE*, 61.

Vieira, M., Yong, X.L.H., Roche, K.W. and Anggono, V., (2020) Regulation of NMDA glutamate receptor functions by the GluN2 subunits. *Journal of Neurochemistry*, 1542, pp.121–143.

Volkert, M.R. and Crowley, D.J., (2020) Preventing Neurodegeneration by Controlling Oxidative Stress: The Role of OXR1. *Frontiers in Neuroscience*, 14December.

Wang, J., Liu, W., Shi, H., Zhai, H., Qian, J. and Zhang, W., (2022) A Role for PGC-1a in the Control of Abnormal Mitochondrial Dynamics in Alzheimer's Disease. *Cells*, 112849, pp.1–26.

Wang, Y.C., Liu, P., Yue, L.Y., Huang, F., Xu, Y.X. and Zhu, C.Q., (2021) NRSF deficiency leads to abnormal postnatal development of dentate gyrus and impairment of progenitors in subgranular zone of hippocampus. *Hippocampus*, 319, pp.935–956.

Wang, Z., Gerstein, M. and Snyder, M., (2009) RNA-Seq: a revolutionary tool for transcriptomics. *Nature Reviews Genetics*, 101, p.57.

Wilhelmsson, U., Bushong, E.A., Price, D.L., Smarr, B.L., Phung, V., Terada, M., Ellisman, M.H. and Pekny, M., (2006) Redefining the concept of reactive astrocytes as cells that remain within their unique domains upon reaction to injury. *Proceedings of the National Academy of Sciences of the United States of America*, 10346, pp.17513–17518.

Winkler, E.A., Nishida, Y., Sagare, A.P., Rege, S. V., Bell, R.D., Perlmutter, D., Sengillo, J.D., Hillman, S., Kong, P., Nelson, A.R., Sullivan, J.S., Zhao, Z., Meiselman, H.J., Wenby, R.B., Soto, J.,

Abel, E.D., Makshanoff, J., Zuniga, E., De Vivo, D.C. and Zlokovic, B. V., (2015) GLUT1 reductions exacerbate Alzheimer's disease vasculo-neuronal dysfunction and degeneration. *Nature Neuroscience*, [online] 184, pp.521–530. Available at: http://dx.doi.org/10.1038/nn.3966.

Wolfe, S.A., Nekludova, L. and Pabo, C.O., (1999) DNA RECOGNITION BY Cys2His2 ZINC FINGER PROTEINS. *Annual Review of Biophysics*, 3, pp.183–212.

World Health Organization, (2022) *World Health Organization - Dementia Fact Sheet*. [online] Available at: https://www.who.int/en/news-room/fact-sheets/detail/dementia.

Xia, C., Yin, M., Wu, C., Ji, Y. and Zhou, Y., (2020) Neuroglial activation in the auditory cortex and medial geniculate body of salicylate-induced tinnitus rats. *American Journal of Translational Research*, 1210, pp.6043–6059.

Xiang, Z., (2006) Advances in Homology Protein Structure Modeling. *Current Protein & Peptide Science*, 73, pp.217–227.

Xu, C., Zhang, M., Zu, L., Zhang, P., Sun, L., Liu, X. and Fang, M., (2021) Repressor element-1 silencing transcription factor regulates. *Aging*, 1311.

Yan, Y., Tao, H., He, J. and Huang, S.Y., (2020) The HDOCK server for integrated protein–protein docking. *Nature Protocols*, [online] 155, pp.1829–1852. Available at: http://dx.doi.org/10.1038/s41596-020-0312-x.

Yu, M., Suo, H., Liu, M., Cai, L., Liu, J., Huang, Y., Xu, J., Wang, Y., Zhu, C., Fei, J. and Huang, F., (2013) NRSF/REST neuronal deficient mice are more vulnerable to the neurotoxin MPTP. *Neurobiology of Aging*, 343, pp.916–927.

Zhang, F., Zhong, R., Qi, H., Li, S., Cheng, C., Liu, X., Liu, Y. and Le, W., (2018) Impacts of acute hypoxia on Alzheimer's disease-like pathologies in APPswe/PS1dE9 mice and their wild type littermates. *Frontiers in Neuroscience*, 12MAY, pp.1–15.

Zhang, R., Miller, R.G., Madison, C., Jin, X., Honrada, R., Harris, W., Katz, J., Forshew, D.A. and McGrath, M.S., (2013) Systemic immune system alterations in early stages of Alzheimer's disease. *Journal of Neuroimmunology*, [online] 2561–2, pp.38–42. Available at: http://dx.doi.org/10.1016/j.jneuroim.2013.01.002.

Zhang, Z., Ma, Z., Zou, W., Guo, H., Liu, M., Ma, Y. and Zhang, L., (2019) The Appropriate Marker for Astrocytes: Comparing the Distribution and Expression of Three Astrocytic Markers in Different Mouse Cerebral Regions. *BioMed Research International*, 2019.

Zhao, J., O'Connor, T. and Vassar, R., (2011) The contribution of activated astrocytes to Aβ production: Implications for Alzheimer's disease pathogenesis. *Journal of Neuroinflammation*, 8, pp.6–16.

Zogopoulos, V., Spaho, K., Ntouka, C., Lappas, G., Kyranis, I., Bagos, P., Spandidos, D. and Michalopoulos, I., (2021) TFBSPred: A functional transcription factor binding site prediction webtool for humans and mice. *International Journal of Epigenetics*, 14, pp.1–11.

Zott, B., Busche, M.A., Sperling, R.A. and Konnerth, A., (2018) What Happens with the Circuit in Alzheimer's Disease in Mice and Humans? *Annual Review of Neuroscience*, 41, pp.277–297.

Zuccato, C., Belyaev, N., Conforti, P., Ooi, L., Tartari, M., Papadimou, E., MacDonald, M., Fossale,

E., Zeitlin, S., Buckley, N. and Cattaneo, E., (2007) Widespread disruption of repressor element-1 silencing transcription factor/neuron-restrictive silencer factor occupancy at its target genes in Huntington's disease. *Journal of Neuroscience*, 2726, pp.6972–6983.

Zuccato, C., Tartari, M., Crotti, A., Goffredo, D., Valenza, M., Conti, L., Cataudella, T., Leavitt, B.R., Hayden, M.R., Timmusk, T., Rigamonti, D. and Cattaneo, E., (2003) Huntingtin interacts with REST/NRSF to modulate the transcription of NRSE-controlled neuronal genes. *Nature Genetics*, 351, pp.76–83.

Zullo, J.M., Drake, D., Aron, L., O'Hern, P., Dhamne, S.C., Davidsohn, N., Mao, C.A., Klein, W.H., Rotenberg, A., Bennett, D.A., Church, G.M., Colaiácovo, M.P. and Yankner, B.A., (2019) Regulation of lifespan by neural excitation and REST. *Nature*, 5747778, pp.359–364.

Zusso, M., Barbierato, M., Facci, L., Skaper, S.D. and Giusti, P., (2018) Neuroepigenetics and Alzheimer's Disease : An Update. *Journal of Alzheimer's Disease*, 64, pp.671–688.

APPENDIX 1 - ANTIBODIES

1. List of antibodies used in this project.

Primary and secondary antibodies used for immunohistochemistry (IHC), immunofluorescence (IF) or Western blot (WB), together with working dilution factors and sources. AR: antigen retrieval.

Antibody	Supplier	Catalogue number	Host Species	Application	Dilution
GFAP	abcam	ab7260	Rabbit	WB	1:50,000
				IHC	1:4,000
GluN2A	Sigma	M264	Rabbit	WB	1:1,000
GluN2B	Neuromab	N59/36	Mouse	WB	1:1,000
GSK3β	abcam	ab32391	Rabbit	WB	1:5,000 (Cortex) 1:500 (Hippocampus)
				IHC	1:500
MAP2	abcam	ab11267	Mouse	WB	1:10,000 (Cortex) 1:3,500 (Hippocampus)
				IHC	1:1,000
NeuN	abcam	ab177487	Mouse	WB	1:10,000
				IHC / IF + AR	1:6,000
PSD-95	abcam	ab18258	Rabbit	WB	1:16,000
				IHC + AR	1: 1,000
p35/p25	Cell signaling	2680S	Rabbit	WB	1:2,000 (Cortex) 1:1,000 (Hippocampus)
				IHC + AR	1:800
Synaptophysin	abcam	ab32127	Rabbit	WB	1:100,000
Total Tau	abcam	ab64193	Rabbit	WB	1:10,000 (Cortex) 1:5,000 (Hippocampus)
Phospho-Tau (pSer396)	abcam	ab109390	Rabbit	WB	1:100,000 (Cortex) 1:20,000 (Hippocampus)
Phospho-Tau AT8 (pSer202+pThr205)	ThermoFisher	MN1020	Mouse	WB	1:100 (Cortex) 1:50 (Hippocampus)
				IHC	1:500
REST	abcam	ab21635	Rabbit	IHC	1:100
α-tubulin	abcam	ab7291	Mouse	WB	1:100,000
β-actin	abcam	ab8226	Mouse	WB	1:8,000 (Cortex) 1:4,000 (Hippocampus)
Histone H3	abcam	ab1791	Rabbit	WB	1:50,000
Anti-Mouse	abcam	ab205719	Goat	WB	1:10,000
Anti-Rabbit	abcam	ab205718	Goat	WB	1:10,000
Alexa Fluor® 488	abcam	ab150077	Goat	WB	1:1,000

2. List of reagents and respective suppliers used in this project.

Reagent	Catalogue N°	Supplier
4x Laemmli Sample Buffer	1610747	Bio-Rad
Citric Acid Anhydrous ($C_6H_8O_7$)	-	Thermo Scientific
Clarity Western ECL Substrate	1705061	Bio-Rad
DAB Peroxidase Substrate Kit	SK-4100	Vector Laboratories
Dried Skimmed Milk	-	Marvel
EDTA 0.5M salt solution	03690	Sigma
Glycine	-	Fisher scientific
Goat serum	9023	Sigma
H_2O_2 30%	-	Fisher Scientific
Histo-Clear	HS-200	National Diagnostics
Horse serum	S-2000	Vector Laboratories
IMS (Industrial Methylated Spirit)	-	Fisher Scientific
Methanol	-	Fisher scientific
NaCL	-	Thermo Scientific
NuPAGE™ 4-12%, Bis-Tris, 1.0–1.5 mm, Mini Protein Gels	NP0335Box	Invitrogen
NuPAGE™ MOPS SDS Running Buffer (20X)	NP0001-02	Invitrogen
NuPAGE™ Sample Reducing Agent (10X)	NP0009	Invitrogen
OCT Embedding Matrix	KMA-0100-00A	Cell Path
Permount™ Mounting Medium	SP15-500	Fisher Scientific
Phosphatase inhibitor cocktail 2	P5726	Sigma
Phosphatase inhibitor cocktail 3	P0044	Sigma
Pierce BCA Protein Assay kit	23227	Thermo Scientific
Pierce™ 20X PBS Tween™ Buffer	28352	ThermoFisher
PMSF 0.1M	93482	Sigma
Precision Plus Protein Dual Colour Standards	1610374	Bio-Rad
Protease inhibitors	P8340	Sigma
RIPA Lysis and Extraction Buffer	89900	Thermo Scientific
SDS 10%	71736	Sigma
Sodium Deoxycholate Detergent	89904	Thermo Scientific
Sodium Phosphate Dibasic Anhydrous (Na_2HPO_4)	-	Thermo Scientific
Sodium phosphate monobasic monohydrate ($NaH_2PO_4 \cdot H_2O$)	-	Acros Organics
Tris base	-	Fisher scientific
Tris Hydrochloride, 1M Solution, pH 7.5	-	Fisher scientific
Trisodium citrate dihydrate ($C_6H_5Na_3O_7 \cdot 2H_2O$)	-	Thermo Scientific
Triton X-100	9002-93-1	Sigma
VECTASHIELD® HardSet™ Antifade Mounting Medium	H-1400	Vector Laboratories
VECTASTAIN® ELITE® ABC anti-mouse HRP Immunodetection Kit	PK-4002	Vector Laboratories
VECTASTAIN® ELITE® ABC anti-rabbit HRP Immunodetection Kit	PK-4001	Vector Laboratories

3. Preparation of reagents:

Buffer A:
10mM Tris HCl, pH 7.5
100mM NaCl
1% Triton
0.1mM EDTA
0.5mM PMSF

RIPA buffer:
25mM Tris HCl, pH 7.5
150mM NaCl
1% NP-40
1% Sodium deoxycholate
0.1% SDS

RIPA supplementary buffer:
75mM Tris HCl, pH 7.5
150mM NaCl
10mM EDTA
1.9% SDS

Lysis buffer:
RIPA buffer and RIPA supplementary buffer (1:1)

Citrate Buffer 10x:
0.1M $C_6H_8O_7$, anhydrous
0.1M $C_6H_5Na_3O_7 \cdot 2H_2O$

PB Stock 0.2M:
0.2M $NaH_2PO_4 \cdot H_2O$
0.2M Na_2HPO_4

Western blot transfer buffer:
15g Glycine
3g Tris Base
800mL dH2O
200mL Methanol 100%

4. List of equipment and respective suppliers used in this project.

Equipment	Supplier
Coplin Staining Jar, Plastic	Bel-Art Scienceware
Glass Rectangular Coverslips, 22x50mm, 0.13-0.17mm	Fisher Scientific
Leica Cryostat CM1850	Leica
Leica DM2500 LED microscope	Leica
PT Link	Dako
Superfrost™ Plus Microscope Slides	ThermoScientific
Centrifuge 5430 R - High-Speed Centrifuge	Eppendorf
ChemiDoc XRS+ System	Bio-Rad
Heat block DRI-BLOCK DB3	Techne
Incubator	Gallenkamp
Mini Gel tank	Invitrogen
Mini Trans-Blot Electrophoretic Transfer Cell	Bio-Rad
PELLET PESTLE® Cordless Motor	Kimble
Plate reader	Tecan
PowerPac™ Basic Power Supply	BioRad
PVDF membrane 0.2 µm (#1620177)	Bio-Rad
Stuart SB3 Rotator	Stuart
Stuart SSM1 Mini Orbital Shaker	Stuart
Vortex-Genie 2	Scientific Industries
VWR rocking platform	VWR

APPENDIX 2 – COMPUTATIONAL DETAILS

1. REST DNA binding domain secondary structure prediction from PSIPRED

The web server PSIPRED was used to predict the secondary structure of REST DBD, based on the FASTA sequence. These results were then imported to Prime software to complement the predictions of the secondary structure proposed by Schrödinger/Prime software.

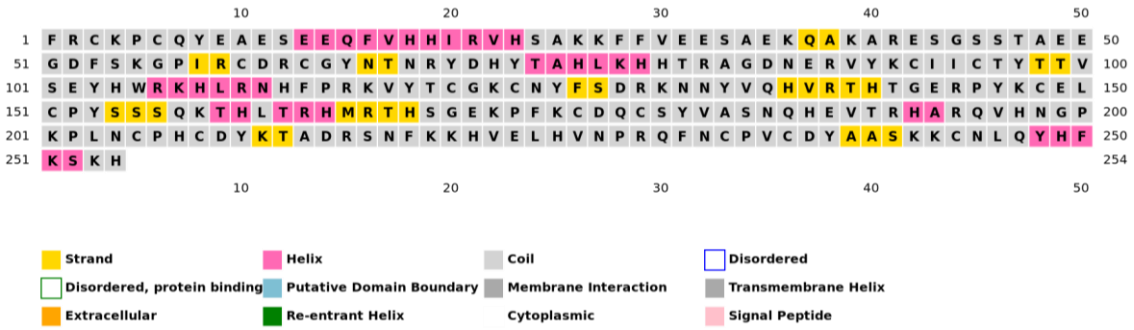

2. Constraints table (next page).

To ensure coordination, the distance between the zinc atom and the residues that compose each ZF motif has to be smaller than 3Å. However, the initial model (before constraints) of REST DBD had several residues that were located beyond this value (highlighted in red). Thus, constraints were added to all four residues that coordinate with the zinc atoms in ZF1, 2, 6, 7 and 8 (i.e. the zinc fingers that initially had residues with distances higher than 3Å). The values of these constraints were defined based on the distances of equivalent residues in the template. REST DBD final model has all the zinc coordination distances smaller than 3Å, except for Zn505-Cys179, however, this mimics what is observed in the equivalent residue in the template (2nd Cys of the ZF9). All the other residues that appear altered in the template (ZF11) were able to be corrected with applications of constraints.

Template 5WJQ	REST DBD	Residue	Distance between S/N and Zn atoms					
			Template 5WJQ	REST DBD				
				Before constraints	Final model		Residue	Constraint (Å)
ZF3 Zn702	**ZF1 Zn500**	1st Cys	2.56	2.80	2.60	**ZF1 Zn500**	Cys 3	2.60
		2nd Cys	2.17	3.55	2.25		Cys 6	2.20
		1st His	2.05	2.39	2.13		His19	2.10
		2nd His	1.96	2.19	2.04		His 23	2.00
ZF5 Zn704	**ZF2 Zn501**	1st Cys	2.44	4.64	2.51	**ZF2 Zn501**	Cys 60	2.50
		2nd Cys	2.39	6.32	2.51		Cys 63	2.50
		1st His	2.60	2.37	2.70		His 76	2.70
		2nd His	2.06	2.26	2.12		His 80	2.10
ZF6 Zn705	**ZF3 Zn502**	1st Cys	2.10	2.61	2.64	**ZF3 Zn502**	Cys 92	-
		2nd Cys	2.39	2.62	2.64		Cys 95	-
		1st His	2.12	2.23	2.23		His 108	-
		2nd His	2.04	2.21	2.21		His 112	-
ZF7 Zn706	**ZF4 Zn503**	1st Cys	2.33	2.79	2.78	**ZF4 Zn503**	Cys 120	-
		2nd Cys	2.36	2.47	2.47		Cys 123	-
		1st His	2.62	2.47	2.45		His 136	-
		2nd His	2.05	2.22	2.21		His 140	-
ZF8 Zn707	**ZF5 Zn504**	1st Cys	2.39	2.56	2.59	**ZF5 Zn504**	Cys 148	-
		2nd Cys	2.57	2.59	2.59		Cys 151	-
		1st His	2.32	2.23	2.22		His 164	-
		2nd His	1.90	2.31	2.33		His 168	-
ZF9 Zn708	**ZF6 Zn505**	1st Cys	2.35	2.58	2.41	**ZF6 Zn505**	Cys 176	2.40
		2nd Cys	3.14	4.77	3.10		Cys 179	3.10
		1st His	1.97	2.23	2.04		His 192	2.00
		2nd His	2.55	2.18	2.59		His 197	2.60
ZF10 Zn709	**ZF7 Zn506**	1st Cys	2.43	5.32	2.51	**ZF7 Zn506**	Cys 205	2.50
		2nd Cys	2.11	2.51	2.25		Cys 208	2.20
		1st His	2.34	2.18	2.40		His 221	2.40
		2nd His	1.91	2.19	2.04		His 225	2.00
ZF11 Zn710	**ZF8 Zn507**	1st Cys	3.42	2.58	2.90	**ZF8 Zn507**	Cys 233	2.90
		2nd Cys	2.33	2.54	2.41		Cys 236	2.40
		1st His	3.06	2.23	2.39		His 249	2.40
		2nd His	3.29	8.28	2.41		His 254	2.40

3. Parameters used to rebuild Re1 DNA structure using the webserver w3DNA 2.0.

The web server from SCFBio IIT Delhi was used to build *de novo* a Re1 3D structure. This model was then analysed using the webserver w3DNA 2.0. and a file containing both base-pair parameters and base-pair step parameters was obtained. The bellow parameters were then used to optimize the Delhi structure by reconstructing of the doubled-stranded structure using the "Rebuilding" option of the webserver with backbone geometry optimization.

21 # base-pairs
0 # ***local base-pair & step parameters***

#	Shear	Stretch	Stagger	Buckle	Prop-Tw	Opening	Shift	Slide	Rise	Tilt	Roll	Twist
T-A	-0.005	-0.089	-0.005	-0.009	-1.234	-2.676	0.000	0.000	0.000	0.000	0.000	0.000
T-A	-0.004	-0.089	-0.005	-0.006	-1.235	-2.676	0.002	-0.205	3.374	-0.007	-2.806	35.901
C-G	0.146	-0.168	-0.004	-0.025	-1.248	-1.642	0.033	-0.156	3.376	-0.028	-2.797	36.830
A-T	0.005	-0.089	-0.005	0.007	-1.234	-2.689	-0.057	-0.216	3.374	-0.029	-2.819	34.778
G-C	-0.146	-0.169	-0.004	0.025	-1.248	-1.649	0.055	-0.225	3.375	0.036	-2.810	34.958
C-G	0.146	-0.168	-0.004	-0.024	-1.248	-1.643	0.000	-0.115	3.378	0.000	-2.782	37.946
A-T	0.005	-0.089	-0.005	0.007	-1.235	-2.679	-0.057	-0.216	3.374	-0.030	-2.819	34.781
C-G	0.146	-0.168	-0.004	-0.025	-1.248	-1.642	0.031	-0.165	3.376	-0.021	-2.789	37.009
C-G	0.146	-0.168	-0.004	-0.026	-1.249	-1.623	-0.023	-0.176	3.376	-0.057	-2.802	35.890
A-T	0.004	-0.089	-0.005	0.006	-1.235	-2.676	-0.057	-0.215	3.374	-0.029	-2.818	34.775
T-A	-0.005	-0.089	-0.005	-0.009	-1.234	-2.676	-0.000	-0.214	3.374	-0.000	-2.797	36.075
G-C	-0.145	-0.168	-0.004	0.025	-1.248	-1.645	0.057	-0.216	3.374	0.029	-2.820	34.790
G-C	-0.146	-0.168	-0.004	0.026	-1.249	-1.623	0.024	-0.176	3.376	0.057	-2.802	35.886
A-T	0.005	-0.089	-0.005	0.007	-1.234	-2.689	-0.034	-0.156	3.376	0.028	-2.798	36.833
C-G	0.145	-0.168	-0.004	-0.025	-1.248	-1.645	0.031	-0.165	3.376	-0.021	-2.789	36.999
A-T	0.005	-0.089	-0.005	0.009	-1.234	-2.676	-0.057	-0.216	3.374	-0.029	-2.820	34.790
G-C	-0.145	-0.168	-0.004	0.025	-1.248	-1.645	0.055	-0.225	3.375	0.036	-2.811	34.964
C-G	0.146	-0.168	-0.004	-0.025	-1.248	-1.642	-0.000	-0.115	3.378	0.000	-2.781	37.941
G-C	-0.146	-0.168	-0.004	0.025	-1.248	-1.642	-0.000	-0.237	3.375	0.000	-2.824	33.836
C-G	0.145	-0.168	-0.004	-0.025	-1.248	-1.645	0.000	-0.115	3.378	-0.000	-2.781	37.941
C-G	0.146	-0.168	-0.004	-0.024	-1.248	-1.643	-0.023	-0.175	3.376	-0.056	-2.803	35.905

4. Docking results of ZFP568 and Aart with their respective native DNA structures.

The software HDOCK (http://hdock.phys.hust.edu.cn/) was used to dock the two proteins with highest homology to the REST DNA-binding domain obtained through the BLAST search with their native DNA, separately. HDOCK displays the best 10 model colour coded and below, the software summarizes the docking scores and the ligand RMSD (Å) in a table. To simplify the analysis, bellow it is shown only the best model.

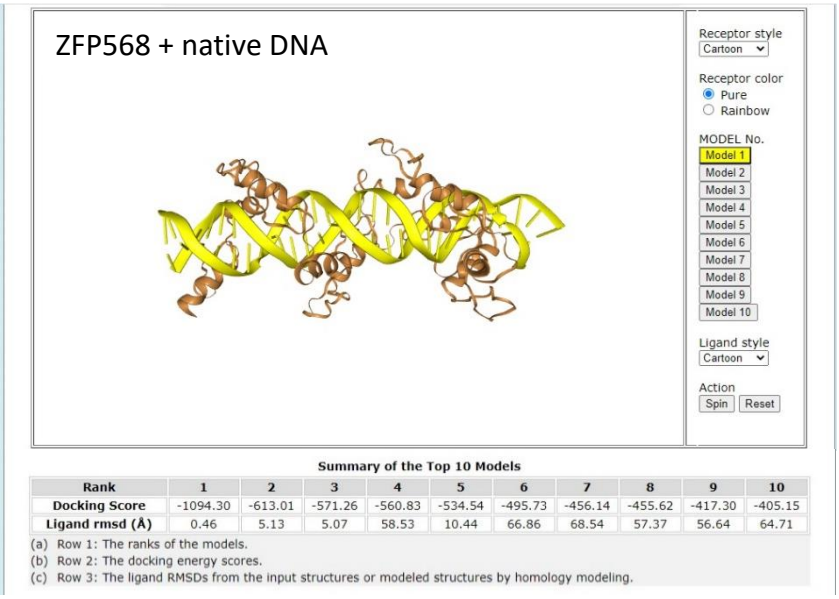

Summary of the Top 10 Models

Rank	1	2	3	4	5	6	7	8	9	10
Docking Score	-1094.30	-613.01	-571.26	-560.83	-534.54	-495.73	-456.14	-455.62	-417.30	-405.15
Ligand rmsd (Å)	0.46	5.13	5.07	58.53	10.44	66.86	68.54	57.37	56.64	64.71

(a) Row 1: The ranks of the models.
(b) Row 2: The docking energy scores.
(c) Row 3: The ligand RMSDs from the input structures or modeled structures by homology modeling.

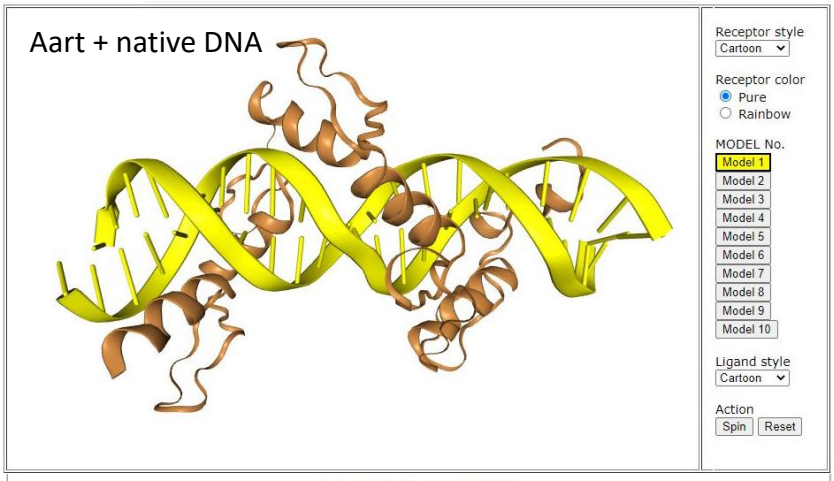

Summary of the Top 10 Models

Rank	1	2	3	4	5	6	7	8	9	10
Docking Score	-811.07	-572.28	-519.85	-474.18	-473.78	-461.06	-453.06	-451.48	-445.02	-432.12
Ligand rmsd (Å)	0.53	5.86	10.50	24.63	21.86	18.31	14.91	26.38	10.58	45.16
Interface residues	model_1	model_2	model_3	model_4	model_5	model_6	model_7	model_8	model_9	model_10

[a] Row 1: The ranks of the models.
[b] Row 2: The docking energy scores.
[c] Row 3: The ligand RMSDs from the input structures or modeled structures by homology modeling.
[d] Row 4: The interface residues within 5.0 Å from their interacting partner or each other, and the corresponding distances.

5. Table comparing the localization of zinc finger motifs from REST DNA binding domain Schrödinger/Prime homology model and the template ZFP568.

REST DBD (UniProt)		ZFP568	
ZF#	**Residues**	**ZF#**	**Residues**
-	-	**2**	(before query sequence)
1	159-181	**3**	159-184
2	216-238	**5**	217-241
3	248-270	**6**	248-273
4	276-298	**7**	276-301
5	304-326	**8**	304-329
6	332-355	**9**	332-357
7	361-383	**10**	361-382
8	389-412	**11**	389-410

ZF4 → "extra"

Note 1: The numeration of the residues corresponds to the numeration in query sequence, after alignment.

Note 2: The template's ZF2 + ZF4 don't interact with DNA bases, they interact with the DNA backbone phosphate. Therefore and because REST only has eight ZF motifs, these ZF were not include in the Schrödinger/Prime homology model.

APPENDIX 3 – NEURONAL COUNT

1. NeuN images revealed by DAB immunohistochemistry.

General representation of neuronal labelling using an anti-NeuN antibody, revealed by DAB immunohistochemistry (as opposed to immunofluorescence). **a)** The whole hippocampus was imaged using a 5x magnification. **b)** A higher magnification, 10x, was used to analyse each different region of the hippocampus. These images were then further enlarged (20x) to allow a better representation of the labelled neurons.

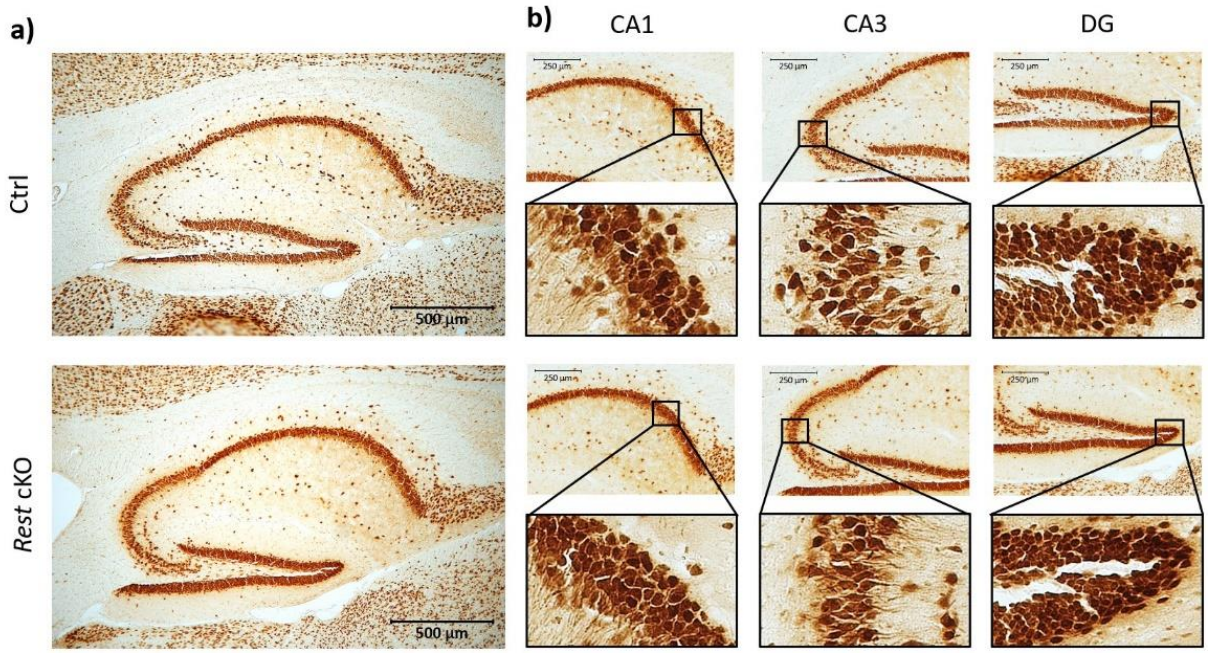

2. Table of the average neuronal counts per atlas page (n=3 per genotypic group)

Atlas 104					
Mouse	**Region of the hippocampus**				
	CA1	**CA2**	**CA3**	**DG**	**TOTAL**
Control	251.00	125.33	-	455.00	831.33
***Rest* cKO**	287.00	142.67	-	568.67	998.33
p-value	0.1610	0.2270	-	0.2728	0.1711

Atlas 107					
Mouse	**Region of the hippocampus**				
	CA1	**CA2**	**CA3**	**DG**	**TOTAL**
Control	347.33	67.67	176.33	997.67	1589.00
***Rest* cKO**	336.33	49.33	160.00	845.00	1390.67
p-value	0.3939	0.1670	0.3402	0.1432	0.1213

Atlas 109					
Mouse	**Region of the hippocampus**				
	CA1	**CA2**	**CA3**	**DG**	**TOTAL**
Control	354.67	63.00	209.00	922.67	1549.33
***Rest* cKO**	326.67	57.33	186.67	864.33	1435.00
p-value	0.1241	0.2974	0.1330	0.3109	0.2285

Atlas 112					
Mouse	**Region of the hippocampus**				
	CA1	**CA2**	**CA3**	**DG**	**TOTAL**
Control	352.33	74.33	221.67	912.67	1561.00
***Rest* cKO**	331.33	75.33	191.67	889.00	1487.33
p-value	0.1061	0.4841	0.1680	0.2912	0.2206

Atlas 114					
Mouse	**Region of the hippocampus**				
	CA1	**CA2**	**CA3**	**DG**	**TOTAL**
Control	336.33	75.00	243.67	984.00	1639.00
***Rest* cKO**	344.00	69.00	227.67	900.00	1540.67
p-value	0.3958	0.3590	0.1948	0.2043	0.1389

Atlas 117					
Mouse	**Region of the hippocampus**				
	CA1	**CA2**	**CA3**	**DG**	**TOTAL**
Control	362.33	71.00	264.67	981.33	1679.33
***Rest* cKO**	338.33	69.33	260.33	948.33	1616.33
p-value	0.2686	0.4611	0.4423	0.4208	0.3895

Atlas 120					
Mouse	**Region of the hippocampus**				
	CA1	**CA2**	**CA3**	**DG**	**TOTAL**
Control	386.00	69.00	366.00	973.00	1794.00
***Rest* cKO**	303.00	71.67	349.00	911.33	1635.00
p-value	0.1418	0.4377	0.4127	0.3878	0.3344

Atlas 122					
Mouse	**Region of the hippocampus**				
	CA1	**CA2**	**CA3**	**DG**	**TOTAL**
Control	320.67	87.67	358.67	760.00	1527.00
***Rest* cKO**	306.67	103.00	482.67	1027.67	1920.00
p-value	0.3591	0.2585	0.2473	0.1218	0.1341

APPENDIX 4 – RNA-Seq

1. List of upregulated genes in *Rest* cKO mice.

Upregulated genes are represented in green and have a positive Log2 FC.

Gene name	Log2 FC (*Rest* cKO vs Control)	p-value	Gene name	Log2 FC (*Rest* cKO vs Control)	p-value
Slc2a1	0.285159	2.22E-07	Rnaseh1	0.183288	0.005704
Acer2	0.260249	1.95E-05	Plcg2	0.183187	0.007304
Blvrb	0.259494	0.000145	Zbtb16	0.182128	0.005675
Ly86	0.257108	0.000164	Emilin2	0.181587	0.007837
Klf15	0.246004	5.88E-05	Gm15506	0.180417	0.004928
Zfp14	0.243377	0.000367	A2ml1	0.180166	0.008169
Acvrl1	0.227981	0.000647	Sdc4	0.178791	0.006965
Xdh	0.222846	0.000551	Tgfbr3	0.177119	0.009044
Syndig1l	0.220476	0.000785	Gm19439	0.176114	0.005961
Agt	0.220161	0.001207	Synm	0.175808	0.006284
Lrrc10b	0.219392	0.001318	Sorbs3	0.175418	0.002843
2900076A07Rik	0.210913	0.001456	Pnkp	0.175287	0.005143
Plekhg2	0.206724	0.002463	Col9a2	0.174711	0.010156
Zfp488	0.205675	0.002144	Mill2	0.174124	0.004507
Tsc22d3	0.203808	0.000659	Robo4	0.173721	0.010941
Folh1	0.202058	0.001685	Bag3	0.173706	0.008776
Hspa12b	0.199884	0.003266	Cd74	0.172486	0.006228
Pim3	0.199666	0.001505	Zfp27	0.171465	0.003321
Phactr4	0.199439	0.003323	Rapgef3	0.170998	0.004700
Prcp	0.198341	0.003272	Myo1f	0.170894	0.011376
Prkd2	0.196471	0.003844	Slfn5	0.170334	0.012645
2310022B05Rik	0.196152	0.000693	Cmklr1	0.169617	0.009471
Padi2	0.195983	0.003243	Tert	0.169457	0.001522
Dbi	0.192594	0.000154	Atp10a	0.167599	0.013143
Fah	0.188629	0.002659	Tpbgl	0.166813	0.013603
Rgs10	0.188447	0.000971	Ifitm3	0.165353	0.015380
Il3ra	0.186520	0.000689	Hif3a	0.164729	0.009712
St6galnac2	0.184892	0.001624	Smim3	0.164448	0.012321
Kptn	0.183921	0.002831	Mdk	0.164049	0.014402
Ramp3	0.183579	0.006818	Gm12992	0.163844	0.005605
Tgm2	0.183525	0.007215	Stra6	0.163806	0.013563
Prkd1	0.183441	0.004116	Csf1r	0.163639	0.007079
Prr5	0.183336	0.006265	Gjc1	0.162927	0.015697

Gene name	Log2 FC (*Rest* cKO vs Control)	p-value	Gene name	Log2 FC (*Rest* cKO vs Control)	p-value
Mamdc2	0.162913	0.012750	Rab24	0.149879	0.016862
Ryr3	0.162874	0.012450	Il15ra	0.149864	0.026617
Inpp5d	0.162245	0.013825	BC024139	0.149364	0.005898
4933407L21Rik	0.162084	0.010328	Ly6c1	0.149173	0.027203
Stard9	0.162053	0.016062	Hexb	0.148734	0.005966
Abcc4	0.161836	0.012733	Tifab	0.148467	0.025738
Me3	0.161575	0.018007	Itgb2	0.146384	0.030059
Zfp182	0.161003	0.018422	Rpl18	0.146353	0.014391
Scarb1	0.160753	0.004703	Nrros	0.146183	0.031873
Ly6a	0.160575	0.018623	Thrsp	0.145945	0.026690
Klf2	0.160573	0.016435	Hemk1	0.145822	0.030109
Olfml1	0.160096	0.017254	Mfsd2a	0.145446	0.027182
Tnni1	0.159778	0.005764	Vsir	0.145421	0.025342
Cd14	0.158678	0.013493	Cd300c2	0.144794	0.031208
Dbp	0.157096	0.003915	Stard10	0.143954	0.022517
1700047M11Rik	0.155686	0.017223	Sardh	0.143644	0.032978
Ccdc88b	0.155610	0.019828	Cd4	0.143287	0.031964
Helz2	0.155421	0.015740	Ppp1r1b	0.143070	0.015593
Snx22	0.154922	0.022571	Coa4	0.143055	0.025380
Gm49702	0.154776	0.003924	Als2cl	0.142816	0.035154
Trappc6a	0.154368	0.012764	Gm45869	0.141936	0.011621
Ccdc141	0.154008	0.018702	Sys1	0.141478	0.023550
Adgrl4	0.153981	0.023817	Lfng	0.141221	0.030651
Piezo1	0.153691	0.023744	Hspg2	0.141215	0.034731
Ciart	0.153002	0.022457	Ostf1	0.141119	0.036093
Alad	0.152647	0.025097	Shroom1	0.140982	0.037141
Tmem119	0.152460	0.015823	Gkn3	0.140777	0.030974
Gm44954	0.152242	0.000461	Zfp619	0.140772	0.039206
Sox17	0.152146	0.020039	Rin2	0.140398	0.020405
Castor1	0.151764	0.015960	Bhlhe41	0.140333	0.004535
Gata2	0.151645	0.015442	Tnxb	0.140279	0.033916
C1qa	0.151445	0.018049	Notch3	0.140248	0.039486
H2-Ab1	0.151333	0.007784	Slc16a12	0.140019	0.038978
Pld4	0.151031	0.025898	Selplg	0.139897	0.035625
Patj	0.150782	0.022620	Rsad2	0.139828	0.013332
Rccd1	0.150694	0.025200	Gm2629	0.139788	0.026529
Plekhg1	0.150457	0.026386	Kirrel2	0.139628	0.029825
Vwf	0.150137	0.024496	Stk32a	0.139464	0.037981
Lama5	0.150047	0.025390	Gm45470	0.139258	0.015122

Gene name	Log2 FC (*Rest* cKO vs Control)	p-value	Gene name	Log2 FC (*Rest* cKO vs Control)	p-value
Ccl9	0.139101	0.010916	Sytl1	0.128723	0.009015
Tnnt2	0.138665	0.040730	Rasd2	0.128401	0.036592
Unc93b1	0.138095	0.041655	S100pbp	0.127881	0.011072
Scn4b	0.137945	0.042143	5930430L01Rik	0.127607	0.031274
Col6a3	0.137650	0.037518	Dll3	0.127503	0.017739
Cebpa	0.137457	0.024078	Psg16	0.124896	0.031290
Trappc2l	0.137149	0.037976	Fam183b	0.124863	0.030765
Cacng4	0.136943	0.019706	Ahnak	0.124466	0.024837
Ssbp4	0.136598	0.031483	Adcy5	0.124033	0.046881
Itga5	0.136540	0.041828	Rps19	0.123550	0.049896
Zfp976	0.136403	0.039275	Cables1	0.123514	0.036624
H2bc21	0.136201	0.045127	Lin7b	0.122900	0.032749
Dnah7b	0.135793	0.016874	Gimap8	0.122020	0.037912
Nat8f4	0.135613	0.046941	Irf7	0.121920	0.037549
Adhfe1	0.135427	0.033189	AW112010	0.121537	0.017495
Lage3	0.135379	0.046979	Angptl2	0.121423	0.043589
Zmynd10	0.135134	0.035077	Hddc3	0.118695	0.018860
Pltp	0.135029	0.041638	Lgmn	0.116774	0.012914
BC028528	0.134942	0.021641	Lamb3	0.116732	0.029938
Scp2	0.134885	0.022805	Dna2	0.116048	0.036177
Drd2	0.134851	0.047306	Atp5d	0.115594	0.044721
Synpo2	0.134776	0.034659	Gm11639	0.115554	0.007219
Fam20a	0.134334	0.046485	H2-T24	0.114709	0.044225
Tbc1d7	0.134001	0.030556	Nucb1	0.114504	0.032066
Arhgef15	0.133589	0.029387	Slc25a1	0.111754	0.042525
Sdr42e1	0.133349	0.046548	Bub1b	0.111377	0.039669
Lamb2	0.133307	0.027793	4632427E13Rik	0.110896	0.018873
Zfp94	0.133038	0.045253	Mlf1	0.109496	0.018827
Alox5ap	0.132440	0.044138	D330041H03Rik	0.105077	0.034014
Knop1	0.131777	0.022349	Polr3e	0.103628	0.039182
Setd6	0.131504	0.049531	Col6a6	0.102750	0.010418
Rnase4	0.131449	0.021729	B230208B08Rik	0.102134	0.014742
Me1	0.131250	0.018103	A730085K08Rik	0.099010	0.011209
Iqgap1	0.129818	0.025802	Gm6089	0.096924	0.034316
Rinl	0.129342	0.021678	Gm17641	0.095598	0.007638
Icosl	0.129199	0.042262	Gm18706	0.095523	0.037710
Foxo1	0.128941	0.025778	Sp110	0.092962	0.031122
Sergef	0.128938	0.033930	Gm14285	0.089796	0.048950
Rpl39	0.128818	0.045415	Nlrc3	0.089794	0.021876

Gene name	Log2 FC (*Rest* cKO vs Control)	p-value	Gene name	Log2 FC (*Rest* cKO vs Control)	p-value
Gm17509	0.088292	0.039175	9130208D14Rik	0.033759	0.044265
Ptpn22	0.087949	0.049164	Ighg2b	0.032784	0.026972
D430018E03Rik	0.087921	0.010432	1700019G24Rik	0.030221	0.044185
Gm9945	0.087793	0.023720	Gm36169	0.026539	0.041497
Gm37019	0.087177	0.024946			
Pnmal1	0.086775	0.043213			
Gpi-ps	0.086373	0.005496			
Exoc3l2	0.085898	0.019540			
C330024D21Rik	0.085479	0.041777			
Gm29093	0.085344	0.047269			
Slc35d2	0.084132	0.037113			
Aoc3	0.079557	0.043289			
Serpina3n	0.077394	0.013188			
Gm4925	0.076645	0.028261			
Uchl1os	0.073486	0.029965			
Phf11d	0.072210	0.037760			
Gm26644	0.069026	0.023538			
Zfp264	0.068447	0.018139			
Slc23a4	0.067745	0.048537			
Masp2	0.067299	0.036782			
Il2rb	0.067252	0.040137			
Arhgap33os	0.066292	0.007401			
Gm44700	0.062920	0.025243			
Gm4864	0.058454	0.007427			
Hp	0.058450	0.013847			
Gm14131	0.055119	0.014926			
Hmga1b	0.054539	0.006189			
Ubb-ps	0.053286	0.012023			
Gm38228	0.052198	0.043571			
Atp12a	0.051709	0.043425			
Gm44219	0.050859	0.028166			
Abhd12b	0.050673	0.045369			
E230015B07Rik	0.050561	0.048799			
Spo11	0.047198	0.049025			
Orc1	0.043558	0.033077			
Gm18736	0.043444	0.026368			
Gm36001	0.043330	0.033471			
Gm26520	0.042365	0.040069			
Rslcan18	0.038517	0.049063			

2. List of upregulated genes in *Rest* cKO mice.

Downregulated genes are represented in red and have a negative Log2 FC

Gene name	Log2 FC (*Rest* cKO vs Control)	p-value	Gene name	Log2 FC (*Rest* cKO vs Control)	p-value
Oxr1	-0.911091	1.95E-66	Sp4	-0.172270	0.007030
Pop4	-0.330085	1.27E-06	Mrpl48	-0.171091	0.010375
Ercc2	-0.261652	5.82E-05	Vstm2b	-0.170337	0.005685
Snhg14	-0.248463	0.000116	Sirt1	-0.169778	0.005316
Kcnj11	-0.247055	0.000236	Dctn5	-0.169407	0.010832
Prss23	-0.243576	0.000169	Gm44644	-0.166372	0.005069
Grin2a	-0.232933	3.12E-05	Zfp758	-0.166105	0.012793
Ramac	-0.232870	0.000652	Zfp93	-0.165948	0.013508
Gm44509	-0.224645	0.000290	C230062I16Rik	-0.165835	0.005196
Zfp109	-0.219333	0.000731	Kctd15	-0.165817	0.015012
Olfm3	-0.216673	0.000790	Pxylp1	-0.165282	0.013060
Tmem267	-0.213802	0.001679	Dcx	-0.164250	0.014785
Krt9	-0.212238	0.001645	Zfp39	-0.162292	0.016692
Matn2	-0.205662	0.000809	Ech1	-0.162051	0.006080
Homer2	-0.205376	0.000573	AI504432	-0.161502	0.009241
Gm45441	-0.198924	0.002447	Zfp180	-0.161153	0.006243
Igf1	-0.193122	0.002386	Rab6a	-0.161032	1.16E-05
Rorb	-0.192587	5.44E-05	Maml3	-0.160620	0.015575
Itpripl2	-0.192389	0.004842	Plekha2	-0.160432	0.008664
Kcnv1	-0.191663	0.001065	Tmem196	-0.160011	0.018108
4930452B06Rik	-0.191419	0.005021	Acan	-0.159626	0.018703
Epha3	-0.191364	0.004956	Kcnh7	-0.159569	0.015227
Kantr	-0.190602	0.002722	Rps15a	-0.157753	0.006512
Pgm2l1	-0.190566	0.000785	Rasa2	-0.157569	0.008372
Trpc6	-0.190352	0.003701	Lmbrd2	-0.157273	0.012587
Ccdc61	-0.188039	0.005887	Med8	-0.157068	0.017786
Wnt7a	-0.187871	0.005619	Ube2e1	-0.155785	0.002611
Rnf169	-0.186494	0.006317	Rhcg	-0.154408	0.001911
Fam71e1	-0.185014	0.003276	Zfp526	-0.153452	0.022051
A030001D20Rik	-0.182930	0.007402	Prkca	-0.153306	0.009969
9330121K16Rik	-0.182284	0.002856	Zfp870	-0.151205	0.023332
Dlx1	-0.180448	0.006355	Cited1	-0.151041	0.013574
Gng4	-0.175716	0.009910	Rasgrf2	-0.150568	0.005918
Zxdb	-0.175316	0.006537	Wee1	-0.150495	0.009531
Pcdh11x	-0.174330	0.004774	Sms	-0.149863	0.002520
Cadm2	-0.172735	0.004479	Pcdhb3	-0.149715	0.025036

Gene name	Log2 FC (*Rest* cKO vs Control)	p-value	Gene name	Log2 FC (*Rest* cKO vs Control)	p-value
Kras	-0.149038	0.004126	Chaf1a	-0.136640	0.044873
Gm48678	-0.148310	0.003204	Sox2	-0.136625	0.020859
Gpatch1	-0.148277	0.018194	Pcdha11	-0.136607	0.036555
Sult2b1	-0.147998	0.030183	Homer1	-0.136414	0.030726
Hspa1b	-0.147415	0.027739	Zfp420	-0.136337	0.031139
Pcdh7	-0.146597	0.010705	Zeb2	-0.136268	0.029247
Doc2g	-0.146342	0.000543	Smg9	-0.136199	0.027930
Mybl1	-0.144916	0.032481	Kcnt2	-0.135986	0.033389
Dennd5b	-0.144776	0.011055	Elavl4	-0.135896	0.021505
9330104G04Rik	-0.144694	0.003645	Esco1	-0.135676	0.024379
Neurod1	-0.144529	0.031414	Rad23b	-0.135255	0.019508
Hnrnpa3	-0.144316	0.016049	Serpini1	-0.134741	0.016446
Nucks1	-0.144264	0.003584	Tmed5	-0.134566	0.024457
Zfp536	-0.144252	0.027916	Efna5	-0.134465	0.014333
Th	-0.143780	0.004449	Pcdhb17	-0.134229	0.043700
Gm765	-0.143677	0.029811	Kbtbd7	-0.134204	0.022493
Trim33	-0.143548	0.003837	Ngf	-0.134091	0.032281
Tmem170b	-0.143240	0.003547	Ipcef1	-0.133825	0.003273
Coq7	-0.142911	0.020724	Hcn1	-0.133763	0.035168
Klhl9	-0.142330	0.034335	Zfx	-0.133688	0.038887
Gm42372	-0.141992	0.022431	Ywhaz	-0.133382	0.002656
Cd47	-0.141397	0.037875	Gabra1	-0.132826	0.021616
Rspo2	-0.141302	0.026139	Zfp81	-0.132819	0.038072
Med29	-0.140179	0.039620	Fzd3	-0.132682	0.026217
Gys1	-0.139920	0.021762	Rab29	-0.132495	0.048273
Sp8	-0.139392	0.012320	Zfp711	-0.132482	0.039347
Erbb4	-0.139359	0.022022	A830018L16Rik	-0.132088	0.023978
Tmtc2	-0.139164	0.020349	1700003M07Rik	-0.131255	0.036285
Napb	-0.138948	0.031049	Paip1	-0.130749	0.004569
Col4a3bp	-0.138316	0.011745	Slc8a1	-0.130139	0.041284
Arfip1	-0.138257	0.039209	Kcnj3	-0.129949	0.012306
Spred1	-0.138099	0.001031	Klhl4	-0.128494	0.049379
Bmpr2	-0.138062	0.024145	Ro60	-0.128369	0.039380
Zfp748	-0.138043	0.033471	Txlng	-0.128121	0.046094
Dlx6os1	-0.137295	0.042429	Rps6ka3	-0.128078	0.018641
Pclo	-0.137206	0.020679	Zfp260	-0.127629	0.023117
Kcnb2	-0.137054	0.040334	mt-Nd6	-0.127467	0.031291
mt-Tq	-0.137027	0.009695	Tsc22d2	-0.127320	0.006775
Nefm	-0.136644	0.011998	Fgf9	-0.127187	0.049222

Gene name	Log2 FC (*Rest* cKO vs Control)	p-value	Gene name	Log2 FC (*Rest* cKO vs Control)	p-value
Dnajb9	-0.127064	0.030026	Slc2a13	-0.118450	0.035494
Gm37056	-0.126786	0.045966	Kcnip1	-0.117802	0.027219
Elavl2	-0.126734	0.021720	Ubxn2b	-0.117545	0.039829
Ube3a	-0.126459	0.047559	Prkaa2	-0.117466	0.044266
Krt80	-0.126244	0.034383	Pcdh9	-0.117303	0.049083
Dr1	-0.125874	0.020638	Rsbn1	-0.116756	0.049285
Lgr4	-0.125723	0.023254	Avl9	-0.116079	0.040073
Hydin	-0.125043	0.039993	Gnai1	-0.115913	0.025665
Ntrk3	-0.124856	0.036825	D630045J12Rik	-0.115821	0.027123
Sipa1l1	-0.124839	0.003675	Bnip3	-0.115264	0.049338
Zdhhc2	-0.124585	0.013194	Ddx6	-0.115165	0.039680
L3mbtl3	-0.124580	0.020976	Usp31	-0.114525	0.025234
Isg20l2	-0.124472	0.047263	Edil3	-0.114481	0.033257
Cyb5r4	-0.124468	0.043010	Magi1	-0.114481	0.034730
Oip5os1	-0.124442	0.023420	Plppr5	-0.114312	0.031820
Klhl28	-0.124136	0.043985	Ids	-0.114259	0.034019
Vstm2a	-0.124105	0.028805	Lrp8	-0.113901	0.012562
Nrxn1	-0.122929	0.021089	Klf3	-0.112390	0.042464
Bmt2	-0.122592	0.045109	Nfat5	-0.112247	0.041384
Yipf6	-0.122332	0.013354	Rock2	-0.112222	0.046769
Cpeb4	-0.122189	0.018548	Sumf1	-0.110717	0.043894
Lrrtm2	-0.121865	0.046786	Arfgef2	-0.110672	0.029143
Kdm7a	-0.121851	0.028090	Otud6b	-0.110185	0.047325
Pold3	-0.121736	0.044225	Lgr6	-0.108956	0.033230
Slc24a2	-0.121500	0.049624	Tbc1d9	-0.108690	0.028463
Btbd3	-0.121438	0.003036	Lin7c	-0.108447	0.028445
Bmpr1a	-0.121393	0.025663	Mgat5	-0.108182	0.019764
Vip	-0.121284	0.042865	Ryr2	-0.108035	0.014765
Fmr1	-0.121143	0.044771	Cyp51	-0.107925	0.042285
Frmd7	-0.121114	0.001252	Arl6ip1	-0.107761	0.027433
Sox5	-0.120509	0.047162	Car3	-0.107735	0.033032
Gnaq	-0.120450	0.021265	Gm14703	-0.107662	0.027208
Pglyrp1	-0.120226	0.040699	Nap1l2	-0.107497	0.046845
Tmx1	-0.119994	0.047417	Marcks	-0.107497	0.026957
1600014C10Rik	-0.119822	0.033591	Ncoa4	-0.107279	0.036803
Igip	-0.119410	0.015280	Mbtps2	-0.107211	0.041153
Ythdf3	-0.119227	0.036977	Atmin	-0.107043	0.013760
Robo2	-0.119013	0.047368	Fam234b	-0.106704	0.045242
Matr3	-0.118505	0.028389	Hdac4	-0.105771	0.044187

Gene name	Log2 FC (*Rest* cKO vs Control)	p-value	Gene name	Log2 FC (*Rest* cKO vs Control)	p-value
Zdhhc5	-0.105759	0.022484	Cpa6	-0.072461	0.042422
Atrnl1	-0.105362	0.025073	Gm37584	-0.070795	0.048575
Spcs3	-0.105071	0.014386	Zfp991	-0.065452	0.049450
Clock	-0.104990	0.033272	Trdn	-0.063273	0.031618
Vxn	-0.104639	0.020719	Myl1	-0.060110	0.011673
Sp7	-0.104285	0.013234	Kcnk15	-0.056283	0.013321
Kmt5b	-0.104038	0.039819	Tfap2c	-0.050205	0.024343
Zfp451	-0.103596	0.033807	Gm31479	-0.047958	0.025302
Cxxc5	-0.103428	0.033393	Eps8l1	-0.046811	0.011317
Lrrc8b	-0.103345	0.042840	Gm30684	-0.045320	0.025317
Tbx21	-0.103340	0.000407	Shisa3	-0.045091	0.043097
Efr3a	-0.103322	0.032223	Gm44985	-0.044088	0.041771
4930426D05Rik	-0.103170	0.049626	Gm45737	-0.039597	0.038678
Clcn4	-0.102412	0.039114	S100a5	-0.038054	0.023070
Chordc1	-0.101594	0.049625	Hephl1	-0.037679	0.018826
Dnajc3	-0.101164	0.035947	E330017L17Rik	-0.035298	0.045358
Zfp354c	-0.100579	0.035459	Nr5a1	-0.035065	0.046435
Tbl1xr1	-0.099909	0.035510	Gm22009	-0.034221	0.043284
Pkp1	-0.099651	0.037711	Gm38224	-0.033844	0.028605
Atl2	-0.098897	0.045254	Foxd3	-0.025254	0.046302
mt-Tp	-0.098198	0.022772			
Sh3gl2	-0.096715	0.016100			
Syt1	-0.094409	0.031744			
9630028B13Rik	-0.093914	0.019729			
Sbno1	-0.093831	0.033905			
Stox2	-0.092052	0.042754			
Ankrd13c	-0.091714	0.048165			
Smim13	-0.091086	0.037160			
Dscam	-0.090696	0.047451			
Gm3636	-0.088108	0.014405			
Arih1	-0.087445	0.046649			
Dnah11	-0.086348	0.031653			
Pate2	-0.085105	0.048391			
Edar	-0.084933	0.032965			
Scgn	-0.083639	0.008172			
Nefl	-0.083486	0.048957			
Gm45793	-0.082763	0.003478			
Myh13	-0.078493	0.047638			
Gm45353	-0.076010	0.043172			

3. **Complete list of significant gene ontology enrichment in biological process aspect in upregulated genes in *Rest* cKO mice, as opposed to the shorter version in the Results section where only root terms are shown.**

	Mus musculus (REF)	upload_1 (▽ Hierarchy NEW!)					
GO biological process complete	#	#	expected	Fold Enrichment	+/-	raw P value	FDR
interleukin-15-mediated signaling pathway	6	3	.06	48.67	+	8.33E-05	4.53E-02
↳cellular response to interleukin-15	6	3	.06	48.67	+	8.33E-05	4.69E-02
↳response to organic substance	2641	53	27.13	1.95	+	1.74E-06	3.91E-03
↳response to chemical	3602	67	37.01	1.81	+	8.02E-07	2.53E-03
↳cellular response to chemical stimulus	2500	46	25.69	1.79	+	9.00E-05	4.58E-02
positive regulation of angiogenesis	176	10	1.81	5.53	+	2.18E-05	2.64E-02
↳regulation of angiogenesis	301	12	3.09	3.88	+	9.31E-05	4.45E-02
↳regulation of vasculature development	305	12	3.13	3.83	+	1.05E-04	4.73E-02
↳regulation of multicellular organismal process	2989	59	30.71	1.92	+	7.52E-07	2.96E-03
↳positive regulation of vasculature development	176	10	1.81	5.53	+	2.18E-05	2.45E-02
↳positive regulation of multicellular organismal process	1699	36	17.46	2.06	+	4.60E-05	3.30E-02
↳positive regulation of biological process	6514	97	66.93	1.45	+	2.71E-05	2.67E-02
↳positive regulation of developmental process	1505	32	15.46	2.07	+	1.03E-04	4.75E-02
regulation of endothelial cell migration	174	9	1.79	5.03	+	1.12E-04	4.51E-02
↳regulation of epithelial cell migration	246	11	2.53	4.35	+	6.90E-05	4.19E-02
↳regulation of cell migration	987	31	10.14	3.06	+	4.98E-08	7.86E-04
↳regulation of cell motility	1044	31	10.73	2.89	+	1.67E-07	1.32E-03
↳regulation of locomotion	1092	31	11.22	2.76	+	4.31E-07	2.27E-03
positive regulation of cell adhesion	512	19	5.26	3.61	+	2.33E-06	4.60E-03
↳regulation of cell adhesion	814	25	8.36	2.99	+	1.62E-06	4.26E-03
↳positive regulation of cellular process	5869	87	60.30	1.44	+	1.11E-04	4.62E-02
positive regulation of response to external stimulus	458	16	4.71	3.40	+	3.04E-05	2.82E-02
↳positive regulation of response to stimulus	2409	46	24.75	1.86	+	3.98E-05	3.14E-02
↳regulation of response to stimulus	4140	67	42.53	1.58	+	1.07E-04	4.70E-02
positive regulation of cell migration	578	20	5.94	3.37	+	3.48E-06	6.10E-03
↳positive regulation of cell motility	605	20	6.22	3.22	+	6.71E-06	9.61E-03
↳positive regulation of locomotion	622	20	6.39	3.13	+	9.93E-06	1.30E-02
blood vessel morphogenesis	447	15	4.59	3.27	+	8.35E-05	4.39E-02
↳tube morphogenesis	746	20	7.66	2.61	+	1.17E-04	4.51E-02
↳blood vessel development	551	17	5.66	3.00	+	7.67E-05	4.48E-02
↳vasculature development	582	18	5.98	3.01	+	4.57E-05	3.43E-02
↳system development	3813	63	39.18	1.61	+	9.26E-05	4.56E-02
inflammatory response	512	17	5.26	3.23	+	3.19E-05	2.79E-02
↳defense response	1554	34	15.97	2.13	+	3.81E-05	3.16E-02
regulation of cytokine production	780	22	8.01	2.75	+	2.54E-05	2.67E-02
positive regulation of immune system process	1123	27	11.54	2.34	+	5.20E-05	3.41E-02
regulation of protein modification process	1586	34	16.29	2.09	+	5.06E-05	3.47E-02
response to other organism	1513	32	15.54	2.06	+	1.11E-04	4.71E-02
↳response to external biotic stimulus	1515	32	15.57	2.06	+	1.13E-04	4.44E-02
↳response to external stimulus	2488	50	25.56	1.96	+	4.18E-06	6.58E-03
sensory perception of chemical stimulus	1235	1	12.69	.08	-	5.66E-05	3.57E-02

4. Complete list of significant gene ontology enrichment in biological processes aspect in downregulated genes in *Rest* cKO mice, as opposed to the shorter version in the Results section where only root terms are shown.

	Mus musculus (REF)	upload_1 (▿ Hierarchy NEW!)					
GO biological process complete	#	#	expected	Fold Enrichment	+/-	raw P value	FDR
regulation of axon diameter	6	3	.07	42.96	+	1.20E-04	1.53E-02
↳regulation of biological quality	3833	67	44.61	1.50	+	4.84E-04	4.49E-02
↳biological regulation	12948	189	150.69	1.25	+	7.41E-07	3.24E-04
↳regulation of axonogenesis	181	12	2.11	5.70	+	2.60E-06	7.31E-04
↳regulation of neuron projection development	549	24	6.39	3.76	+	5.71E-08	6.92E-05
↳regulation of plasma membrane bounded cell projection organization	740	29	8.61	3.37	+	2.21E-08	3.49E-05
↳regulation of cell projection organization	756	29	8.80	3.30	+	3.46E-08	4.95E-05
↳regulation of cellular component organization	2474	48	28.79	1.67	+	4.61E-04	4.33E-02
↳regulation of cellular process	11607	174	135.08	1.29	+	1.06E-06	4.17E-04
↳regulation of biological process	12315	181	143.32	1.26	+	1.75E-06	5.42E-04
↳regulation of anatomical structure morphogenesis	989	26	11.51	2.26	+	1.28E-04	1.58E-02
↳regulation of developmental process	2652	62	30.86	2.01	+	1.21E-07	1.06E-04
intermediate filament bundle assembly	7	3	.08	36.83	+	1.70E-04	1.93E-02
regulation of postsynaptic density assembly	14	4	.16	24.55	+	4.61E-05	6.92E-03
↳regulation of postsynaptic specialization assembly	18	4	.21	19.09	+	1.06E-04	1.36E-02
↳regulation of postsynaptic density organization	19	4	.22	18.09	+	1.28E-04	1.60E-02
↳regulation of postsynapse organization	111	9	1.29	6.97	+	1.06E-05	2.22E-03
↳regulation of synapse organization	263	13	3.06	4.25	+	2.04E-05	3.57E-03
↳regulation of synapse structure or activity	271	13	3.15	4.12	+	2.75E-05	4.37E-03
↳regulation of excitatory synapse assembly	17	5	.20	25.27	+	4.35E-06	1.09E-03
glutamate receptor signaling pathway	40	6	.47	12.89	+	1.39E-05	2.64E-03
positive regulation of cardiac muscle tissue growth	46	5	.54	9.34	+	2.96E-04	3.11E-02
↳positive regulation of heart growth	49	5	.57	8.77	+	3.87E-04	3.74E-02
↳positive regulation of multicellular organismal process	1699	37	19.77	1.87	+	2.44E-04	2.63E-02
↳positive regulation of biological process	6514	117	75.81	1.54	+	8.91E-08	8.77E-05
↳regulation of multicellular organismal process	2989	57	34.79	1.64	+	1.60E-04	1.84E-02
↳positive regulation of developmental growth	217	12	2.53	4.75	+	1.48E-05	2.79E-03
↳positive regulation of developmental process	1505	43	17.52	2.46	+	7.13E-08	8.03E-05
↳positive regulation of growth	310	12	3.61	3.33	+	3.78E-04	3.68E-02
↳regulation of multicellular organismal development	1545	38	17.98	2.11	+	2.13E-05	3.65E-03
forebrain neuron differentiation	46	5	.54	9.34	+	2.96E-04	3.09E-02
↳central nervous system neuron differentiation	201	12	2.34	5.13	+	7.16E-06	1.61E-03
↳central nervous system development	913	29	10.63	2.73	+	1.51E-06	5.30E-04
↳nervous system development	2038	57	23.72	2.40	+	8.13E-10	4.27E-06
↳system development	3813	80	44.38	1.80	+	7.60E-08	7.99E-05
↳anatomical structure development	5341	97	62.16	1.56	+	1.61E-06	5.53E-04
↳developmental process	5724	104	66.62	1.56	+	4.42E-07	2.32E-04
↳multicellular organism development	4559	89	53.06	1.68	+	2.44E-07	1.54E-04
↳neuron differentiation	1147	40	13.35	3.00	+	9.51E-10	3.75E-06
↳generation of neurons	1226	41	14.27	2.87	+	1.87E-09	5.89E-06
↳neurogenesis	1396	46	16.25	2.83	+	2.57E-10	4.05E-06
↳cell differentiation	3675	76	42.77	1.78	+	3.27E-07	1.78E-04
↳cellular developmental process	3702	77	43.08	1.79	+	2.21E-07	1.51E-04
↳forebrain development	395	15	4.60	3.26	+	8.83E-05	1.15E-02
↳brain development	673	23	7.83	2.94	+	6.28E-06	1.48E-03
↳head development	731	23	8.51	2.70	+	2.25E-05	3.77E-03
↳animal organ development	3306	67	38.48	1.74	+	4.16E-06	1.07E-03
tissue regeneration	53	5	.62	8.11	+	5.40E-04	4.89E-02
↳developmental growth	496	19	5.77	3.29	+	9.04E-06	1.95E-03
↳growth	500	19	5.82	3.27	+	1.01E-05	2.15E-03
↳regeneration	105	8	1.22	6.55	+	4.97E-05	7.32E-03
positive regulation of axonogenesis	98	9	1.14	7.89	+	4.12E-06	1.08E-03
↳positive regulation of neurogenesis	298	16	3.47	4.61	+	8.09E-07	3.35E-04
↳positive regulation of nervous system development	359	20	4.18	4.79	+	1.85E-08	3.64E-05
↳regulation of nervous system development	554	23	6.45	3.57	+	2.63E-07	1.59E-04
↳positive regulation of cell development	377	17	4.39	3.87	+	3.54E-06	9.46E-04
↳positive regulation of cell differentiation	991	29	11.53	2.51	+	7.11E-06	1.62E-03
↳regulation of cell differentiation	1677	43	19.52	2.20	+	1.37E-06	5.01E-04
↳positive regulation of cellular process	5869	108	68.30	1.58	+	1.13E-07	1.05E-04
↳regulation of cell development	596	24	6.94	3.46	+	2.43E-07	1.60E-04
↳regulation of neurogenesis	456	20	5.31	3.77	+	7.26E-07	3.27E-04

↳positive regulation of cell projection organization	438	22	5.10	4.32	+	2.06E-08	3.61E-05
↳positive regulation of cellular component organization	1180	32	13.73	2.33	+	1.10E-05	2.29E-03
dendrite morphogenesis	80	7	.93	7.52	+	6.56E-05	9.23E-03
↳cell morphogenesis involved in neuron differentiation	482	18	5.61	3.21	+	2.16E-05	3.67E-03
↳cell morphogenesis involved in differentiation	615	19	7.16	2.65	+	1.48E-04	1.73E-02
↳cell development	1915	46	22.29	2.06	+	3.43E-06	9.32E-04
↳cell morphogenesis	785	23	9.14	2.52	+	6.50E-05	9.24E-03
↳anatomical structure morphogenesis	2337	56	27.20	2.06	+	2.19E-07	1.57E-04
↳neuron development	921	29	10.72	2.71	+	1.79E-06	5.33E-04
↳dendrite development	145	9	1.69	5.33	+	7.62E-05	1.04E-02
↳neuron projection development	747	22	8.69	2.53	+	8.76E-05	1.16E-02
↳plasma membrane bounded cell projection organization	1174	28	13.66	2.05	+	3.96E-04	3.76E-02
↳cell projection organization	1225	29	14.26	2.03	+	3.25E-04	3.30E-02
↳neuron projection morphogenesis	517	21	6.02	3.49	+	1.24E-06	4.67E-04
↳plasma membrane bounded cell projection morphogenesis	523	21	6.09	3.45	+	1.48E-06	5.31E-04
↳cell projection morphogenesis	529	21	6.16	3.41	+	1.76E-06	5.34E-04
↳cell part morphogenesis	556	23	6.47	3.55	+	2.79E-07	1.63E-04
↳cellular component morphogenesis	653	24	7.60	3.16	+	1.17E-06	4.49E-04
positive regulation of protein localization to cell periphery	69	6	.80	7.47	+	2.27E-04	2.48E-02
↳regulation of localization	2297	49	26.73	1.83	+	3.44E-05	5.37E-03
osteoblast differentiation	107	9	1.25	7.23	+	8.01E-06	1.75E-03
↳ossification	255	11	2.97	3.71	+	2.75E-04	2.93E-02
chondrocyte differentiation	90	7	1.05	6.68	+	1.31E-04	1.59E-02
↳tissue development	1785	39	20.77	1.88	+	1.97E-04	2.18E-02
positive regulation of synapse assembly	80	6	.93	6.44	+	4.76E-04	4.44E-02
potassium ion transmembrane transport	146	10	1.70	5.89	+	1.37E-05	2.64E-03
↳potassium ion transport	170	10	1.98	5.05	+	4.70E-05	6.98E-03
↳inorganic cation transmembrane transport	460	16	5.35	2.99	+	1.38E-04	1.62E-02
↳cation transmembrane transport	504	16	5.87	2.73	+	3.70E-04	3.65E-02
↳inorganic ion transmembrane transport	516	17	6.01	2.83	+	1.60E-04	1.85E-02
positive regulation of synaptic transmission	169	9	1.97	4.58	+	2.28E-04	2.48E-02
↳positive regulation of cell communication	1784	38	20.76	1.83	+	3.26E-04	3.30E-02
↳regulation of cell communication	3348	71	38.96	1.82	+	4.58E-07	2.33E-04
↳modulation of chemical synaptic transmission	526	21	6.12	3.43	+	1.62E-06	5.42E-04
↳regulation of trans-synaptic signaling	527	21	6.13	3.42	+	1.66E-06	5.35E-04
↳regulation of signaling	3356	71	39.06	1.82	+	4.69E-07	2.31E-04
↳positive regulation of signaling	1791	38	20.84	1.82	+	3.42E-04	3.43E-02
negative regulation of neuron apoptotic process	194	10	2.26	4.43	+	1.33E-04	1.59E-02
↳negative regulation of cellular process	4808	93	55.96	1.66	+	1.79E-07	1.49E-04
↳negative regulation of biological process	5444	100	63.36	1.58	+	5.98E-07	2.77E-04
↳negative regulation of neuron death	266	11	3.10	3.55	+	3.88E-04	3.70E-02
stem cell differentiation	199	10	2.32	4.32	+	1.62E-04	1.85E-02
regulation of neuron differentiation	233	11	2.71	4.06	+	1.30E-04	1.59E-02
regulation of nervous system process	191	9	2.22	4.05	+	5.36E-04	4.89E-02
↳regulation of system process	651	19	7.58	2.51	+	2.98E-04	3.09E-02
rhythmic process	263	12	3.06	3.92	+	8.82E-05	1.16E-02
positive regulation of neuron projection development	223	10	2.60	3.85	+	3.87E-04	3.72E-02
synapse organization	315	14	3.67	3.82	+	3.03E-05	4.77E-03
↳cell junction organization	524	16	6.10	2.62	+	5.57E-04	4.99E-02
learning or memory	319	13	3.71	3.50	+	1.34E-04	1.59E-02
↳behavior	720	20	8.38	2.39	+	5.49E-04	4.94E-02
↳cognition	356	13	4.14	3.14	+	3.73E-04	3.65E-02
regulation of membrane potential	467	17	5.43	3.13	+	4.99E-05	7.28E-03
regulation of ion transmembrane transport	525	19	6.11	3.11	+	1.94E-05	3.43E-03
↳regulation of ion transport	769	24	8.95	2.68	+	1.69E-05	3.13E-03
↳regulation of transport	1940	42	22.58	1.86	+	9.69E-05	1.25E-02
↳regulation of transmembrane transport	625	21	7.27	2.89	+	2.05E-05	3.56E-03
cellular chemical homeostasis	518	18	6.03	2.99	+	5.35E-05	7.74E-03
↳cellular homeostasis	618	18	7.19	2.50	+	4.39E-04	4.14E-02
↳chemical homeostasis	942	24	10.96	2.19	+	4.88E-04	4.50E-02
heart development	577	19	6.72	2.83	+	6.64E-05	9.26E-03
↳circulatory system development	945	26	11.00	2.36	+	6.96E-05	9.63E-03
tube morphogenesis	746	22	8.68	2.53	+	8.59E-05	1.15E-02
↳tube development	976	27	11.36	2.38	+	4.58E-05	6.94E-03
negative regulation of cell differentiation	714	21	8.31	2.53	+	1.29E-04	1.59E-02
↳negative regulation of developmental process	999	26	11.63	2.24	+	2.14E-04	2.36E-02
cell-cell signaling	894	25	10.40	2.40	+	8.37E-05	1.13E-02
animal organ morphogenesis	1057	29	12.30	2.36	+	2.54E-05	4.18E-03

positive regulation of transcription by RNA polymerase II	1249	34	14.54	2.34	+	5.23E-06	1.29E-03
↳positive regulation of DNA-templated transcription	1612	39	18.76	2.08	+	1.82E-05	3.30E-03
↳regulation of DNA-templated transcription	3261	65	37.95	1.71	+	1.25E-05	2.56E-03
↳regulation of gene expression	4744	94	55.21	1.70	+	4.22E-08	5.54E-05
↳regulation of macromolecule metabolic process	6101	118	71.00	1.66	+	6.27E-10	4.94E-06
↳regulation of metabolic process	6619	121	77.03	1.57	+	9.86E-09	2.59E-05
↳regulation of nucleic acid-templated transcription	3265	65	38.00	1.71	+	1.27E-05	2.50E-03
↳regulation of RNA biosynthetic process	3273	65	38.09	1.71	+	1.31E-05	2.55E-03
↳regulation of macromolecule biosynthetic process	3726	76	43.36	1.75	+	5.95E-07	2.84E-04
↳regulation of biosynthetic process	3993	77	46.47	1.66	+	4.23E-06	1.08E-03
↳regulation of RNA metabolic process	3576	71	41.62	1.71	+	5.30E-06	1.28E-03
↳regulation of nucleobase-containing compound metabolic process	3887	76	45.24	1.68	+	3.27E-06	9.05E-04
↳regulation of nitrogen compound metabolic process	5528	106	64.33	1.65	+	1.73E-08	3.90E-05
↳regulation of cellular metabolic process	5458	102	63.52	1.61	+	1.86E-07	1.47E-04
↳regulation of primary metabolic process	5714	105	66.50	1.58	+	2.00E-07	1.50E-04
↳regulation of cellular biosynthetic process	3909	77	45.49	1.69	+	1.62E-06	5.33E-04
↳positive regulation of nucleic acid-templated transcription	1612	39	18.76	2.08	+	1.82E-05	3.33E-03
↳positive regulation of RNA biosynthetic process	1618	39	18.83	2.07	+	1.92E-05	3.43E-03
↳positive regulation of RNA metabolic process	1754	41	20.41	2.01	+	2.33E-05	3.87E-03
↳positive regulation of nucleobase-containing compound metabolic process	1963	44	22.85	1.93	+	3.65E-05	5.64E-03
↳positive regulation of nitrogen compound metabolic process	3071	63	35.74	1.76	+	7.31E-06	1.62E-03
↳positive regulation of metabolic process	3825	74	44.52	1.66	+	6.47E-06	1.50E-03
↳positive regulation of cellular metabolic process	3078	65	35.82	1.81	+	1.92E-06	5.61E-04
↳positive regulation of macromolecule metabolic process	3479	71	40.49	1.75	+	1.73E-06	5.44E-04
↳positive regulation of cellular biosynthetic process	1951	45	22.71	1.98	+	1.25E-05	2.53E-03
↳positive regulation of biosynthetic process	2002	45	23.30	1.93	+	2.63E-05	4.27E-03
↳positive regulation of macromolecule biosynthetic process	1835	45	21.36	2.11	+	2.28E-06	6.54E-04
↳regulation of transcription by RNA polymerase II	2484	58	28.91	2.01	+	2.82E-07	1.59E-04
cellular response to endogenous stimulus	931	25	10.83	2.31	+	1.32E-04	1.59E-02
↳response to endogenous stimulus	1156	28	13.45	2.08	+	3.43E-04	3.43E-02
negative regulation of protein metabolic process	1057	27	12.30	2.19	+	1.79E-04	2.00E-02
↳regulation of protein metabolic process	2563	52	29.83	1.74	+	7.86E-05	1.07E-02
↳negative regulation of macromolecule metabolic process	2746	61	31.96	1.91	+	9.08E-07	3.67E-04
↳negative regulation of metabolic process	2982	62	34.70	1.79	+	5.58E-06	1.33E-03
↳negative regulation of nitrogen compound metabolic process	2365	55	27.52	2.00	+	7.79E-07	3.32E-04
epithelium development	1161	29	13.51	2.15	+	1.27E-04	1.60E-02
embryo development	1231	30	14.33	2.09	+	1.75E-04	1.97E-02
negative regulation of macromolecule biosynthetic process	1462	33	17.01	1.94	+	3.48E-04	3.45E-02
negative regulation of cellular metabolic process	2205	47	25.66	1.83	+	5.94E-05	8.52E-03
cellular response to organic substance	1903	40	22.15	1.81	+	3.10E-04	3.19E-02
↳cellular response to chemical stimulus	2500	48	29.09	1.65	+	5.15E-04	4.72E-02
↳response to chemical	3602	65	41.92	1.55	+	2.47E-04	2.65E-02
↳response to organic substance	2641	51	30.74	1.66	+	3.20E-04	3.28E-02
regulation of signal transduction	2924	59	34.03	1.73	+	2.66E-05	4.28E-03
↳regulation of response to stimulus	4140	72	48.18	1.49	+	2.91E-04	3.08E-02
sensory perception of smell	1133	1	13.19	.08	-	4.06E-05	6.22E-03
↳sensory perception of chemical stimulus	1235	1	14.37	.07	-	1.26E-05	2.51E-03

5. Complete list of significant gene ontology enrichment in molecular function aspect in downregulated genes in *Rest* cKO mice, as opposed to the shorter version in the Results section where only root terms are shown.

	Mus musculus (REF)	upload_1 (▽ Hierarchy NEW!)					
GO molecular function complete	#	#	expected	Fold Enrichment	+/-	raw P value	FDR
voltage-gated potassium channel activity	95	7	1.11	6.33	+	1.79E-04	2.89E-02
↳voltage-gated ion channel activity	197	10	2.29	4.36	+	1.50E-04	2.69E-02
↳voltage-gated channel activity	198	10	2.30	4.34	+	1.56E-04	2.70E-02
↳channel activity	482	17	5.61	3.03	+	7.25E-05	1.60E-02
↳passive transmembrane transporter activity	482	17	5.61	3.03	+	7.25E-05	1.67E-02
↳cation channel activity	333	14	3.88	3.61	+	5.39E-05	1.31E-02
↳ion channel activity	438	17	5.10	3.34	+	2.30E-05	6.19E-03
↳potassium channel activity	121	9	1.41	6.39	+	2.01E-05	5.73E-03
↳potassium ion transmembrane transporter activity	156	10	1.82	5.51	+	2.35E-05	5.99E-03
chromatin binding	651	20	7.58	2.64	+	1.07E-04	2.07E-02
↳binding	14027	201	163.25	1.23	+	5.29E-07	2.84E-04
RNA polymerase II cis-regulatory region sequence-specific DNA binding	1143	35	13.30	2.63	+	2.61E-07	3.16E-04
↳cis-regulatory region sequence-specific DNA binding	1164	35	13.55	2.58	+	3.96E-07	2.74E-04
↳transcription cis-regulatory region binding	1451	42	16.89	2.49	+	8.17E-08	3.96E-04
↳transcription regulatory region nucleic acid binding	1456	42	16.94	2.48	+	8.69E-08	2.10E-04
↳nucleic acid binding	3401	63	39.58	1.59	+	1.71E-04	2.85E-02
↳heterocyclic compound binding	5386	89	62.68	1.42	+	2.48E-04	3.88E-02
↳organic cyclic compound binding	5468	91	63.64	1.43	+	1.50E-04	2.79E-02
↳sequence-specific double-stranded DNA binding	1508	42	17.55	2.39	+	1.89E-07	3.04E-04
↳double-stranded DNA binding	1611	43	18.75	2.29	+	4.40E-07	2.66E-04
↳DNA binding	2332	48	27.14	1.77	+	9.81E-05	1.98E-02
↳sequence-specific DNA binding	1602	43	18.64	2.31	+	3.92E-07	3.17E-04
↳RNA polymerase II transcription regulatory region sequence-specific DNA binding	1357	38	15.79	2.41	+	7.21E-07	3.49E-04
DNA-binding transcription factor activity, RNA polymerase II-specific	1288	34	14.99	2.27	+	1.19E-05	3.60E-03
↳DNA-binding transcription factor activity	1343	35	15.63	2.24	+	1.03E-05	3.56E-03
↳transcription regulator activity	1809	47	21.05	2.23	+	2.74E-07	2.65E-04
metal ion binding	3593	73	41.82	1.75	+	1.08E-06	4.76E-04
↳cation binding	3692	74	42.97	1.72	+	2.01E-06	8.10E-04
↳ion binding	5304	90	61.73	1.46	+	9.16E-05	1.93E-02
protein binding	9570	147	111.38	1.32	+	1.09E-05	3.52E-03
olfactory receptor activity	1149	0	13.37	< 0.01	-	2.44E-06	9.07E-04

6. **Complete list of significant gene ontology enrichment in cellular component aspect in downregulated genes in *Rest* cKO mice, as opposed to the shorter version in the Results section where only root terms are shown.**

	Mus musculus (REF)		upload_1 (▿ Hierarchy NEW! ⓘ)				
GO cellular component complete	#	#	expected	Fold Enrichment	+/-	raw P value	FDR
presynaptic intermediate filament cytoskeleton	2	2	.02	85.93	+	7.79E-04	3.88E-02
↳presynaptic cytoskeleton	11	3	.13	23.43	+	4.99E-04	2.75E-02
↳presynapse	591	23	6.88	3.34	+	7.73E-07	1.43E-04
↳synapse	1434	49	16.69	2.94	+	1.73E-11	1.77E-08
↳cell junction	2081	55	24.22	2.27	+	1.09E-08	2.77E-06
↳intracellular organelle	12654	176	147.27	1.20	+	2.76E-04	1.87E-02
↳intracellular anatomical structure	14305	192	166.48	1.15	+	7.44E-04	3.80E-02
↳organelle	12965	180	150.89	1.19	+	2.00E-04	1.46E-02
messenger ribonucleoprotein complex	15	4	.17	22.91	+	5.79E-05	5.37E-03
presynaptic cytosol	25	4	.29	13.75	+	3.24E-04	2.00E-02
↳cytosolic region	43	5	.50	9.99	+	2.22E-04	1.56E-02
hippocampal mossy fiber to CA3 synapse	49	5	.57	8.77	+	3.87E-04	2.32E-02
↳neuron to neuron synapse	433	20	5.04	3.97	+	3.34E-07	6.81E-05
excitatory synapse	79	7	.92	7.61	+	6.09E-05	5.18E-03
GABA-ergic synapse	108	8	1.26	6.36	+	5.99E-05	5.31E-03
potassium channel complex	90	6	1.05	5.73	+	8.54E-04	4.15E-02
↳cation channel complex	223	11	2.60	4.24	+	8.99E-05	7.05E-03
↳ion channel complex	294	13	3.42	3.80	+	6.11E-05	4.99E-03
↳transmembrane transporter complex	372	14	4.33	3.23	+	1.66E-04	1.25E-02
↳transporter complex	394	14	4.59	3.05	+	2.92E-04	1.92E-02
Schaffer collateral - CA1 synapse	115	7	1.34	5.23	+	5.35E-04	2.87E-02
growth cone	199	12	2.32	5.18	+	6.50E-06	8.84E-04
↳distal axon	376	18	4.38	4.11	+	8.06E-07	1.37E-04
↳axon	732	29	8.52	3.40	+	1.76E-08	3.99E-06
↳neuron projection	1563	47	18.19	2.58	+	2.85E-09	1.16E-06
↳plasma membrane bounded cell projection	2392	55	27.84	1.98	+	9.65E-07	1.51E-04
↳cell projection	2635	56	30.67	1.83	+	1.08E-05	1.16E-03
↳site of polarized growth	206	12	2.40	5.01	+	9.06E-06	1.09E-03
axon terminus	194	9	2.26	3.99	+	5.97E-04	3.12E-02
↳neuron projection terminus	216	10	2.51	3.98	+	3.04E-04	1.94E-02
neuronal cell body	734	32	8.54	3.75	+	3.15E-10	1.61E-07
↳cell body	822	35	9.57	3.66	+	7.91E-11	5.38E-08
↳somatodendritic compartment	1064	42	12.38	3.39	+	8.20E-12	1.67E-08
glutamatergic synapse	517	21	6.02	3.49	+	1.24E-06	1.81E-04
postsynaptic density	394	16	4.59	3.49	+	2.38E-05	2.31E-03
↳asymmetric synapse	402	17	4.68	3.63	+	7.98E-06	1.02E-03
↳postsynaptic specialization	434	17	5.05	3.37	+	2.06E-05	2.10E-03
↳postsynapse	741	24	8.62	2.78	+	9.35E-06	1.06E-03
dendrite	740	30	8.61	3.48	+	5.92E-09	2.01E-06
↳dendritic tree	743	30	8.65	3.47	+	6.47E-09	1.89E-06
intrinsic component of plasma membrane	1822	37	21.20	1.74	+	9.23E-04	4.38E-02
nucleus	7212	111	83.93	1.32	+	4.82E-04	2.81E-02
↳membrane-bounded organelle	12045	168	140.18	1.20	+	4.96E-04	2.81E-02

7. PPI network in upregulated genes in *Rest* cKO mice – Immune response (directly associated)

Functional enrichment of biological process aspect in PPI network in upregulated genes in *Rest* cKO mice. The terms selected are directly associated with immune response (network is depicted in the next page).

Biological Process (Gene Ontology)				
GO-term	description	count in network	strength	false discovery rate
GO:0035723	interleukin-15-mediated signaling pathway	3 of 6	1.7	0.0153
GO:0010996	Response to auditory stimulus	4 of 28	1.15	0.0407
GO:0016064	Immunoglobulin mediated immune response	7 of 80	0.94	0.0081
GO:1904018	Positive regulation of vasculature development	10 of 201	0.69	0.0126
GO:0045766	Positive regulation of angiogenesis	9 of 181	0.69	0.0227
GO:0010594	Regulation of endothelial cell migration	8 of 166	0.68	0.0493
GO:0010632	Regulation of epithelial cell migration	10 of 232	0.63	0.0283
GO:1903039	Positive regulation of leukocyte cell-cell adhesion	9 of 210	0.63	0.0493
GO:0002696	Positive regulation of leukocyte activation	13 of 324	0.6	0.0102
GO:0022409	Positive regulation of cell-cell adhesion	10 of 254	0.59	0.0469
GO:0042063	Gliogenesis	10 of 255	0.59	0.0478
GO:0045785	Positive regulation of cell adhesion	16 of 425	0.57	0.0045
GO:0010038	Response to metal ion	14 of 374	0.57	0.0104
GO:1901342	Regulation of vasculature development	13 of 349	0.57	0.0150
GO:0001525	Angiogenesis	12 of 325	0.56	0.0265
GO:0006954	Inflammatory response	17 of 481	0.55	0.0049
GO:0030335	Positive regulation of cell migration	20 of 567	0.54	0.0015
GO:0048514	Blood vessel morphogenesis	15 of 433	0.54	0.0119
GO:0002252	Immune effector process	15 of 435	0.53	0.0123
GO:0001819	Positive regulation of cytokine production	15 of 436	0.53	0.0123
GO:0050778	Positive regulation of immune response	15 of 450	0.52	0.0144
GO:0032103	Positive regulation of response to external stimulus	13 of 399	0.51	0.0407
GO:0030334	Regulation of cell migration	29 of 915	0.5	0.00078
GO:0001817	Regulation of cytokine production	22 of 698	0.5	0.0023
GO:0001944	Vasculature development	18 of 562	0.5	0.0074
GO:0001568	Blood vessel development	17 of 534	0.5	0.0111
GO:0050776	Regulation of immune response	20 of 645	0.49	0.0049
GO:0010035	Response to inorganic substance	17 of 556	0.48	0.0139
GO:0045087	Innate immune response	17 of 558	0.48	0.0142
GO:0006955	Immune response	29 of 979	0.47	0.00078
GO:0002684	Positive regulation of immune system process	24 of 815	0.47	0.0023
GO:0001775	Cell activation	18 of 599	0.47	0.0123
GO:0006952	Defense response	33 of 1133	0.46	0.00078
GO:0009617	Response to bacterium	19 of 660	0.46	0.0126
GO:0045321	Leukocyte activation	15 of 511	0.46	0.0407
GO:0051270	Regulation of cellular component movement	30 of 1048	0.45	0.00078
GO:0098542	Defense response to other organism	22 of 775	0.45	0.0061
GO:0030155	Regulation of cell adhesion	20 of 705	0.45	0.0111
GO:0030097	Hemopoiesis	18 of 637	0.45	0.0198
GO:0051707	Response to other organism	32 of 1145	0.44	0.00078
GO:0035239	Tube morphogenesis	20 of 728	0.44	0.0137
GO:0048646	Anatomical structure formation involved in morphogenesis	25 of 952	0.42	0.0059
GO:0002520	Immune system development	19 of 727	0.41	0.0297
GO:0002682	Regulation of immune system process	30 of 1252	0.38	0.0049
GO:0032101	Regulation of response to external stimulus	21 of 871	0.38	0.0380
GO:0002376	Immune system process	43 of 1842	0.37	0.00078
GO:1901698	Response to nitrogen compound	25 of 1064	0.37	0.0176
GO:0051050	Positive regulation of transport	24 of 1020	0.37	0.0227
GO:0010243	Response to organonitrogen compound	23 of 975	0.37	0.0283

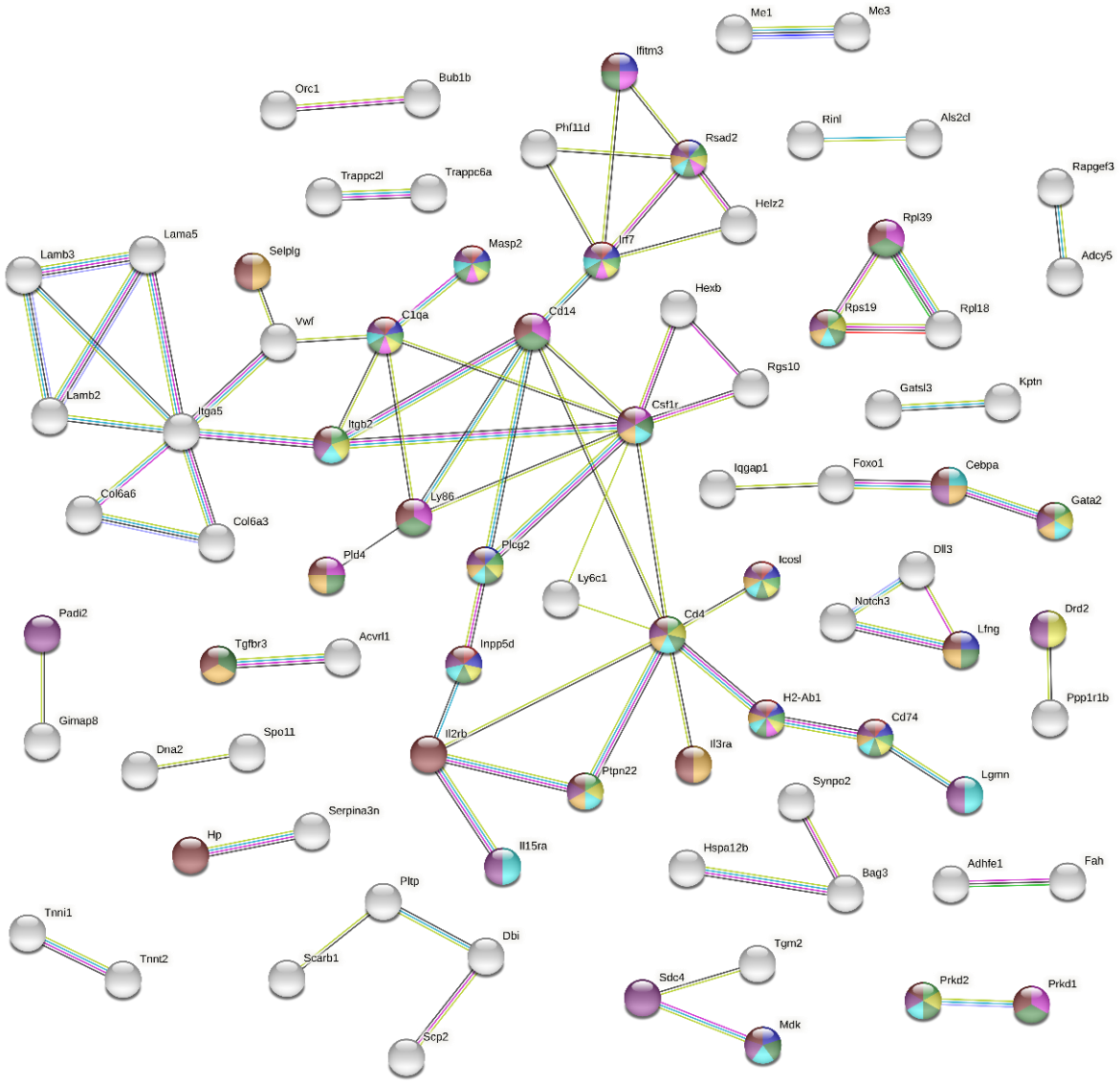
Me1
Me3
Ifitm3
Orc1
Bub1b
Phf11d
Rsad2
Rinl
Als2cl
Trappc2l
Trappc6a
Rapgef3
Helz2
Rpl39
Lama5
Lamb3
Selplg
Masp2
Irf7
Adcy5
Hexb
Vwf
C1qa
Cd14
Rps19
Rpl18
Rgs10
Lamb2
Itga5
Itgb2
Csf1r
Gatsl3
Kptn
Iqgap1
Foxo1
Cebpa
Col6a6
Ly86
Gata2
Col6a3
Plcg2
Dll3
Pld4
Icosl
Ly6c1
Padi2
Cd4
Notch3
Drd2
Tgfbr3
Acvrl1
Inpp5d
Lfng
H2-Ab1
Ppp1r1b
Gimap8
Cd74
Il2rb
Il3ra
Spo11
Dna2
Ptpn22
Lgmn
Synpo2
Serpina3n
Hp
Il15ra
Hspa12b
Bag3
Adhfe1
Fah
Pltp
Tnni1
Dbi
Scarb1
Tnnt2
Tgm2
Sdc4
Prkd2
Prkd1
Scp2
Mdk

8. PPI network in upregulated genes in *Rest* cKO mice – Immune response (indirectly associated)

Functional enrichment of biological process aspect in PPI network in upregulated genes in *Rest* cKO mice. The terms selected are indirectly associated with immune response (network is depicted in the next page).

Biological Process (Gene Ontology)				
GO-term	description	count in network	strength	false discovery rate
GO:0035723	interleukin-15-mediated signaling pathway	3 of 6	1.7	0.0153
GO:0010996	Response to auditory stimulus	4 of 28	1.15	0.0407
GO:0016064	Immunoglobulin mediated immune response	7 of 80	0.94	0.0081
GO:1904018	Positive regulation of vasculature development	10 of 201	0.69	0.0126
GO:0045766	Positive regulation of angiogenesis	9 of 181	0.69	0.0227
GO:0010594	Regulation of endothelial cell migration	8 of 166	0.68	0.0493
GO:0010632	Regulation of epithelial cell migration	10 of 232	0.63	0.0283
GO:1903039	Positive regulation of leukocyte cell-cell adhesion	9 of 210	0.63	0.0493
GO:0002696	Positive regulation of leukocyte activation	13 of 324	0.6	0.0102
GO:0022409	Positive regulation of cell-cell adhesion	10 of 254	0.59	0.0469
GO:0042063	Gliogenesis	10 of 255	0.59	0.0478
GO:0045785	Positive regulation of cell adhesion	16 of 425	0.57	0.0045
GO:0010038	Response to metal ion	14 of 374	0.57	0.0104
GO:1901342	Regulation of vasculature development	13 of 349	0.57	0.0150
GO:0001525	Angiogenesis	12 of 325	0.56	0.0265
GO:0006954	Inflammatory response	17 of 481	0.55	0.0049
GO:0030335	Positive regulation of cell migration	20 of 567	0.54	0.0015
GO:0048514	Blood vessel morphogenesis	15 of 433	0.54	0.0119
GO:0002252	Immune effector process	15 of 435	0.53	0.0123
GO:0001819	Positive regulation of cytokine production	15 of 436	0.53	0.0123
GO:0050778	Positive regulation of immune response	15 of 450	0.52	0.0144
GO:0032103	Positive regulation of response to external stimulus	13 of 399	0.51	0.0407
GO:0030334	Regulation of cell migration	29 of 915	0.5	0.00078
GO:0001817	Regulation of cytokine production	22 of 698	0.5	0.0023
GO:0001944	Vasculature development	18 of 562	0.5	0.0074
GO:0001568	Blood vessel development	17 of 534	0.5	0.0111
GO:0050776	Regulation of immune response	20 of 645	0.49	0.0049
GO:0010035	Response to inorganic substance	17 of 556	0.48	0.0139
GO:0045087	Innate immune response	17 of 558	0.48	0.0142
GO:0006955	Immune response	29 of 979	0.47	0.00078
GO:0002684	Positive regulation of immune system process	24 of 815	0.47	0.0023
GO:0001775	Cell activation	18 of 599	0.47	0.0123
GO:0006952	Defense response	33 of 1133	0.46	0.00078
GO:0009617	Response to bacterium	19 of 660	0.46	0.0126
GO:0045321	Leukocyte activation	15 of 511	0.46	0.0407
GO:0051270	Regulation of cellular component movement	30 of 1048	0.45	0.00078
GO:0098542	Defense response to other organism	22 of 775	0.45	0.0061
GO:0030155	Regulation of cell adhesion	20 of 705	0.45	0.0111
GO:0030097	Hemopoiesis	18 of 637	0.45	0.0198
GO:0051707	Response to other organism	32 of 1145	0.44	0.00078

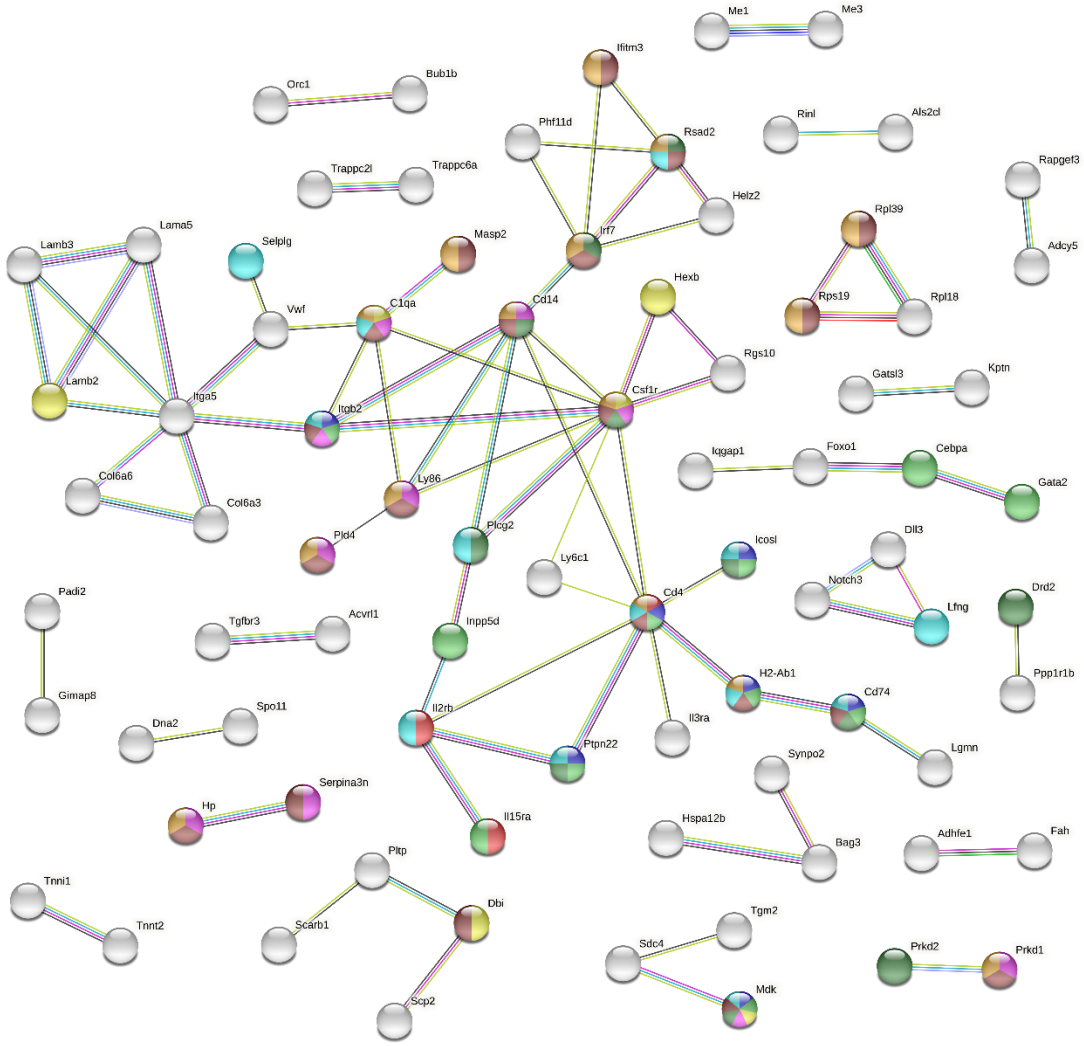
Me1
Me3
Ifitm3
Orc1
Bub1b
Phf11d
Rsad2
Rinl
Als2cl
Trappc2l
Trappc6a
Rapgef3
Helz2
Rpl39
Lama5
Lamb3
Selplg
Masp2
Irf7
Adcy5
Hexb
Vwf
C1qa
Cd14
Rps19
Rpl18
Rgs10
Lamb2
Itga5
Itgb2
Csf1r
Gatsl3
Kptn
Iqgap1
Foxo1
Cebpa
Col6a6
Ly86
Gata2
Col6a3
Dll3
Plcg2
Icosl
Ly6c1
Notch3
Padi2
Cd4
Lfng
Drd2
Tgfbr3
Acvrl1
Inpp5d
H2-Ab1
Ppp1r1b
Cd74
Gimap8
Spo11
Il2rb
Il3ra
Dna2
Ptpn22
Lgmn
Synpo2
Serpina3n
Hp
Il15ra
Hspa12b
Bag3
Adhfe1
Fah
Pkp
Tnni1
Dbi
Scarb1
Tgm2
Tnnt2
Sdc4
Prkd2
Prkd1
Mdk
Scp2

9. PPI network in upregulated genes in *Rest* cKO mice – Angiogenesis

Functional enrichment of biological process aspect in PPI network in upregulated genes in *Rest* cKO mice. The terms selected are indirectly associated with angiogenesis (network is depicted in the next page).

explain columns

Biological Process (Gene Ontology)				
GO-term	*description*	*count in network*	*strength*	*false discovery rate*
GO:0035723	interleukin-15-mediated signaling pathway	3 of 6	1.7	0.0153
GO:0010996	Response to auditory stimulus	4 of 28	1.15	0.0407
GO:0016064	Immunoglobulin mediated immune response	7 of 80	0.94	0.0081
GO:1904018	Positive regulation of vasculature development	10 of 201	0.69	0.0126
GO:0045766	Positive regulation of angiogenesis	9 of 181	0.69	0.0227
GO:0010594	Regulation of endothelial cell migration	8 of 166	0.68	0.0493
GO:0010632	Regulation of epithelial cell migration	10 of 232	0.63	0.0283
GO:1903039	Positive regulation of leukocyte cell-cell adhesion	9 of 210	0.63	0.0493
GO:0002696	Positive regulation of leukocyte activation	13 of 324	0.6	0.0102
GO:0022409	Positive regulation of cell-cell adhesion	10 of 254	0.59	0.0469
GO:0042063	Gliogenesis	10 of 255	0.59	0.0478
GO:0045785	Positive regulation of cell adhesion	16 of 425	0.57	0.0045
GO:0010038	Response to metal ion	14 of 374	0.57	0.0104
GO:1901342	Regulation of vasculature development	13 of 349	0.57	0.0150
GO:0001525	Angiogenesis	12 of 325	0.56	0.0265
GO:0006954	Inflammatory response	17 of 481	0.55	0.0049
GO:0030335	Positive regulation of cell migration	20 of 567	0.54	0.0015
GO:0048514	Blood vessel morphogenesis	15 of 433	0.54	0.0119
GO:0002252	Immune effector process	15 of 435	0.53	0.0123
GO:0001819	Positive regulation of cytokine production	15 of 436	0.53	0.0123
GO:0050778	Positive regulation of immune response	15 of 450	0.52	0.0144
GO:0032103	Positive regulation of response to external stimulus	13 of 399	0.51	0.0407
GO:0030334	Regulation of cell migration	29 of 915	0.5	0.00078
GO:0001817	Regulation of cytokine production	22 of 698	0.5	0.0023
GO:0001944	Vasculature development	18 of 562	0.5	0.0074
GO:0001568	Blood vessel development	17 of 534	0.5	0.0111
GO:0050776	Regulation of immune response	20 of 645	0.49	0.0049
GO:0010035	Response to inorganic substance	17 of 556	0.48	0.0139
GO:0045087	Innate immune response	17 of 558	0.48	0.0142
GO:0006955	Immune response	29 of 979	0.47	0.00078
GO:0002684	Positive regulation of immune system process	24 of 815	0.47	0.0023
GO:0001775	Cell activation	18 of 599	0.47	0.0123

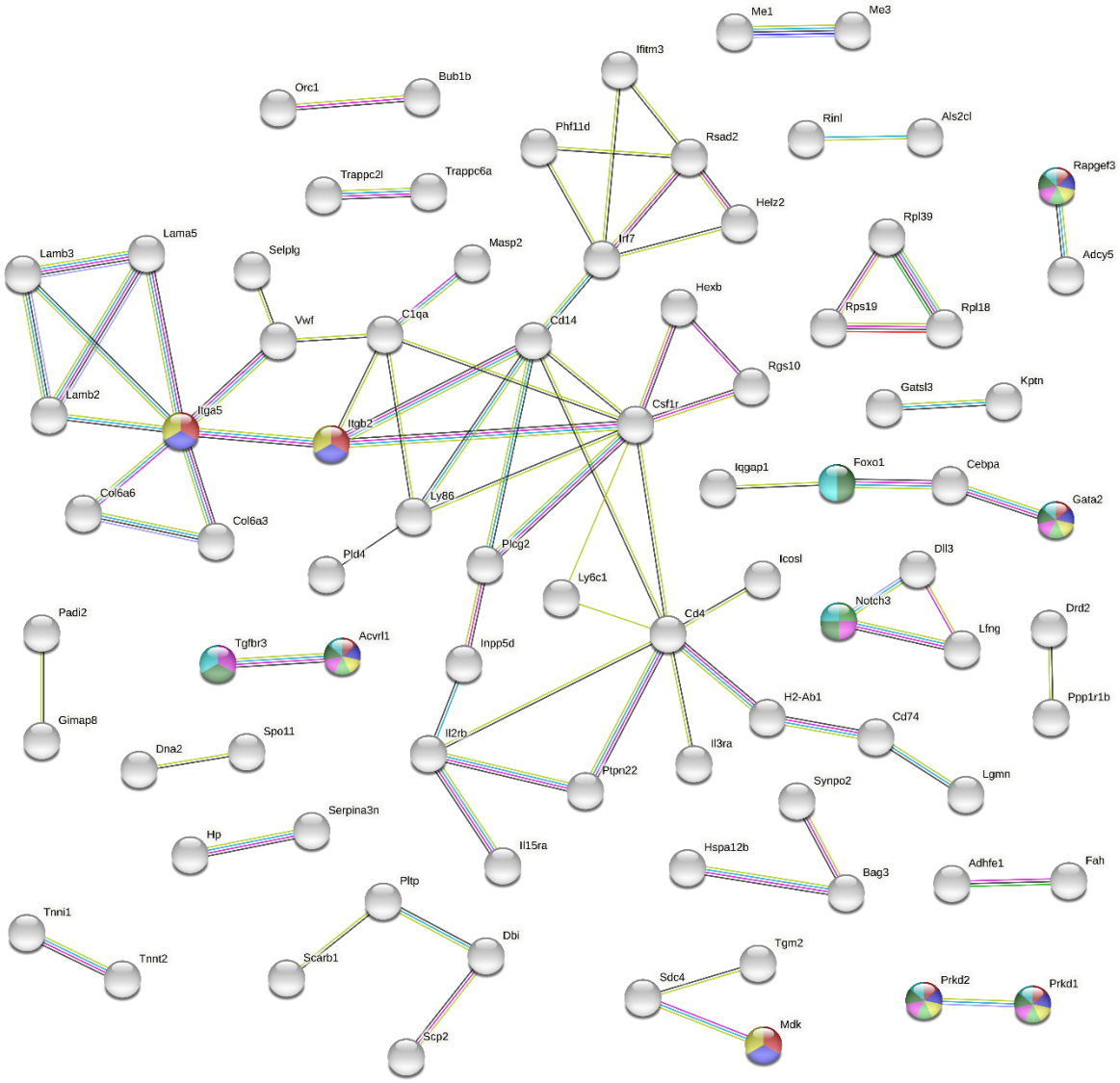
Me1
Me3
Ifitm3
Orc1
Bub1b
Phf11d
Rsad2
Rinl
Als2cl
Trappc2l
Trappc6a
Rapgef3
Helz2
Rpl39
Lama5
Lamb3
Selplg
Masp2
Irf7
Adcy5
Hexb
Vwf
C1qa
Cd14
Rps19
Rpl18
Rgs10
Lamb2
Itga5
Itgb2
Csf1r
Gatsl3
Kptn
Iqgap1
Foxo1
Cebpa
Col6a6
Ly86
Gata2
Col6a3
Pld4
Plcg2
Ly6c1
Icosl
Dll3
Padi2
Cd4
Notch3
Drd2
Tgfbr3
Acvrl1
Inpp5d
Lfng
H2-Ab1
Ppp1r1b
Gimap8
Cd74
Il2rb
Il3ra
Dna2
Spo11
Ptpn22
Lgmn
Synpo2
Serpina3n
Hp
Il15ra
Hspa12b
Bag3
Adhfe1
Fah
Pltp
Tnni1
Dbi
Tnnt2
Scarb1
Tgm2
Sdc4
Prkd2
Prkd1
Mdk
Scp2

10. PPI network in downregulated genes in *Rest* cKO mice – Neuronal pathways

Functional enrichment of biological process aspect in PPI network in downregulated genes in *Rest* cKO mice. The terms selected are associated with neuronal pathways (network is depicted in the next page).

Biological Process (Gene Ontology)				
GO-term	description	count in network	strength	false discovery rate
GO:0045105	Intermediate filament polymerization or depolymerization	2 of 2	1.94	0.0484
GO:0045110	Intermediate filament bundle assembly	3 of 5	1.71	0.0077
GO:0031133	Regulation of axon diameter	3 of 6	1.63	0.0107
GO:1904889	Regulation of excitatory synapse assembly	5 of 17	1.4	0.0010
GO:0099151	Regulation of postsynaptic density assembly	4 of 14	1.39	0.0050
GO:0045109	Intermediate filament organization	4 of 25	1.14	0.0241
GO:0007215	Glutamate receptor signaling pathway	6 of 47	1.04	0.0037
GO:0021879	Forebrain neuron differentiation	7 of 58	1.02	0.0016
GO:0055023	Positive regulation of cardiac muscle tissue growth	5 of 41	1.02	0.0152
GO:0048813	Dendrite morphogenesis	7 of 73	0.92	0.0043
GO:0001754	Eye photoreceptor cell differentiation	5 of 52	0.92	0.0348
GO:0002062	Chondrocyte differentiation	8 of 86	0.9	0.0019
GO:1990090	Cellular response to nerve growth factor stimulus	5 of 55	0.89	0.0418
GO:0042461	Photoreceptor cell development	5 of 55	0.89	0.0418
GO:0042220	Response to cocaine	5 of 55	0.89	0.0418
GO:0050772	Positive regulation of axonogenesis	9 of 104	0.87	0.0012
GO:1904377	Positive regulation of protein localization to cell periphery	6 of 69	0.87	0.0185
GO:0046530	Photoreceptor cell differentiation	6 of 69	0.87	0.0185
GO:0043279	Response to alkaloid	9 of 117	0.82	0.0022
GO:0051965	Positive regulation of synapse assembly	6 of 78	0.82	0.0300
GO:0007416	Synapse assembly	6 of 81	0.8	0.0348
GO:0099175	Regulation of postsynapse organization	9 of 130	0.78	0.0039
GO:0001649	Osteoblast differentiation	7 of 100	0.78	0.0193
GO:0001678	Cellular glucose homeostasis	7 of 101	0.78	0.0199
GO:0007269	Neurotransmitter secretion	6 of 86	0.78	0.0441
GO:0016358	Dendrite development	9 of 135	0.76	0.0049
GO:0099173	Postsynapse organization	7 of 106	0.75	0.0247
GO:0021987	Cerebral cortex development	8 of 127	0.73	0.0146
GO:0050770	Regulation of axonogenesis	12 of 203	0.71	0.0013
GO:0021953	Central nervous system neuron differentiation	12 of 210	0.69	0.0017
GO:0021543	Pallium development	11 of 193	0.69	0.0032
GO:0051963	Regulation of synapse assembly	7 of 122	0.69	0.0468
GO:0006836	Neurotransmitter transport	7 of 123	0.69	0.0484
GO:0048639	Positive regulation of developmental growth	12 of 214	0.68	0.0019
GO:0010770	Positive regulation of cell morphogenesis involved in differe...	10 of 189	0.66	0.0098
GO:0023061	Signal release	10 of 194	0.65	0.0115
GO:0050808	Synapse organization	15 of 303	0.63	0.0010
GO:0043524	Negative regulation of neuron apoptotic process	9 of 182	0.63	0.0278
GO:0051216	Cartilage development	9 of 184	0.62	0.0297
GO:0045666	Positive regulation of neuron differentiation	22 of 465	0.61	3.77e-05
GO:0050807	Regulation of synapse organization	13 of 275	0.61	0.0037
GO:0050806	Positive regulation of synaptic transmission	9 of 189	0.61	0.0348
GO:0030307	Positive regulation of cell growth	9 of 192	0.61	0.0369
GO:0010976	Positive regulation of neuron projection development	17 of 366	0.6	0.00065
GO:0021537	Telencephalon development	13 of 288	0.59	0.0052
GO:0061448	Connective tissue development	11 of 244	0.59	0.0158
GO:0031346	Positive regulation of cell projection organization	21 of 474	0.58	0.00013
GO:0010769	Regulation of cell morphogenesis involved in differentiation	15 of 343	0.58	0.0025
GO:0097305	Response to alcohol	11 of 252	0.58	0.0195
GO:0051962	Positive regulation of nervous system development	28 of 651	0.57	7.18e-06
GO:0032412	Regulation of ion transmembrane transporter activity	11 of 254	0.57	0.0205
GO:0001505	Regulation of neurotransmitter levels	11 of 255	0.57	0.0209
GO:0048511	Rhythmic process	13 of 305	0.56	0.0081
GO:0050769	Positive regulation of neurogenesis	24 of 579	0.55	6.98e-05
GO:0045664	Regulation of neuron differentiation	31 of 774	0.54	5.78e-06
GO:0032990	Cell part morphogenesis	21 of 522	0.54	0.00043
GO:0034765	Regulation of ion transmembrane transport	19 of 477	0.54	0.0011
GO:0010975	Regulation of neuron projection development	24 of 607	0.53	0.00013
GO:0048812	Neuron projection morphogenesis	19 of 479	0.53	0.0011
GO:0010721	Negative regulation of cell development	15 of 384	0.53	0.0065
GO:0030900	Forebrain development	17 of 438	0.52	0.0029
GO:0050768	Negative regulation of neurogenesis	13 of 336	0.52	0.0178
GO:0051960	Regulation of nervous system development	39 of 1071	0.5	1.47e-06
GO:0050767	Regulation of neurogenesis	35 of 948	0.5	5.18e-06
GO:0120035	Regulation of plasma membrane bounded cell projection or...	29 of 788	0.5	4.54e-05
GO:0034762	Regulation of transmembrane transport	21 of 568	0.5	0.0011
GO:0050804	Modulation of chemical synaptic transmission	19 of 521	0.5	0.0024
GO:0070848	Response to growth factor	18 of 485	0.5	0.0029
GO:0040007	Growth	17 of 466	0.5	0.0051

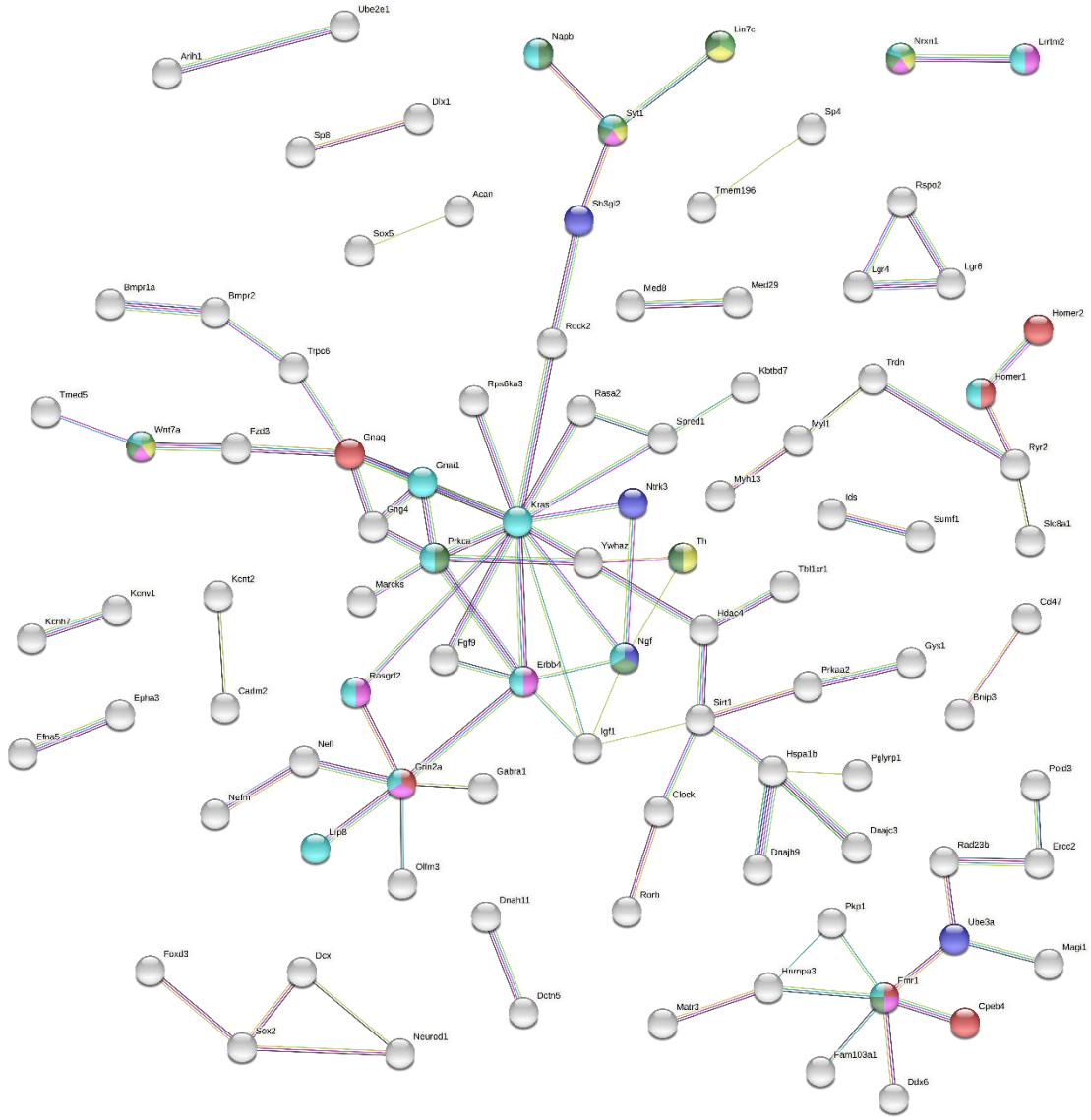
Ube2e1
Arih1
Napb
Lin7c
Nrxn1
Lrfn2
Dlx1
Sp8
Syt1
Sp4
Tmem196
Acan
Sox5
Sh3gl2
Rspo2
Lgr4
Lgr6
Bmpr1a
Bmpr2
Med8
Med29
Rock2
Homer2
Trpc6
Homer1
Trdn
Kbtbd7
Rps6ka3
Rasa2
Tmed5
Wnt7a
Fzd3
Gnaq
Spred1
Myl1
Ryr2
Gnai1
Myh13
Ntrk3
Gng4
Kras
Ids
Sumf1
Slc8a1
Prkca
Ywhaz
Th
Tbl1xr1
Kcnv1
Kcnh7
Kcnt2
Marcks
Hdac4
Cd47
Fgf9
Ngf
Gys1
Rasgrf2
Erbb4
Prkaa2
Cadm2
Bnip3
Epha3
Efna5
Sirt1
Nefl
Igf1
Hspa1b
Pglyrp1
Gnn2a
Gabra1
Pold3
Nefm
Clock
Lip8
Dnajc3
Rad23b
Ercc2
Olfm3
Dnajb9
Rorh
Dnahl1
Pkp1
Ube3a
Magi1
Foxd3
Dcx
Hnrnpa3
Fmr1
Dctn5
Matr3
Cpeb4
Sox2
Neurod1
Fam103a1
Ddx6

11. PPI network in downregulated genes in *Rest* cKO mice – Synaptic assembly

Functional enrichment of biological process aspect in PPI network in downregulated genes in *Rest* cKO mice. The terms selected are associated with synaptic assembly (network is depicted in the next page).

Biological Process (Gene Ontology)					
GO-term	description	count in network	strength	false discovery rate	
GO:0045105	Intermediate filament polymerization or depolymerization	2 of 2	1.94	0.0484	
GO:0045110	Intermediate filament bundle assembly	3 of 5	1.71	0.0077	
GO:0031133	Regulation of axon diameter	3 of 6	1.63	0.0107	
GO:1904889	Regulation of excitatory synapse assembly	5 of 17	1.4	0.0010	
GO:0099151	Regulation of postsynaptic density assembly	4 of 14	1.39	0.0050	
GO:0045109	Intermediate filament organization	4 of 25	1.14	0.0241	
GO:0007215	Glutamate receptor signaling pathway	6 of 47	1.04	0.0037	
GO:0021879	Forebrain neuron differentiation	7 of 58	1.02	0.0016	
GO:0055023	Positive regulation of cardiac muscle tissue growth	5 of 41	1.02	0.0152	
GO:0048813	Dendrite morphogenesis	7 of 73	0.92	0.0043	
GO:0001754	Eye photoreceptor cell differentiation	5 of 52	0.92	0.0348	
GO:0002062	Chondrocyte differentiation	8 of 86	0.9	0.0019	
GO:1990090	Cellular response to nerve growth factor stimulus	5 of 55	0.89	0.0418	
GO:0042461	Photoreceptor cell development	5 of 55	0.89	0.0418	
GO:0042220	Response to cocaine	5 of 55	0.89	0.0418	
GO:0050772	Positive regulation of axonogenesis	9 of 104	0.87	0.0012	
GO:1904377	Positive regulation of protein localization to cell periphery	6 of 69	0.87	0.0185	
GO:0046530	Photoreceptor cell differentiation	6 of 69	0.87	0.0185	
GO:0043279	Response to alkaloid	9 of 117	0.82	0.0022	
GO:0051965	Positive regulation of synapse assembly	6 of 78	0.82	0.0300	
GO:0007416	Synapse assembly	6 of 81	0.8	0.0348	
GO:0099175	Regulation of postsynapse organization	9 of 130	0.78	0.0039	
GO:0001649	Osteoblast differentiation	7 of 100	0.78	0.0193	
GO:0001678	Cellular glucose homeostasis	7 of 101	0.78	0.0199	
GO:0007269	Neurotransmitter secretion	6 of 86	0.78	0.0441	
GO:0016358	Dendrite development	9 of 135	0.76	0.0049	
GO:0099173	Postsynapse organization	7 of 106	0.75	0.0247	
GO:0021987	Cerebral cortex development	8 of 127	0.73	0.0146	
GO:0050770	Regulation of axonogenesis	12 of 203	0.71	0.0013	
GO:0021953	Central nervous system neuron differentiation	12 of 210	0.69	0.0017	
GO:0021543	Pallium development	11 of 193	0.69	0.0032	
GO:0051963	Regulation of synapse assembly	7 of 122	0.69	0.0468	
GO:0006836	Neurotransmitter transport	7 of 123	0.69	0.0484	
GO:0048639	Positive regulation of developmental growth	12 of 214	0.68	0.0019	
GO:0010770	Positive regulation of cell morphogenesis involved in differe...	10 of 189	0.66	0.0098	
GO:0023061	Signal release	10 of 194	0.65	0.0115	
GO:0050808	Synapse organization	15 of 303	0.63	0.0010	
GO:0043524	Negative regulation of neuron apoptotic process	9 of 182	0.63	0.0278	
GO:0051216	Cartilage development	9 of 184	0.62	0.0297	
GO:0045666	Positive regulation of neuron differentiation	22 of 465	0.61	3.77e-05	
GO:0050807	Regulation of synapse organization	13 of 275	0.61	0.0037	
GO:0050806	Positive regulation of synaptic transmission	9 of 189	0.61	0.0348	
GO:0030307	Positive regulation of cell growth	9 of 192	0.61	0.0369	

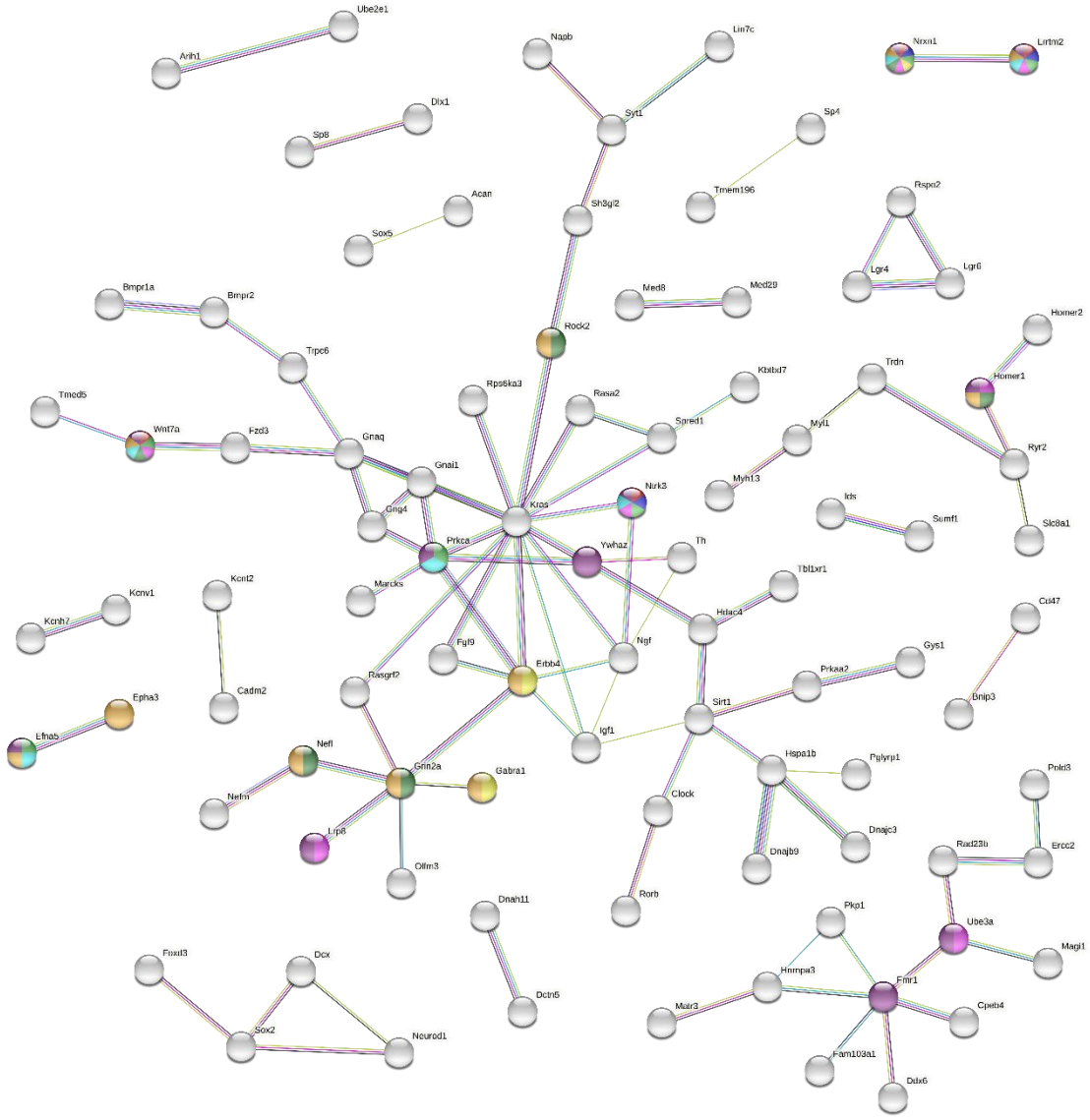
Ube2e1
Anh1
Napb
Lin7c
Nrxn1
Lrrtm2
Dlx1
Sp8
Syt1
Sp4
Tmem196
Acan
Sox5
Sh3gl2
Rspo2
Lgr4
Lgr6
Bmpr1a
Bmpr2
Med8
Med29
Rock2
Homer2
Trpc6
Kbtbd7
Trdn
Homer1
Tmed5
Rps6ka3
Rasa2
Spred1
Wnt7a
Fzd3
Gnaq
Myl1
Ryr2
Gnai1
Myh13
Nrk3
Ids
Sumf1
Gng4
Kras
Slc8a1
Prkca
Ywhaz
Th
Marcks
Tbl1xr1
Kcnv1
Kcnh7
Kcnt2
Hrlac4
Cd47
Fgf9
Ngf
Gys1
Erbb4
Prkaa2
Rasgrf2
Cadm2
Bnip3
Epha3
Efna5
Sirt1
Igf1
Nefl
Hspa1b
Plglyrp1
Grin2a
Gabra1
Nefm
Clock
Prdm3
Lrp8
Dnajc3
Rad23b
Ercc2
Olfm3
Dnajb9
Rorb
Dnah11
Pkp1
Ube3a
Magi1
Foxd3
Dcx
Hnrnpa3
Fmr1
Dctn5
Mair3
Cpeb4
Sox2
Neurod1
Fam103a1
Ddx6

12. PPI network in downregulated genes in *Rest* cKO mice – Binding

Functional enrichment of molecular function aspect in PPI network in downregulated genes in *Rest* cKO mice. The terms selected are associated with binding.

Molecular Function (Gene Ontology)				
GO-term	*description*	*count in network*	*strength*	*false discovery rate*
GO:0046872	Metal ion binding	76 of 3513	0.27	5.18e-05
GO:0043167	Ion binding	95 of 5439	0.18	0.0049
GO:0005515	Protein binding	117 of 6764	0.17	0.00030
GO:0005488	Binding	177 of 11199	0.13	7.83e-06

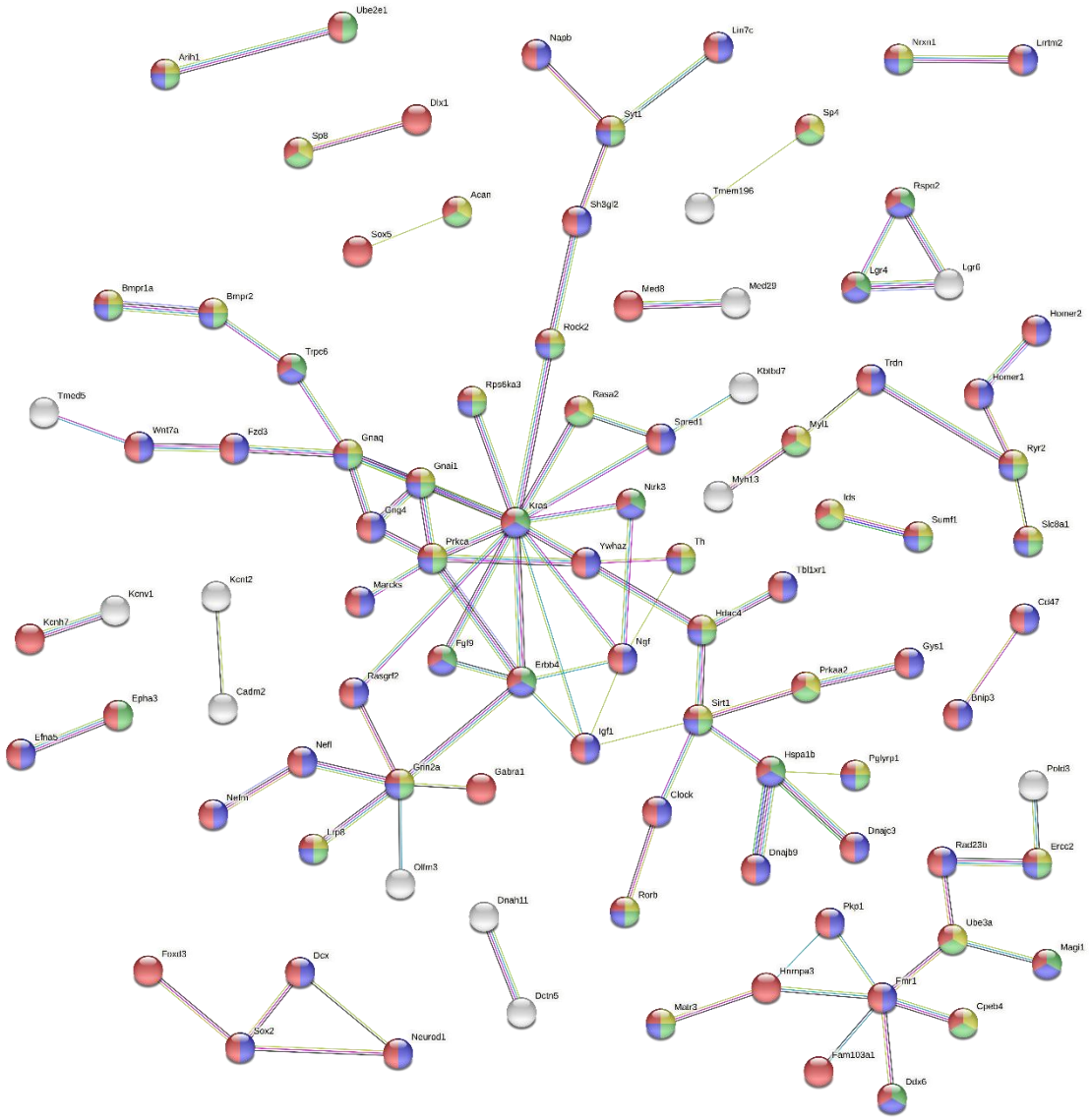

13. PPI network in downregulated genes in *Rest* cKO mice – Synaptic components

Functional enrichment of cellular component aspect in PPI network in downregulated genes in *Rest* cKO mice. The terms selected are associated with synaptic components (network is depicted in the next page).

Cellular Component (Gene Ontology)

GO-term	description	count in network	strength	false discovery rate
GO:0099182	Presynaptic intermediate filament cytoskeleton	2 of 2	1.94	0.0292
GO:0099569	Presynaptic cytoskeleton	3 of 10	1.41	0.0171
GO:1990124	Messenger ribonucleoprotein complex	4 of 14	1.39	0.0035
GO:0005790	Smooth endoplasmic reticulum	4 of 36	0.98	0.0404
GO:0098686	Hippocampal mossy fiber to ca3 synapse	5 of 50	0.94	0.0173
GO:0060076	Excitatory synapse	6 of 72	0.86	0.0131
GO:0098982	GABA-ergic synapse	8 of 102	0.83	0.0033
GO:0034705	Potassium channel complex	6 of 82	0.8	0.0205
GO:0005901	Caveola	7 of 97	0.79	0.0102
GO:0098685	Schaffer collateral - CA1 synapse	7 of 113	0.73	0.0193
GO:0031234	Extrinsic component of cytoplasmic side of plasma membr...	6 of 98	0.72	0.0452
GO:0034703	Cation channel complex	11 of 207	0.66	0.0035
GO:0098984	Neuron to neuron synapse	21 of 446	0.61	2.60e-05
GO:0034702	Ion channel complex	13 of 276	0.61	0.0027
GO:0044306	Neuron projection terminus	10 of 213	0.61	0.0130
GO:0032279	Asymmetric synapse	19 of 420	0.59	0.00015
GO:0030426	Growth cone	10 of 224	0.58	0.0171
GO:0043025	Neuronal cell body	32 of 743	0.57	2.76e-07
GO:0014069	Postsynaptic density	18 of 414	0.57	0.00033
GO:0099572	Postsynaptic specialization	19 of 449	0.56	0.00029
GO:0044297	Cell body	34 of 836	0.54	2.76e-07
GO:0150034	Distal axon	16 of 399	0.54	0.0024
GO:0030425	Dendrite	28 of 753	0.51	2.60e-05
GO:0098978	Glutamatergic synapse	19 of 501	0.51	0.0011
GO:0036477	Somatodendritic compartment	40 of 1080	0.5	2.76e-07
GO:0098793	Presynapse	23 of 636	0.49	0.00030
GO:0030424	Axon	27 of 791	0.47	0.00015
GO:0045202	Synapse	48 of 1492	0.44	2.76e-07
GO:0098794	Postsynapse	24 of 761	0.43	0.0014
GO:0043005	Neuron projection	45 of 1583	0.39	1.07e-05

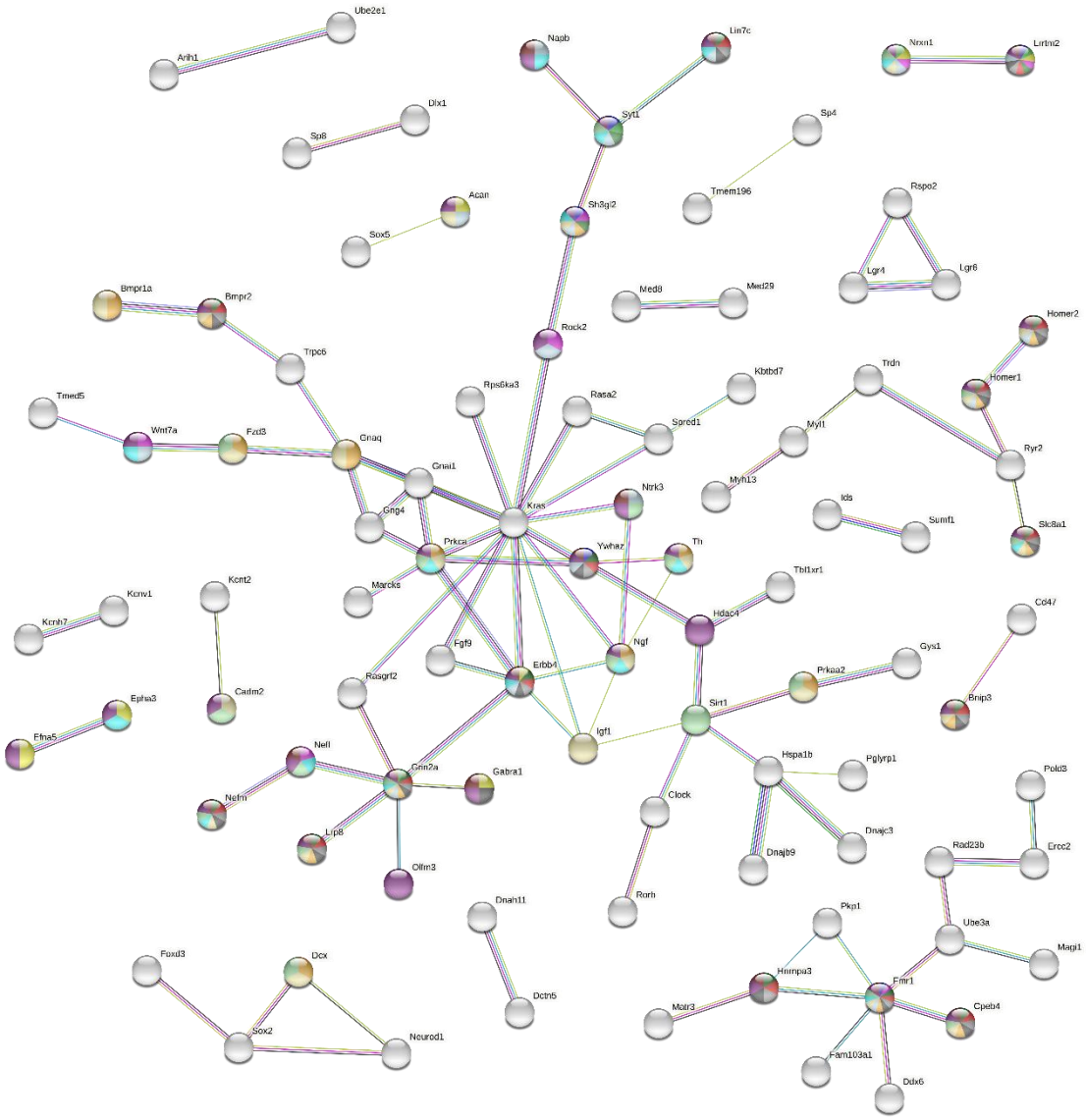
Ube2e1
Anln1
Napb
Lin7c
Nrxn1
Lrrtm2
Dlx1
Sp8
Syt1
Sp4
Tmem196
Acan
Sox5
Sh3gl2
Rspo2
Lgr4
Lgr6
Bmpr1a
Bmpr2
Med8
Med29
Rock2
Homer2
Trpc6
Kbtbd7
Trdn
Homer1
Tmed5
Rps6ka3
Rasa2
Spred1
Myl1
Wnt7a
Fzd3
Gnaq
Ryr2
Gnai1
Myh13
Ntrk3
Ids
Sumf1
Slc8a1
Gng4
Kras
Prkca
Ywhaz
Th
Marcks
Tbl1xr1
Kcnv1
Kcnh7
Kcnt2
Hdac4
Cd47
Fgf9
Ngf
Gys1
Erbb4
Prkaa2
Rasgrf2
Bnip3
Cadm2
Epha3
Efna5
Sirt1
Igf1
Nefl
Hspa1b
Pglyrp1
Grin2a
Gabra1
Nefm
Clock
Pold3
Dnajc3
Lin8
Dnajb9
Rad23b
Ercc2
Olfm3
Rorb
Dnah11
Pkp1
Ube3a
Magi1
Fuxd3
Dcx
Hnrnpa3
Fmr1
Dctn5
Mdh3
Cpeb4
Sox2
Neurod1
Fam103a1
Ddx6